Nanofiber-Based Scaffold for Integrative Anterior Cruciate Ligament Reconstruction

Siddarth D. Subramony

Submitted in partial fulfillment of the requirements for the degree of Doctor of Philosophy

in the Graduate School of Arts and Science

Columbia University

2014

ABSTRACT

Nanofiber-Based Scaffold for Integrative Anterior Cruciate Ligament Reconstruction

Siddarth D. Subramony

The anterior cruciate ligament (ACL) is the most frequently injured ligament of the knee, with upwards of 100,000 ACL reconstructions performed annually. Current grafting techniques are limited by insufficient integration with subchondral bone and donor site morbidity issues related to graft harvest, potentially resulting in revision surgery and long-term joint pain. Therefore, significant demand exists for alternative grafting solutions that do not require additional surgery and can regenerate the native ACL-to-bone interface to promote biological fixation of the implanted ACL graft. To address this need, the ideal system must be able to withstand the functional demands of the native tissue by demonstrating physiologically equivalent mechanical properties, be comprised of compositionally varying phases in order to recapitulate the inherent heterogeneity of the native ligament to bone transition and be biodegradable such that it is gradually replaced by the regenerated tissue following implantation. It is hypothesized that a biomimetic, multi-phased scaffold comprised of optimized bone, interface and ligament regions coupled with controlled chemical and/or mechanical stimulation *in vitro* will guide phase-specific differentiation of mesenchymal stem cells (MSC) and result in a biologically integrated bone-ligament-bone complex *in vivo*. Mesenchymal stem cells are particularly attractive for this application as they can be routinely harvested from bone marrow, have been shown to respond to chemical, mechanical and structural cues, and are capable of differentiating towards the primary cell types (fibroblasts, osteoblasts and chondrocytes) found within ligament, bone and the ligament-to-bone interface.

To this end, a nanofiber-based synthetic graft was designed with compositionally-varying phases to regenerate ligament, bone and interface tissues. The ligament phase was optimized in terms of nanofiber alignment, composition, mechanical stimulation and chemical stimulation. It was demonstrated that an aligned nanofiber substrate coupled with controlled mechanical stimulation was necessary to differentiate MSCs towards a fibroblastic phenotype. The bone phase was optimized in terms of ceramic content and it was shown that a threshold of mineral incorporation into nanofibers was necessary to differentiate MSCs towards an osteogenic phenotype. Lastly, a mechanoactive nanofiber collar was

designed to induce interface formation. It was demonstrated that compressive stimulation applied via nanofiber collar contraction induced chondrogenic differentiation of MSCs. Subsequently, the three phases were incorporated to form a synthetic graft, for which graft architecture and cell seeding density were optimized. The resulting graft was cultured *in vitro* under the optimized parameters, demonstrating the formation of distinct and structurally continuous regions of bone, interface and ligament tissue. The graft was implanted *in vivo* where it was shown to be suitable for ACL reconstruction as it maintained knee stability and promoted ligament regeneration.

In summary, this thesis focuses on the design of a biomimetic, nanofiber-based, integrated bone-ligament-bone construct, and elucidates chemical, mechanical and scaffold design-related parameters that can guide MSC differentiation towards desired tissue types. The impact of these studies extends beyond ligament reconstruction as they yield valuable scaffold design criteria, establish scaffold and culturing-related parameters to induce stem cell differentiation and can readily be applied to the formation of interfaces between soft-to-hard tissues as well as other complex tissues.

TABLE OF CONTENTS

LIST OF FIGURES

LIST OF TABLES

LIST OF ABBREVIATIONS

ACL: Anterior Cruciate Ligament

ALP: Alkaline Phosphatase

ANOVA: Analysis of Variance

bFGF: Basic Fibroblast Growth Factor

BPTB: Bone-Patellar Tendon-Bone

DMEM: Dulbecco's Modification of Eagle's Medium

DNA: Deoxyribose Nucleic Acid

E: Young's Modulus

EDAX: Energy Dispersive X-ray Analysis

Fb: Fibroblast

FBS: Fetal Bovine Serum

FTIR: Fourier Transform Infrared Spectroscopy

GAG: Glycosaminoglycan

HA: Hydroxyapatite

IR: Infrared

MFC: Mineralized fibrocartilage

Micro-CT: Micro Computerized Tomography

MSC: Mesenchymal Stem Cell

M_w: Weight-Averaged Molecular Weight

NEAA: Non-Essential Amino Acids

NFC: Non-mineralized fibrocartilage

P/S: Penicillin/Streptomycin

PCL: Polycaprolactone

PLGA: Polylactide-co-glycolide

PMMA: Poly(methylmethacrylate)

RT-PCR: Reverse Transcription – Polymerase Chain Reaction

SEM: Scanning Electron Microscopy

TGF-β3: Transforming Growth Factor Beta-3

ACKNOWLEDGEMENTS

Over the course of completing my doctoral studies at Columbia University, I have had the opportunity to work with an outstanding group of faculty, staff, and students. To begin, I would like to acknowledge my advisor, Dr. Helen Lu, who not only guided my research studies but who was also both a personal and professional mentor. In addition, my thesis committee, including Dr. Stephen Doty, Dr. X. Edward Guo, Dr. Scott Rodeo and Dr. Gordana Vunjak-Novakovic, has been a source of knowledge and wisdom. I am also grateful to the many collaborators who have been extremely generous with their time and continuously provided valuable insight to guide my research.

I would like to thank my colleagues in the Biomaterials and Interface Tissue Engineering Laboratory who played an instrumental role in helping me perform the research outlined in this thesis. I am particularly grateful to my fellow graduate students and post-doctoral scholars, namely Kristen Moffat, Elaine Wang, Nora Khanarian, Philip Chuang, Sagaw Prateepchinda, Margaret Boushell, Xinzhi Zhang, Nancy Lee, Danielle Bogdanowicz, Dovina Qu, Cevat Erisken, Marissa Solomon, Booth Dargis, and Mario Castillo as well as the undergraduate students that worked directly with me, including Michael Tracey, Amanda Su and Joshua Heisler. Furthermore, I would like to acknowledge the contributions of several staff members and graduate students from other laboratories in the Biomedical Engineering department, including Keith Yeager, Bin Zhou and Eric Yu, members of the Laboratory for Soft Tissue Research at the Hospital for Special Surgery (HSS), including Demetris Delos, Richard Ma, Michael Schär, Tina Chen and Marco Sisto and also thank the research staff and veterinary staff at HSS, including Orla O'Shea, Anthony Labissiere, Theresa Cunningham, Franky Colon, Mariel Rauer, and Xiomara Santiago.

Research funding for the studies in this thesis has been provided by the National Institutes of Health (NIH), National Institute of Arthritis and Musculoskeletal and Skin Diseases (NIAMS), New York Stem Cell Foundation (NYSTEM) and the National Science Foundation through a Graduate Research Fellowship and a Graduate K-12 Teaching Fellowship.

DEDICATION

This thesis is dedicated to my wife and family who provided unending support throughout all my years at Columbia. Without them, this work would not have been possible.

CHAPTER 1: INTRODUCTION

1.1 Specific Aims

The anterior cruciate ligament (ACL) is the most frequently injured ligament of the knee[4] with upwards of 100,000 ACL reconstructions performed annually in the United States alone[5]. Due to the ligament's intrinsically poor healing capability, ACL ruptures require surgical intervention[6-8]. The current standard of treatment is ACL reconstruction, which utilizes a biological graft to replace the damaged ligament, typically consisting of autologous bone-patellar tendon-bone (BPTB) or hamstring tendon tissue. Clinically, there has been a shift towards hamstring tendon grafts due to concerns related to the donor site morbidity associated with BPTB grafts, including patellar tendon rupture and persistent anterior knee pain[9;10]. However, the integration of hamstring tendon grafts with bone following reconstruction has been especially challenging as they lack the intact soft tissue-to-bone transitions inherent to BPTB grafts[11]. Studies evaluating graft-to-bone healing have shown that fibrovascular tissue forms within the bone tunnel and surrounds the graft following ACL reconstruction[12]. This disorganized tissue results in non-anatomical attachment sites that are prone to failure as well as insufficient bone formation within the tibial and femoral tunnels, which prevents the re-establishment of the structure-function relationship found in the native ligament[13]. In addition, failure rates for the reconstruction procedure, regardless of graft source, have been reported to exceed 20% in some instances[14] and frequently fail due to insufficient graft integration with bone[15]. As a result, there is a pressing clinical need for functional grafting solutions that can enable integrative ACL reconstruction through regeneration of the native ligament and ligament-bone interfaces.

To this end, tissue engineering has emerged as a promising method for integrative ACL reconstruction[16]. Recent efforts in ACL tissue engineering have primarily focused on the use of fibrous scaffolds[17-19], fabricated from a wide range of polymers, to mimic the structure of the native ligament which consists primarily of highly aligned bundles of collagen fibers[20]. These systems have been shown to exhibit mechanical properties, in terms of stiffness and failure strength, similar to those of the native ACL, and are also capable of directing cell attachment and matrix production[16;18;21]. However, these systems fail to promote biological fixation of the ligament to bone via interface regeneration, which is essential for long-term functionality of the ACL graft. To date, techniques to simultaneously regenerate the ligament as well as the complex femoral and tibial ligament-to-bone transitions have yet to be

realized. The native ligament-to-bone interface consists of distinct-yet-continuous regions of mineralized and non-mineralized fibrocartilage[22]. This transition is characterized by differences in cell type (including osteoblasts, chondrocytes and fibroblasts), matrix composition, mineral content and mechanical properties[23] and serves to minimize the formation of stress concentrations and mediate load transfer from ligament-to-bone[23]. Given its functional significant, the goal of this thesis project is to enable the regeneration of the native ligament as well as the femoral and tibial ligament-to-bone insertion sites following ACL reconstruction using a multi-phased scaffold (Fig. 1). With this approach, long-term clinical outcomes could be improved by eliminating a secondary surgical procedure plus the associated limitations of biological grafts. The primary advantage of this approach is that by engineering an *in vitro* integrated multi-phased scaffold with pre-connected ligament-to-bone interfaces, only osteointegration is required *in vivo*. The proposed techniques are intended to lead to the formation of multiple, distinct-yet-continuous cellular and matrix regions mimicking the organization of native tissue, with a gradation of mechanical and structural properties.

As this integrative scaffold is intended to replace traditional soft tissue grafts used for ACL reconstruction, there are several key design criteria that the ideal system must meet. First, it must be able to withstand the functional demands of the native tissue by demonstrating physiologically equivalent viscoelastic and elastic mechanical properties as immediate joint stability is required following reconstruction. Second, the scaffold must be comprised of compositionally varying phases in order to recapitulate the inherent heterogeneity of the native ligament to bone transition. Lastly, the scaffold must be biodegradable such that it is gradually replaced by the regenerated tissue following implantation.

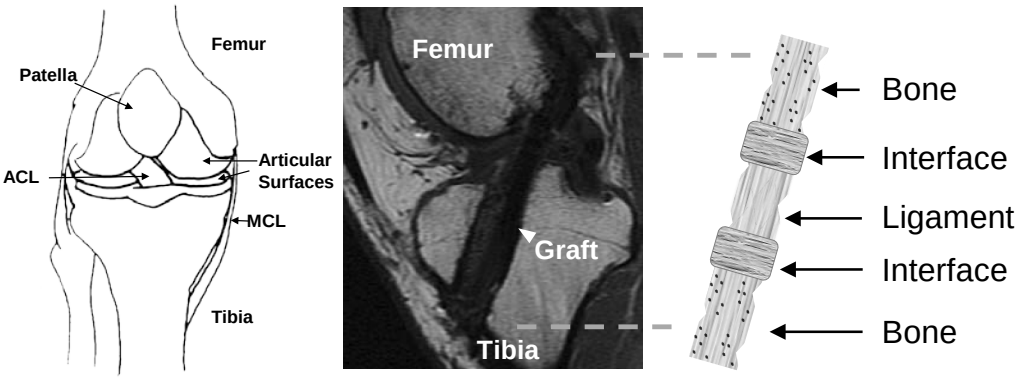

Figure 1.1. Schematic of the proposed integrative ACL scaffold. The scaffold comprises individually optimized phases for bone, interface or ligament regeneration, respectively. A schematic of the knee and an MRI following ACL reconstruction is shown to the left[1].

Collectively, these criteria will support multi-tissue formation and integrative ACL regeneration.

The strategy described in this thesis for integrative ligament tissue engineering centers on the design of a multi-phased, biomimetic scaffold by forming a continuous tissue encompassing the femoral bone and interface, ligament proper and tibial interface and bone (*Fig. 1.1*). To accomplish this, the graft will consist of nanofibers with a bone phase and ligament-to-bone interface phase at each end of the scaffold along with a central ligament phase to regenerate the ligament proper. Nanofibers are particularly advantageous for this application as their nano-architecture emulates the collagenous ultrastructure of the native ligament and insertions[24]. Moreover, nanofiber alignment, diameter and composition has also been reported to guide cell attachment, orientation, biosynthesis and differentiation[24]. In addition, while differentiated primary cells have largely been used for orthopaedic tissue engineering, such an approach is not as clinically translative as the ligament, fibrocartilage interface, and bone are populated by distinct cell types[25]. Therefore, pluri-potent stem cells represent a more feasible option for the regeneration of multiple tissue types using a single cell source. To this end, this thesis will utilize mesenchymal stem cells (MSC), which can be routinely harvested from bone marrow[26], have been shown to respond to chemical, mechanical and structural cues, and are capable of differentiating towards the primary cell types (fibroblasts, osteoblasts and chondrocytes) found within ligament, bone and the ligament-to-bone interface. To address the challenge of controlling MSC differentiation and design a clinically translatable scaffold, this thesis will focus on using chemical and mechanical cues to guide MSC differentiation on each phase. Specifically, fibroblastic differentiation can be stimulated using tensile and torsional mechanical loading[27] as well as fibrogenic growth factors[28], osteoblastic differentiation has been guided using osteointegrative ceramics[29] and osteogenic induction media[26], and differentiation into chondrocytes has been stimulated with compressive loading[30] and chondrogenic induction factors[26]. The first three aims will focus on optimizing design and culturing conditions of each phase to guide MSC differentiation for the formation of ligament, bone and interface tissue, followed by *in vitro* culture and *in vivo* evaluation of the integrated ACL scaffold in Aims 4 and 5. The **working hypothesis** of this thesis is that a biomimetic, multi-phased scaffold comprised of optimized bone, interface and ligament regions coupled with controlled chemical and/or mechanical stimulation *in vitro* will guide phase-specific MSC differentiation and result in a biologically integrated bone-ligament-bone complex *in vivo*.

Aim 1: Design, characterize and optimize a nanofiber-based phase to direct MSC-mediated formation of a ligament-like matrix.

Hypothesis: Ligament formation will be induced by nanofiber composition, nanofiber alignment, mechanical stimulation and/or fibrogenic factors.

Aim 2: Design, characterize and optimize a nanofiber-based phase to direct MSC-mediated formation of a bone-like matrix.

Hypothesis: Bone formation by MSCs on nanofibers will be induced by nanofiber mineral content.

Aim 3: Design, characterize and optimize a mechanoactive nanofiber-based collar to direct MSC-mediated formation of an interface-like matrix.

Hypothesis: Interface formation by MSCs on nanofibers will be induced by compressive loading with nanofiber collar contraction.

Aim 4: Fabricate and evaluate a multi-phased, nanofiber-based ACL scaffold *in vitro*.

Hypothesis: Scaffold mechanical properties will be dictated by architecture and the incorporation of all three phases optimized in Aims 1-3 will enable the formation of a biologically integrated bone-ligament-bone complex *in vitro*.

Aim 5: *In vivo* evaluation of a multi-phased nanofiber-based scaffold for integrative ACL reconstruction.

Hypothesis: The scaffold will enable the formation of a biologically integrated bone-ligament-bone complex *in vivo*.

The overall **objective** of this thesis is to design a multi-phased, nanofiber-based scaffold for integrative ACL reconstruction. To this end, Aims 1-3 encompass the fabrication, characterization and optimization of the three phases of the system, with each aim focusing on ligament, interface or bone formation, respectively. Following the design of each individual phase, in Aim 4, a stratified scaffold will be fabricated by combining these phases and the multi-phased scaffold will then be evaluated *in vitro* and, per Aim 5, *in vivo*.

More specifically, **Aim 1** will focus on the formation of a ligament-like tissue on polymeric nanofibers by inducing the differentiation of MSC into the ligament fibroblast-like phenotype. Three parameters will be tested in this aim. First, dynamic tensile stimulation will be utilized to induce MSC differentiation towards a fibroblastic phenotype, as this is the primary mode of loading experienced by the ligament[31] (*Chapter 2*). Mechanical loading has also been shown to induce MSC differentiation towards a fibroblast-like phenotype in published studies[27]. Second, the effect of nanofiber organization will be assessed in this aim to determine if aligned nanofibers, which mimic the underlying collagenous structure of the native ligament, are necessary for fibroblastic differentiation (*Chapter 2*). Third, the addition of fibrogenic factors[28] will be evaluated to determine if chemical stimulation is necessary in addition to mechanical stimulation (*Chapter 3*). It is expected that mechanical stimulation and nanofiber alignment are sufficient to drive ligament-like tissue formation. Lastly, the effect of nanofiber composition will be assessed to select the optimal material based on mechanical properties, degradation and cell response for the ligament phase (Chapter 4).

Following development of the ligament phase, **Aim 2** addresses the optimization of the bone phase by guiding MSC-mediated bone formation. To accomplish this, hydroxyapatite (HA) particles, the primary mineral identified in bone[32], will be incorporated into nanofibers to induce MSC differentiation towards an osteoblastic phenotype[33]. The osteogenic differentiation of MSCs will be evaluated as a function of nanofiber mineral content (*Chapter 5*) as it has previously been shown that hydroxyapatite can induce osteoblastic differentiation[33;34] of stem cells.

Aim 3 focuses on optimizing the interface phase. As fibrocartilage formation has been shown to be induced by compressive loading[35], this aim will incorporate the application of compression to induce MSC-mediated formation of a matrix rich in types I and II collagen and proteoglycans. To this end, a mechanoactive, nanofiber-based collar composed of polylactide-*co*-glycolide (PLGA) will be used to apply compression to MSCs as it contracts when placed in a physiological environment. Compressive loading via a nanofiber collar system has previously been shown to induce upregulation of fibrocartilage-related markers when applied to soft tissue *in vitro*[36]. Similarly, compression has also been shown to enhance MSC chondrogenesis[30;37]. The effect of compression via nanofiber collar contraction on MSCs will be assessed *in vitro* (*Chapter 6*) and the system will be further validated by assessing its ability to induce

fibrocartilage formation on biological grafts *in vivo* (*Chapter 7*). It is hypothesized that the application of compressive loading, via nanofiber scaffold contraction *in situ*, will initiate fibrocartilage formation and enable soft tissue-to-bone interface formation.

Incorporating the outcomes of Aims 1-3, **Aim 4** encompasses the design, characterization and *in vitro* evaluation of a stratified scaffold that incorporates all three optimized phases to form an integrated bone-ligament-bone complex. This multi-phased scaffold will be designed to guide MSC differentiation in order to form distinct-yet-continuous regions of bone, interface and ligament tissues *in vitro*. The effect of scaffold architecture on mechanical properties (*Chapter 8)* will be evaluated and the effect of cell seeding density will be evaluated *in vitro* (*Chapter 8*) within a bioreactor to provide mechanical stimulation under the optimized culture conditions and assess the formation of all three tissue types over time. Subsequently, in **Aim 5,** the system will be evaluated *in vivo* using a well-established rodent model of ACL reconstruction[38] to assess its efficacy for integrative ACL reconstruction (*Chapter 9*) in terms of biomechanical properties and matrix formation, focusing on regenerating a biologically integrated bone-ligament-bone complex.

In summary, in order to tissue engineer an integrative and functional anterior cruciate ligament graft, the studies discussed in this thesis consist of **1)** biomimetic scaffold fabrication and optimization, **2)** incorporation and differentiation of MSC towards interface-relevant phenotypes and **3)** *in vitro* and *in vivo* evaluation of the novel stratified scaffold. The approach outlined in this thesis is innovative as it focuses on the design of a biomimetic, nanofiber-based, integrated bone-ligament-bone construct, and elucidates chemical, mechanical and scaffold design-related parameters that can guide MSC differentiation towards desired tissue types. The impact of these studies extends beyond ligament reconstruction as they will likely yield valuable scaffold design criteria, establish scaffold and culturing-related parameters to induce stem cell differentiation and can readily be applied to the formation of interfaces between soft-to-hard tissues as well as other complex tissues.

1.2 Significance

1.2.1 ACL Injuries and Current Reconstruction Techniques

The anterior cruciate ligament (ACL) spans from the anterior tibial plateau to the medial aspect of the lateral femoral condyle and primarily serves to resist tibial translation and rotational loads[39]. The

ACL is the most frequently injured ligament of the knee, with upwards of 250,000 injuries reported each year and over 100,000 ACL reconstructions performed annually in the United States alone[4;5]. Due to the avascular nature of the tissue as well as the synovial environment within the joint, the ACL does not heal upon injury and requires surgical intervention in the form of the ACL reconstruction procedure[6-8]. This procedure is considered the gold standard for ACL rupture and necessitates the use of a graft to replace the damaged ligament and restore knee stability. Importantly, the graft must be capable of bearing loads almost immediately after surgery and withstand the intensive rehabilitation process that is required to regain mobility. This requirement has become even more critical in light of an increasing number of ACL injuries due to an aging yet active population.

While ACL reconstruction has traditionally utilized autologous bone-patellar tendon-bone (BPTB) grafts, hamstring tendon grafts have become increasingly popular due to the anterior knee pain and patellar tendonitis often associated with BPTB graft harvest[40-42]. Furthermore, hamstring tendon grafts have been shown to withstand higher loads at failure as compared to BPTB grafts with similar stiffness[43]. Despite this, however, clinical studies have shown that ACL reconstructions utilizing hamstring tendon grafts do not result in a complete return to pre-injury activity levels for over 30% of patients[44]. This finding is attributed to the inability of hamstring tendon grafts to fully integrate with bone and an increase in knee laxity due to insufficient graft fixation[45]. In addition, frequent complaints of weakness in knee flexion have been reported following reconstruction with hamstring tendon grafts[46] indicating that the harvest of these grafts may result in donor site morbidity issues, such as a significant decrease in hamstring muscle strength.

Whereas BPTB grafts are secured by bone-to-bone healing, fixation of hamstring tendon grafts requires healing between soft tissue and bone. Studies evaluating tendon graft-to-bone healing have shown that the native insertion site is not reformed following ligament reconstruction with a tendon graft as a fibrovascular scar-tissue interface forms between tendon and bone[12;47]. These fixation sites, therefore, represent the weakest point during the early postoperative healing period and the lack of mechanical stability may lead to graft failure[11;13;47]. As a result, techniques that promote the regeneration of the native interface are critical for long-term graft functionality.

1.2.2 Challenges in ACL Graft Harvest and Fixation

While advances in surgical technique and rehabilitation have resulted in marked improvement in the outcome of ACL reconstruction, the optimal graft for the procedure remains controversial. The BPTB grafts require excising the central third of the patellar tendon and therefore have been associated with a variety of complications including anterior knee pain and patellar tendon rupture as well as patellar and tibial fracture[48]. Hamstring tendon grafts have become a more frequent alternative as they can minimize the incidence of these symptoms but have also been reported to cause hamstring weakness as well as increased joint long-term joint laxity[48]. Further complicating outcomes is that graft harvesting is highly dependent upon the individual surgeon and patient as each graft represents a unique set of technical challenges[49]. Allogenic grafts, which have the potential to address these issues, have been shown to undergo a slower rate of biologic incorporation and decreased long-term stability as compared to autologous grafts[50]. These challenges indicate that alternative grafting solutions that can eliminate the variable graft harvesting process and also enable rapid integration with existing tissue would be ideal for the ACL reconstruction procedure.

In addition to graft selection and composition, a variety of factors have been shown to determine the long-term performance of ACL grafts, including the initial graft tension[51;52], the intraarticular position of the graft[53;54], and graft fixation[13;47]. Graft fixation, specifically, has increasingly gained importance as post-surgical rehabilitation methods require the immediate ability to regain full range of motion, re-establish neuromuscular function and bear weight[12;55]. The BPTB graft is particularly advantageous due to its ability to integrate with the femoral and tibial subchondral bone via the bony ends while also possessing intact fibrocartilaginous insertion sites that can serve as functional transitions between soft tissue and bone. In contrast, semitendinosus grafts require more extensive mechanical fixation within the bone tunnels and, while the physiological range of motion is restored, anatomical graft-to-bone integration is not achieved as the native insertion site is lost during surgery and fibrous tissue forms within the tendon-bone junction [12;47]. Due to this, these fixation sites represent the weakest point during the early postoperative healing period and the lack of mechanical stability often results in graft failure[11;13;47]. As a result, techniques that promote the regeneration of the native interface on soft tissue-based ACL grafts are critical to achieve long-term functionality.

1.2.3 Graft Fixation Strategies

Following ACL reconstruction, tendon-to-bone healing does not result in the regeneration of a native fibrocartilaginous transition between soft tissue and bone. Several groups have studied the process of tendon-to-bone healing in animal models and have shown that a non-mineralized fibrovascular interface forms instead of the native transition[38;56;57]. Initial attempts to improve ligament graft-to-bone fixation have focused on augmenting the surgical graft with mineralized components in order to encourage bone tissue formation[58-64] as the strength of the tendon-to-bone interface has been shown to correlate with the degree of bone in-growth[12]. For example, Tien *et al.* used calcium phosphate cements within the bone tunnels in a rabbit ACL reconstruction study and found that the addition of ceramic helped to improve bone tissue growth and organization[58]. Similarly, Mutsuzaki *et al.* demonstrated that hybridization of calcium phosphate onto tendon grafts in a goat ACL reconstruction model reduced bone tunnel enlargement and resulted in more organized bone tissue formation than compared to the control[64]. These findings indicate that the incorporation of hydroxyapatite is a viable strategy for enhancing tendon-to-bone integration. However, although these methods have improved osteointegration between the ACL graft and the bone tunnel, they do not result in the regeneration of an anatomical fibrocartilage interface between graft and bone which is critical for biological fixation. To this end, engineering a biomimetic scaffold to direct cellular response and support multi-tissue formation is a key component in functional interface formation.

1.2.4 Biochemical Structure of the ACL and ACL Insertion Sites

The anterior cruciate ligament is a dense, collagenous tissue that connects the tibia to the femur and serves to resist rotational and translational loads[39]. It is primarily composed of types I and III collagen along with elastin, fibronectin, decorin, tenascin-C and biglycan, with a specific ratio of type I to type III collagen (approximately 7:1) that serves to distinguish ligaments from tendons[16;65]. It is populated by spindle-shaped fibroblasts that

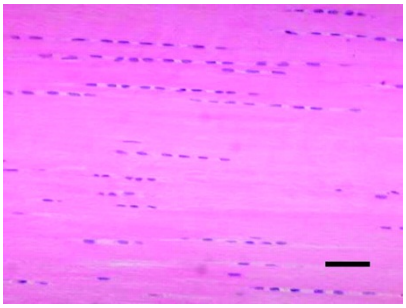

Figure 1.2. Collagen alignment. The ACL consists of dense bundles of collagen fibers populated primarily with spindle-shaped fibroblasts[3].

remain closely attached to the extracellular collagen and follow the ultrastructure of the fibrous matrix[66] (*Fig. 1.2*). Macroscopically, the ACL contains a unique helical organization of collagen fibers that is thought to be essential for ligaments to perform their stabilizing function[20]. In addition, the fibers also have a distinct crimp pattern that allows for creep elongation prior to permanent deformation and ligament damage[39]. Characterization of the ACL has typically divided the ligament into either two functional bundles, the anteromedial bundle and posterolateral bundle, or three bundles, with the addition of an intermediate bundle between the two[67;68]. These bundles experience different patterns of length changes during knee flexion and enable the ligament to withstand the multi-axial stresses and varying tensile strains that accompany joint motion[69].

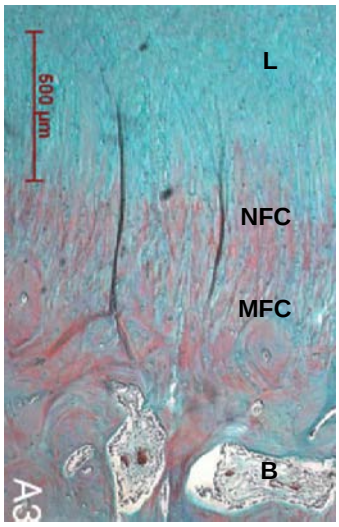

Figure 1.3. The ligament-to-bone interface. The interface consists of a transition from ligament (L) to non-mineralized fibrocartilage (NFC), mineralized fibrocartilage (NFC) and then bone (B)[2].

The native ACL insertion sites consist of direct fibrocartilaginous interfaces which serve to minimize stress concentrations and facilitate load transfer between distinct tissue types[22;23;70-73]. Variations in cell type and matrix composition occur as the tissue transitions from ligament to bone and this interface has been reported to be histologically similar for both the tibial and femoral sites[2]. The interface consists of four distinct, yet continuous, tissue regions: ligament proper, non-mineralized fibrocartilage (NFC), mineralized fibrocartilage (MFC), and bone[2] (*Fig. 1.3*). As previously discussed, the ligament region is primarily composed of aligned types I and III collagen populated by fibroblasts, along with small amounts of proteoglycans[65]. The non-mineralized fibrocartilage region contains ovoid fibrochondrocytes within of a matrix of types I and II collagen present within a proteoglycan-rich matrix[74]. The mineralized fibrocartilage zone is composed of hypertrophic fibrochondrocytes surrounded by a calcified matrix containing types I, II and X collagen[75]. Lastly, the subchondral bone contains osteoblasts, osteocytes, and osteoclasts in a mineralized type I collagen matrix[22]. The specific organization and controlled heterogeneity are believed to be important for minimizing stress concentrations and facilitating the transfer of complex loads between soft and hard tissues[23].

1.2.5 Current Efforts in ACL Tissue Engineering

Synthetic systems have been evaluated for ligament replacement but have met with limited clinical success to date, as none are currently FDA approved. These attempts include grafts manufactured from carbon fiber[76], polytetrafluoroethylene (PTFE)[77;78], polyester[79;80],polypropylene[81], and polyarylamide[82;83]. Among the earliest attempts at a prosthetic ligament were the carbon fiber implant and the composite carbon fiber-polyester braid ligament. While these ligaments provided initial mechanical stability, long term studies reported the generation and migration of carbon wear particles into the joint space following implantation. In addition, frequent incidence of implant stretching and rupture led to poor long-term functional outcomes[80]. Alternatively, polymer-based grafts have also been evaluated, such as the Gore-Tex ACL, fabricated out of expanded PTFE. While the Gore-Tex graft was implanted in more than 18,000 patients worldwide, it ultimately failed due to a lack of tissue ingrowth, likely due to the hydrophobicity of the material, and fatigued in response to normal cyclic loads[84]. In contrast, synthetic ligaments fabricated from polyester (Dacron) resulted in improved outcomes but were still susceptible to failure due to the lack of organized tissue formation over time[79;83].

In response to the previous failures of synthetic ligaments, tissue engineering has arisen as a promising method by which to synthetically regenerate the ACL. Beginning with natural materials, Dunn *et al.* were among the first to evaluate a tissue engineered ACL replacement in vivo[85]. Studies were performed using a type I collagen fiber-based prosthesis with polymethylmethacrylate (PMMA) bone fixation plugs on the ends. While neo-ligamentous tissue formation was reported, the majority of scaffolds ruptured after 20 weeks in a rabbit model[85], demonstrating that this system was insufficient to support long-term knee stability. Chvapil *et al.* similarly evaluated a collagen fiber-based scaffold in vivo using a goat model and, after reporting significant decreases in mechanical properties over the course of 11 months, concluded that a collagen fiber-based scaffold alone was insufficient for ACL replacement[86]. In an effort to bolster the mechanical properties of a collagen-based scaffold, Cai *et al.* investigated a composite collagen-polyvinylalcohol (PVA) scaffold *in vitro* and in vivo in a porcine model[87]. It was reported that scaffolds retained 75% of native ACL strength after 24 weeks in vivo and ligament-like

tissue was formed within the scaffolds. Dunn *et al.* have similarly sought to enhance the mechanical strength of their collagen scaffold system and recently reported on a composite silk-collagen scaffold [88]. While this system has been shown to retain mechanical properties similar to the native ACL after eight weeks implantation in a rabbit model, it has yet to be shown to support tissue growth. Altman *et al.* performed a series of studies focusing on the development of a silk-only anterior cruciate ligament replacement both *in vitro*[21;89-91] and in vivo[17]. Specifically, a silk-fiber based scaffold was designed and several studies were performed to assess the impact of chemical and mechanical stimulation on the differentiation of seeded MSCs. It was demonstrated that individually, soluble chemical factors, such as basic fibroblast growth factor (bFGF), as well as tensile and torsional stimulation could drive matrix elaboration and fibroblastic differentiation of MSCs on the silk scaffold[21]. In addition, it was also reported that chemical and mechanical stimulation could be applied concomitantly and be varied temporally to enhance MSC response[89;91]. The system was implanted in an in vivo goat model with promising results in terms of histological and mechanical outcomes after 12 months[17] and is currently undergoing human clinical trials in Europe[92]. Li *et al.* optimized the architecture of silk ACL scaffold by evaluating wired, braided, and straight fiber scaffold designs[93]. It was reported that the wired system, which consists of twisted silk fibers, exhibited biomechanical properties most similar to the native ACL.

In terms of synthetic approaches, Lin *et al.* evaluated cylindrical scaffolds composed of poly(glycolic acid) (PGA) fibers coated with poly(ε-caprolactone) (PCL) *in vitro* and reported that they supported fibroblast proliferation and matrix deposition[94], demonstrating that polymeric scaffolds are a viable alternative to biopolymer systems. Freeman *et al.* developed a PLLA microfiber system and evaluated the effect of both braiding and twisting on scaffold mechanical properties[95;96], demonstrating that twisting coupled with braiding could increase scaffold ultimate tensile strength and toe-region length. A composite braid-twist scaffold combined with a polyethylene glycol diacrylate (PEDGA) hydrogel was also developed and shown to have mechanical properties similar to the native ACL and also support fibroblast growth[97]. The braid-twist design has also recently been extended to the development of composite collagen and gelatin-based ligament scaffolds[98]. Recently, Barber *et al.* reported on the development of a braided nanofiber-based scaffold for ACL replacement[99]. Scaffold architecture was optimized by varying the number of braided bundles and evaluating mechanical properties, with minimal

differences in toe-region or elastic modulus as a function of braid number. The system was seeded with MSCs and cultured *in vitro*, demonstrating that it supported cell viability and proliferation. Other than scaffold architecture, scaffold composition and fiber diameter also have significant impact on scaffold mechanical properties and compatibility. Surrao *et al.* reported that nanofibrous scaffolds composed of poly(L-lactide-co-D,L-lactide) (PLDLA) develop a crimp pattern similar to that of native ligament collagen when heated in an aqueous environment and support bovine fibroblast proliferation *in vitro*[100]. Vaquette *et al.* reported on two hybrid scaffold systems, a knitted PLGA suture system and a knitted silk suture system, each coated with electrospun PLA/PCL microfibers[101]. These systems had tensile properties similar to native ligaments and resulted in the formation of a ligament-like matrix by rat MSCs *in vitro*. Bach *et al.* performed a preliminary mechanical evaluation of a PVA hydrogel fiber-based scaffold and reported non-linear mechanical characteristics similar to the native ACL[102]. Collectively, these studies have established critical design parameters for ligament engineering but do not address one of the primary drawbacks of current reconstruction techniques: namely, the inability of grafts to integrate with subchondral bone following implantation.

As tissue engineering approaches have advanced, multi-phased designs focused on regenerating bone and the ligament-to-bone interfaces simultaneously with the ligament have been developed. Cooper *et al.* reported on the *in vitro*[103;104] optimization and in vivo[18] evaluation of a braided, α-hydroxyester microfiber-based scaffold for ligament engineering. The architecture and porosity was optimized *in vitro* using a braiding technique to recapitulate the native ligament mechanical properties and incorporated a multi-phased design consisting of a denser fiber arrangement at each end of the construct for bone formation[103]. Scaffold composition was optimized based on *in vitro* degradation and cell response with poly(L-lactide) (PLLA) selected based on its ability to maintain structural integrity over the eight-week culture duration[104]. Subsequently, the optimized scaffold was evaluated in vivo using a rabbit ACL reconstruction model. It was demonstrated that cell seeding of the implanted scaffold resulted in a marked improvement in functional outcomes but scaffolds in both groups ruptured after 12 weeks of implantation[18]. Kimura *et al.* evaluated a multi-phased system composed of braided PLLA wrapped with collagen for ligament formation and a gelatin hydrogel containing bFGF within the bone tunnels[105]. The multi-phased design resulted in distinct regions of bone and ligament formation as well as enhanced

mechanical properties compared to single-phase controls. Goh *et al.* performed a series of studies to optimize a knitted silk scaffold which was combined with a microporous silk sponge[106;107]. This bi-phasic system was designed to mimic the ECM of native tissue and provide sufficient mechanical strength for ligament replacement. The scaffold was implanted in vivo using a rabbit model[108] as well as a pig model[109]. After 24-weeks in each model, substantial ligament-like tissue was formed on the scaffold and an insertion-like structure was regenerated between scaffold and bone. In addition, several *in vitro* studies were performed to further optimize the scaffold, including the use of silk cables to increase tensile strength[110], the incorporation of bFGF-releasing PLGA[111] and RADA16 peptide[112] nanofibers to enhance cell biosynthesis, and the addition of a silk-based aligned nanofiber topography to direct cell orientation and matrix production[113].

In contrast with these scaffold-based approaches, Ma *et al.* reported on the *in vitro*[114] and in vivo[115] evaluation of a scaffold-less system for bone-ligament-bone regeneration. The system consisted of self-assembled bone constructs co-cultured with a ligament monolayer rolled between them to form a bone-ligament-bone replacement. After six months of implantation using a sheep model of ACL reconstruction, the constructs increased in cross section, native bone integration, and functional insertion-like tissue, though with a sample size of only three sheep. Using a similar approach, Paxton *et al.* developed an *in vitro* model of bone-ligament-bone using calcium phosphate brushite-based anchors connected to a fibrin gel-based ligament sinew[116;117]. It was reported that fibroblasts seeded within the sinew produced an interface between the anchors and gel that resembled the in vivo tidemark at the ligament-to-bone insertion[116]. These studies represent important advancements in the engineering of the ligament-to-bone interface but do not represent a functional ligament construct.

While the aforementioned studies establish the ability of scaffold design as well as chemical and mechanical stimulation strategies to direct ligament tissue regeneration, the systems reviewed here do not facilitate the formation of the native ligament-to-bone interface. This structure is critical to accomplish biological fixation of the regenerated ligament tissue and will be required for long-term clinical success. To this end, Spalazzi *et al.* reported on the development of a multi-phased scaffold for ligament-to-bone interface tissue regeneration. Utilizing a tri-phasic design to mimic the ligament, fibrocartilage and bone regions of the native transition, phase-specific matrix heterogeneity was demonstrated *in vitro* by co-

culturing osteoblasts and fibroblasts on the bone and ligament phases, respectively[118]. In addition, using a subcutaneous rodent model, it was demonstrated that fibrocartilage-like tissue could be regenerated in vivo by tri-culturing primary cells from each tissue type on each of the phases[119]. These studies demonstrate the ability to use stratified scaffold design for multi-tissue regeneration of the ACL-to-bone interface and this thesis aims to extend upon this work by engineering a system for complete bone-ligament-bone regeneration.

1.2.6 Mesenchymal Stem Cells

In addition to scaffold design, cell source is a critical parameter for the clinical translation of tissue engineered strategies. While primary cell sources have largely been used to test the feasibility of engineered constructs, adult stem cells are considered an ideal cell source due to their versatility and clinical translation potential. Mesenchymal stem cells (MSC), in particular, are considered to be advantageous for musculoskeletal tissue engineering applications[26;120]. These cells, which reside within the bone marrow, can be routinely harvested via conventional biopsy techniques and are able to maintain their differentiation capabilities even after long term *in vitro* culture[26]. Moreover, differentiation of MSCs has been shown to be sensitive to chemical, mechanical and structural cues as well as combinations of these stimuli[26;91;121]. For the purpose of ligament tissue engineering, it has been established that MSCs are capable of differentiating into the primary cell types found within the ligament (fibroblasts)[27], bone (osteoblasts)[26], and ligament-to-bone interface (chondrocytes)[26]. More specifically, Altman *et al.* demonstrated that fibroblastic differentiation can be stimulated using tensile and torsional stimulation[27] as well as fibrogenic growth factors[28]. Osteoblastic differentiation has been guided using osteogenic induction medium containing dexamethasone[26], osteointegrative ceramics such as hydroxyapatite[34] and tricalcium phosphate[122] as well as shear stress[123]. Lastly, chondrogenic differentiation has been induced with chondrogenic induction factors including transforming growth factor-beta 3 (TGF-β3)[26] and compressive stimuli[30].

1.3 Summary

Despite advances in surgical techniques, the failure rates of biological grafts and donor site morbidity issues related to conventional graft harvesting techniques remain a significant clinical problem. In addition, the native ligament-to-bone interface is not re-established following ACL reconstruction and is critical for long term knee stability and functionality. Therefore, a significant demand exists for alternative grafting solutions that do not require additional surgery and can regenerate the native ACL-to-bone interface to promote biological fixation of the implanted ACL graft. In order to tissue engineer an integrative and functional anterior cruciate ligament graft, the studies outlined in this thesis consist of **1)** biomimetic scaffold fabrication and optimization, **2)** incorporation and differentiation of MSC towards relevant phenotypes and **3)** *in vitro* and *in vivo* evaluation of the novel stratified scaffold. A ligament (*Chapters 2-4*), bone (*Chapter 5*) and interface (*Chapters 6-7*) phase will be individually optimized and a scaffold incorporating all the phases will be fabricated and evaluated *in vitro* (*Chapter 8*). Subsequently, the optimized scaffold will be implanted *in vivo* (*Chapter 9*) to evaluate its functional and integrative potential. The findings of these studies will yield valuable scaffold design criteria, establish scaffold and culturing-related parameters to induce stem cell differentiation and, further, can readily be applied to the formation of interfaces between other unmineralized-to-mineralized tissues.

CHAPTER 2: LIGAMENT PHASE: THE EFFECT OF NANOFIBER ORGANIZATION AND MECHANICAL STIMULATION ON FIBROBLASTIC DIFFERENTIATION OF MESENCHYMAL STEM CELLS

2.1 Introduction

This thesis begins by focusing on the ligament phase of the ACL scaffold in order to determine the cues necessary to direct fibroblastic differentiation of mesenchymal stem cells. Stem cells have been shown to respond to both physical and chemical cues in order to guide differentiation. In particular, this study will evaluate the effects of tensile mechanical stimulation and nanofiber organization on the fibroblastic differentiation of MSCs. The findings from this study will provide the physical parameters necessary to direct differentiation of MSCs into a ligament fibroblast phenotype on the ligament phase of the scaffold.

2.1.1 Background and Motivation

An emerging trend in biomaterial and scaffold design has been the incorporation of strategic biomimicry in order to more effectively guide MSC differentiation and accelerate the healing process. Specifically, nanofibers been investigated for the regeneration of connective tissues, such as bone[124;125], meniscus[126], intervertebral disk[127], cartilage[128], tendons and ligaments[24;129;130], as they are biomimetic and can be fabricated to replicate the structural organization of the collagenous matrix that dominates these tissues. Moreover, nano-scale fibers have been shown to direct cell attachment and matrix deposition[24;99;106;131] and represent an ideal system to model the collagenous matrices present within native tissue structures. These fibers exhibit high aspect ratio, surface area, permeability and porosity, making them advantageous for tissue engineering applications. Furthermore, they can be fabricated from a variety of polymers, both natural and synthetic, with tunable fiber diameter and matrix alignment[132;133].

Given their similarity to the native extracellular matrix (ECM), nanofibers have been used to promote MSC response and differentiation. For example, Ma *et al.* studied the effect of poly(L-lactic) acid (PLLA) nanofiber alignment on the osteogenic differentiation of rat MSC in conjunction with osteogenic medium[134]. It was found that total calcium content was the highest on aligned nanofibers albeit no difference in cell proliferation or osteogenic markers was observed between cells cultured on aligned and unaligned nanofibers. Similarly, Baker *et al.* investigated the impact of poly(ε-caprolactone) (PCL) nanofiber alignment on bovine MSC fibrochondrogenesis when coupled with chondrogenic induction

medium[126]. It was reported that a greater increase in construct mechanical properties was measured when MSCs were cultured on aligned nanofibers in contrast to cells on unaligned controls after 10 weeks. Notably, the majority of these studies have employed chemical factors along with scaffold cues, making it difficult to decouple the effects of these distinct stimuli[135]. Recently, Schofer *et al.* reported that culturing MSCs on type I collagen or PLLA nanofibers modulated cell proliferation and expression of osteogenic markers, even in the absence of osteogenic induction medium[136]. Similarly, Jiang *et al.* reported that culture on PCL nanofibers upregulated the expression of neural markers by MSCs, as compared to monolayer controls[137].

In addition to matrix-guided cues, mechanical stimulation has been found to direct MSC differentiation[27;123;138]. For example, dynamic tensile (10%) and torsional (25%) strains applied at 1 cycle/minute upregulated types I and III collagen expression by human MSCs in collagen gels and direct these cells towards a fibroblastic phenotype without the use of chemical induction medium[27]. In addition, Terranciano *et al.* demonstrated that 10% compressive strain applied at a frequency of 1 Hz to MSC-encapsulated poly(ethylene glycol)-diacrylate hydrogels resulted in the upregulation of cartilaginous markers and greater matrix production when combined with chemical stimulation[138]. Recently, Grayson *et al.* also reported that osteogenic differentiation and mineral production by MSCs correlated to the intensity and pattern of shear flow applied by a custom bioreactor when coupled with osteogenic induction medium[123].

2.1.2 Objectives

Collectively, the aforementioned studies suggest that mechanical loading and nanofiber architecture are important in guiding MSC differentiation. Therefore, the purpose of this study is to investigate the role of nanofiber matrix alignment and mechanical stimulation on MSC differentiation towards a fibroblastic phenotype for the ligament phase of the synthetic ACL graft. To this end, this study will evaluate the fibroblastic differentiation of human MSCs on nanofibers as a function of fiber alignment and mechanical stimulation. It is hypothesized that tensile stimulation combined with a biomimetic nano-scale substrate will direct MSC differentiation towards a ligament fibroblast-like phenotype and the subsequent production of a ligament-like matrix. To test this hypothesis, the attachment, proliferation,

biosynthesis and differentiation of MSCs stimulated by dynamic tensile loading will be evaluated on aligned and unaligned nanofibers over a four-week culturing period. It is expected that the results of this study will elucidate fundamental substrate and culture environment-related rules to systematically control MSC differentiation and determine if loading or matrix alignment is a more dominant determinant of cell behavior, without confounding effects from concurrent chemical stimulation. These outcomes of this study will establish the nanofiber alignment and mechanical stimulation parameters for the ligament phase of the synthetic ACL graft.

2.2 Materials and Methods

2.2.1 Nanofiber Mesh Fabrication

Unaligned and aligned nanofiber meshes composed of poly(lactide-co-glycolide) (PLGA, 85:15, Mw = 123.6 kDa; Lakeshore Biomaterials, Birmingham, AL) were produced via electrospinning[24;139]. Briefly, 35% PLGA (v/v) was solubilized in 55% N,N-dimethylformamide (Sigma-Aldrich, St. Louis, MO) and 10% ethyl alcohol. The solution was loaded into a syringe with an 18.5-gauge stainless steel blunt tip needle and electrospun at 8-10kV and 1 mL/hour using a custom electrospinning device. Polymer was dispensed via a syringe pump (Harvard Apparatus, Holliston, MA; 1 ml/hr) and unaligned meshes were fabricated using a static collector plate whereas the aligned meshes were produced by electrospinning onto rotating mandrel (20 m/s). With the exception of fiber alignment, the resultant meshes were identical with respect to fiber diameter, pore size and porosity[24].

2.2.2 Cells and Cell Culture

Human mesenchymal stem cells (MSC) were obtained commercially (Lonza, Walkersville, MD) and maintained in culture with fully supplemented (FS) DMEM containing 10% FBS (stem cell certified, Atlanta Biologicals, Atlanta, GA), 1% penicillin-streptomycin, 1% non-essential amino acids, 0.1% amphotericin B and 0.1% gentamicin. Cells were cultured to 80% confluence and then passaged using 0.25% trypsin/1 mM ethylenediaminetetraacetate (EDTA) and re-plated at a density of $5x10^3$ cells/cm^2. Cells from passage two were seeded on meshes for all studies. Prior to cell seeding, the stemness of these cells was ascertained using flow cytometry (BD FACSCalibur, Franklin Lakes, NJ) to confirm

characteristic MSC surface markers, with cells determined to be positive for markers CD29, CD71, CD106 (BD Biosciences) and negative for markers CD14, CD31 and CD34 (BD Biosciences).

Meshes were secured in a custom high-throughput bioreactor to apply uniaxial tensile strain. Briefly, electrospun meshes (5x6cm) were excised after fabrication and subsequently sterilized via ultraviolet irradiation (15minutes/side). meshes were secured in loading cartridges via teflon clamps, sectioned into 5 cm x 1 cm strips and pre-incubated in FS medium at 37ºC and 5% carbon dioxide for 16 hours. Cells were seeded on the meshes at a density of $3x10^4$ cells/cm2 and allowed to attach for 15 min before the addition of FS DMEM. Following an initial five-day period of static culture to allow for matrix elaboration, the effects of a loading physiologically relevant regimen[140], similar to previous studies[141], consisting of 1% strain at 1 Hz for 90 minutes twice daily (10.5 hours rest between cycles) on MSC morphology, attachment, proliferation, gene expression and matrix production were determined after 1, 7, 14 and 28 days of mechanical stimulation. Aligned and unaligned meshes cultured in identical bioreactor cartridges without loading served as controls.

2.2.3 Cell Attachment and Alignment

Cell attachment and alignment were imaged via scanning electron microscopy (SEM, 1.0kV, Hitachi S-4700, Pleasanton, CA). Following fixation, samples were dehydrated in an ethanol series and then sputter-coated with gold-palladium to reduce charging effects.

Cell viability and morphology (n=3/group) were evaluated using Live/Dead staining (Invitrogen, Carlsbad, CA) following the manufacturer's suggested protocol. The samples were imaged under confocal microscopy (Leica Microsystems TCS-SP5, Bannockburn, IL) at excitation wavelengths of 488nm and 594nm. Cell penetration was evaluated by taking a z-series of confocal images over a depth of 20μm, equivalent to 15 to 20 layers of nanofibers.

The effects of mechanical loading and nanofiber architecture on MSC alignment were quantified following the methods of Costa *et al.* Briefly, confocal images (n=3/group) of cell-seeded meshes were analyzed using circular statistics software customized for evaluating fiber alignment (Fiber 3). The circular statistics parameters determined included mean vector angle, which represents the average fiber alignment in the matrix ($-90º < \theta < 90º$; 0º indicates horizontal orientation); mean vector length, which

ranges from zero for a randomly distributed sample to unity for an aligned sample ($0 < r < 1$); and angular deviation, which characterizes the dispersion of the non-Gaussian angle distribution of the nanofibers (0-40.5º). Specifically, an angular deviation of 0º represents an aligned sample, and 40.5º is indicative of random distribution.

2.2.4 Cell Proliferation

Total DNA content was measured using the PicoGreen dsDNA assay (Invitrogen). At each time point, the samples (n=5/group) were homogenized in 0.1% Triton-X (Sigma-Aldrich) and subjected to 20 seconds of ultrasonication at 5W. Fluorescence was measured using a microplate reader (Tecan, Research Triangle Park, NC) at an excitation wavelength of 485 nm and an emission wavelength of 535 nm. A standard curve was derived and used to correlate DNA concentration to fluorescence intensity, and cell number was determined based on a conversion factor of 8pg DNA/cell[104].

2.2.5 Matrix Deposition

Total collagen content per sample (n=5/group) was calculated using the hydroxyproline assay[142]. Briefly, the samples were first desiccated for 24 hours and then digested for 16 hours at 65°C with papain (600 µg protein/ml) in 0.1M sodium acetate (Sigma), 10 mM cysteine HCl (Sigma), and 50 mM ethylenediaminetetraacetate (Sigma). A 40 µl aliquot of the digest was hydrolyzed with 10 µl 10 M sodium hydroxide and autoclaved for 25 minutes. The hydrolyzate was then oxidized by a buffered chloramine-T reagent for 25 minutes before the addition of Ehrlich's reagent. Sample absorbance was measured at 550nm (Tecan), and the collagen content was obtained by interpolation along a standard curve of bovine type I collagen (Sigma).

Collagen distribution was also visualized using picrosirius red staining of frozen sections (n=2/group). Briefly, after fixation, samples were embedded in 5% polyvinyl alcohol (PVA, Sigma-Aldrich) and 7-micrometer thick sections (spanning the depth and width of the mesh) were obtained using a cryostat (Hacker-Bright OTF model, Hacker Instruments and Industries, Winnsboro, SC). Collagen distribution was visualized with picrosirius red staining under light microscopy (Axiovert 25, Zeiss).

Elaboration of type I and type III collagen (n=3 samples/group) on nanofibers was evaluated using immunohistochemistry. After rinsing with PBS, samples were fixed with 10% neutral buffered formalin for 24 hours. Monoclonal antibodies for type I collagen (1:20 dilution in serum-free Protein Block, Dako Cytomation, Carpinteria, CA) and type III collagen (1:100 dilution in serum-free Protein Block) were obtained from Abcam (Cambridge, MA) and Sigma-Aldrich, respectively. Samples were treated with 1% hyaluronidase for 30 min at 37ºC and incubated with primary antibody overnight. After a PBS wash, Alexa Fluor 488-conjugated secondary antibody (Invitrogen) was added and incubated for 1 hour. Propidum iodide (Invitrogen) was used as a nuclear counterstain. Images were obtained using a confocal microscope (Leica TCS SP5) with 488 nm and 594 nm excitation wavelengths.

2.2.6 Fibroblastic Markers

Gene expression (n=5/group) was measured using quantitative real-time reverse transcriptase polymerase chain reaction (qPCR). Expression of fibroblastic markers type I collagen, type III collagen, fibronectin, tenascin-C, tenomodulin and scleraxis as well as integrins α2, αV, α5 and β1 was determined with GAPDH as the house-keeping gene using custom-designed primers as follows:

Gene	***Sense***	***Anti-Sense***
GAPDH	5'- GGCGATGCTGGCGCTGAGTA-3'	5'-ATCCACAGTCTTCTGGGTGG-3'
Collagen I	5'-TGGTCCACTTGCTTGAAGAC-3'	5'-ACAGATTTGGGAAGGAGTGG-3'
Collagen III	5'-GGCTACTTCTCGCTCTGCTT-3'	5'-CATATTTGGCATGGTTCTGG-3'
Fibronectin	5'-TTGAACCAACCTACGGATGA-3'	5'-AAATGACCACTTCCAAAGCC-3'
Tenascin-C	5'-TGCCCATTACAGGAGGTACA-3'	5'-CACTTTCCTCAAAGCCCTTC-3'
Scleraxis	5'-CAGCGGCACACGGCGAAC-3'	5'-CGTTGCCCAGGTGCGAGATG-3'
Tenodmoulin	5'-TTTGAGGAGGAGGGAGAAGA-3'	5'-TTCCTCACTTGCTTGTCTGG-3'
α2	5'-CAGAATTTGGAACGGGACTT-3'	5'- CAGGTAGGTCTGCTGGTTCA-3'
αV	5'-GATGGACCAATGAACTGCAC-3'	5'-TTGGCAGACAATCTTCAAGC-3'
α5	5'-GTGGCCTTCGGTTTACAGTC-3'	5'-AATAGCACTGCCTCAGGCTT-3'
β1	5'-GAGGAATACAGCCTGTGGGT-3'	5'-ATTGCAGGATTCAGGGTTTC-3'

Total RNA was isolated using the TRIzol reagent (Invitrogen, Carlsbad, CA) extraction method. The isolated RNA was reverse-transcribed into cDNA via the SuperScript III First-Strand Synthesis System (Invitrogen) following the manufacturer's suggested protocol. The cDNA product was amplified and quantified through real-time PCR using iQ SYBR Green Supermix (BioRad, Hercules, CA). All reactions were run for 50 cycles using the iCycler iQ Real-Time PCR Detection System (BioRad). Normalized expression levels reported were calculated based on difference between threshold cycles, namely, the difference in threshold cycle values between the gene of interest and the housekeeping gene GAPDH.

2.2.7 Statistical Analysis

Results are presented in the form of mean ± standard deviation, with n equal to the number of samples per group. Two-way ANOVA was used to determine the effects of loading and time on cell alignment, proliferation, gene expression and matrix deposition. The Tukey-Kramer post-hoc test was used for all pair-wise comparisons and significance was attained at $p<0.05$. Statistical analyses were performed with JMP IN (4.0.4, SAS Institute, Inc., Cary, NC).

2.3 Results

2.3.1 Cell Attachment and Alignment

The MSCs were cultured on aligned and unaligned nanofiber meshes in a custom designed loading bioreactor (*Fig. 2.1*). It was observed that cells remained viable and proliferated on both aligned and unaligned nanofibers. On unaligned nanofibers, a significantly greater number of cells were measured after 28 days of loading (*Fig. 2.2*). Similarly, significantly more cells were found on loaded aligned nanofibers by day 7, with cell number plateauing after 28 days. In terms of cell attachment, on unaligned nanofibers, as expected, random orientation of cells was observed without loading and this cell morphology was maintained over time. Interestingly, upon loading, the cells adopted a markedly different morphology and aligned in the direction of applied strain by day 28. In contrast, a characteristic elongated fibroblast-like morphology was maintained on aligned nanofibers with no change observed due to either mechanical loading or culture duration.

To further investigate these apparent differences between groups, cell alignment on loaded and unloaded nanofibers was quantified using circular statistical analysis, focusing on changes in mean vector angle (MVA), angular deviation (AD) and mean vector length (MVL)[24;143] (*Fig. 2.3*). In general, values for the MVL range from 0 to 1, with the upper bound indicating greater horizontal alignment whereas the MVA ($-90° < \theta < 90°$) represents the angle of cells with respect to the horizontal axis, with a lower angle indicating horizontal alignment. Values for AD characterize the dispersion of the non-Gaussian angle of distribution (0-40.5°) with 0° representing horizontal alignment and 40.5° indicating random distribution. In this study, it was observed that on unaligned nanofibers, loading resulted in a significantly greater MVL (loaded: 0.94; unloaded: 0.33) and a significant decrease in AD after 28 days of culture as well as a distinct cell alignment profile ($p<0.05$), represented as a histogram of cell orientation measured in each group (*Fig. 2.3*), all indicating a greater degree of horizontal alignment with respect to the unloaded group. In contrast, on aligned nanofibers, no difference in the MVL (0.91 vs. 0.93; unloaded vs. loaded) or AD (11.74° vs. 9.21°; unloaded vs. loaded) was found between the loaded and unloaded group.

2.3.2 Matrix Deposition

In terms of collagen production (*Fig. 2.4*), on both aligned and unaligned nanofibers, a significant increase in total collagen content was found after 28 days of loading. Further analysis revealed that on a per-cell basis, mechanical loading upregulated cellular biosynthesis on both unaligned and aligned nanofibers, with significantly greater collagen production per-cell measured for both groups after 28 days of loading when compared to unloaded controls. Moreover, immunohistochemistry revealed that, independent of loading, the matrix formed on unaligned nanofibers consisted primarily of type I collagen. Similarly, a predominantly type I collagen matrix was seen on aligned nanofibers in the absence of loading. Interestingly, upon the application of loading, a matrix of both types I and III collagen was produced by the cells only on aligned nanofibers while the matrix deposited on the unaligned nanofibers is still predominantly of type I collagen.

2.3.3 Cell Differentiation

To further ascertain MSC differentiation, markers characteristic of the ligament fibroblast phenotype, including types I and III collagen, fibronectin, tenascin-C, scleraxis and tenomodulin, were assessed using quantitative real-time RT-PCR. On unaligned nanofibers, a mean increase in type I collagen was observed after seven days of loading and expression remained elevated after 28 days. The expression of type III collagen increased (6.1±1.0 fold higher with respect to the unloaded control) after seven days of loading but returned to control levels by day 28. Fibronectin expression was upregulated after 14 days (2.0±1.2 fold increase relative to unloaded control) and remained upregulated after 28 days in the loaded group. Notably, key fibroblastic markers tenascin-C, scleraxis and tenomodulin remained at basal level and were not upregulated by loading over time on unaligned nanofibers (*Fig. 2.5*). In contrast, on aligned nanofibers, type I collagen expression remained statistically similar both between groups and over time, although a three-fold increase in mean expression was observed after 28 days of loading compared to the unloaded group. Expression of type III collagen (4.1±1.1 fold increase relative to unloaded control), fibronectin (5.1±1.2 fold increase relative to unloaded control) and tenascin-C (4.3±1.0 fold increase relative to unloaded control) was significantly upregulated after 14 days of mechanical stimulation, with the higher expression level maintained after 28 days of loading. (*Fig. 2.5*). While no change in tenomodulin expression was observed over time on aligned nanofibers regardless of loading, scleraxis was downregulated after 28 days of static culture whereas its expression was maintained over time in the loaded group (*Fig. 2.5*). In addition, phenotype specificity was evaluated by measuring the expression of various osteogenic (Runx-2, osteocalcin) and chondrogenic markers (sox9, type II collagen). No upregulation of any of these markers was observed over time or with loading on either unaligned or aligned nanofibers.

2.3.4 Integrin Expression

Next, to better understand the mechanisms behind MSC mechanotransduction and the observed cell-matrix interactions, the expression of key integrins (α2, αV, α5, β1) was assessed as these surface-membrane receptors have been shown to mediate cell response to physical stimulation as well as matrix alignment[24;144-148]. It was observed that on unaligned nanofibers, both α2 and β1 were upregulated

after 14 days of loading and expression levels were maintained thereafter, while the expression of α5 became significantly higher after seven days and plateaued thereafter (*Fig. 2.6*). On the aligned nanofibers, similar to the response on unaligned nanofibers, αV expression did not change in response to loading. However, distinct expression profiles, as compared to the unloaded control, were measured with integrin subunits α2, α5 and β1 being upregulated after 14 days of culture, and expression levels were maintained after 28 days on the loaded nanofibers($p<0.05$, *Fig. 2.6*).

2.4 Discussion

The objectives of this study are to investigate the role of nanofiber matrix alignment and mechanical stimulation on MSC differentiation, focusing on elucidating the relative contribution of each parameter as well as their interaction. It is shown that fibroblastic differentiation of MSCs is only possible when cultured on aligned nanofibers and co-stimulated with mechanical loading. In contrast, when loading was applied to MSCs cultured on unaligned nanofibers, while cells adapted their morphology to align in the direction of loading, they fail to undergo fibroblastic differentiation and do not deposit a ligament-like matrix. The findings of this study provide the first evidence that there is an interactive effect between matrix alignment and mechanical loading, and co-stimulation is required for the induction of MSC differentiation into fibroblasts.

In terms of cell alignment and morphology, it was observed in this study that cells aligned in the direction of strain on the unaligned nanofibers whereas no change in alignment occurred over time on the aligned nanofibers in response to tensile stimulation. These findings suggest that the underlying nanofiber organization is the primary determinant of cellular alignment and that contact guidance drives long-term cellular organization. However, similar to what has been previously reported for fibroblasts on non-patterned substrates[149;150], cell alignment can also be modulated by exogenous factors such as the direction of applied strain and oriented in a more physiologically relevant arrangement.

In evaluating cell proliferation, the significant increase in cell number on unaligned nanofibers in response to loading, despite similar numbers of initially seeded cells on both the unloaded and loaded groups, may be due to a greater cell density that could be achieved with linear cell alignment in the direction of applied strain, as opposed to the random fiber-directed adhesion of cells on control

nanofibers. Though alternatively, mechanical loading may also enhance nutrient diffusion through the culture medium and promote cell survival over the unloaded groups. Notably, however, a consistently greater number of cells were measured on aligned nanofibers at all time points after day 1 as compared to unaligned nanofibers, supporting the implication that linear matrix alignment may allow for greater cell density on nanofibers.

Total matrix deposition by MSCs was found to increase significantly with tensile stimulation on both aligned and unaligned nanofiber nanofibers. These observations corroborate previous reports of elevated MSC biosynthesis, such as in studies performed by Baker *et al.* who applied both tensile and chemical stimulation to MSCs cultured on PCL nanofibers[151] as well as for human fibroblasts cultured on polyurethane nanofibers[152] and subjected to tensile strain. However, in contrast to these reports, the results of this study reveal that mechanical stimulation alone can enhance MSC matrix deposition in the absence of growth factors as per-cell collagen production was enhanced on both aligned and unaligned nanofibers after 28 days of loading.

In addition to enhanced matrix production, the production of type III collagen by MSCs in response to tensile strain only occurs on aligned nanofibers. The production of type III collagen is essential for the fibroblastic differentiation of cells as this protein represents approximately 12% (by dry weight) of the native ligament matrix[65] and provides tendons and ligaments with their strength and elasticity by forming heterotypic fibers incorporating type I collagen[153] while also playing a critical role in the healing processes of connective tissues[66]. These results indicate that only loading in conjunction with nanofiber alignment can stimulate the production of type III collagen. In short, for MSC to differentiate towards the ligament fibroblast phenotype, it is observed that a combination of physiologically-relevant cell-material interactions and mechanical stimulation is required.

Analysis of MSC differentiation revealed that several key fibroblastic markers were upregulated only with the combination of nanofiber alignment and dynamic tensile loading. On unaligned nanofibers, an increase in type III collagen expression was observed after seven days of loading, accompanied by an increase in fibronectin expression after 14 days. Though type III collagen deposition was not found on unaligned nanofibers, the increase in expression may arise due to the similarity of the unaligned matrix to the disorganized collagen matrix of scar tissue, as five- to ten-fold increases in type III collagen content

have been reported at the Achilles' tendon rupture sites during healing[154]. The changes in gene expression on aligned nanofibers are similar to those reported by Altman *et al.* who evaluated the effect of tensile strain and torsion on MSCs in type I collagen gels[27] and on silk fibers[91], reporting a similar upregulation of types I and III collagen as well as tenascin-C. Upregulation of both types I and III collagen expression is in agreement with the increase in total collagen deposition as well as the production of type III collagen by MSCs on aligned nanofibers in response to loading. Hsieh *et al.* also observed elevated type I collagen expression in fibroblasts cultured on silicone elastomer membranes and subjected to tensile strain[155]. The results of this study, however, represent a comprehensive characterization of fibroblastic differentiation of MSCs as a function of scaffold architecture and mechanical stimulation. Additionally, as no specific marker serves to distinguish ligament fibroblasts from other fibroblasts present in connective tissues, the type I:III collagen ratio is an important indicator of cell phenotype as it varies significantly between ligaments (~7:1) and tendons (~20:1)[65] and is substantially decreased in scar tissue (~1:1)[156]. In this study, cells on unaligned nanofibers demonstrated a type I:III collagen ratio of 0.51±1.26 without loading and 1.03±0.99 with loading. In contrast, cells on aligned nanofibers measured a type I:III collagen expression ratio of 8.35±2.12 after 28 days of loading, as opposed to approximately 2.07±1.11 for the unloaded group, thereby suggesting that cells assumed a ligament fibroblast-like phenotype in response to mechanical stimulation only on the aligned nanofibers.

Furthermore, scleraxis, a transcription factor that has been shown to be critical for tendon and ligament formation during development in both avian and murine models[157;158], was maintained on nanofibers subjected to mechanical stimulation while decreasing in unloaded scaffolds, a trend similar to that reported by Kuo *et al.* using a collagen gel system seeded with human MSCs[159]. However, tenomodulin, a transmembrane glycoprotein induced by scleraxis and implicated in collagen organization[160;161], was not upregulated with stimulation in this study. Tenomodulin, a late marker of tendon and ligament formation, is regulated by scleraxis[162] and will likely be upregulated in long term culture.

In addition, mechanical stimulation, on both substrates, leads to significant changes in integrin expression, indicating that these receptors mediate both cell-matrix interaction and mechanotransduction. The upregulation of α2, α5 and β1 on both unaligned and aligned nanofibers, though with distinct

temporal patterns, in response to loading indicates that these integrins play a role in MSC mechanotransduction. Integrin upregulation has also been observed for MSCs cultured on silk fibers and subjected to dynamic torsion, whereby a significant increase in α2 expression was found albeit without a concurrent upregulation of β1[89]. The elevated expression of these integrins is likely in response to mechanical loading, ensuring that there are sufficient numbers of surface receptors to translate the physical stimulation. Interestingly, a similar enhancement of integrin expression was reported for differentiated cells in response to nanofiber alignment. Moffat *et al.* observed α2 upregulation by tendon fibroblasts when cultured on aligned versus unaligned PLGA nanofibers[24] and it was proposed that fibroblasts may signal recognition of fiber alignment with upregulated integrin expression. Therefore, the biomimetic aligned nanofibers, which resembles the native collagenous ECM, may also contribute to the observed increase in α2 expression as the β1 subunit complexes with α2 to bind to collagen[163]. As such, no upregulation in α2 expression was observed for MSCs on unaligned or aligned nanofibers in the absence of loading, indicating that for MSCs, upregulation of such a key collagen-binding molecule is linked primarily to mechanical stimulation.

Upregulation of the α5 and β1 subunits has also been associated with mechanotransduction by Hannafin *et al.* who observed α5 and β1 subunit upregulation by canine ligament fibroblasts cultured in tethered and strained collagen gels[149;164]. Additionally, the α5 integrin complexes with β1 to bind to fibronectin[165] and has been demonstrated to be upregulated by MSCs upon binding to fibronectin functionalized surfaces[166]. The concomitant increase in fibronectin expression observed here may be coupled with the upregulation of these integrins as fibronectin plays a central role in cell adhesion and also can influence a variety of downstream pathways. For example, binding to the α5β1 receptor has been shown to activate the Shc pathway which promotes cell proliferation and is potentially responsible for the observed increase in cell number on meshes subjected to mechanical stimulation this study[167]. In addition, Song *et al.* reported that rat MSC proliferation on silicone elastomers was enhanced with mechanical loading and postulated that such a response may be due to activation of the focal adhesion kinase (FAK) pathway via integrin signaling[168]. The downstream effects of these cell-matrix interactions will be investigated in future studies.

In addition to systematically elucidating the role of scaffold architecture and mechanical stimulation in stem cell differentiation, the findings of this study have broad implications for scar-less wound healing and guided soft tissue repair. All three of the integrin subunits upregulated in this study have been implicated in ligament and tendon healing and published studies have shown that α5, αV and β1 integrin production increases in injured rabbit medial collateral ligaments (MCL)[165]. Moreover, mechanical stimulation has been demonstrated to accelerate the wound healing process, such as that of skin wounds using a rabbit model[169]. The α2β1 integrin, specifically, is known to be utilized by cells to contract collagen fibrils during matrix reorganization and wound healing[170], and the upregulation of these integrins suggest a nanofiber-driven matrix remodeling response by these stem cells. In addition, by modulating alignment, the nanofiber matrix can be used to model both the healthy tissue (aligned) and a disorganized wound site (unaligned) during repair. Specifically, the ability of mechanical loading to 'rescue' cell alignment towards a more physiologically relevant organization is significant as these observations demonstrate that controlled physical stimulation may be a more potent driver of MSC differentiation than substrate morphology. However, the lack of fibroblastic differentiation by MSCs on the unaligned substrate and the statically cultured aligned substrate indicates that neither mechanical loading nor substrate alignment alone is sufficient to drive MSCs towards a fibroblastic phenotype, thereby demonstrating that both biomimetic architecture and physiologic mechanical stimulation are needed to control MSC differentiation and guide tissue healing. Clinically, it is envisioned that a strategy of concurrent stimulation with a biomimetic ECM and physiological loading could be utilized to direct the differentiation of MSCs on scaffolds for connective tissue engineering as well as extended applications in scar-less wound repair. Future work will more closely investigate the effects of cellular deformation on the aligned and unaligned nanofibers, as previous work has established that actin and myosin stress-fibre alignment is substrate-dependent and can influence differentiation[171], while also evaluating further optimization of the loading regiment for both differentiation and matrix production.

2.5 Conclusions

This study investigated the coupled effects of nanofiber matrix alignment and mechanical stimulation on stem cell differentiation. It was demonstrated that MSCs differentiate into ligament

fibroblast-like cells when cultured on aligned nanofibers and subjected to tensile loading. In contrast, on unaligned nanofibers, mechanical loading only modulates cell attachment morphology without subsequent induction of fibroblastic differentiation. These results demonstrate the deterministic role biomaterial substrate alignment plays in stem cell response to mechanical loading, as both biomimetic alignment and tensile loading are required for the induction of MSCs into ligament fibroblasts. As a result, the ligament phase of the graft should consist of aligned nanofibers subjected to dynamic tensile loading to drive fibroblastic differentiation of seeded MSCs. Next, the effect of combined chemical and mechanical stimulation will be evaluated to determine if fibroblastic differentiation on aligned nanofibers can be enhanced with the addition of exogenous growth factors.

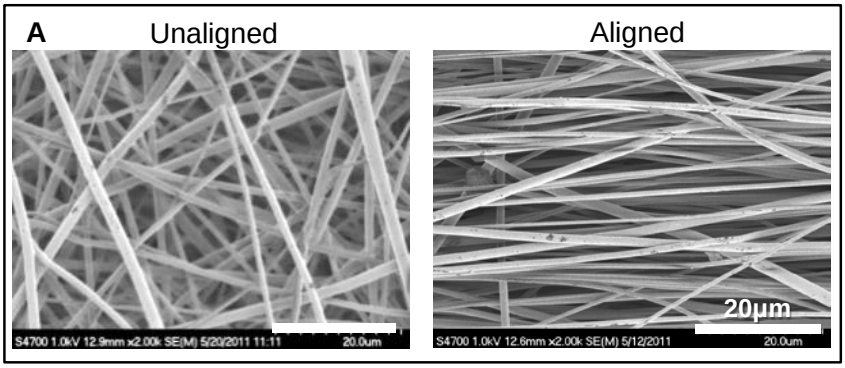

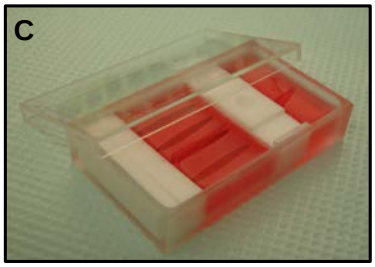

	Unaligned	*Aligned*
Fiber Diameter (nm)	667 ± 128	615 ± 152
Pore Size (µm)	4.91 ± 0.78	4.23 ± 1.06
Porosity (%)	81.76 ± 3.93	80.75 ± 2.97

Figure 2.1. Modular bioreactor system for applying tensile strain to nanofiber meshes. **A)** Scanning electron micrographs of unaligned and aligned PLGA nanofibers. **B)** Nanofiber meshes are cultured in a custom bioreactor with load applied via a linear actuator and stepper motor. **C)** Five nanofiber meshes are cultured in each individual bioreactor. The apparatus is housed within a cell culture incubator for the duration of the culture period.

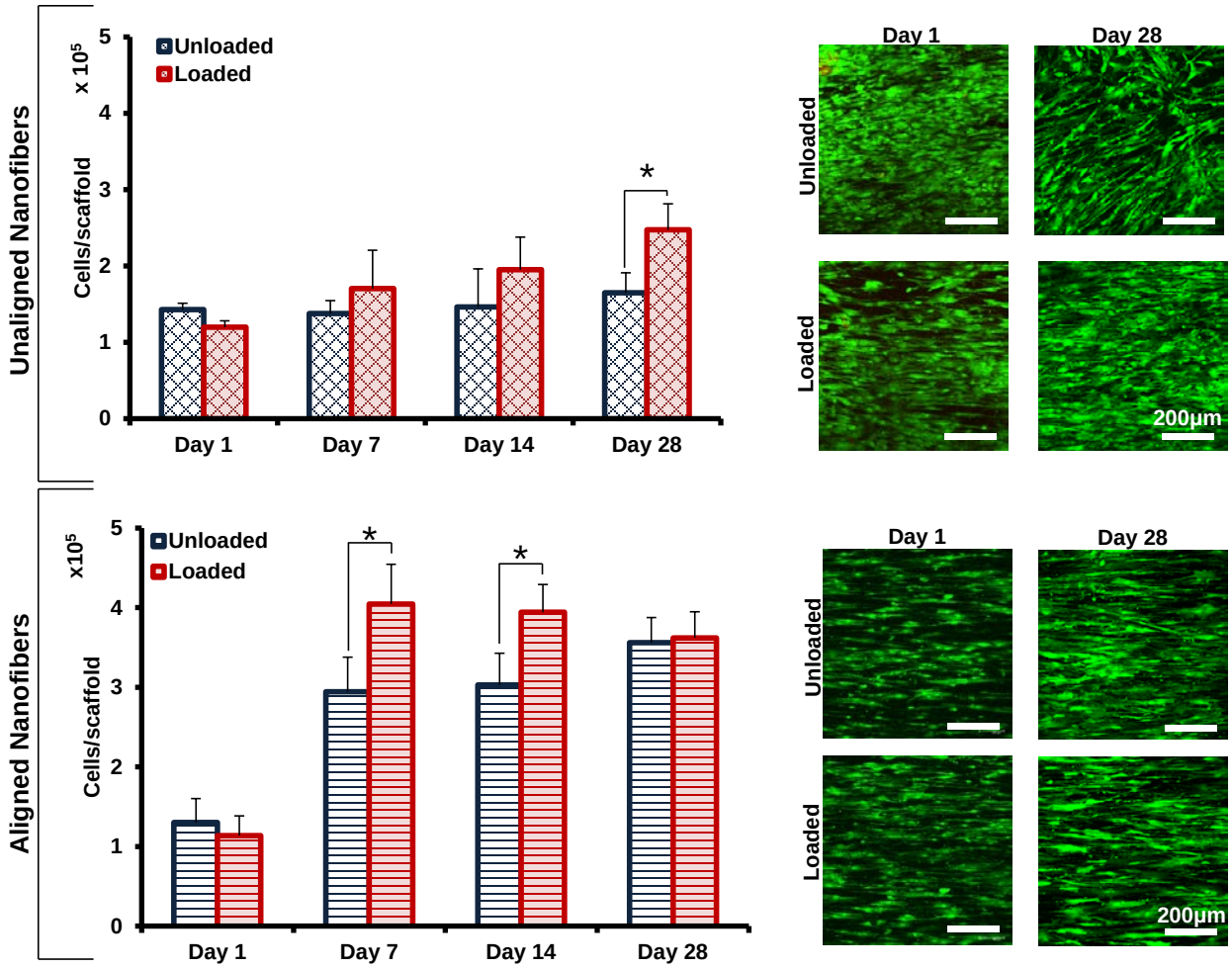

Figure 2.2. Effect of alignment and mechanical stimulation on cell attachment and proliferation. On unaligned nanofibers, a significantly greater number of MSC were found after 28 days of loading. Cells attachment conformed to the underlying nanofiber architecture in the control group but appeared to align in the direction of loading with the application of mechanical stimulation. On aligned nanofibers, an increase in total cell number was observed after seven days with equal numbers of cells present after 28 days. Cell morphology was similar both with and without loading.

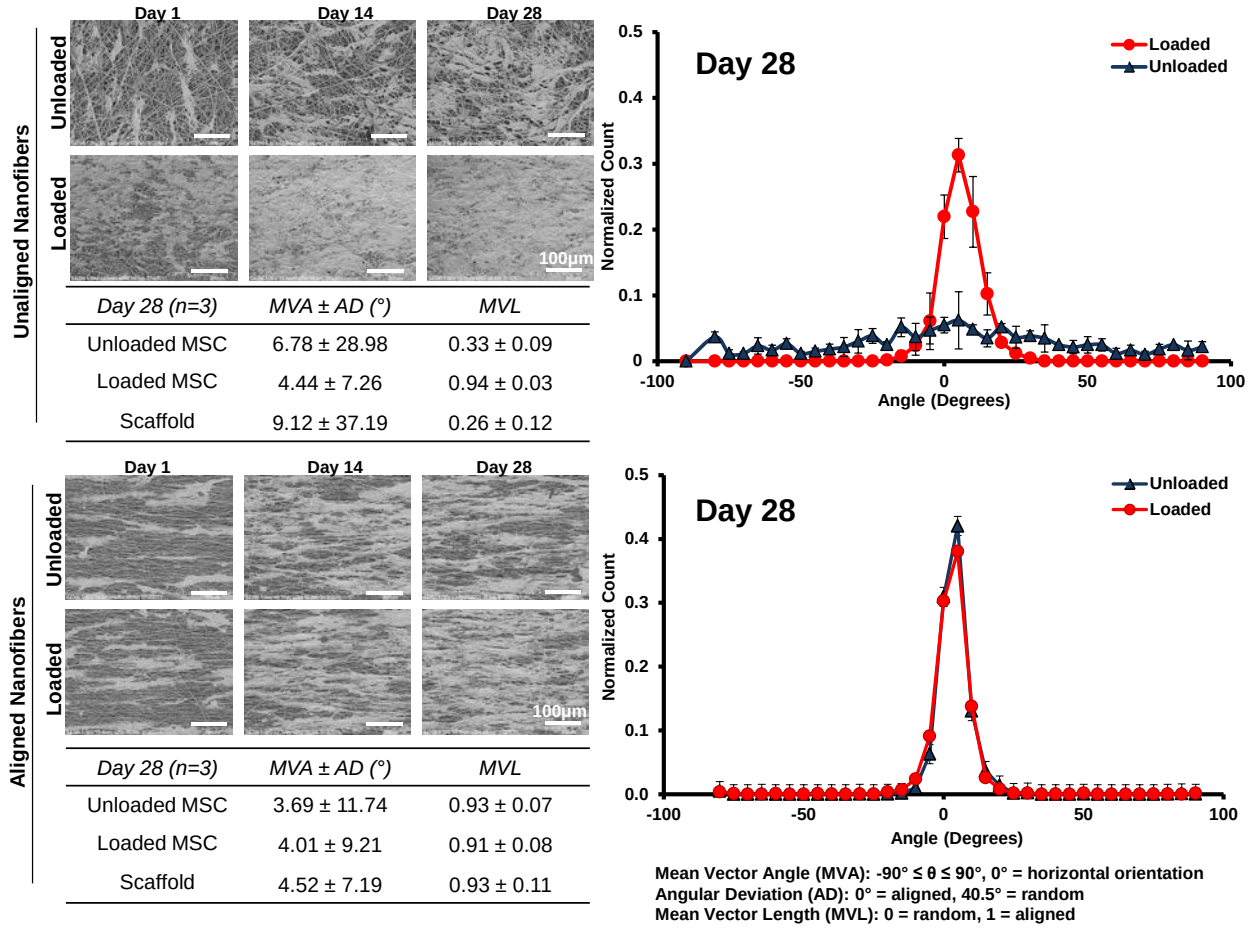

Figure 2.3. Effect of alignment and mechanical stimulation on cell alignment. A distinct difference in MSC alignment was observed on unaligned nanofibers after 28 days of loading with cells predominantly aligned in the direction of loading on strained nanofibers, as quantified via circular statistical analysis. Analysis via SEM indicated that cells spanned across fibers as opposed to following individual fibers. No difference in alignment was observed on aligned nanofibers due to loading.

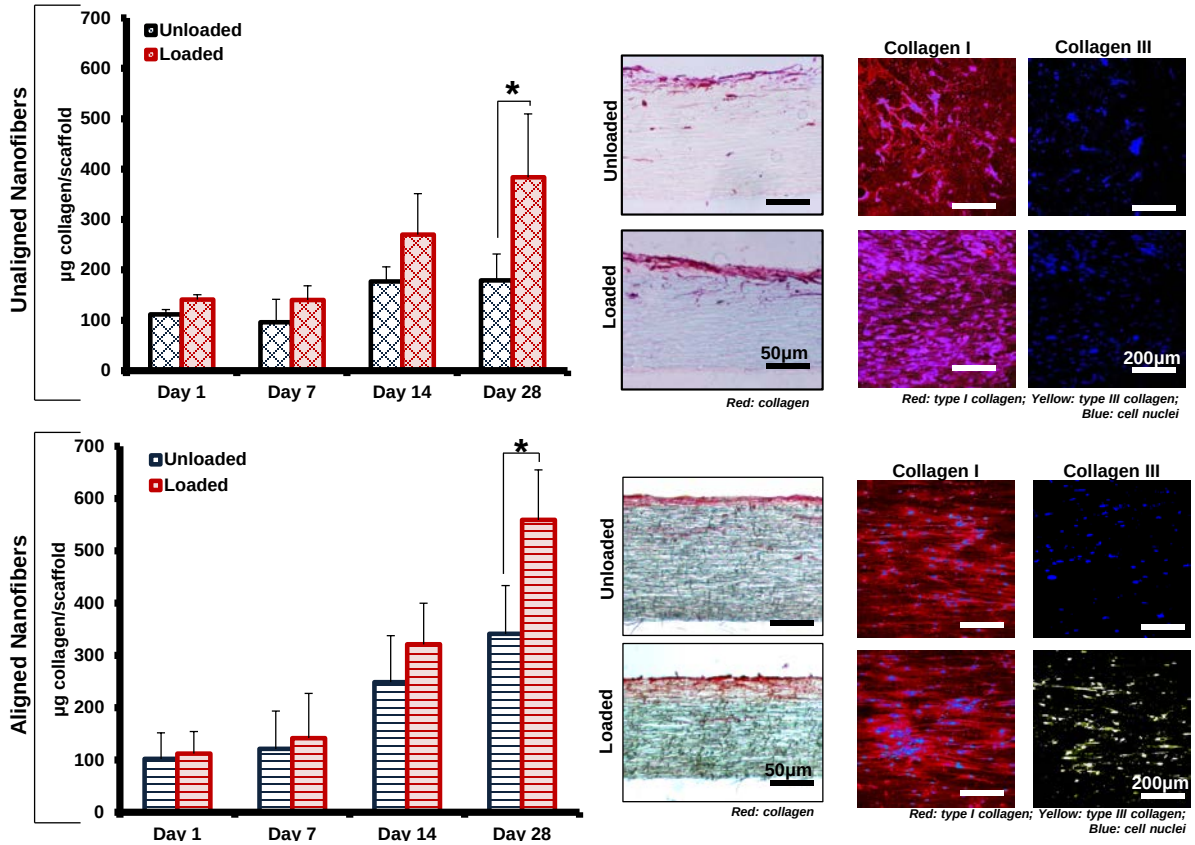

Figure 2.4. Effect of alignment and mechanical stimulation on matrix deposition. A significant increase in total collagen was measured, using the hydroxyproline assay, on both aligned and unaligned nanofibers after 28 days of dynamic loading. Immunohistochemistry after 28 days of culture also indicated that the ECM was primarily composed of type I collagen on unaligned nanofibers with type III collagen only present on aligned nanofibers subjected to mechanical loading.

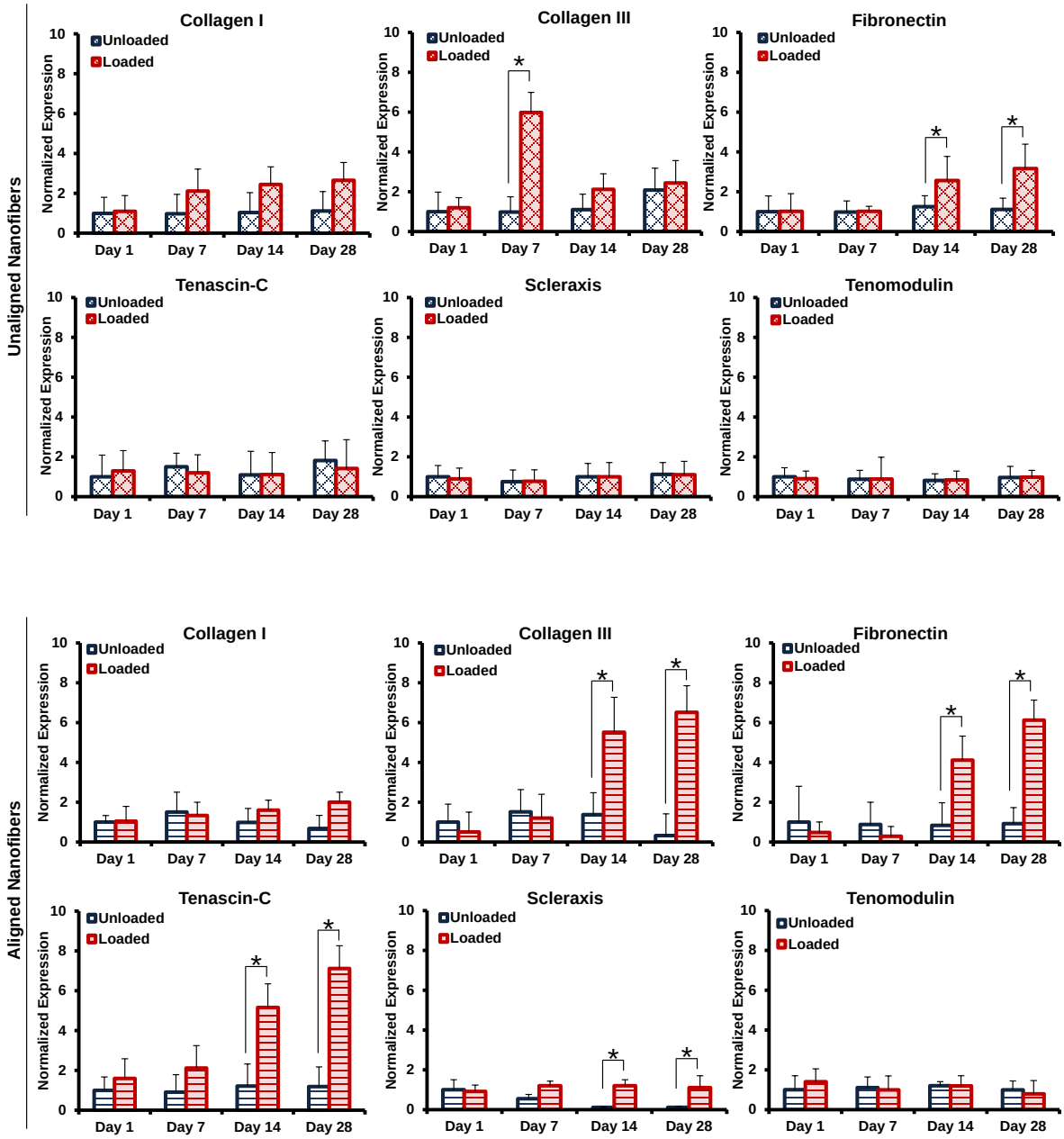

Figure 2.5. Effect of alignment and mechanical stimulation on cell differentiation. Gene expression of fibroblast makers by *MSC*s on unloaded and loaded nanofibers versus time (*p<0.05). On unaligned nanofibers, type III collagen was upregulated after 7 days of loading but returned to control levels after 14 days. Fibronectin expression was upregulated after 14 days and remained elevated after 28 days of loading. In contrast, on aligned nanofibers, types I and III collagen, fibronectin, tenascin-C and scleraxis were all upregulated. The ratio of collagen type I:III was 8.35 ± 2.12 by cells on loaded nanofibers after 28 days of culture.

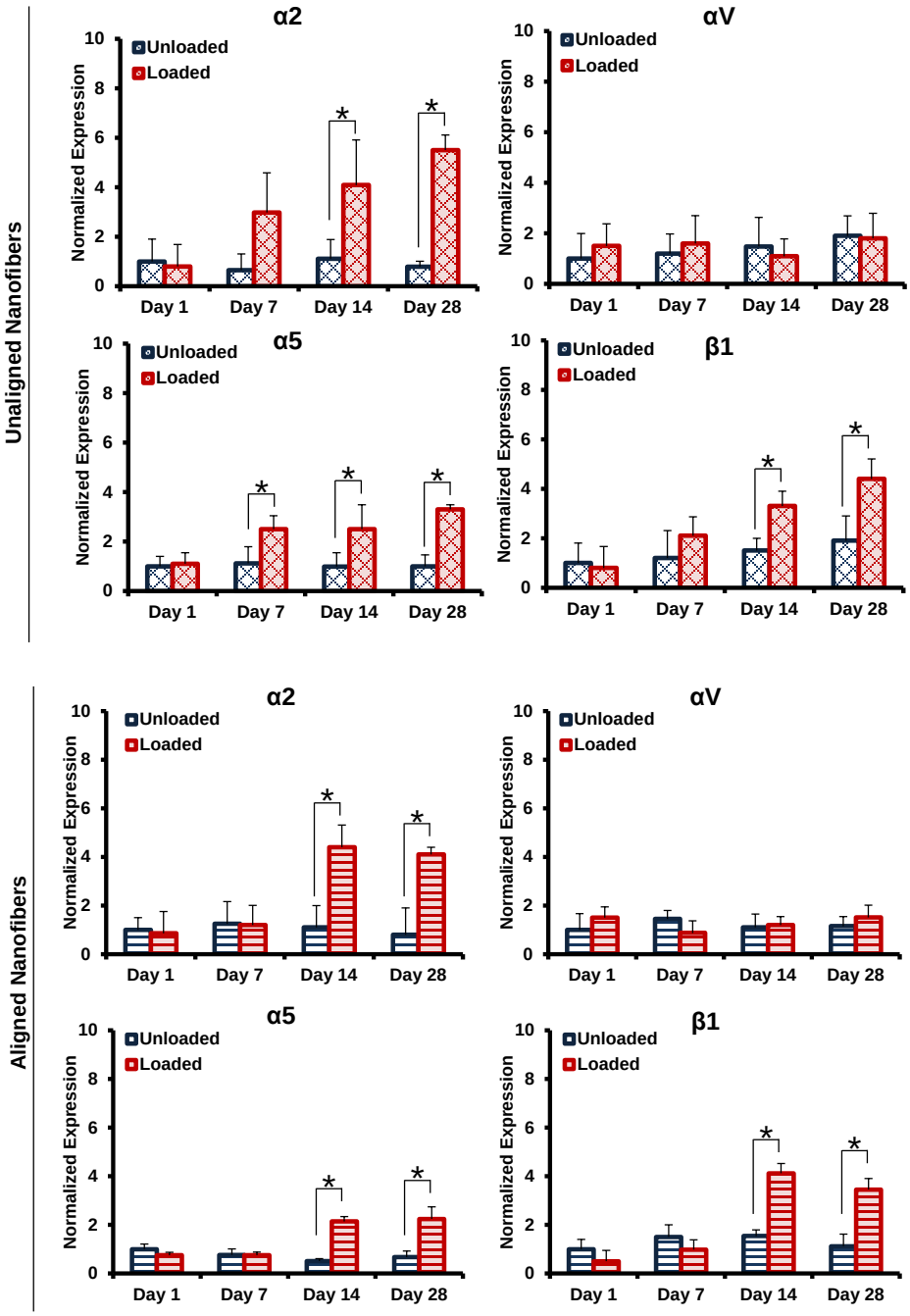

Figure 2.6. Effect of alignment and mechanical stimulation on integrin expression. Gene expression of integrin subunit by *MSC*s on unaligned nanofibers revealed the upregulation of integrin subunits α2, α5 and β1. (*p<0.05). Similarly, on aligned nanofibers upregulation of integrin subunits α2, α5 and β1 was observed, with differing temporal patterns as compared to cells on unaligned nanofibers. (*p<0.05)

CHAPTER 3: LIGAMENT PHASE: THE EFFECT OF FIBROGENIC CULTURE CONDITIONS ON FIBROBLASTIC DIFFERENTIATION OF MESENCHYMAL STEM CELLS

3.1 Introduction

Based on the previous study in *Chapter 2*, fibroblastic differentiation of MSCs requires physiologically-relevant mechanical stimulation coupled with an aligned nanofiber substrate. It has also been demonstrated that chemical stimulation, using growth factors such as basic fibroblast growth factor (bFGF) and transforming growth factor-beta can induce fibrogenic differentiation of MSCs and that differentiation can be further enhanced when coupled with mechanical loading. This chapter aims to determine the synergistic effects of chemical and mechanical stimulation to determine if adding growth factors prior to applying the mechanical strain regimen, identified in *Chapter 2*, is necessary to enhance fibrogenesis.

3.1.1 Background and Motivation

Despite the versatility of MSCs for tissue engineering purposes, standardized methods to differentiate these cells towards a fibroblastic lineage have not been well established. To this end, several groups have demonstrated that mechanical stimulation can be used to drive fibroblastic differentiation of MSCs. Among the earliest to evaluate fibrogenic differentiation of MSC were Altman *et al.* who demonstrated that MSCs could be induced into a fibroblastic phenotype when seeded in type I collagen gels and subjected to a combination of tensile and rotational strain. Specifically, It was reported that the application of mechanical stress upregulated the expression of ligament fibroblast markers, resulted in the production of type III collagen and guided cell alignment in the direction of applied load[27]. Studies performed by Butler *et al.* evaluating a range of mechanical stimulation parameters using a type I collagen sponge system have similarly demonstrated that tensile strain can upregulate the expression of fibroblastic markers and enhance MSC matrix deposition[172-175]. Recently, it was demonstrated that the application of dynamic mechanical stimulation to human MSCs cultured on aligned nanofibers results in fibroblastic differentiation and the production of a ligament-like matrix[176] Mechanical loading resulted in the upregulation of several fibroblastic genes including type III collagen, fibronectin, tenascin-C and scleraxis while also resulting in the production of a matrix rich in types I and III collagen.

To augment ligament engineering strategies, methods to further enhance MSC response and biosynthesis have been explored in order to facilitate the formation of functional ligament tissue. Mitogens

such as the transforming growth factor-beta (TGF-β) family, basic fibroblast growth factor (bFGF) and epidermal growth factor (EGF) have been shown to induce proliferation both *in vitro* and in vivo for cell types including fibroblasts and MSCs and have also been shown to affect MSC differentiation and biosynthesis. In particular, bFGF has been shown to maintain MSC differentiation potential, stimulate proliferation, and induce fibroblastic differentiation. Studies performed by Hankemier *et al.* demonstrated that low-dose (3ng/ml) bFGF increased MSC proliferation as measured after 7 days and, on days 14 and 28, upregulated the expression of type I and III collagen, fibronectin and smooth muscle actin[177]. Furthermore, chemical stimulation has been shown to synergistically enhance cell response when combined with mechanical stimulation. For example, Moreau *et al.* evaluated the sequential application of biochemical and mechanical stimulation to MSCs cultured on silk fiber-based scaffolds. It was reported that stimulating cells with bFGF or EGF for five days prior to the application of mechanical load modulated matrix protein expression and cell activity[91].

3.1.2 Objectives

Building upon previous results, bFGF was selected for further investigation to enhance MSC-based ligament engineering for the ligament phase of the synthetic ACL graft. Specifically, the objective of this study is to evaluate the synergistic effect of chemical and mechanical stimulation on the fibroblastic differentiation of human MSC when seeded on nanofiber meshes. It is hypothesized that chemical priming of MSCs with bFGF prior to the application of mechanical stimulation will enhance MSC matrix production and upregulate the expression of relevant fibroblastic genes.

3.2 Materials and Methods

3.2.1 Nanofiber Mesh Fabrication

Aligned nanofiber meshes composed of PLGA (85:15, M_w = 123.6 kDa; Lakeshore Biomaterials, Birmingham, AL) were produced using electrospinning[24;139]. Briefly, PLGA nanofibers were fabricated by producing a solution composed of 35% PLGA (v/v) in 55% N,N-dimethylformamide (Sigma-Aldrich, St. Louis, MO) and 10% ethyl alcohol. The solution was loaded into a syringe with an 18.5-gauge stainless steel blunt tip needle and electrospun at 8-10kV and 1 mL/hour using a custom electrospinning device.

Aligned fibers were produced by electrospinning onto a custom rotating mandrel (20 m/s) with polymer dispensation via a syringe pump (Harvard Apparatus, Holliston, MA; 1 ml/hr).

3.2.2 Cells and Cell Culture

Human mesenchymal stem cells (MSC) were obtained commercially (Lonza, Walkersville, MD) and maintained in culture with DMEM containing 10% fetal bovine serum (FBS, embryonic stem cell certified, Atlanta Biologicals, Atlanta, GA), 1% penicillin-streptomycin, 1% non-essential amino acids, 0.1% amphotericin B and 0.1% gentamicin. Cells were cultured to 80% confluence and then passaged using 0.25% trypsin/1 mM ethylenediaminetetraacetate (EDTA) and re-plated at a density of $5x10^3$ cells/cm^2. Passage 2 cells were used for nanofiber mesh seeding.

All studies were performed using low-serum medium as adapted from previously published studies. This medium was identical to MSC maintenance media but contained 5% FBS and was utilized for the duration of the culture period. To evaluate chemical stimulation, the low-serum medium was supplemented with 10ng/mL bFGF (Invitrogen).

Meshes were secured in a custom bioreactor to apply uniaxial tensile strain. Briefly, electrospun meshes (5x6cm) were excised after fabrication and subsequently sterilized via ultraviolet irradiation (15minutes/side). Meshes were secured in loading cartridges via teflon clamps, sectioned into 5 cm x 1 cm strips and pre-incubated in culture medium at 37ºC and 5% carbon dioxide for 16 hours. Cells were seeded on the meshes at a density of $3x10^4$ cells/cm^2 and allowed to attach for 15 min before the addition of culture medium.

3.2.3 Cell Attachment and Alignment

Cell viability and morphology (n=3/group) was evaluated using Live/Dead staining (Invitrogen, Carlsbad, CA) following the manufacturer's suggested protocol. The samples were imaged under confocal microscopy (Leica TCS SP5, Bannockburn, IL) at excitation wavelengths of 488nm and 594nm. Cell penetration was evaluated by taking a z-series of confocal images over a depth of 20μm, equivalent to 15 to 20 layers of nanofibers.

3.2.4 Cell Proliferation

Total DNA content was measured using the PicoGreen dsDNA assay (Invitogen). At each time point, the samples (n=5/group) were homogenized in 0.1% Triton-X (Sigma-Aldrich) and subjected to 20 seconds of ultrasonication at 5W. Fluorescence was measured using a microplate reader (Tecan) at an excitation wavelength of 485 nm and an emission wavelength of 535 nm. A standard curve was derived and used to correlate DNA concentration to fluorescence intensity, and cell number was determined based on a conversion factor of 8pg DNA/cell[104].

3.2.5 Matrix Deposition

Total collagen content per sample (n=5/group) was calculated using the hydroxyproline assay[142]. Briefly, the samples were first desiccated for 24 hours and then digested for 16 hours at 65°C with papain (600 µg protein/ml) in 0.1M sodium acetate (Sigma), 10 mM cysteine HCl (Sigma), and 50 mM ethylenediaminetetraacetate (Sigma). A 40 µl aliquot of the digest was hydrolyzed with 10 µl 10 M sodium hydroxide and autoclaved for 25 minutes. The hydrolyzate was then oxidized by a buffered chloramine-T reagent for 25 minutes before the addition of Ehrlich's reagent. Sample absorbance was measured at 550nm (Tecan), and the collagen content was obtained by interpolation along a standard curve of bovine type I collagen (Sigma).

Collagen penetration was also visualized using picrosirius red staining of frozen sections (n=2/group) after 28 days of culture. Briefly, after fixation, samples were embedded in 5% polyvinyl alcohol (PVA, Sigma-Aldrich) and 7-micrometer thick sections (spanning the depth and width of the mesh) were obtained using a cryostat (Hacker-Bright OTF model, Hacker Instruments and Industries, Winnsboro, SC). Collagen distribution was visualized with picrosirius red staining under light microscopy (Axiovert 25, Zeiss).

3.2.5 Cell Differentiation

Gene expression (n=5/group) was measured using quantitative real-time reverse transcriptase polymerase chain reaction (qPCR) at 1, 7, 14 and 28 days. Total RNA was isolated using the Trizol extraction method (Invitrogen). Isolated RNA was then reverse-transcribed into complementary DNA

using the SuperScript First-Strand Synthesis System (Invitrogen), and the cDNA product was amplified using recombinant Taq DNA polymerase (Invitrogen). Expression of fibroblastic markers type I collagen, type III collagen, fibronectin tenascin-C, tenomodulin and scleraxis was determined. GAPDH served as the house-keeping gene. Primer sequences were as follows:

Gene	***Sense***	***Anti-Sense***
GAPDH	5'- GGCGATGCTGGCGCTGAGTA-3'	5'-ATCCACAGTCTTCTGGGTGG-3'
Collagen I	5'-TGGTCCACTTGCTTGAAGAC-3'	5'-ACAGATTTGGGAAGGAGTGG-3'
Collagen III	5'-GGCTACTTCTCGCTCTGCTT-3'	5'-CATATTTGGCATGGTTCTGG-3'
Fibronectin	5'-TTGAACCAACCTACGGATGA-3'	5'-AAATGACCACTTCCAAAGCC-3'
Tenascin-C	5'-TGCCCATTACAGGAGGTACA-3'	5'-CACTTTCCTCAAAGCCCTTC-3'
Scleraxis	5'-CAGCGGCACACGGCGAAC-3'	5'-CGTTGCCCAGGTGCGAGATG-3'
Tenodmoulin	5'-TTTGAGGAGGAGGGAGAAGA-3'	5'-TTCCTCACTTGCTTGTCTGG-3'

All genes were amplified for 50 cycles in a thermocycler (Bio-Rad iCycler, Hercules, CA) with a fluorescent probe (SYBR Green, Invitrogen). Quantitative analysis of gene expression was performed using the delta-delta CT method.

3.2.6 Mechanical Properties

Mechanical properties of the loaded and unloaded meshes (n = 5 samples/group) were determined at 1, 7, 14 and 28 days after priming. At each time point, samples were tested to failure under uniaxial tension. Meshes were secured with custom clamps tested to failure at a strain rate of 5mm/minute (Instron, Model 8841, Norwood, MA) with an average gauge length of 3cm. Samples were evaluated to failure at a strain rate of 5mm/min with load applied in the direction of fiber alignment. Mesh yield strength and ultimate tensile stress were determined, and elastic modulus was calculated from the linear region of the stress-strain curve.

3.2.7 Experimental Design & Bioreactor Culture

The effect of exogenous bFGF stimulation on MSC response was first evaluated in a two-week study in which cell viability, proliferation, matrix deposition and differentiation were assessed.

Subsequently, a four-week study was conducted in which MSCs were primed statically for 5 days with bFGF and then subjected to dynamic tensile stimulation in a custom bioreactor. Loaded samples were subjected to 1% strain at 1Hz for 90 minutes twice daily and evaluated over a period of 28 days. Control meshes, cultured in identical bioreactor cartridges, were subjected to the same growth factor priming regimen without subsequent mechanical stimulation.

3.2.8 Statistical Analysis

Results are presented in the form of mean ± standard deviation, with *n* equal to the number of samples per group. Two-way ANOVA was used to determine the effects of chemical stimulation and mechanical loading on cell proliferation, matrix deposition, gene expression and mechanical properties. The Tukey-Kramer post-hoc test was used for all pair-wise comparisons and significance was attained at $p<0.05$. Statistical analyses were performed with JMP IN (4.0.4, SAS Institute, Inc., Cary, NC).

3.3 Results

3.3.1 MSC Response to Chemical Stimulation

Cell viability and attachment morphology was visualized using confocal microscopy. The MSCs displayed an elongated fibroblastic morphology that conformed to the alignment of the underlying nanofibers (*Fig. 3.1*). Similarly viable cells were observed both with and without the treatment of bFGF. Cell number was quantified for both groups at each time point. Chemical stimulation resulted in a significant difference in the number of cells per mesh after 7 days of culture, with a significantly greater number of cells present on nanofibers subjected to bFGF stimulation. The total number of cells was also significantly greater than that measured after 1 day of culture for both groups (*Fig. 3.1*). After 14 days of culture, there remained significant difference in number of cells present in the control and bFGF stimulated group. Total collagen deposition was evaluated for both groups over time. Total collagen deposited by cells was similar after 1 day of culture with a significant increase in the bFGF stimulated group after 7 days of culture (*Fig. 3.1*). A significantly greater amount of collagen was measured on nanofibers subjected to bFGF stimulation after 14 days. No significant change in total collagen was measured over time in the control group.

Differentiation of MSCs in both groups was assessed over the 14 day culture period by measuring the expression of types I and III collagen, fibronectin, tenascin-C, scleraxis and tenomodulin. Significant changes in gene expression occurred only after 14 days in the bFGF stimulation group. Specifically, types I and III collagen, fibronectin and tenascin-C were all upregulated after 14 days of chemical stimulation as compared to the control group (*Fig. 3.2*). The expression of these genes did not change over time in the control group. In both the control and bFGF stimulated groups, the mean expression of scleraxis and tenomodulin decreased over time though no significant change was measured.

Nanofiber mesh mechanical properties were measured over the duration of the study via uniaxial tensile testing. No differences in mechanical properties were measured between the unloaded and loaded groups in terms of elastic modulus, yield strength, ultimate tensile strength or ductility. A significant decrease in elastic modulus and ductility were observed after 28 days of culture in both groups.

3.3.2 MSC Response to Sequential Chemical and Mechanical Stimulation

After determining the effect of chemical stimulation on MSC response, a four-week study was conducted to assess MSC response to sequential chemical and mechanical stimulation. Confocal microscopy of cells seeded revealed no differences in cell viability or morphology between the loaded and unloaded control group as cells aligned in the direction of the underlying nanofibers and remained viable over the duration of the study (*Fig 3.3*). A significant increase in total cells was observed after 7 days of culture in both the loaded and unloaded group. Total cell number on nanofiber meshes was significantly greater in the loaded group after 7 days of mechanical stimulation, as compared to unloaded controls. No significant difference between groups was measured after 14 days, though significantly greater cells were once again measured on the loaded group after 28 days.

Matrix deposition was evaluated both quantitatively to determine total collagen content and qualitatively to evaluate matrix morphology and penetration. Total collagen deposition increased over the duration of the culture period with significantly greater collagen deposited by cells subjected to dynamic loading as compared to loaded controls after 28 days (*Fig. 3.4*). In addition, histological analysis of matrix

deposition via Picrosirius Red staining revealed deeper matrix penetration into loaded meshes after 28 days.

To evaluate MSC differentiation, the expression of several key fibroblastic genes was measured using quantitative PCR (*Fig. 3.5*). In the unloaded group, type I collagen expression was unregulated significantly 7 days after the priming culture period but decreased significantly after 28 days. In contrast, type I collagen was upregulated to a greater extent in the loaded group after 7 days of mechanical stimulation and remained elevated after 28 days. The expression of type III collagen was significantly upregulated after 14 days in both groups though the expression levels on mechanically stimulated nanofiber meshes were significantly higher at both 14 and 28 days. Fibronectin expression increased over time in both the unloaded and loaded groups with expression levels remaining similar regardless of the application of mechanical stimulation. Tenascin-C expression increased over time in both groups over the first 14 days following priming. A significant decrease in tenascin-C expression was measured in the unloaded group after 28 days whereas the expression level was maintained with mechanical stimulation. Expression of scleraxis remained similar in both groups over the duration of the study though expression of tenomodulin increased significantly after 28 days of loading.

The effect of combined chemical and mechanical stimulation on nanofiber mesh mechanical properties was assessed over the duration of the culture period (*Fig 3.6*). No difference in mesh mechanical properties was measured between groups at any time point. A significant decrease in yield strength, ultimate tensile strength (UTS) and ductility were measured 4 weeks after priming in both groups as compared to day 1 ($p<0.05$).

3.4 Discussion

This study focuses on the differentiation of mesenchymal stem cells into fibroblast-like cells on nanofiber meshes using a combination of chemical and mechanical stimulation. In this study, the effects of treating MSCs seeded on nanofibers with bFGF alone and also sequentially with bFGF followed by dynamic tensile strain were systematically investigated. It is observed that bFGF stimulation alone can enhance MSC proliferation and matrix deposition and that mechanical stimulation can synergistically

enhance these effects to drive MSCs towards a fibroblastic phenotype. Based on these findings, it is apparent that combinatorial stimulation techniques could be used to engineer ligament tissue *in vitro*.

In this study, biochemical stimulation of MSCs with bFGF resulted in an increase in the total number of cells and collagen on nanofiber meshes after 14 days as well as an increase in the expression of types I and III collagen, fibronectin and tenascin-C. It has previously been established that bFGF is a mitogen which can enhance the proliferation of MSCs. Pitaru *et al.* reported that bFGF in conjunction with osteogenic medium containing dexamethasone stimulated proliferation. Hankemeier *et al.* also reported that bFGF stimulation results in dose-dependent effects on MSCs and low doses (3ng/ml) stimulated cell proliferation while upregulating the expression types I and III collagen, fibronectin and alpha-smooth muscle actin (α-SMA). In contrast, high doses (30ng/ml) decreased proliferation and ECM protein expression. The dose used in this study (10ng/ml) is closer in magnitude to the low-dose condition. In addition, an increase in total collagen was observed on nanofibers with chemical stimulation as compared to unstimulated controls after 14 days. This difference is likely due to the increased number of cells, as normalizing collagen content per-cell indicated no difference in per-cell collagen production. Previous groups have reported similar findings when utilizing bFGF to stimulate MSCs on tissue engineered scaffold systems. For example, Sahoo *et al.* extended upon this and evaluated the incorporation of bFGF into a silk/PLGA hybrid fiber scaffold for ligament tissue engineering{5313}. Local release from the biohybrid scaffold resulted in an increase in cell number and total collagen and also increased scaffold mechanical properties after three weeks of culture *in vitro*.

Based upon the ability of bFGF to enhance cell response and elicit the upregulation of fibroblast-related matrix proteins, chemical priming of MSCs with bFGF prior to mechanical stimulation was investigated. Notably, in this study, it was shown that applying mechanical stimulation following chemical priming resulted in a greater number of cells and total collagen present on nanofiber meshes after 28, as compared to applying a bFGF priming regimen alone. These findings indicate that mechanical stimulation can synergistically enhance cell proliferation and biosynthetic response on nanofibers. In addition, mechanical stimulation maintained the expression of types I and III collagen over the four week period following priming. This finding indicates that that chemical stimulation may not result in cells fully obtaining a fibroblastic phenotype, whereas mechanical stimulation could maintain differentiation or

potentially result in cells committing to fibrogenesis. Interestingly, combined mechanical and chemical stimulation resulted in the upregulation of tenomodulin 28 days after chemical priming. Tenomoduling ia an anti-angiogenic transmembrane protein that has been shown to be predominantly expressed in tendons and ligaments. While previous work evaluating mechanical stimulation without chemical priming of MSCs on nanofibers did not show any effect on tenomodulin expression, this finding indicates that bFGF priming may result in MSCs further differentiating towards a ligament or tendon fibroblast phenotype.

The effect of combined bFGF and mechanical stimulation has been previously investigated on other tissue engineered constructs with similar results. Petrigliano *et al.* reported on the development of a bFGF-eluting porous polycaprolactone-based construct[178]. It was shown that cells subjected to both chemical and mechanical stimulation resulted in the greatest upregulation of types I and III collagen and tenascin-C. Moreau *et al.* demonstrated that bFGF priming followed by mechanical stimulation enhanced matrix development and better supported overall tissue development, as compared to EGF priming[91].

It has previously been shown that mechanical stimulation may result in increased cell responsiveness to growth factors, potentially due to mechanical forces initiating enhanced matrix production and remodeling. In a study performed by Shin *et al.*, bFGF signaling was investigated as a mechanotransduction pathway for human umbilical vein endothelial cells (HUVEC) subjected to cyclic pressure[179]. It was shown that the enhanced proliferation of cells was associated with rapid tyrosine phosphoryliation of the bFGF receptor, fibroblast growth receptor 2 (FGFR-2), but not with increased synthesis of bFGF. Studies performed by Vincent *et al.* also demonstrated that cyclic loading of porcine cartilage resulted in the rapid activation of the bFGF-dependent extracellular signal-regulated kinase (ERK) mitogen-activated protein (MAP) kinase pathway[180;181]. These findings collectively implicate bFGF in mechanical signaling and suggest that priming of cells with this protein may increase cell response to mechanical stimulation.

Sequential chemical and mechanical stimulation resulted in no difference in nanofiber mesh mechanical properties as compared to chemical priming alone. It is likely that longer-term culture or further strategies to enhance matrix deposition may be necessary in order for cells to produce sufficient

ECM to augment nanofiber mesh mechanical properties. Previous studies using electrospun nanofibers have shown increases in cell-seeded mechanical properties as late as 10 weeks post-seeding[126].

One limitation of this study is the use of serum-containing medium in conjunction with growth factor stimulation. This parameter was determined based on previous work in which low-serum levels in conjunction with growth factors elicited a favorable response[28;91]. While these conditions may be suitable for ligament tissue engineering strategies, a further investigation of growth factor stimulation on MSC response requires serum-free condition as the proteins present in serum may mask or synergistically enhance the effects of bFGF. In addition to bFGF, other growth factors, such as TGF-β[28;182] or growth/differentiation factor-5 (GDF-5)[182;183], may be able to further enhance cell response, either simultaneously or in sequence, as these proteins have been shown to enhance MSC biosynthesis as well as ligament and tendon tissue formation.

While this study produced several promising findings, significant further investigation is required to understand the temporal effects of chemical and mechanical stimulation on MSC response. Specifically, future work should assess dose-dependent response, priming duration and variations in mechanical stimulation parameters are necessary to optimize MSC differentiation into a fibroblast-like phenotype. These studies represent a foundation upon which further investigation can be performed and it is anticipated that combined stimulation techniques of mesenchymal stem cells on tissue engineered scaffolds will enable functional ligament regeneration.

3.5 Conclusions

In summary, it is shown that bFGF stimulation of MSCs can enhance MSC proliferation and matrix deposition and that applying chemical stimulation prior to mechanical stimulation can synergistically enhance these effects to drive MSCs towards a fibroblastic phenotype. Based on these findings, it is apparent that combinatorial stimulation techniques could be used to engineer ligament tissue *in vitro*. Next, the composition of the ligament phase will be optimized.

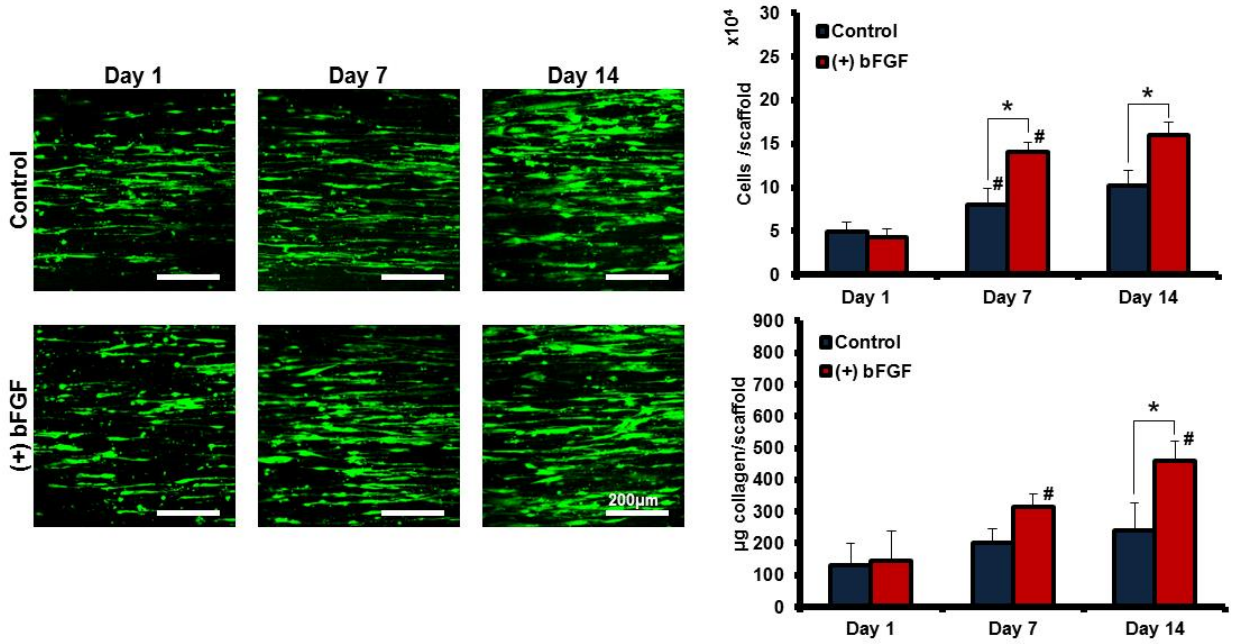

Figure 3.1. Effect of bFGF on MSC Proliferation and Matrix Production. Treatment with exogenous bFGF resulted in significantly greater cells on nanofibers after 7 days of culture. Growth factor treatment also resulted in a significant increase in matrix deposition after 14 days of culture.

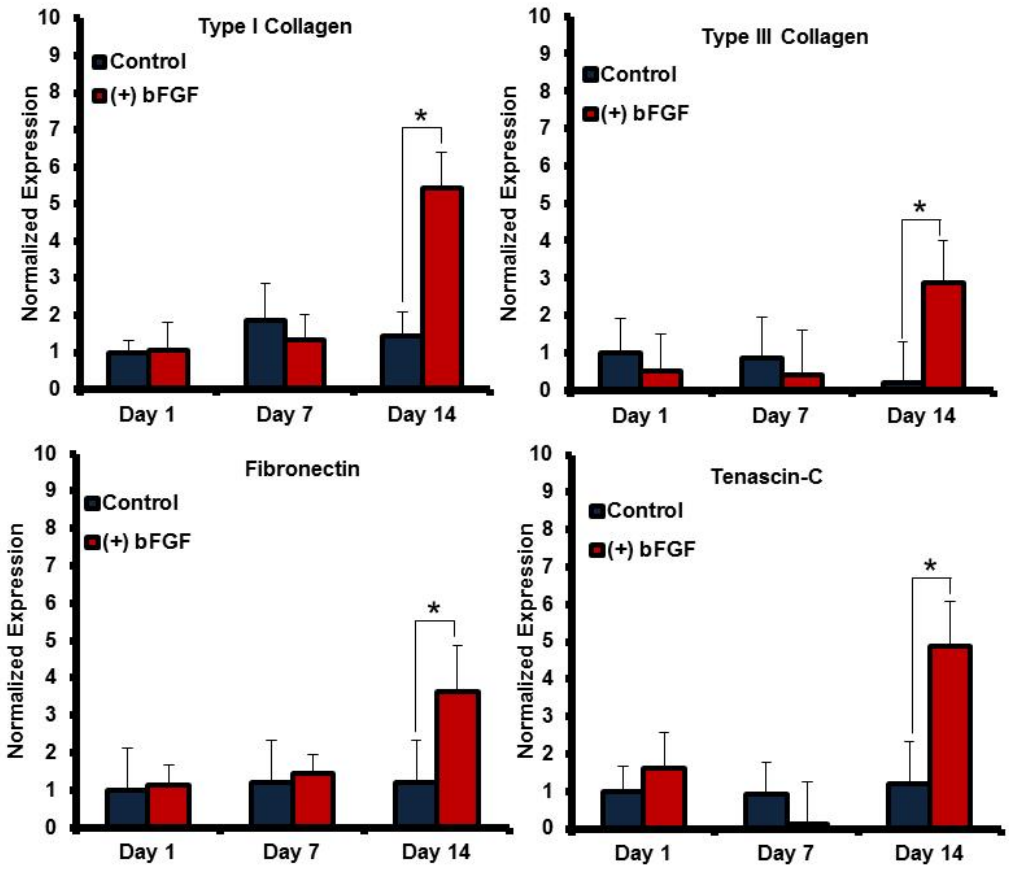

Figure 3.2. Effect of bFGF on MSC Differentiation. Growth factor treatment resulted in the upregulation of types I and III collagen, fibronectin and tenascin-C. In contrast, the mean expression of scleraxis and tenomodulin decreased over time.

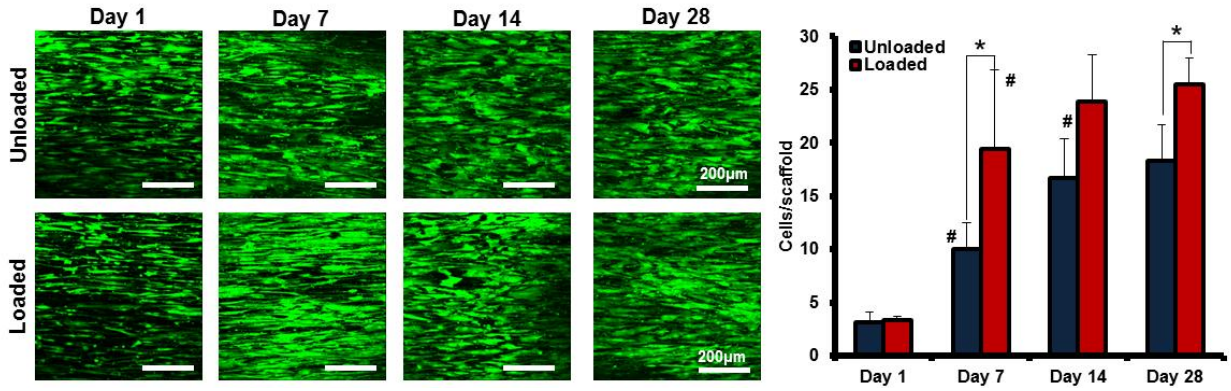

Figure 3.3. Effect of chemical and mechanical stimulation on cell attachment and proliferation. Cells remained similarly viable on both unloaded and loaded scaffolds. A significantly greater number of cells was measured on loaded meshes as compared to unloaded scaffolds after 28 days.

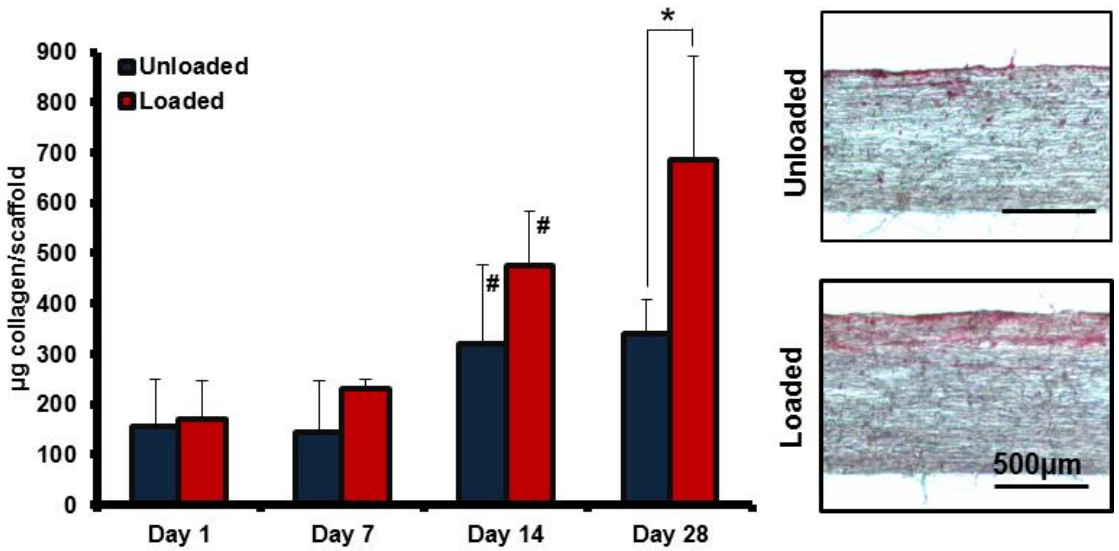

Figure 3.4. Effect of chemical and mechanical stimulation on MSC biosynthesis. Mechanical stimulation in conjunction with growth factor priming resulted in enhanced collagen deposition after 28 days of loading, as compared to unloaded controls. Histological analysis indicated deeper matrix penetration into loaded meshes after 28 days.

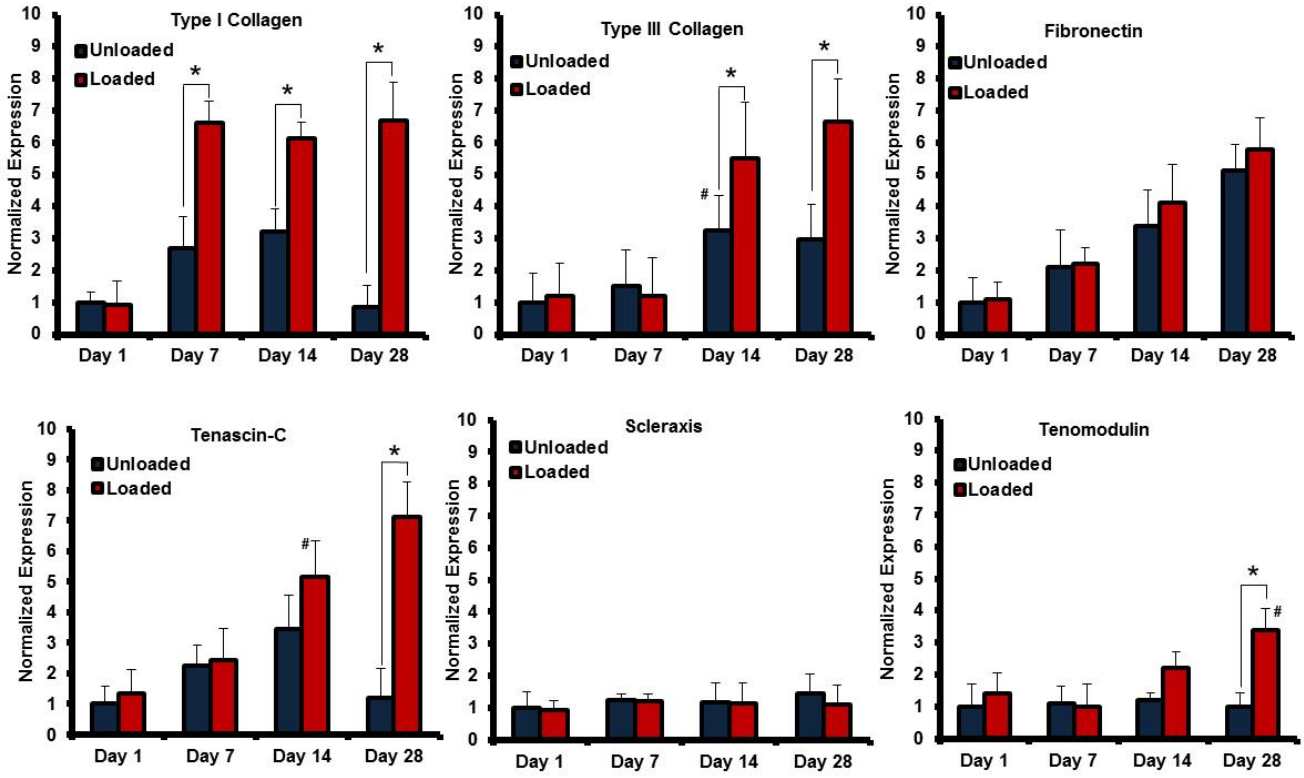

Figure 3.5. Effect of chemical and mechanical stimulation on MSC differentiation. Mechanical stimulation in conjunction with chemical priming resulted in a significant upregulation of types I and III collagen, tenascin-C and tenomodulin expression.

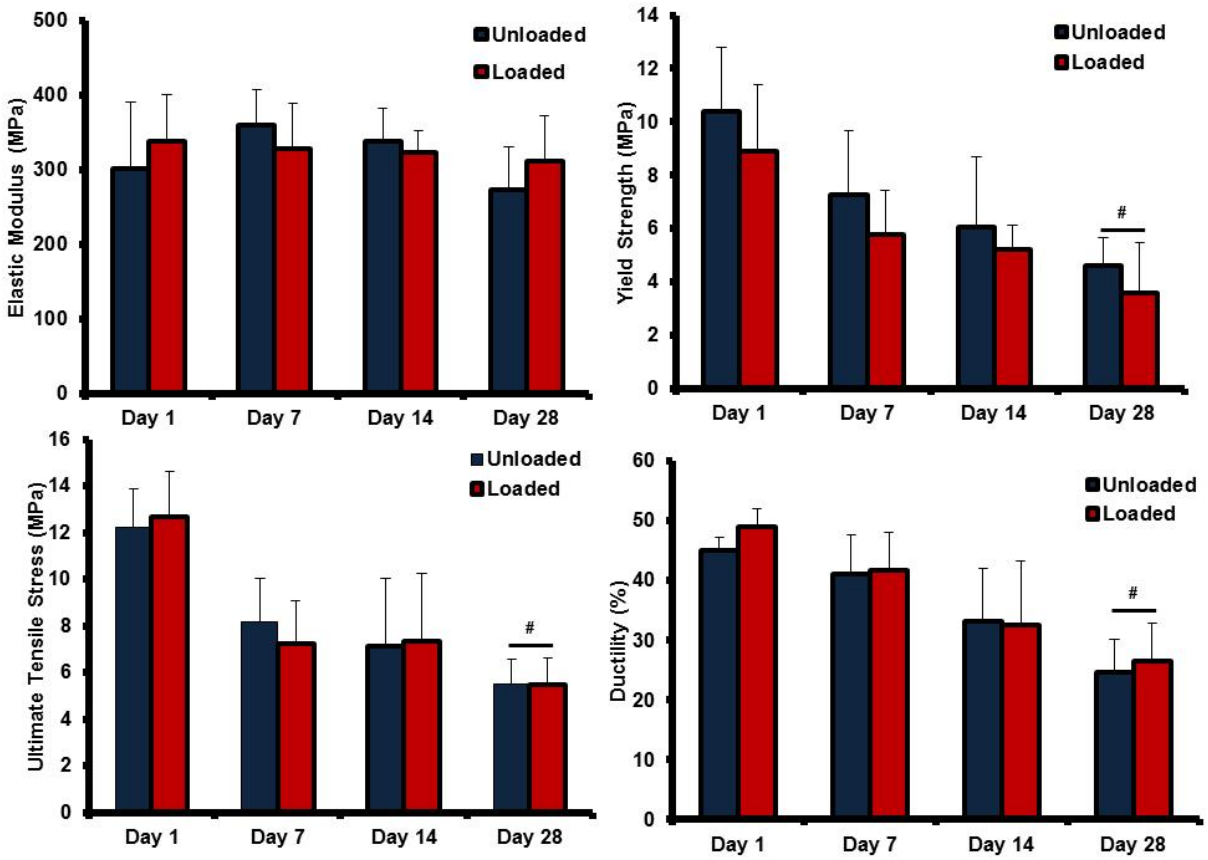

Figure 3.6. Effect of chemical and mechanical stimulation on nanofiber mesh mechanical properties. No difference in mesh mechanical properties was measured between groups over time. A significant decrease in yield strength, ultimate tensile strength (UTS) and ductility were measured 4 weeks after priming in both groups as compared to day 1 (#, $p<0.05$).

CHAPTER 4: LIGAMENT PHASE: THE EFFECT OF NANOFIBER COMPOSITION ON LIGAMENT TISSUE FORMATION

4.1 Introduction

In the previous chapters, cues to induce fibroblastic differentiation of MSCs were investigated. In chapter 2, it was demonstrated that mechanical stimulation alone on an aligned nanofiber substrate could induce the expression of fibroblastic markers and the deposition of a ligament-like matrix by MSCs. Subsequently, in chapter 3, it was shown that these effects could be enhanced when combined with chemical stimulation. However, in addition to supporting fibroblastic cell response, the ligament phase of the ACL scaffold must be sufficiently mechanically suitable for ligament replacement. This chapter investigates the optimal nanofiber composition for the ligament phase of the scaffold to select a material that mimics the mechanical properties of the native ligament and supports long-term ligament tissue formation.

4.1.1 Background and Motivation

A number of synthetic ACL prosthetic devices have been previously investigated with limited clinical success to date, as none are currently FDA approved. These attempts include grafts manufactured from carbon fiber[76], polytetrafluoroethylene (PTFE)[77;78], polyester[79;80] and polypropylene[81]. Among the earliest attempts at a prosthetic ligament were the carbon fiber implant and the composite carbon fiber-polyester braid ligament. While these ligaments provided initial mechanical stability, long term studies reported the generation and migration of carbon wear particles into the joint space following implantation. In addition, frequent incidence of implant stretching and rupture led to poor long-term functional outcomes[80]. Alternatively, polymer-based grafts have also been evaluated, such as the Gore-Tex ACL, fabricated out of expanded PTFE. While the Gore-Tex graft was implanted in more than 18,000 patients worldwide, it ultimately failed due to a lack of tissue ingrowth, likely due to the hydrophobicity of the material, and fatigued in response to normal cyclic loads[84]. In contrast, synthetic ligaments fabricated from polyester (Dacron) resulted in improved outcomes but were still susceptible to failure due to the lack of organized tissue formation over time[79;83]. In response to the previous failures of synthetic ligaments, tissue engineering has arisen as a promising method by which to synthetically regenerate the ACL. A number of approaches have been reported in the literature, including poly(methyl methacrulate)[85], silk[17;21;89-91;107-109] and PLLA-based[18;95;96;99;103;104] systems.

In terms of material selection, nanofibers have been fabricated from a wide variety of polymers. These include poly(lactide-co-glycolide) (PLGA)[24], poly(ε-caprolactone) (PCL)[126;128], polyurethane[152], silk[112], and collagen[184], among others. As the elastic modulus of the human ACL are reported to be within the range of 49-163 MPa[185;186], the ideal ACL scaffold must have mechanical properties within this range. Two suitable polymers for this purpose are PLGA and PCL as these materials have been widely investigated for tissue engineering applications[24;126;128]. An alpha-hydroxyester, PLGA degrades via bulk erosion on the order of six months to one year in vivo[187], and can be used to form nanofibers with an elastic modulus on the order of 400 MPa[24]. In contrast, PCL, also a polyester, degrades via surface erosion on the order of one to two years[188] with PCL nanofibers exhibiting an elastic modulus of approximately 50-100 MPa[126]. Due to the wide range of mechanical properties and degradation characteristics represented by these two polymers, it is anticipated that an ideal ligament scaffold, in terms of mechanical properties, degradation characteristics, and cell response could be fabricated by blending these two materials together.

4.1.2 Objectives

This study focuses on the fabrication of nanofibers from PLGA and PCL and assesses fibroblast response as a function of nanofiber composition in order to determine the optimal composition for a synthetic nanofiber-based ligament. The objective of this study is to evaluate the response of human ACL fibroblasts (hACL Fb) on PCL, PLGA and blends of PCL/PLGA nanofibers in order to determine the optimal composition for the ligament phase of the multi-phased ACL scaffold. It is hypothesized that blending the two polymers will allow for the fabrication of nanofibers with tunable mechanical and degradation characteristics and that changes in the underlying nanofiber composition will dictate cell response.

4.2 Materials and Methods

4.2.1 Nanofiber Mesh Fabrication

Nanofiber meshes were fabricated via electrospinning. For PLGA mesh fabrication, a 35% (v/v) solution of PLGA (85:15, DL, High IV, Lakeshore Biomaterials, Birmingham, AL) was mixed with 55%

N,N-dimethylformamide (DMF, Sigma-Aldrich) and 10% ethyl alcohol. To fabricate the PCL nanofibers, a mixture of 16% (w/v) PCL (Sigma-Aldrich, Mw=70,000-90,000) was dissolved in a mixture of 60/40 dichloromethane (DCM, Sigma-Aldrich) and DMF. Blend PLGA-PCL nanofibers fabricated by varying the ratio of PLGA and PCL in the solution, while using a 60/40 DCM/DMF mixture as a solvent. Each polymer solution was loaded into a 5 mL syringe with a 18.5-gauge stainless steel blunt tip needle, and electrospun at 8-10kV using a custom electrospinning device. The polymer solution was deposited (1 mL/hour) using a syringe pump (Harvard Apparatus, Holliston, MA) onto a custom rotating mandrel (20 m/s) to produce aligned fibers.

4.2.2 Nanofiber Characterization

The structural and material properties of the nanofibers were characterized post-fabrication. Nanofiber morphology and organization was imaged using scanning electron microscopy (SEM, 1.0 kV, S-4700, Hitachi, Japan). For SEM analysis, the nanofibers were sputter-coated (108Auto, Cressington Scientific, Watford, UK) with a gold-palladium coating to reduce charging effects. Fiber diameter was quantified using image analysis of SEM micrographs (2000x, n=3 images/group, ImageJ, National Institutes of Health, Bethesda, MD).

Fourier Transform Infrared Spectroscopy (FTIR, FTS 3000MX Excalibur Series, Digilab, Randolph, MA) was performed on as-fabricated nanofibers to further investigate composition. Briefly, FTIR spectra were collected in Attenuated Total Reflectance (ATR) mode (200 scans, resolution at 4 cm−1) and analyzed for characteristic peaks to confirm the presence of both polymers: PLGA (C=O, 1780 cm^{-1}), PCL (C=O, 1724 cm^{-1}).

The mechanical properties of the as-fabricated nanofibers were evaluated under uniaxial tensile testing. Briefly, the meshes (6cm x 1 cm, n=5/group) were secured with custom clamps and mounted on a mechanical testing device (Instron, Model 8841, Norwood, MA) with an average gauge length of 3 cm. The samples were evaluated to failure at a strain rate of 5mm/min along the nanofiber long axis. Nanofiber mesh yield strength and ultimate tensile stress were determined, and elastic modulus was calculated from the linear region of the stress-strain curve.

Polymer degradation was examined *in vitro* after 1, 7, 14, 28, and 56 days of culture in fully supplemented medium. At each time point, total weight loss (n=5) was determined for each sample. After incubation in plain DMEM, the samples were rinsed with deionized water, allowed to dry under vacuum using a lyophilizer for 24 h and the dry weight was measured over time.

4.2.3 Cells and Cell Culture

Human ACL fibroblasts were derived from explant culture of tissues obtained from a patient (male, aged 24) undergoing ACL reconstruction surgery. Briefly, the tissue samples were rinsed in phosphate buffered saline (PBS, Sigma-Aldrich), plated in tissue culture dishes, and maintained in Dulbecco's modifies Eagle medium supplemented with 10% fetal bovine serum, 1% non-essential amino acids, 1% penicillin/streptomycin, 0.1% amphotericin B and 0.1% gentamicin sulfate. The cells from the first migration were subsequently discarded, and the tissue was re-plated in fresh fully supplemented medium. Only cells obtained from the second and third migrations were used in this study because this method has been shown to yield a relatively homogenous fibroblast population. All medium and supplements were purchased from Mediatech (Herndon, VA).

Nanofiber meshes were secured using custom-made clamps to prevent contraction. After ultraviolet sterilization, the nanofibers were pre-incubated in fully supplemented medium at 37C and 5% carbon dioxide for 16 hours. Human ACL fibroblasts (passage 2) were seeded on the nanofiber meshes at a density $3x10^4$ cells/cm^2 and allowed to attach for 15 minutes before the addition of fully supplemented medium. The cells were cultured on the nanofibers for four weeks and the effects of nanofiber composition on cell morphology, gene expression, proliferation, and matrix production were determined throughout the culturing period. In addition, the effects of *in vitro* culture on nanofiber mechanical properties were evaluated over time.

4.2.4 Cell Proliferation and Matrix Production

Total DNA content was measured using the PicoGreen dsDNA assay (Invitrogen). At each time point, the samples (n=5/group) were homogenized in 0.1% Triton-X (Sigma-Aldrich) and subjected to 20 seconds of ultrasonication at 5W. Fluorescence was measured using a microplate reader (Tecan,

Research Triangle Park, NC) at an excitation wavelength of 485 nm and an emission wavelength of 535 nm. A standard curve was derived and used to correlate DNA concentration to fluorescence intensity, and cell number was determined based on a conversion factor of 8pg DNA/cell[104].

Total collagen content per sample (n=5/group) was calculated using the hydroxyproline assay[142]. Briefly, the samples were first desiccated for 24 hours and then digested for 16 hours at 65°C with papain (600 µg protein/ml) in 0.1M sodium acetate (Sigma), 10 mM cysteine HCl (Sigma), and 50 mM ethylenediaminetetraacetate (Sigma). A 40 µl aliquot of the digest was hydrolyzed with 10 µl 10 M sodium hydroxide and autoclaved for 25 minutes. The hydrolyzate was then oxidized by a buffered chloramine-T reagent for 25 minutes before the addition of Ehrlich's reagent. Sample absorbance was measured at 550nm (Tecan), and the collagen content was obtained by interpolation along a standard curve of bovine type I collagen (Sigma).

Collagen distribution was visualized using picrosirius red staining of frozen sections (n=2/group). Briefly, after fixation, samples were embedded in 5% polyvinyl alcohol (PVA, Sigma-Aldrich) and 7-micrometer thick sections (spanning the depth and width of the mesh) were obtained using a cryostat (Hacker-Bright OTF model, Hacker Instruments and Industries, Winnsboro, SC). Collagen distribution was visualized with picrosirius red staining under light microscopy (Axiovert 25, Zeiss).

4.2.5 Nanofiber Mechanical Properties

The effects of *in vitro* fibroblast culture on the mechanical properties of nanofiber mehses were determined at day 1, 7, 14, 28 and 56. For tensile testing, the meshes (6 cm x 1 cm, n=5/group) were secured with custom clamps and mounted on an Instron (Model 8841, Norwood, MA), equipped with a 25 lb load cell. The samples had an average gauge length of 3 cm and were tested to failure along the nanofiber long axis at a strain rate of 5 mm/min. Nanofiber yield strength and ultimate tensile stress were determined, and elastic modulus was calculated from the linear region of the stress-strain curve.

4.2.6 Cell Differentiation

Fibroblastic phenotype was assessed quantitative real-time reverse transcriptase polymerase chain reaction (n=5/group) after 28 days of culture. Total RNA was isolated using the Trizol extraction

method (Invitrogen). Isolated RNA was then reverse-transcribed into complementary DNA using the SuperScript First-Strand Synthesis System (Invitrogen), and the cDNA product was amplified using recombinant Taq DNA polymerase (Invitrogen). Expression of fibroblastic markers type I collagen, type III collagen, fibronectin, tenascin-C, tenomodulin and scleraxis was determined. GAPDH served as the house-keeping gene. All primer sequences were as follows:

Gene	***Sense***	***Anti-Sense***
GAPDH	5'-GGCGATGCTGGCGCTGAGTA-3'	5'-ATCCACAGTCTTCTGGGTGG-3'
Collagen I	5'-TGGTCCACTTGCTTGAAGAC-3'	5'-ACAGATTTGGGAAGGAGTGG-3'
Collagen III	5'-GGCTACTTCTCGCTCTGCTT-3'	5'-CATATTTGGCATGGTTCTGG-3'
Fibronectin	5'-TTGAACCAACCTACGGATGA-3'	5'-AAATGACCACTTCCAAAGCC-3'
Tenascin-C	5'-TGCCCATTACAGGAGGTACA-3'	5'-CACTTTCCTCAAAGCCCTTC-3'
Scleraxis	5'-CAGCGGCACACGGCGAAC-3'	5'-CGTTGCCCAGGTGCGAGATG-3'
Tenodmoulin	5'-TTTGAGGAGGAGGGAGAAGA-3'	5'-TTCCTCACTTGCTTGTCTGG-3'

All genes were amplified for 50 cycles in a thermocycler (Bio-Rad iCycler, Hercules, CA) with a fluorescent probe (SYBR Green, Invitrogen). Quantitative analysis of gene expression was performed using the delta-delta CT method.

4.2.7 Statistical Analysis

Results are presented in the form of mean ± standard deviation, with n equal to the number of samples per group. Two-way ANOVA was used to determine the effects of nanofiber composition on cell degradation, proliferation, matrix deposition, gene expression and mechanical properties. The Tukey-Kramer post-hoc test was used for all pair-wise comparisons and significance was attained at $p<0.05$. Statistical analyses were performed with JMP IN (4.0.4, SAS Institute, Inc., Cary, NC).

4.3 Results

4.3.1 Nanofiber Characterization

The structural and material properties of the nanofiber meshes were characterized post-fabrication. The nanofibers displayed a characteristic aligned morphology when examined via SEM

regardless of composition (*Fig 4.1*). Nanofibers with greater PCL content exhibited a more evident crimp pattern in the fibers. Fiber diameter was also measured for each composition (*Table 4.1*) with no significant difference between groups.

The presence of PLGA and PCL within each composition was verified via FTIR-ATR. The 1724 cm-1 carbonyl peak attributed to PCL was present only within blend and pure PCL nanofibers (*Fig 4.1*). Similarly, the 1780 cm-1 carbonyl peak of PLGA is present only within blend and pure PLGA nanofibers. The relative intensity of these peaks also qualitatively reflects the amount of each polymer present within the blends.

Analysis of blend nanofiber mechanical properties via uniaxial tensile testing revealed a gradient of moduli and a composition-dependent elastic stress-strain curve (*Fig 4.2*). The stress-strain curve of PLGA nanofibers displayed no toe-region whereas the PCL nanofibers demonstrated a toe-region from approximately 0-2.5% strain. The curves of blend nanofibers displayed composition-dependent characteristics, more closely mimicking PLGA in the 1:1 PLGA:PCL blend as opposed to PCL in the 1:5 PLGA:PCL blend. The nanofibers also exhibited composition-dependent elastic moduli (*Table 4.1*). Yield strength was similar regardless of composition, except for the 1:5 PLGA:PCL group for which a significantly higher yield stress (16.6±3.0 MPa) was measured. Ultimate tensile strength increased with increasing PCL content, though 1:5 PLGA:PCL nanofibers exhibited the highest UTS (58.3±7.4 MPa). The ductility of PCL and blend nanofibers was significantly greater than that of PLGA nanofibers.

Composition-dependent degradation was assessed by measuring dry weight over the course of a 56 day *in vitro* culture period (*Fig 4.3*). As shown in Figure X, the PLGA nanofibers exhibited the greatest degradation, with 56.09±3.51% remaining after 56 days. Greater mass was retained with increasing PCL content as PCL nanofibers retained 96.04±0.57% of their initial mass after 56 days.

4.3.2 Cell Attachment and Proliferation

The attachment morphology and growth of human ACL fibroblasts on the nanofiber meshes were visualized using confocal microscopy (*Fig 4.4*). The fibroblasts attached and assumed similar morphologies on all compositions. The cells adopted a phenotypic elongated morphology and aligned in

the direction of the underlying fiber arrangement. This cell shape and organization was maintained over the duration of culture in all groups.

Cell number on all compositions was similar on day one and day seven of culture (*Fig 4.4*). A significantly greater number of cells was measured on the 1:5 PLGA:PCL nanofibers as compared to the 1:1 PLGA:PCL and 1:2 PLGA:PCL groups after 14 days. This trend was maintained after 28 days with the PLGA, PCL and 1:5 PLGA:PCL groups all have a significantly greater number of cells than the 1:1 and 1:2 PLGA:PCL blends.

4.3.3 Matrix Deposition

Total collagen deposition was measured over the duration of the study (*Fig 4.5*). Significantly greater total collagen deposition was measured in the 5:1 and PCL groups after 28 days as compared to that of cells on the 1:1 and 1:2 blend nanofibers. Significantly greater total collagen was also deposited by cells on the 1:5 and PCL nanofibers on day 28 as compared to day 1, with only a mean increase over time observed for the other groups. Collagen distribution as visualized by picrosirius red staining showed similar matrix deposition on all compositions. The greatest matrix penetration into the mesh was observed for the PCL nanofibers.

4.3.5 Mechanical Properties

The mechanical properties of ACL fibroblast-seeded nanofiber meshes were determined over time and compared as a function of composition and culturing time (*Fig 4.6*). A significant decrease in elastic modulus, yield strength, ultimate tensile strength and ductility were measured over time for the PLGA nanofibers. The elastic modulus, ultimate tensile stress and ductility remained statistically similar over the duration of the culture period for blend nanofiber groups as well as the PCL group, except for a significant increase in yield strength measured for the PCL group at day 28 which was maintained through day 56. Nanofibers retained mechanical properties similar to their as fabricated characteristics until day 28. At day 56, the PLGA nanofibers had a significantly lower yield strength, ultimate tensile strength and ductility as compared to all other groups.

4.3.4 Fibroblastic Phenotype

The fibroblastic phenotype of cells was evaluated after 28 days by determining the expression of several characteristic markers, specifically types I and III collagen, fibronectin, tenascin-C and tenomodulin (*Fig 4.7*). The expression of type III collagen, fibronectin and tenascin-C remained similar on all nanofiber compositions. A mean increase in type I collagen expression was measured with increasing PCL content and a significant upregulation in type I collagen expression was measured for cells on PCL nanofibers as compared to those on PLGA nanofibers. A similar trend was observed for tenomodulin expression with greater expression on the PCL nanofibers as compared to PLGA.

4.4 Discussion

This study aimed to identify the optimal composition for the ligament phase of a nanofiber-based synthetic ACL scaffold. In this study, nanofibers with controlled mechanical properties were fabricated using blends of PCL and PLGA to determine the effect of nanofiber composition on human ACL fibroblast response. These nanofibers exhibit mechanical properties within range of the human ACL, with tunable linear elastic and toe-regions, and were found to support the proliferation and biosynthesis of human ACL fibroblasts.

The mechanical properties of the blend nanofibers varied as a function of PLGA and PCL content. Specifically, it was shown that a higher PLGA to PCL ratio resulted in an increase elastic modulus, lower yield strength and greater toe-region, as expected when comparing the mechanical properties of pure PLGA and PCL nanofibers. Baker *et al.* reported similarly tunable characteristics for blended PLGA and PCL nanofibers containing approximately 60% PLGA and 40% PCL[189]. Interestingly, in this study, blending also resulted in nanofibers with unique characteristics such as the 5:1 PLGA:PCL nanofibers which exhibited the greatest ultimate tensile strength and the 1:1 PLGA:PCL nanofibers which had the greatest ductility. These findings suggest interactive effects between PLGA and PCL that result in unique mechanical properties when the two polymers are blended together. Degradation kinetics of the nanofibers was also modulated by PLGA and PCL content. As expected, increasing PLGA content resulted in a more rapid degradation rate though the inclusion of PCL resulted in a significantly greater residual mass after 56 days of culture in all blend nanofibers, as compared to

PLGA nanofibers. These findings demonstrate that nanofiber degradation can be controlled to suit specific tissue engineering applications. Collectively, these findings suggest that a blend nanofiber system is optimal for ACL tissue engineering as all of the compositions had mechanical properties within range of the native tissue and allows for modulation of the degradation rate to match neo-tissue formation.

In terms of ACL fibroblast response, while similar numbers of cells attached on all compositions, a significantly greater number of cells was measured on the 1:5 PLGA:PCL nanofibers as compared to the 1:1 PLGA:PCL and 1:2 PLGA:PCL groups after 14 days. Further, this trend was maintained after 28 days with the PLGA, PCL and 1:5 PLGA:PCL groups all having a significantly greater number of cells than the 1:1 and 1:2 PLGA:PCL blends. These findings suggest composition-based effects on fibroblast proliferation but do not elucidate a composition-based trend between groups. Baker *et al.* investigated PLGA and PCL foams on urinary tract stromal cells for bladder tissue engineering[189]. It was reported that cell attachment and proliferation was increased on the PCL foams as compared to PLGA foams. It was hypothesized that this occurred because the PCL foams more closely mimicked the mechanical properties of the native bladder. In this study, the 1:5 PLGA:PCL and PCL nanofibers were also more within range of the native human ACL, with elastic moduli of 205±41 MPa and 170±15 MPa respectively, as compared to the native ACL modulus of 49-163 MPa[186].

Total collagen deposition was measured to assess matrix production on each nanofiber composition. Interestingly, we observed that nanofibers incorporating greater amounts of PCL resulted in the highest total collagen deposition indicating that PCL directs human ACL fibroblasts towards a matrix deposition response as compared to PLGA. These findings were also supported by a significant increase in type I collagen expression after 14 days on PCL nanofibers and may again be attributable to the lower rigidity associated with increasing PCL content. Substrate rigidity modulating cell response has been extensively investigated on a variety of cell types[121], in particular for human mesenchymal stem cells, in which differentiation has shown to be regulated by matrix rigidity[121] and indicates that ligament fibroblasts may be similarly responsive to their culture environment. In addition to type I collagen upregulation, the upregulation of tenomodulin was also reported on the PCL nanofibers. The upregulation of this protein, a late marker of tendon and ligament formation[162], may indicate a long-term tissue

formation response as the PCL nanofibers more closely mimic the native ACL environment. The increased matrix synthesis on the 5:1 blend and PCL nanofibers and marker upregulation suggest that, in terms of cell response, nanofibers primarily composed of PCL may be optimal for ACL tissue engineering.

Collectively, the results of this study suggest that a 1:5 PLGA:PCL blend is the optimal composition for nanofibers used for ligament tissue engineering. However, further studies will be required in order to further investigate these findings. In particular, *in vivo* studies are required to determine the degradation rate of each composition within a physiologic environment and also to select the optimal composition that balances nanofiber degradation with neo-ligament formation.

4.5 Conclusions

This study focused on determining the optimal nanofiber composition for the ligament phase of the ACL scaffold. Two biodegradable polymers, PCL and PLGA, were blended to fabricate nanofibers with tunable mechanical properties and degradation characteristics. Mechanical properties of all compositions remained within range of the native human ACL. Although cells remained viable and proliferated regardless of composition, the greatest matrix deposition and fibroblastic marker expression was measured on nanofibers composed primarily of PCL. In contrast, the slow degradation rate of PCL may hinder long-term matrix formation within the scaffold, there by indicating that incorporation of PLGA is necessary to balance degradation kinetics and cell response. These findings suggest that a 1:5 PLGA:PCL blend is optimal for the ligament phase of the scaffold. The findings of *Chapters 2-4* demonstrate that an aligned nanofiber matrix composed of a 1:5 PLGA:PCL blend coupled with mechanical stimulation is suitable for ligament regeneration. In the following chapter, the bone phase will be optimized.

Table 4.1.Structural and mechanical characteristics of nanofibers as function of composition.

	Elastic Modulus (MPa)	Yield Strength (Mpa)	UTS (MPa)	Ductility (%)	Fiber Diameter (nm)
PLGA	373 ± 99*	10.7 ± 2.4	13.5 ± 2.4	39 ± 1.6*	615 ± 152
1:1 PLGA:PCL	326 ± 31*	8.87 ± 1.0	16.3 ± 1.5	85 ± 3.9*	663 ± 156
1:2 PLGA:PCL	330 ± 37	10.3 ± 0.7	36.6 ± 4.2	69 ± 3.8	678 ± 109
1:5 PLGA:PCL	227 ± 45	16.6 ± 3.0	58.3 ± 7.4*	67 ± 1.8	691 ± 181
PCL	170 ± 15	11.6 ± 0.8	43.5 ± 6.7*	65 ± 3.5	712 ± 146
Human ACL	49 - 163	-	16.3 – 36.4	25 – 40	20 – 45

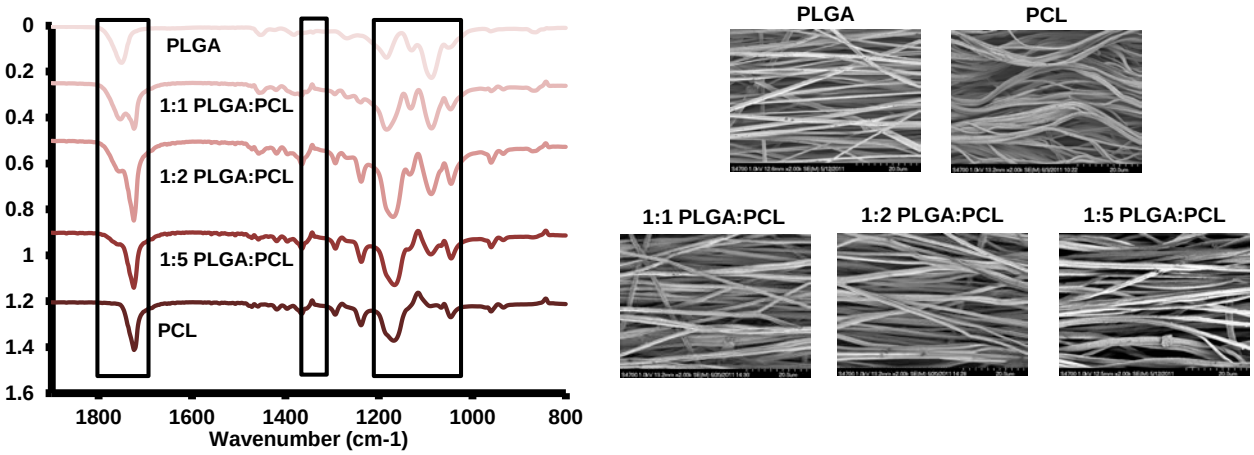

Figure 4.1. Blend nanofiber characterization. Incorporation of PLGA and PCL was verified via FTIR analysis. Blends displayed peaks at 1172, 1361, and 1724 cm-1 attributable to PCL and at 1780 cm-1 for PLGA. Fiber morphology was also verified via SEM with scaffolds displaying characteristic aligned nanofiber morphology.

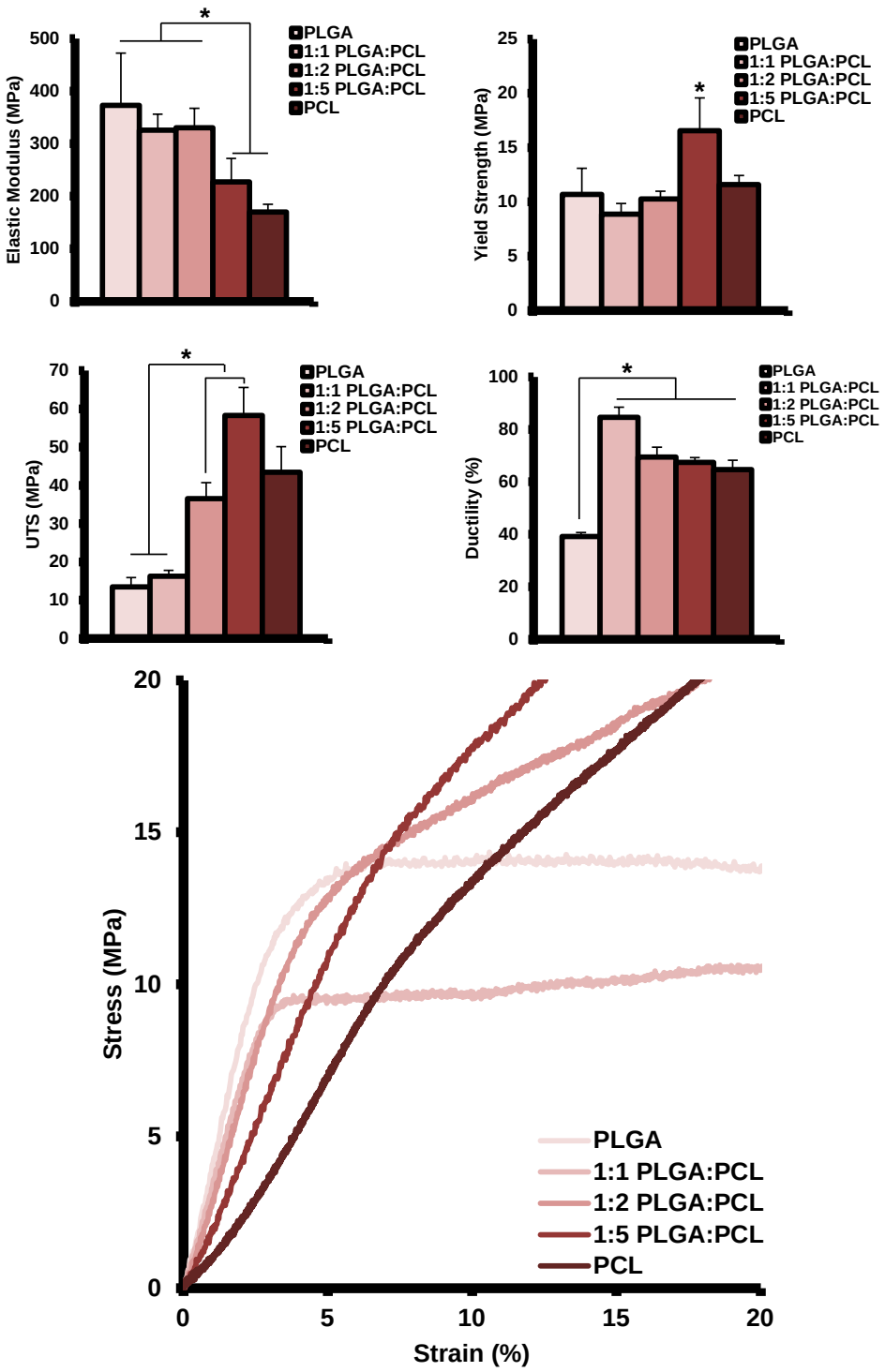

Figure 4.2. Effect of nanofiber composition on mechanical properties. Nanofiber mechanical properties were modulated by the ratio of PLGA to PCL. Elastic modulus decreased with increasing PCL incorporation while 1:5 blend nanofibers exhibited the highest ultimate tensile strength (UTS) and yield strength.

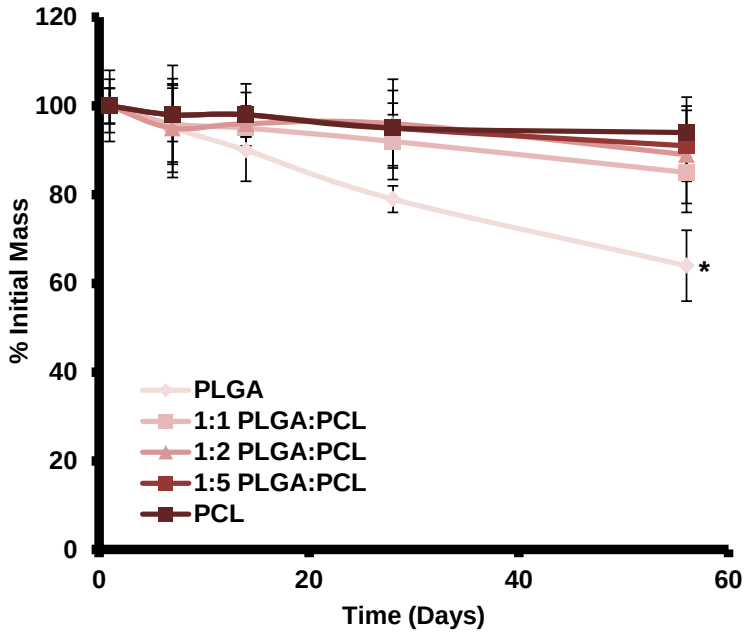

Figure 4.3. Effect of nanofiber composition on degradation. Degradation was characterized by measuring dry weight over time after incubating nanofiber meshes in culture media. Dry weight was the lowest for the PLGA nanofibers after 56 days of culture, indicating faster degradation than PCL-containing nanofibers.

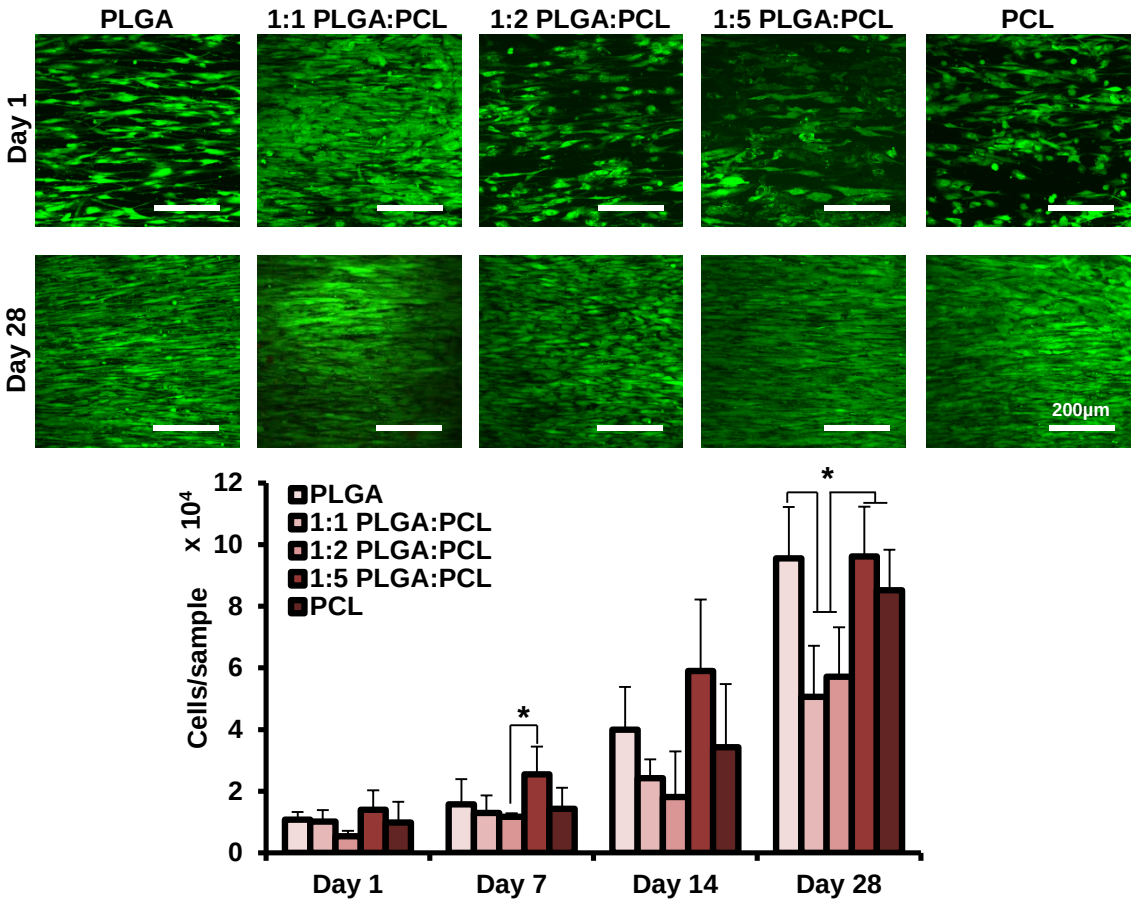

Figure 4.4. Effect of nanofiber composition on cell attachment and proliferation. Cell attachment was similar on all compositions with cells displaying a characteristic elongated morphology and conforming to the alignment of the underlying nanofibers. Cells proliferated on all compositions over time with a significantly greater number of cells present on PLGA, 1:5 PLGA:PCL and PCL scaffolds after 28 days of culture.

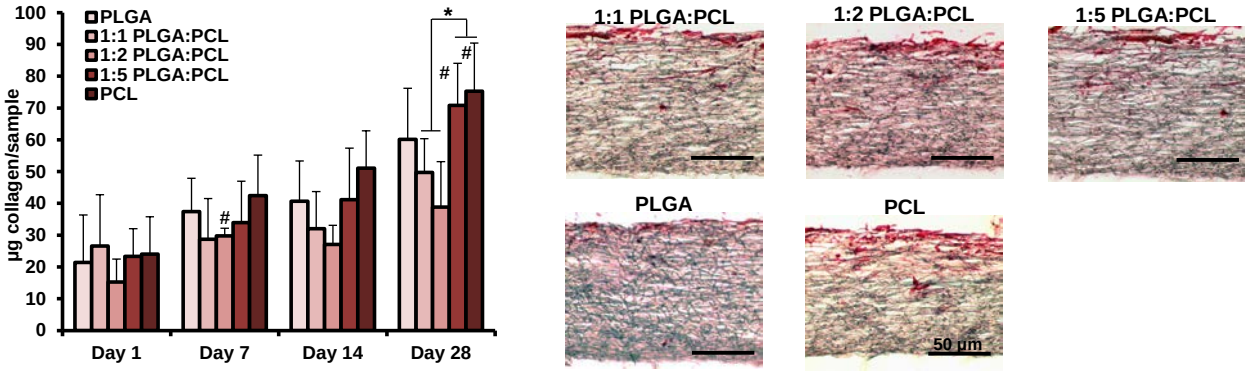

Figure 4.5. Effect of nanofiber composition on collagen deposition. Significantly greater total collagen deposition was measured in the 5:1 and PCL groups after 28 days as compared to that of cells on the 1:1 and 1:2 blend nanofibers. Significantly greater total collagen was also deposited by cells on the 1:5 and PCL nanofibers on day 28 as compared to day 1, with only a mean increase over time observed for the other groups. Matrix deposition as visualized via picrosirius red staining (red=collagen) indicated greatest collagen penetration into PCL scaffolds.

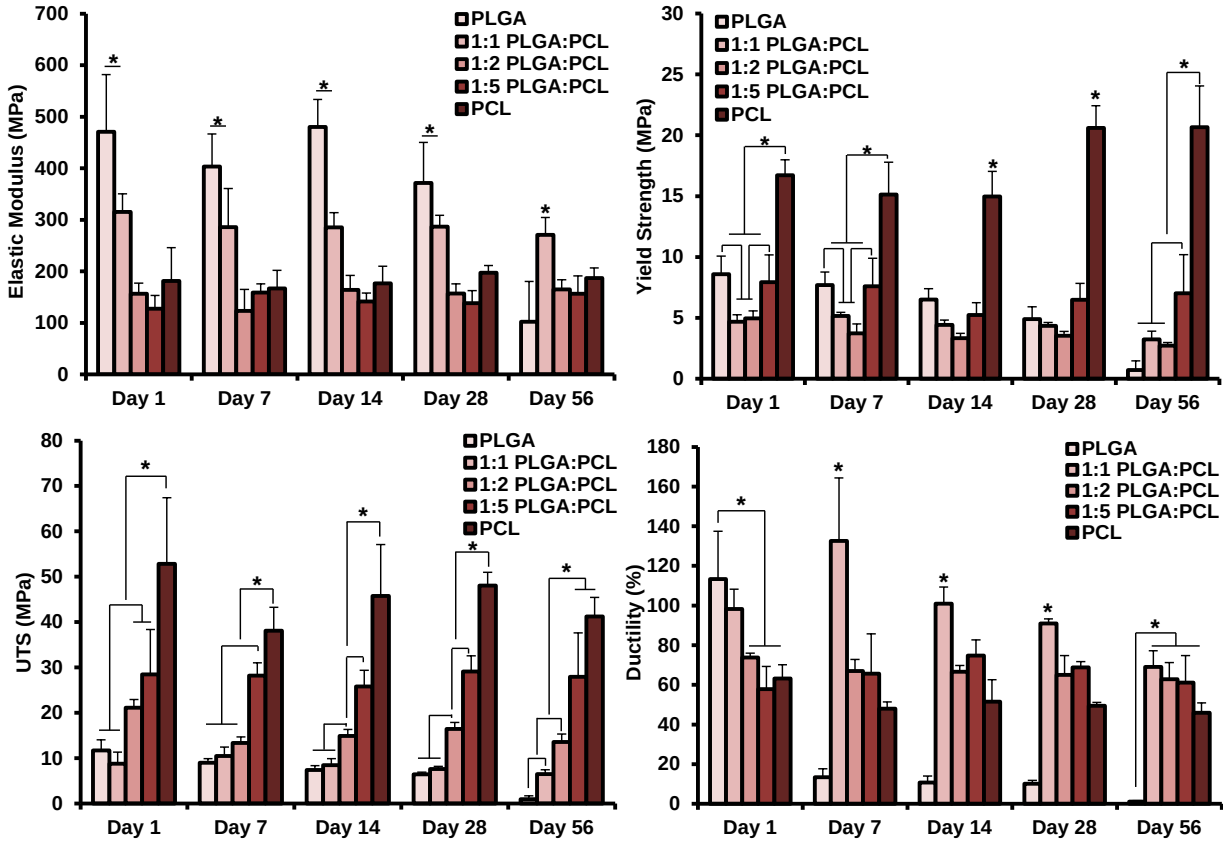

Figure 4.6. Effect of *in vitro culture* on nanofiber mechanical properties. A significant decrease in elastic modulus, yield strength, ultimate tensile strength and ductility were measured over time for the PLGA nanofibers. The elastic modulus, ultimate tensile stress and ductility remained statistically similar over the duration of the culture period for blend nanofiber groups as well as the PCL group, except for a significant increase in yield strength measured for the PCL group at day 28 which was maintained through day 56. At day 56, the PLGA nanofibers had a significantly lower yield strength, ultimate tensile strength and ductility as compared to all other groups.

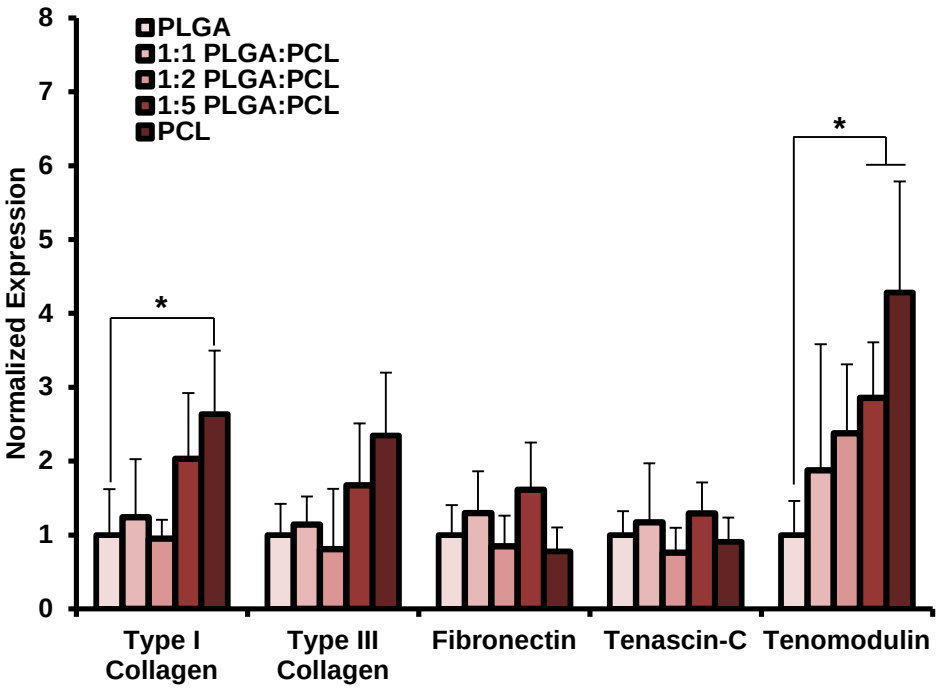

Figure 4.7. Effect of nanofiber composition on fibroblastic phenotype at day 28. A mean increase in type I collagen expression was measured with increasing PCL content and a significant upregulation in type I collagen expression was measured for cells on PCL nanofibers as compared to those on PLGA nanofibers after 28 days of culture

CHAPTER 5: BONE PHASE: THE EFFECT OF NANOFIBER MINERAL CONTENT ON HUMAN MESENCHYMAL STEM CELL OSTEOGENESIS

5.1 Introduction

While the previous chapters focused on the design and optimization of the ligament phase, demonstrating that fibroblastic differentiation of MSCs can be induced using mechanical stimulation as well as chemical stimulation. In addition, it was shown that nanofibers composed of a blend of PLGA and PCL are suitable for ligament tissue formation. This chapter focuses on the next phase of the multi-phased synthetic ACL scaffold, the bone phase.

The bone phase of the ACL scaffold must be osteconductive in order to integrate with subchondral bone within the femoral and tibial tunnels after ACL reconstruction. In addition, it must also be osteoinductive in order to induce osteoblastic differentiation of MSCs and thereby enable cell-mediated bone formation. To this end, composite polymer-ceramic nanofibers containing hydroxyapatite will be investigated for the bone phase. Hydroxyapatite is particularly advantageous for this purpose as it is the primary mineral found in bone and has been widely used for commercial bone regeneration products[190-192]. To optimize the composition of the bone phase, this chapter investigates the effect of nanofiber mineral content on osteogenic differentiation of MSCs.

5.1.1 Background and Motivation

Polymer and polymer-ceramic nanofibers have been widely investigated for bone tissue engineering. Composite polymer-ceramic nanofibers have been reportedly fabricated by incorporating nanoparticles of hydroxyapatite (HA)[33;193-195], beta tricalcium phosphate (TCP)[33;196] or demineralized bone powder directly into the fibers[197]. Hydroxyapatite is particularly advantageous for this purpose as it is the primary mineral found in bone and has been widely used for commercial bone regeneration products[190-192]. In addition, composite nanofibers incorporating HA have been shown to promote osteoblast proliferation and enable mineralized tissue formation both *in vitro* and *in vivo*[33;196;197].

In addition to scaffold parameters, the incorporation of cells into tissue engineered systems has been established a method to augment tissue formation. Mesenchymal stem cells (MSCs) are considered an ideal cell source for this purpose as they can be easily obtained from the bone marrow, as well as other tissues, and can readily differentiate into an osteoblastic phenotype using chemical induction

medium or scaffold-based cues[26;198]. Dexamethasone and bone morphogenetic protein-2 (BMP-2) are among the most common chemical supplements used to induce osteogenic differentiation[26]. In contrast, the precise scaffold-based cues to drive osteogenic differentiation have not been determined. Reports have indicated that cues such as scaffold mineral incorporation[33;197;199] and surface roughness[200] can induce the MSC mineralization. However, many studies investigating the use of MSCs for bone tissue engineering have been performed in conjunction with osteogenic induction medium, making it difficult to identify the independent effects of scaffold-based and chemical cues.

This study focuses on identifying the optimal nanofiber mineral content for the osteogenic differentiation of MSCs, in the absence of osteogenic chemical factors, in order to identify parameters to direct osteogenic differentiation of MSCs on nanofibers. To this end, HA nanoparticles will be incorporated into nanofibers to fabricate a composite polymer-ceramic system. Ostegenesis will be evaluated in terms of cell mineralization potential, mineralized matrix production and osteogenic marker expression. It is hypothesized that increasing nanofiber mineral content, in terms of hydroxyapatite nanoparticle weight-percent, will increase the expression of osteogenic markers and enhance mineralized matrix deposition.

5.1.2 Objectives

The objective of this study is to determine the optimal nanofiber mineral content to support bone formation and induce MSC osteogenesis. Previous studies have reported that the incorporation of ceramics, such as HA and tricalcium phosphate, into polymer nanofibers can modulate the proliferation and osteoblastic activity of stem cells[199]. In addition, it has been shown that the effect of ceramic presence can be content dependent, such as in studies performed by He *et al.* with composite PLGA microspheres incorporating various ratios of hydroxyapatite[201], where greater mineral content resulted in increased mineralized tissue formation. It is hypothesized that increasing nanofiber mineral content, in terms of hydroxyapatite nanoparticle weight-percent, will increase the expression of osteogenic markers and enhance mineralized matrix deposition.

5.2. Materials and Methods

5.2.1 Nanofiber Mesh Fabrication

Composite polymer-ceramic nanofibers were fabricated via electrospinning. Briefly, a 5:1 mixture of PLGA and PCL was dissolved in a 60:40 mixture of dichloromethane and dimethyl formamide (DMF) and mixed for one hour. Simultaneously, a suspension of HA nanoparticles (Nanocerox, Ann Arbor, MI) and DMF was sonicated for one hour. The nanoparticle suspension and polymer solution were then mixed rigorously to produce an 18% (wt%) polymer solution containing 0%, 15%, 25% or 35% (wt ceramic/wt polymer) HA. To produce the nanofibers, each polymer solution was loaded into a 5 mL syringe with a 18.5-gauge stainless steel blunt tip needle, and electrospun at 8-10kV using a custom electrospinning device. The polymer solution was deposited (1 mL/hour) using a syringe pump (Harvard Apparatus, Holliston, MA) onto a rotating mandrel (20m/s) to produce the aligned fibers.

5.2.2 Nanofiber Characterization

As-fabricated nanofibers were imaged with secondary scanning electron microscopy (SEM, 1-2 kV, Hitachi 4700, Hitachi Ltd.) to evaluate nanofiber morphology. Nanofibers were sputter-coated (108 Auto, Cressington Scientific, Watford, UK) with gold-palladium to reduce charging effects. Nanofiber diameter was quantified via image analysis of SEM micrographs (2000x, n=3 images/group, ImageJ, NIH, Bethesda, MD). The elemental composition of as-fabricated nanofibers was evaluated with backscattered SEM coupled with energy dispersive x-ray analysis (EDAX). After coating, the samples were imaged in the backscattered mode and EDXA was performed at 2 kV.

To further assess nanofiber mineral presence, Fourier Transform Infrared Spectroscopy (FTIR, FTS 3000MX Excalibur Series, Digilab, Randolph, MA) was performed on as-fabricated nanofibers. Briefly, FTIR spectra were collected in Attenuated Total Reflectance (ATR) mode (200 scans, resolution at 4 cm−1) and analyzed for characteristic peaks: PLGA (C=O, 1780 cm-1), PCL (C=O, 1724 cm-1) and HA (PO4 bending, 605 cm-1 and 560 cm-1).

The mineral content (n=5/group) of the as-fabricated nanofibers was evaluated with thermogravimetric analysis (TGA, Q50, TA Instruments, New Castle, DE). The sample was loaded into a calibrated platinum pan, heated to 100oC, followed by a 20ºC/minute ramp to 700ºC, and the residual

weight was then determined. The degradation temperature of PLGA and PCL is approximately 400°C, therefore the residual weight corresponded to the weight percent of mineral in the nanofibers.

5.2.3 Cells and Cell Culture

Human mesenchymal stem cells (MSC) were obtained commercially (Lonza, Walkersville, MD) and maintained in culture with DMEM containing 10% fetal bovine serum (FBS, embryonic stem cell certified, Atlanta Biologicals, Atlanta, GA), 1% penicillin-streptomycin, 1% non-essential amino acids, 0.1% amphotericin B and 0.1% gentamicin. All media supplements were purchased from Cellgro-Mediatech unless otherwise specified. Cells were cultured to 80% confluence and then passaged using 0.25% trypsin/1 mM ethylenediaminetetraacetate (EDTA) and re-plated at a density of $5x10^3$ cells/cm^2. Passage 2-3 cells were used for nanofiber mesh seeding.

5.2.4 Cell Proliferation

Total DNA content was measured using the PicoGreen dsDNA assay (Invitrogen). At each time point, the samples (n=5/group) were homogenized in 0.1% Triton-X (Sigma-Aldrich) and subjected to 20 seconds of ultrasonication at 5W. Fluorescence was measured using a microplate reader (Tecan, Research Triangle Park, NC) at an excitation wavelength of 485 nm and an emission wavelength of 535 nm. A standard curve was derived and used to correlate DNA concentration to fluorescence intensity, and cell number was determined based on a conversion factor of 8pg DNA/cell[104].

5.2.5 Matrix Production and Mineralization

Total collagen content per sample (n=5/group) was calculated using the hydroxyproline assay[142]. Briefly, the samples were first desiccated for 24 hours and then digested for 16 hours at 65°C with papain (600 µg protein/ml) in 0.1M sodium acetate (Sigma), 10 mM cysteine HCl (Sigma), and 50 mM ethylenediaminetetraacetate (Sigma). A 40 µl aliquot of the digest was hydrolyzed with 10 µl 10 M sodium hydroxide and autoclaved for 25 minutes. The hydrolyzate was then oxidized by a buffered chloramine-T reagent for 25 minutes before the addition of Ehrlich's reagent. Sample absorbance was

measured at 550nm (Tecan), and the collagen content was obtained by interpolation along a standard curve of bovine type I collagen (Sigma).

Collagen distribution (n=2/group) was also visualized using picrosirius red staining of frozen sections. Briefly, after fixation, samples were embedded in 5% polyvinyl alcohol (PVA, Sigma-Aldrich) and 7-micrometer thick sections (spanning the depth and width of the mesh) were obtained using a cryostat (Hacker-Bright OTF model, Hacker Instruments and Industries, Winnsboro, SC). Collagen distribution was visualized with picrosirius red staining under light microscopy (Axiovert 25, Zeiss).

Mineralization potential was determined by measuring ALP activity (n=5) using an colorimetric assay based on the hydrolysis of *p*-nitrophenyl phosphate (*p*NP-PO_4) to *p*-nitrophenol (pNP)[202]. Briefly, the samples were lysed in 0.1% Triton-X solution, then added to *p*NP-PO_4 solution (Sigma) and allowed to react for 30 min at 37°C. The reaction was terminated with 0.1 N NaOH (Sigma), and sample absorbance was measured at 415nm using a microplate reader (Tecan). In addition, mineral distribution (n=2/group) was evaluated by von Kossa staining of frozen sections with 5% silver nitrate, followed by 30 minutes of UV exposure[203]. Media calcium concentrations (n=5) were quantified using the Arsenazo III dye (Pointe Scientific, Lincoln Park, MI) and a malachite green, ammonium molybdate based phosphate colorimetric assay (BioVision, San Francisco, CA) was used to assess media phosphate concentration. Both assays were read at an absorbance wavelength of 620nm.using a microplate reader[204].

5.2.6 Cell Differentiation

Osteoblastic differentiation of MSCs was assessed via quantitative real-time reverse transcriptase polymerase chain reaction (qPCR, n=5/group) after 14 and 28 days. Total RNA was isolated using the Trizol extraction method (Invitrogen). Isolated RNA was then reverse-transcribed into complementary DNA using the SuperScript First-Strand Synthesis System (Invitrogen), and the cDNA product was amplified using recombinant Taq DNA polymerase (Invitrogen). Expression of osteogenic markers type I collagen, RUNX-2, bone sialoprotein (BSP), osteocalcin, osteopontin, and osteonectin was determined. GAPDH served as the house-keeping gene. All primer sequences are listed in Table 2. All genes were amplified for 50 cycles in a thermocycler (Bio-Rad iCycler, Hercules, CA) with a fluorescent probe (SYBR

Green, Invitrogen). Quantitative analysis of gene expression was performed using the delta-delta CT method.

5.2.7 Statistical Analysis

Results are presented in the form of mean ± standard deviation, with n equal to the number of samples per group. Two-way ANOVA was used to determine the effects of nanofiber mineral content on cell proliferation, matrix deposition and differentiation. The Tukey-Kramer post-hoc test was used for all pair-wise comparisons and significance was attained at $p<0.05$. Statistical analyses were performed with JMP IN (4.0.4, SAS Institute, Inc., Cary, NC).

5.3 Results

5.3.1 Nanofiber Characterization

A distinct aligned nanofiber morphology was observed using SEM for all groups. The addition of ceramic nanoparticles resulted in visible nodules on the surface of the fibers, evident at higher magnifications (*Fig. 5.1*). The elemental composition of the fibers was also determined using EDAX (*Fig 5.1*). The incorporation of was confirmed for the 15%, 25% and 35% HA groups with the presence of calcium (Ca) and phosphorous (P) peaks. No such peaks were observed for the 0% HA group, confirming the lack of ceramic content. The chemical composition of the nanofibers, further investigated via FTIR-ATR, confirmed the presence of ceramic within the nanofibers (*Fig 5.2*). Typical infrared bands for the PCL and PLGA stretching modes were observed in the ceramic-free (0% HA) and ceramic-containing (15%, 25%, 35% HA) groups. The composite nanofibers showed characteristic peaks corresponding to the PO_4^{3-} absorption bands at 564, 603 and 1031 cm^{-1} attributable to hydroxyapatite, as has been reported previously[33;205;206]. Ceramic content was verified using TGA to confirm mineral content of the composite nanofibers. Residual weight of the 0% HA nanofibers was 0.96±0.41% and 16.4±1.20%, 26.2±0.39% and 35.8±0.31% for the 15%, 25% and 35% HA nanofibers, respectively.

5.3.2 Cell Proliferation and Collagen Deposition

Cells remained similarly viable on all groups over time as evident in the confocal microscopy images, with green staining for live cells (*Fig 5.3*). The cells also displayed a characteristic spindle-shaped aligned morphology in the direction of the underlying fiber alignment. In terms of cell proliferation, no significant difference in cell number was measured between groups at any of the time points (*Fig 5.3*). However, a significant increase in cell number was measured in all groups between day 1 and day 7 as well as between days 7 and 14, indicating that cells proliferated over time.

Total collagen content was measured to assess cell matrix deposition over time. No significant difference in total collagen was measured between groups at any time points (*Fig 5.4*). A mean increase in total collagen was observed over time in all groups and significantly greater total collagen was present on all groups after 28 days as compared to day 1. Collagen distribution was also visualized via picrosirius red staining, which stains for collagen types I, II and III, of histological sections (*Fig 5.4*). Similar collagen distribution was evident in all groups, with collagenous matrix primarily found on the seeded surface of the mesh.

5.3.3 Mineralization

Alkaline phosphatase activity was quantified to measure MSC mineralization potential over time (*Fig. 5.5*). A significant increase in ALP activity was measured after 12 hours of culture on the 25% and 35% HA groups as compared to the 0% and 15% HA groups. Significantly elevated ALP activity in these groups persisted through day 7, after which it returned to basal levels similar to the 0% and 15% HA groups. Mineral deposition visualized via von Kossa staining showed similar mineral distribution on the composite nanofibers and no mineral present in the 0% HA group (*Fig 5.5*).

Media calcium and phosphate concentration was also measured over the duration of the study to better understand mineralization mechanics on the nanofibers (*Fig. 5.6*). Significantly lower media calcium content was measured in the 35% HA group after 7 days of culture and this difference was maintained through the 28 day culture period. Significantly lower media calcium content was also measured in the 25% HA though only at day 28. Measurement of media phosphate concentration showed

no significant differences between groups, though a mean decrease in phosphate content was observed with increasing nanofiber ceramic content at all time points.

5.3.4 Cell Differentiation

The expression of several key osteogenic markers was evaluated after 28 days to determine if MSCs underwent osteogenic differentiation (*Fig. 5.7*). While type I collagen expression was not upregulated for any groups, the expression of ALP, RUNX-2 and osteocalcin was increased by cells on the 25% and 35% HA nanofibers. In addition, osteopontin and osteonectin were upregulated on the 35% HA nanofibers only. A mean increase in BSP expression was also measured on the 35% HA nanofibers as compared to all other groups.

5.4 Discussion

The objective of this study was to determine the optimal nanofiber mineral content to induce osteoblastic differentiation of MSCs in the absence of osteogenic chemical factors. To this end, the response of MSCs was evaluated over time on nanofibers both with and without hydroxyapatite nanoparticles. It was found that MSCs underwent osteogenic differentiation in response to nanofiber mineral content alone. Interestingly, differentiation, in terms of ALP activity and osteogenic marker expression, was only observed on the nanofibers with the greatest mineral content and osteogenic response increased with increasing nanofiber mineral content, indicating that a minimum threshold of mineral is required to elicit a response.

In terms of mineralization, an increase in ALP activity early within the culture period on the 25% and 35% HA nanofibers, beginning at the 12 hour time point and remaining elevated until 7 days of culture. This finding likely indicates a rapid mineralization response by the cells as ALP is known to increase inorganic phosphate concentration and thereby promote mineralization[207]. This response also suggests that the composite nanofibers quickly induce a mineralization response by the cells, potentially attributable to the increase surface roughness of the mineral-containing fibers. It has been reported that nano-scale surface roughness regulates osteoblast response[208;209] and can also induce an osteogenic response by stem cells[210-213]. For example, Balloni et al. reported the upregulation of

RUNX-2, BMP-2 and osterix by MSCs cultured on an acid-etched titanium surfaces as compared to a machined titanium surface. Similarly, the nodules visible on the surface of the composite nanofibers may represent a rougher, osteoinductive surface for attached MSCs.

In addition, in this study, a sustained decrease in media calcium content was measured for MSCs cultured on the 35% HA nanofibers after 7 days, which persisted through the remainder of the 28 day culture period. A significant decrease in media calcium content was also measured for the 25% HA group, through only after 28 days. These finding suggests that cell-mediated mineralization is occurring as calcium and phosphate are precipitating from the media for mineralized matrix formation, as it has been shown that large quantities of these ions are accumulated during the cellular mineralization process[214;215]. Though, only a mean decrease in phosphate concentration was measured with increasing nanofiber mineral content. It is also notable that the decrease in calcium concentration occurs earlier on the 35% HA nanofibers, indicating that greater nanofiber content elicits a more rapid mineralization response.

Analysis of MSC differentiation reveled that several osteogenic markers were upregulated after 28 days on the 25% and 35% HA nanofibers. Specifically, ALP and RUNX-2, a transcription factor essential for osteoblastic differentiation, along with osteocalcin, a pro-osteoblastic protein characterized as a late marker of bone formation were upregulated on the 25% and 35% HA nanofibers. Interestingly, osteopontin, a protein which plays a role in anchoring osteoclasts, and osteonectin, an important factor in bone mineralization, both of which are characterized as early markers of bone formation, were only upregulated on the 35% HA nanofibers. These results could be attributed to different temporal sequence of osteoblastic marker expression by MSCs on the 25% HA nanofibers as compared to the 35% HA nanofibers, with a more complete phenotype assumed by cells in the 35% HA group.

Previous studies exploring the effects of nanofiber mineral content have also found that ceramic incorporation can induce MSC osteogenesis in the absence of osteogenic chemical factors. Peng et al. reported increased ALP activity as well as upregulation of ALP and osteocalcin by murine MSC on composite chitosan-HA nanofibers containing 30% HA[216]. Similarly, Lu et al. reported the upregulation of ALP and osteocalcin by rat MSC cultured on poly(3-hydroxybutyrate-co-3-hydroxyvalerate) (PHBV) nanofibers containing 10% HA[217]. Phipps et al. reported that a composite PCL, collagen and 10% HA

mesh can increase phosphorylate FAK production, a signaling molecule in osteogenic differentiation, in human MSC[218]. Other ceramics have also been shown to be capable of directing osteogenesis when incorporated into nanofibers. For example, Polini et al. demonstrated that nanofibers containing approximately 35% tricaclium phosphate (TCP) nanoparticles upregulate BSP and RUNX-2 expression in human MSC[33]. However, unlike previous reports, this study represents a systematic investigation into the requirements to drive osteoblastic differentiation of MSCs on nanofibers without concurrent chemical factors, elucidating that a threshold of ceramic particles is required.

Several groups have also demonstrated that osteogenesis of MSC on composite nanofibers can be further enhanced when combined with osteogenic medium, typically containing dexamethasone or BMP-2. Chen et al. reported elevated ALP activity by MSCs on unaligned PCL nanofibers incorporating 50% HA and also similarly demonstrated that a threshold of mineral was required, as no difference in ALP activity was measured on nanofibers containing 25% HA. Lee et al. reported upregulation of ALP and osteocalcin on PLGA nanofibers containing approximately 28% HA. Lastly, Ko *et al.* reported increased human MSC calcium deposition composite poly(L-lactide) (PLA) and demineralized bone powder (DBP) nanofibers containing approximately 17% DBP.

In summary, the composite polymer-ceramic nanofiber system presented here represents a promising system for bone tissue engineering. The results of this study demonstrate that composite nanofibers can result in osteogenic differentiation of MSCs, in the absence of chemical stimulation, provided a sufficient threshold of mineral is incorporated. These findings indicate that bone tissue engineering scaffolds will benefit from increased mineral content that more closely mimics the composition of native bone.

5.5 Conclusions

Collectively, the results of this study provide the optimal design specifications for the bone phase of the multi-phased ACL scaffold. A nanofiber-based system incorporating 35% HA results in a mineralization response by MSCs as well as the upregulation of several osteoblastic markers. Therefore the bone phase of the synthetic ACL scaffold will consist of composite polymer-ceramic nanofibers containing 35% HA and the interface phase will be optimized in the following chapters.

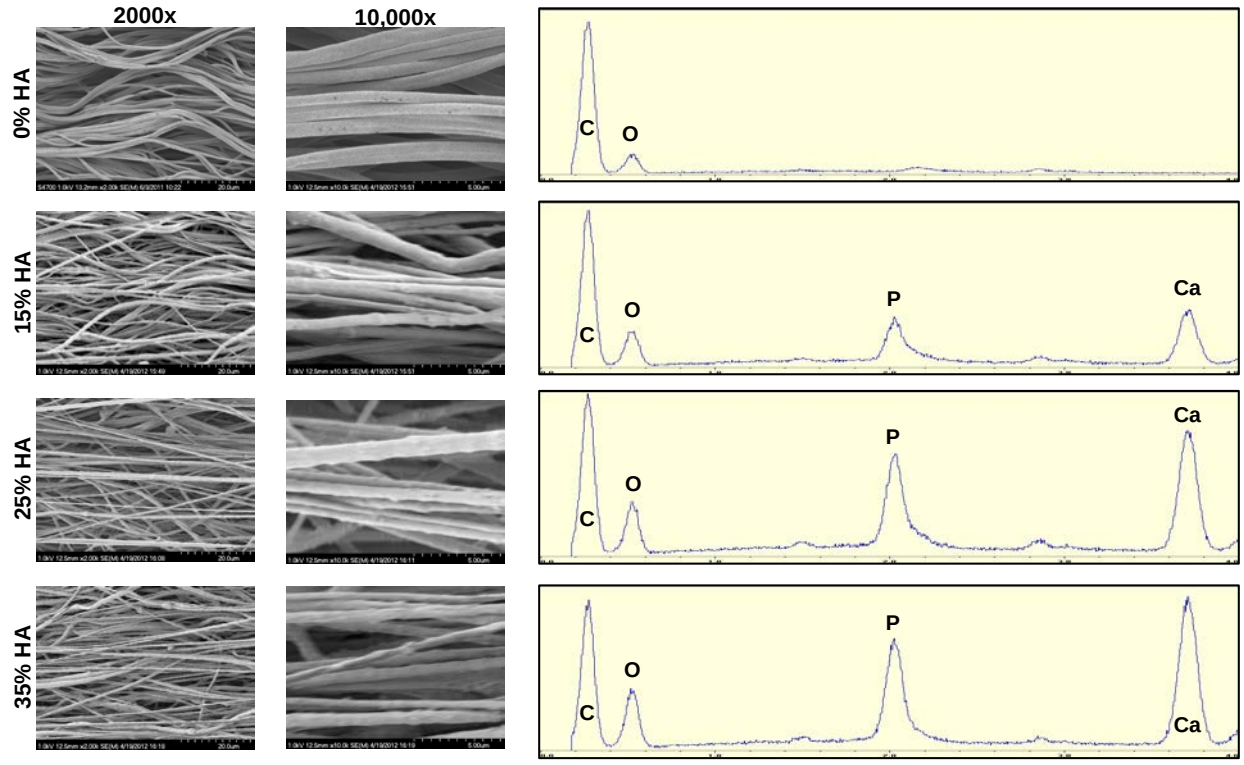

Figure 5.1. Composite polymer-ceramic nanofiber morphology and composition. Nanofibers were examined under SEM and displayed a characteristic aligned nanofiber morphology. More visible nodules were evident on the surface of the fibers with increasing mineral content. EDAX analysis confirmed the presence of Ca and P within nanofibers containing HA.

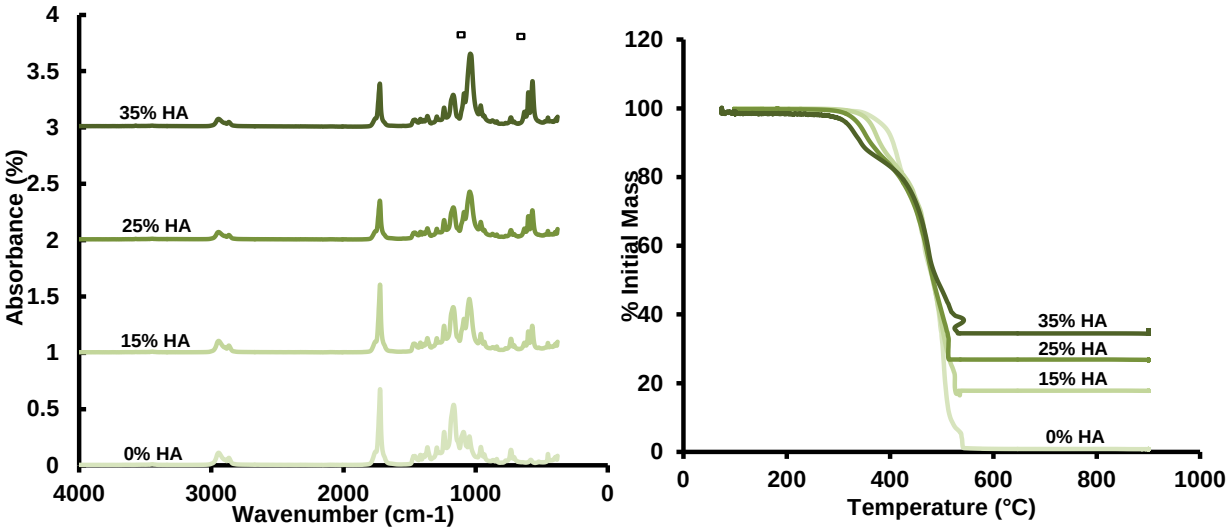

Figure 5.2. Composite polymer-ceramic nanofiber composition and mineral incorporation. FTIR-ATR was used to assess nanofiber chemical composition. Infrared bands for the PCL and PLGA stretching modes were observed in the ceramic-free (0% HA) and ceramic-containing (15%, 25%, 35% HA) groups. The composite nanofibers showed characteristic peaks corresponding to the PO_4^{3-} absorption bands at 564, 603 and 1031 cm^{-1}. Ceramic content was verified using TGA to confirm mineral content. Residual weight of the 0% HA nanofibers was 0.96±0.41% and 16.4±1.20%, 26.2±0.39% and 35.8±0.31% for the 15%, 25% and 35% HA nanofibers, respectively.

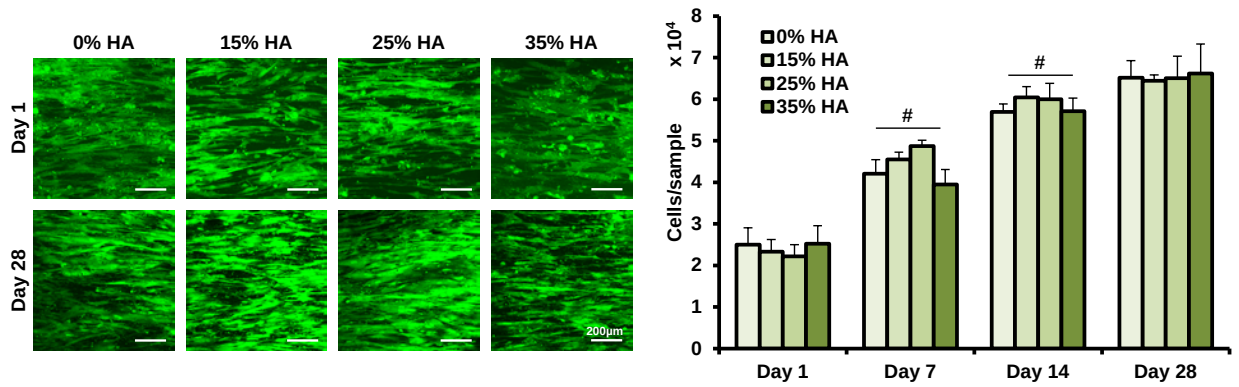

Figure 5.3. Effect of nanofiber mineral content on cell attachment and proliferation. Cells displayed an elongated morphology aligned in the direction of the underlying fiber organization. Cells also remained similarly viable on all groups over time. No significant difference in cell number was measured between groups at any of the time points. However, a significant increase in cell number was measured in all groups between day 1 and day 7 as well as between days 7 and 14.

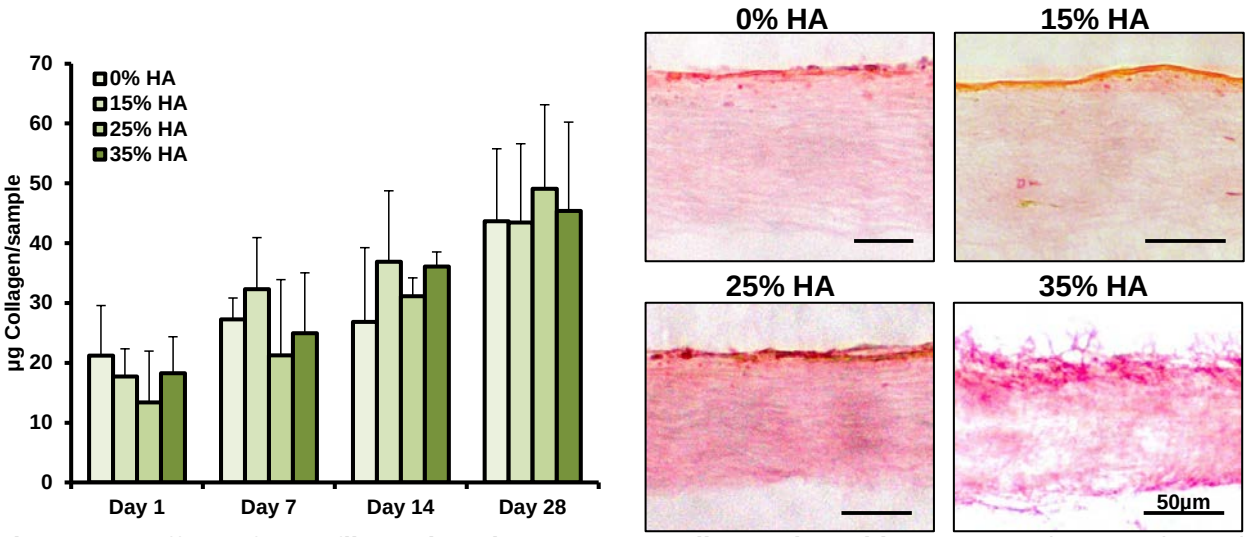

Figure 5.4. Effect of nanofiber mineral content on collagen deposition. A mean increase in total collagen was observed over time in all groups and significantly greater total collagen was present on all groups after 28 days as compared to day 1. Collagen distribution at day 28 was also visualized via picrosirius red staining, which displayed similar collagen distribution in all groups, with collagenous matrix primarily found on the seeded surface of the mesh.

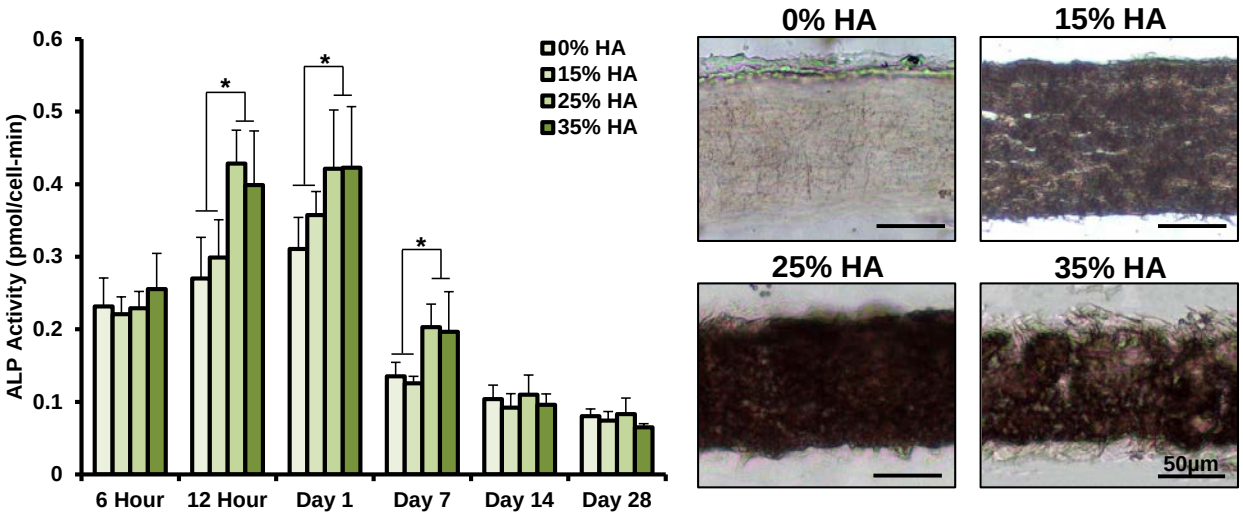

Figure 5.5. Effect of nanofiber mineral content on mineralization. A significant increase in ALP activity was measured after 12 hours of culture on the 25% and 35% HA groups as compared to the 0% and 15% HA groups. Elevated ALP activity in these groups persisted through day 7, after which it returned to basal levels. Mineral distribution visualized via von Kossa staining showed similar mineral distribution on the composite nanofibers and no mineral present in the 0% HA group.

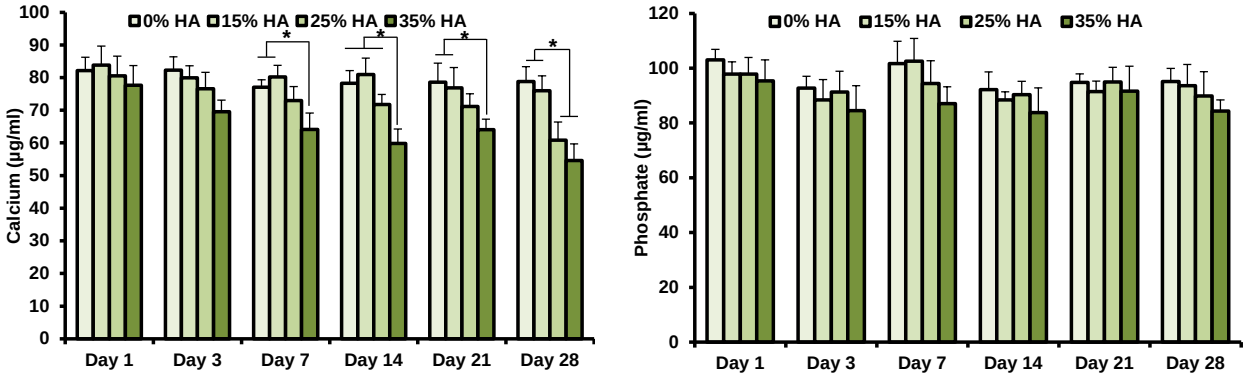

Figure 5.6. Cell-mediated mineralization mechanism on polymer-ceramic nanofibers. Significantly lower media calcium content was measured in the 35% HA group after 7 days of culture and this difference was maintained through day 28. Significantly lower media calcium content was also measured in the 25% HA group, though only at day 28. Measurement of media phosphate concentration showed no significant differences between groups, though a mean decrease in phosphate content was observed with increasing nanofiber ceramic content at all time points.

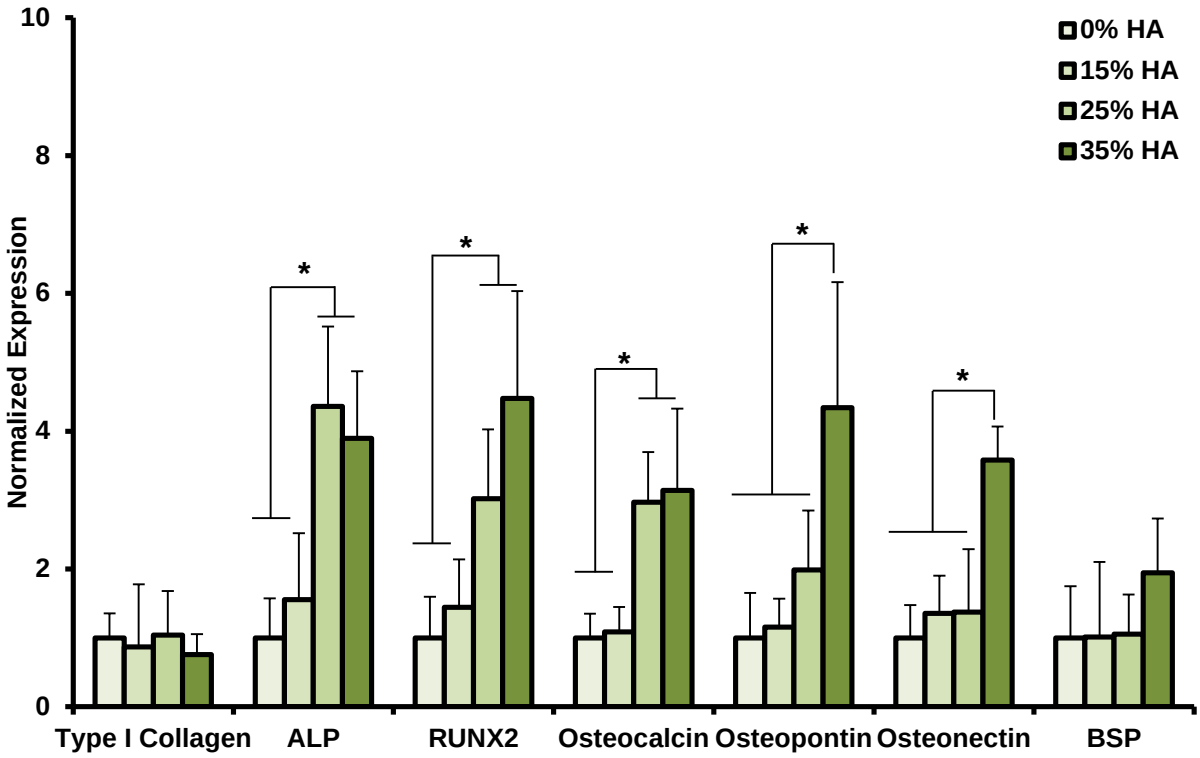

Figure 5.7. Effect of nanofiber mineral content on MSC differentiation. At day 28, the expression of ALP, RUNX-2 and osteocalcin was increased by cells on the 25% and 35% HA nanofibers. In addition, osteopontin and osteonectin were upregulated on the 35% HA nanofibers only. A mean increase in BSP expression was also measured on the 35% HA nanofibers as compared to all other groups.

CHAPTER 6: INTERFACE PHASE: EFFECT OF NANOFIBER COLLAR CONTRACTION ON MESENCHYMAL STEM CELL CHONDROGENESIS

6.1 Introduction

In the previous chapters, the ligament and bone phases of the multi-phased ACL scaffold were optimized in terms of composition and cell response. This chapter focuses on the final phase of the scaffold, the interface phase. As the scaffold must integrate tissue on the ligament and bone phases via the formation of a fibrocartilage interface, a system to induce cartilage-like tissue formation by MSCs will be investigated. To this end, a nanofiber-based collar system to apply compression and induce fibrocartilage formation will be investigated and evaluated *in vitro*.

6.1.1 Background and Motivation

At the ACL-bone interface, there exists a gradual transition from soft tissue-to-bone. With the exception of the mode of collagen fiber insertion into the subchondral bone, the transition from ACL-to-bone is histologically similar for the femoral and tibial insertion sites. The interface consists of four different zones: ligament (L), non-mineralized fibrocartilage (NFC), mineralized fibrocartilage (MFC), and bone (B)[219-223]. The ligament proper is composed of fibroblasts embedded in a type I and type III collagen matrix. The NFC is composed of ovoid chondrocytes, and type II collagen is detectable within the pericellular matrix. The primary sulfated proteoglycan is aggrecan. The next zone is the MFC, with hypertrophic chondrocytes surrounded by a large pericellular matrix[221]. Type X collagen, a specific marker for hypertrophic chondrocytes, is detected only within this zone[220]. The last zone is the subchondral bone and the cells present are osteoblasts, osteocytes and osteoclasts embedded in a type I collagen matrix. The principal function of the fibrocartilage interface is to minimize stress concentrations and to facilitate load transfer between distinct tissue types[23;72].

The majority of current interface regeneration efforts centers on the formation of ligament-interface-bone[36;224] or tendon-interface-bone[24] complexes for orthopaedic tissue engineering. In terms of improving the osteointegration potential of tendon grafts, early attempts focused on augmenting the surgical graft with a material that would encourage bone tissue growth. For example, Tien *et al.* used calcium phosphate cements to fill the tendon-to-bone junction in a rabbit ACL reconstruction study and found that the addition of this ceramic helped to improve bone growth and organization[58]. Using a different approach, Mutsuzaki *et al.* soaked tendon grafts in a series of solutions which coated the

tendons with a calcium phosphate layer prior to implantation[60]. The modified graft was tested using a rabbit ACL reconstruction model, and it was found that the pre-coated tendons enhanced healing and promoted integration. Although these methods have improved osteointegration between the ACL graft and the bone tunnel, they do not result in the regeneration of the fibrocartilage interface. Thus there exists a significant clinical need for integrative fixation devices that will promote interface formation and osteointegration.

The mechanisms governing the formation of this interface are not well understood; though it has been reported that metaplasia of tendon or ligament tissue plays a role in this process[225;226]. Specifically, Nawata *et al.*, using a rodent model, reported that ACL insertion fibrochondrocytes arise from ligament fibroblasts[226]. Similarly, Gao *et al.* used a rodent model to show that ligament fibroblasts begin to synthesize type II collagen during the development of the ligament-bone enthesis[225]. In addition, mechanical stimulation has been implicated in the process of enthesis development and fibrocartilage formation[75]. Vogel *et al.* investigated this process extensively in a bovine model, focusing on the effect of compressive loading on fibrocartilage formation in flexor tendons[227-231]. It was reported that compressive loading induced metaplasia of tendinous matrix and initiated its transformation into fibrocartilage-like tissue as gene expression of fibrocartilage markers, such as aggrecan and type II collagen, was not observed in the wrap-around regions of fetal and neonatal bovine flexor tendons, but was strongly expressed in those of mature animals[229], thereby suggesting that physiological compressive loading induces post-natal fibrocartilage formation. Extending this work, it was reported that translocation of rabbit flexor digitorum profundus tendon to remove compressive loading resulted in a decrease in the size of the fibrocartilage region, looser collagen organization and a lower glycosaminoglycan content in the tissue[228]. It was also reported that re-establishing cyclic compression *in vitro* enhanced the expression of aggrecan, biglycan and versican in bovine flexor tendons[230]. Collectively, these findings suggest that compressive loading modulates fibrocartilage formation and may be responsible for matrix remodeling in tendon tissue.

6.1.2 Objectives

Based on the aforementioned studies, compression will be evaluated as a stimulus to induce fibrocartilage formation by MSCs. To this end, a novel mechanoactive collar will be investigated for the interface phase of the synthetic ACL scaffold. This collar, composed of an aligned poly(lactic-*co*-glycolic) acid (PLGA) nanofiber mesh, undergoes anisotropic contraction when placed in a physiological environment[24;36;232]. The efficacy this mechnoactive collar has previously been demonstrated *in vitro* as it was reported to upregulate the gene expression of fibrocartilage markers, such as transforming growth factor-beta 3 (TGF-β3), aggrecan and type II collagen when applied to bovine patellar tendons *in vitro*[36]. To mimic the heterogeneity of the native ligament-to-bone interface, the collar will consist of two phases: a PLGA phase, to induce and support non-mineralized fibrocartilage formation, and a composite PLGA-HA phase incorporating hydroxyapatite to support mineralized fibrocartilage formation. The first objective of this study is to characterize the contractile properties of the bi-phasic nanofiber collar while the second is to evaluate the use of the mechanoactive system *in vitro* to apply compression to MSCs and induce fibrocartilage-like tissue formation. It is hypothesized that collar-mediated compression will result in the upregulation of cartilage-related markers and the production of a cartilage-like matrix.

6.2 Materials and Methods

6.2.1 Scaffold Fabrication

Bi-phasic nanofiber collars were produced via electrospinning. Briefly, a polymer solution consisting of 35% PLGA (w/v, 85:15, M_w=123.6 kDa; Lakeshore Biomaterials) in 55% N,N-dimethylformamide (Sigma-Aldrich, St. Louis, MO) and 10% ethanol (Pharmco-AAPER, Brookfield, CT) was loaded into a syringe fitted with an 18.5-gauge blunt tip needle (Becton Dickinson, Franklin Lakes, NJ). Composite PLGA-hydroxyapatite (PLGA-HA) nanofibers were fabricated similarly by adding a suspension of HA nanoparticles immersed in DMF to the PLGA solution, resulting in a 15% HA (w/w) polymer-ceramic suspension. Aligned fibers were obtained using an aluminum mandrel rotating at a velocity of 20m/s with a constant polymer flow rate of 1 mL/hr maintained via a syringe pump (Harvard Apparatus, Holliston, MA)[233]. An electrical potential was applied between the needle and the drum using a high-voltage DC power supply (Spellman, Hauppauge, NY). The bi-phasic collar system was

fabricated by electrospinning parallel regions of PLGA and PLGA-HA nanofibers. After depositing a layer of aligned PLGA nanofibers on the mandrel, a custom masking system was applied upon which a layer of PLGA-HA nanofibers was deposited. The resulting multi-phase collar consisted of a PLGA region, a PLGA/PLGA-HA overlapping region (1mm in length) and a PLGA-HA region.

Braided nanofiber constructs, around which the collars were secured prior to cell seeding, were fabricated via electrospinning. A mixture of 18% (w/v) poly(ε-caprolactone) (PCL, Sigma-Aldrich, Mw=70,000-90,000) and PLGA (85:15, Lakeshore) was dissolved in a mixture of 60/40 dichloromethane (DCM, Sigma-Aldrich) and DMF. The polymer solution was loaded into a 5 mL syringe with a 18.5-gauge stainless steel blunt tip needle, and electrospun at 8-10kV using a custom electrospinning device. The polymer solution was deposited (1 mL/hour) using a syringe pump (Harvard Apparatus, Holliston, MA) onto a custom rotating mandrel (20 m/s) to produce aligned fibers. To standardize the amount of fibers in each construct, the solution was electrospun for 45 minutes to create a 20μm-thick nanofiber mesh. The resulting meshes were rolled into bundles 0.8mm in diameter and three fibrous bundles were then braided together. Once braided, the three bundles were cut into 1 cm length sections and melted at the ends to form a construct. Collars were secured to the braided constructs using a 7-0 Prolene suture (Ethicon, Somerville, NJ).

6.2.3 Collar Contraction

The effect of mineral content and incubation time on nanofiber collar contraction was measured *in vitro* by comparing length and width changes of the bi-phasic collar with those of single phase PLGA and PLGA-HA collars. Briefly, collars (1cm x 2cm) were incubated in phosphate buffered saline (PBS) and cultured for 72 hours. Collar dimensions were measured by taking digital images after 1, 2, 24 and 72 hours and measuring length and width using ImageJ image analysis software.

6.2.4 Cells and Cell Culture

Human mesenchymal stem cells were obtained commercially (Lonza, Walkersville, MD) and maintained in culture with DMEM containing 10% fetal bovine serum (FBS, embryonic stem cell certified, Atlanta Biologicals, Atlanta, GA), 1% penicillin-streptomycin, 1% non-essential amino acids, 0.1%

amphotericin B and 0.1% gentamicin. All media supplements were purchased from Cellgro-Mediatech unless otherwise specified. Cells were cultured to 80% confluence and then passaged using 0.25% trypsin/1 mM ethylenediaminetetraacetate (EDTA) and re-plated at a density of $5x10^3$ cells/cm^2. Passage 2-3 cells were used for scaffold seeding.

Constructs were seeded dynamically using an orbital shaker. Briefly, after sterilization, constructs were placed in conical tubes (BD Biosciences) containing cell suspension with a density of 1 million MSC/ml. Tubes containing constructs were placed on an orbital shaker, rotating at a rate of 100 RPM, for four hours in a cell culture incubator which was shown in optimization studies to result in approximately $1x10^6$ cells attached to each construct. Following the seeding process, constructs were placed in individual tubes for culture. To study the effect of nanofiber contraction on mesenchymal stem cell (MSC) response, braided nanofiber constructs with and without nanofiber collars were evaluated.

6.2.5 Cell Proliferation

Total DNA content was measured using the PicoGreen dsDNA assay (Invitrogen). At each time point, the samples (n=5/group) were homogenized in 0.1% Triton-X (Sigma-Aldrich) and subjected to 20 seconds of ultrasonication at 5W. Fluorescence was measured using a microplate reader (Tecan, Research Triangle Park, NC) at an excitation wavelength of 485 nm and an emission wavelength of 535 nm. A standard curve was derived and used to correlate DNA concentration to fluorescence intensity, and cell number was determined based on a conversion factor of 8pg DNA/cell[104].

6.2.6 Matrix Production

Total collagen content per sample (n=5/group) was calculated using the hydroxyproline assay. The assay was performed following a 16-hour sample digestion in Papain (Sigma-Aldrich) to solubilize ECM proteins. Absorbance was measured using a microplate reader (Tecan) at 555 nm. A standard curve was generated and used to correlate total collagen content to absorbance.

Sample glycosaminogylcan content (GAG, n=5) was determined with a modified 1, 9-dimethylmethylene blue (DMMB) binding assay[234-236], with chondrotin-6-sulfate (Sigma) as the standard. To account for the anionic nature of the carboxyl groups on the alginate hydrogel, the pH of the

DMMB dye solution was adjusted to 1.5 with concentrated formic acid (Sigma) so that only the sulfated GAG-DMMB complexes were detectable. Additionally, the absorbance difference between 540nm and 595nm was used to improve the sensitivity in signal detection.

6.2.7 Cell Differentiation

The phenotype of MSCs was assessed quantitative real-time reverse transcriptase polymerase chain reaction (n=5/group). Total RNA was isolated using the Trizol extraction method (Invitrogen). Isolated RNA was then reverse-transcribed into complementary DNA using the SuperScript First-Strand Synthesis System (Invitrogen), and the cDNA product was amplified using recombinant Taq DNA polymerase (Invitrogen). The oligonucleotide primer sequences were: type I collagen: TGGTCCACTTGCTTGAAGAC (sense), ACAGATTTGGGAAGGAGTGG (antisense); type II collagen: GGACATAGGGCCTGTCTGTT (sense), CCGGACTGTGAGGTTAGGAT (antisense); aggrecan: CAGATCTGCATGGAATCACC (sense); AAGTGCCTGCATCTATGTCG (antisense); and transforming growth factor beta-3 (TGF-β3): AAACTCCAGCTCTCTTCCCA (sense); ACGAAGTAGCGGACTGTGTG (antisense) was determined. GAPDH served as the house-keeping gene. All genes were amplified for 50 cycles in a thermocycler (Bio-Rad iCycler, Hercules, CA) with a fluorescent probe (SYBR Green, Invitrogen). Quantitative analysis of gene expression was performed using the delta-delta CT method.

6.3 Results

6.3.1. Collar Contraction

Prior to performing the cell-seeded, collar contraction was characterized as the effect of incubation on nanofiber collar contraction was evaluated over time and compared as a function of collar composition (*Fig. 6.1*). All compositions contracted in length to less than 45% of original length within 12 hours of incubation with no significant change in length over the remainder of the study. In addition, no significant difference in change in length was measured as a function of nanofiber composition. Similarly, in terms of width, the PLGA and PLGA-HA collars contracted to approximately 60% of original width within 12 hours of incubation with no significant change over the remainder of the incubation period. In addition, no difference was observed between these groups. In contrast, the bi-phasic collar contracted

to only 80% of original width. No delamination was observed between the PLGA and PLGA-HA phases of the bi-phasic collar over time.

6.3.2 Cell Proliferation and Matrix Deposition

Total cell number was measured for constructs without and without nanofibers collars at days 1, 3 and 7 (*Fig 6.2*) No difference in cell number was measured between groups at any time points, though a mean increase was observed over time in both groups.

Matrix deposition was quantified in terms of total collagen content and sulfated GAG content (*Fig. 6.3*) No significant difference in collagen content was measured between groups or over time, though a mean increase was observed over time in both groups. In contrast, a significant increase in total GAG content was measured after 7 days with the nanofiber collar as compared to the control group.

6.3.3 Cell Differentiation

Stem cell differentiation was assessed by measuring the expression of several fibrocartilage-related proteins, specifically type II collagen, aggrecan and TGF-β3 (*Fig 6.4*). At day 1, the expression of type II collagen, aggrecan, and TGF-β3 was significantly upregulated with the nanofiber collar. At day 3, only TGF-β3 was upregulated in the nanofiber collar group and, at day 7, no difference in the expression of these genes was measured between groups. In addition, type I collagen expression was measured at each time point to determine phenotype specificity (*Fig 6.4*). No change in type I collagen expression was observed over time in either group.

6.4 Discussion

This study focused on the evaluation of a novel mechanoactive nanofiber collar system to apply *in situ* compression to tissue engineering scaffold systems. The first objective of this study was to characterize the contractile behavior of the nanofiber collar system and the second was to evaluate its ability to induce chondrogenic differentiation of MSCs *in vitro*. It was hypothesized that collar-mediated contraction would result in the upregulation of fibrocartilage-related markers by MSCs and the deposition of a cartilaginous matrix. To this end, a braided nanofiber construct, simulating a synthetic ACL graft, was

wrapped with the nanofiber collar and then seeded with MSCs. The MSC-seeded constructs were cultured for 7 days and evaluated in terms of cell proliferation, matrix deposition and differentiation.

In this study, MSCs were subjected to compression via nanofiber collar contraction which resulted in the short-term upregulation of fibrocartilage-related markers. In particular, TGF-β3, aggrecan and type II collagen were all upregulated after 1 day of culture. However, the lack of long-term marker upregulation in this study potentially suggests an adaptive response by MSCs to the static compressive loading provided by the collar thereby indicating that continued compression or dynamic loading may be necessary to sustain a response. Alternatively, sustained chondrogenic chemical factors could also, absent in the culture medium used in this study, could also help further drive cells towards a fibrochondrogenic lineage.

In this study, aggrecan expression by MSCs was upregulated after 1 day of compression and returned to basal levels at subsequent time points. However, despite this short-term upregulation in marker expression, a significant increase in GAG production was measured after 7 days of compression. This is of particular importance because proteoglycans are one of the principal types of proteins found in cartilaginous tissues and serve to help these structures retain water and resist compressive loading[237]. Compressive loading has previously been shown to increase proteoglycan production by MSCs and is widely used in cartilage tissue engineering applications[238-240] to enhance the biochemical and mechanical properties of cartilage constructs. In addition, compressive loading of the enthesis regions of tendons has been demonstrated to enhance aggrecan gene expression and increase the synthesis of and large proteoglycans[35;227].

Of the fibrocartilage markers investigated in this study, TGF-β3 expression was upregulated the longest. Studies investigating the function of TGF-β3 have reported that it has a range of functions in cell differentiation and development[241;242]. In terms of tissue engineering, this protein is widely used to differentiate MSCs towards a cartilaginous lineage[243]. Exogenous addition of TGF- β3 has also been shown to increase aggrecan expression and subsequent proteoglycan production, suggesting a possible mechanism for the GAG findings observed in this study[244]. In addition, He *et al.* developed a co-culture silk scaffold system and reported fibrocartilaginous differentiation of MSCs when stimulated with TGF-β3, similar to their response when co-cultured with chondrocytes[245]. Collectively, these results imply that

the upregulation of TGF-β3 coupled with aggrecan upregulation and increased proteoglycan production indicate the differentiation of MSCs towards a cartilage or fibrocartilage-like lineage.

The nanofiber collar system developed in this study also has the potential to enable biological fixation by being applied to soft tissue grafts. Spalazzi *et al.* reported on the use of a combined nanofiber mesh and microsphere collar system to upregulate the expression of the same fibrocartilage markers after 24 hours of compression *in vitro* indicating that connective tissues containing viable cells may respond similarly[36]. It is anticipated that autografts, typically utilized for ACL reconstruction surgeries could be augmented using this system by applying the collar to the proximal and distal ends of the graft prior to securing it within the bone tunnels during surgery.

6.5 Conclusions

In summary, this study demonstrates that the nanofiber collar system can be applied to induce chondrogenic differentiation of MSCs *in vitro,* in terms of cartilaginous matrix deposition and the expression of fibrocartilage-related proteins. These findings indicate that the collar represents a promising system for the interface phase of the synthetic ACL graft. However, due to the lack of sustained marker expression, the system will be evaluated *in vivo* in the next chapter to determine if it can induce long-term fibrocartilage formation.

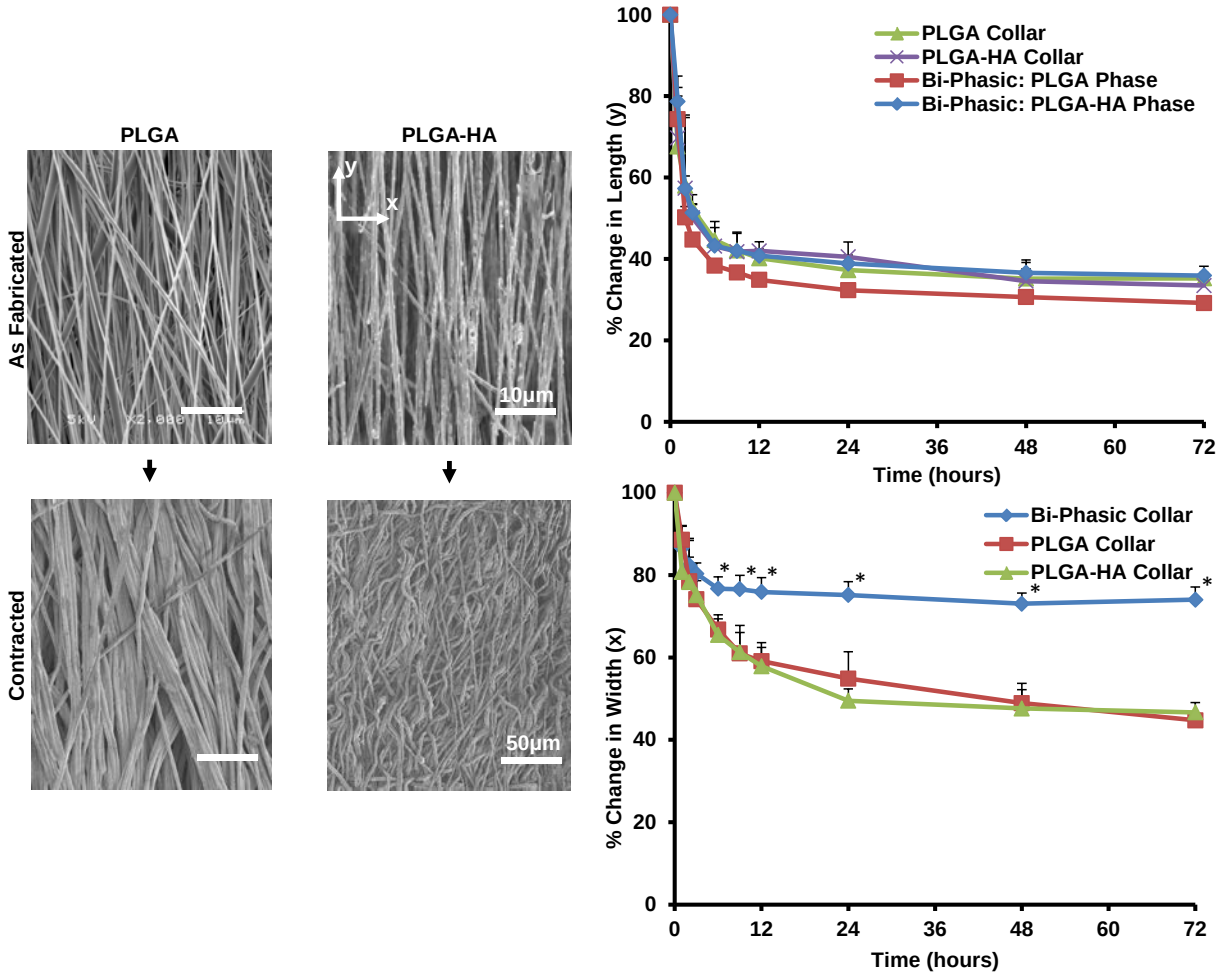

Figure 6.1. Mechanoactive nanofiber collar contraction. Nanofiber collars were fabricated via electrospinning. The collars underwent anisotropic contraction when incubated in a physiological environment with a decrease in length of over 60% regardless of composition.

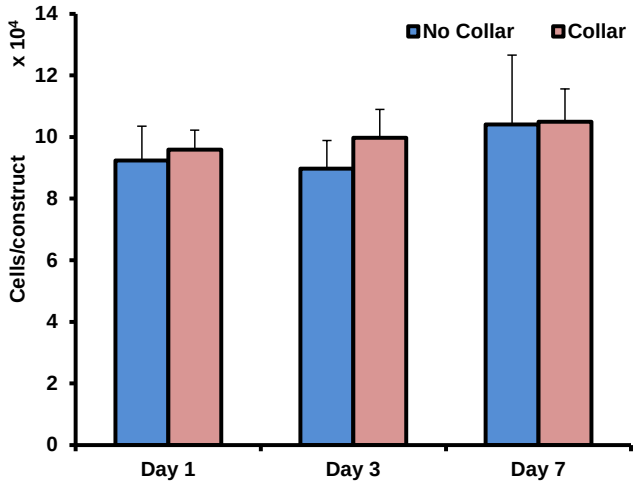

Figure 6.2. Effect of nanofiber collar contraction on MSC attachment and proliferation. No significant difference in cell number was measured between groups or over time indicating that the presence of the collar did not impede cell attachment.

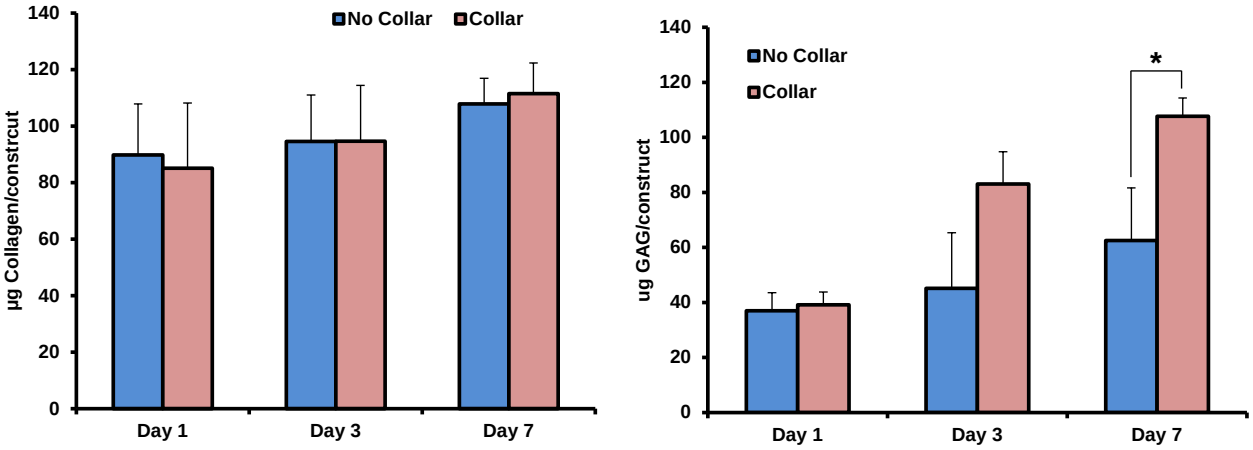

Figure 6.3. Effect of nanofiber collar contraction of MSC matrix deposition. No difference in total collagen content was measured between groups or over time though a mean increase was observed over time in both groups. A mean increase in GAG content was measured at day 3 and GAG content was significantly increased after 7 days with the nanofiber collar.

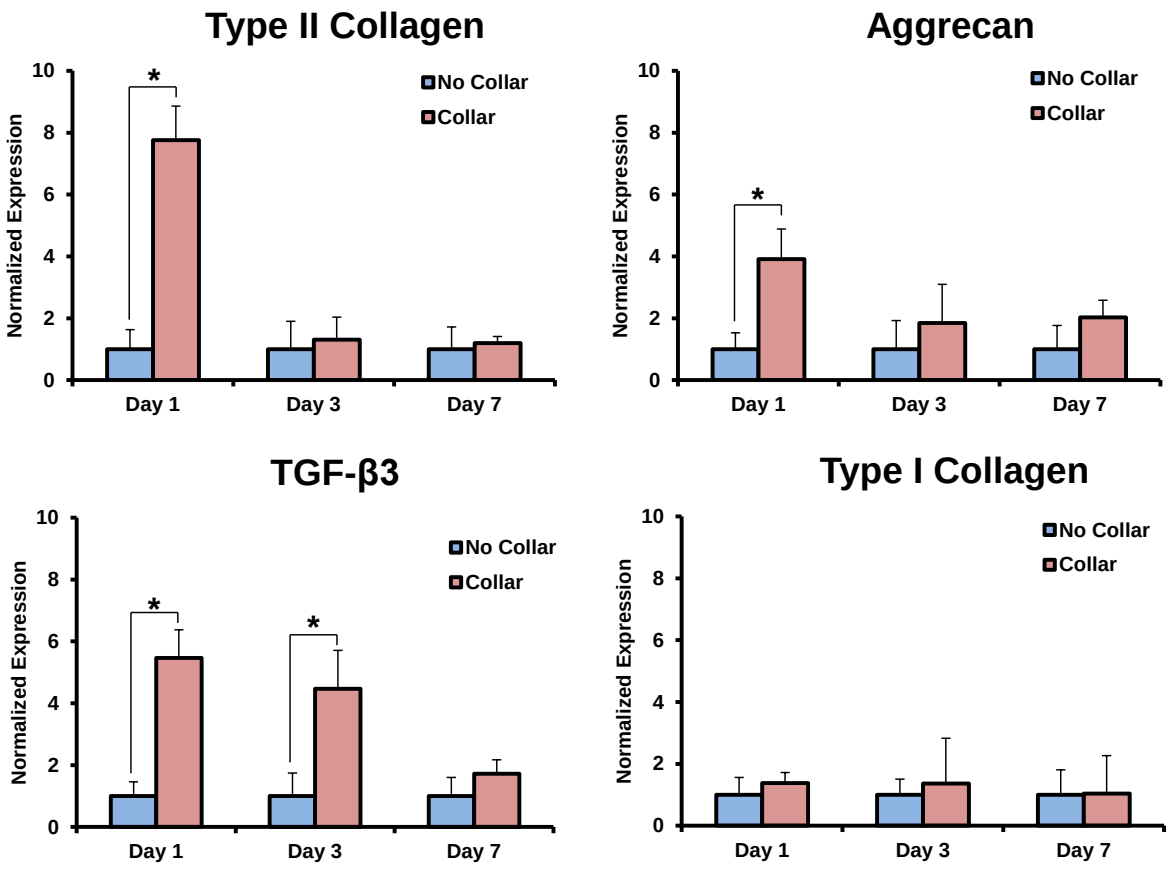

Figure 6.4. Effect of nanofiber collar contraction on MSC differentiation. The application of the nanofiber collar resulted in the upregulation of type II collagen, aggrecan and TGF-β3 at day 1 as compared to the control group. Only TGF-β3 remained upregulated at day 3 and no difference in marker expression was measured between groups at day 7.

CHAPTER 7: INTERFACE PHASE: IN VIVO EVALUATION OF THE NANOFIBER COLLAR FOR FIBROCARTILAGE FORMATION

7.1 Introduction

In *Chapter 6*, a nanofiber collar system was designed and it was demonstrated that using this system to apply compression to MSCs resulted in the upregulation of fibrocartilage-related markers and the production of a cartilaginous extracellular matrix. However, due to the lack of sustained fibrocartilage market expression, the collar system will be validated *in vivo* using a rodent model to determine if it can induce fibrocartilage formation on soft tissue grafts.

7.1.1 Background and Motivation

Initial attempts to improve ligament graft-to-bone fixation have focused on augmenting the surgical graft with mineralized components in order to encourage bone formation[58-63] as the strength of the tendon-to-bone interface has been shown to correlate with the degree of bony in-growth[12]. For example, Tien *et al.* used calcium phosphate cements within the bone tunnels in a rabbit ACL reconstruction study and found that the addition of this ceramic helped to improve osseous tissue in-growth and organization[58]. Similarly, the injection of tricalcium phosphate cement to the tendon-bone junction within the bone tunnel in a canine ACL reconstruction model resulted in more organized bone tissue formation compared to the uncemented control[59]. Using an alternative approach, Mutsuzaki *et al.* soaked tendon grafts in a series of solutions which coated the tendons with a calcium phosphate layer prior to surgery[60;61]. The modified graft displayed enhanced healing and promoted tendon-to-bone integration when tested in a rabbit ACL reconstruction model. These findings indicate that the inclusion of calcium phosphate is a viable strategy for enhancing tendon-to-bone integration. However, although these methods have improved osteointegration between the ACL graft and the bone tunnel, they do not result in the regeneration of the fibrocartilage interface.

The native ACL-to-bone enthesis consists of a fibrocartilaginous transition which serves to minimize stress concentrations and facilitates load transfer between two distinct tissue types[22;23;70-73]. The mechanisms governing the formation of this interface are not well understood; though it has been reported that metaplasia of tendon or ligament tissue plays a role in this process[225;226]. Specifically, Nawata *et al.*, using a rodent model, reported that ACL insertion fibrochondrocytes arise from ligament fibroblasts[226]. Similarly, Gao *et al.* used a rodent model to show that ligament fibroblasts begin

to synthesize type II collagen during the development of the ligament-bone enthesis[225]. In addition, mechanical stimulation has been implicated in the process of enthesis development and fibrocartilage formation[75]. Vogel *et al.* investigated this process extensively in a bovine model, focusing on the effect of compressive loading on fibrocartilage formation in flexor tendons[227-231]. It was reported that compressive loading induced metaplasia of tendinous matrix and initiated its transformation into fibrocartilage-like tissue as gene expression of fibrocartilage markers, such as aggrecan and type II collagen, was not observed in the wrap-around regions of fetal and neonatal bovine flexor tendons, but was strongly expressed in those of mature animals[229], thereby suggesting that physiological compressive loading induces post-natal fibrocartilage formation. Extending this work, it was reported that translocation of rabbit flexor digitorum profundus tendon to remove compressive loading resulted in a decrease in the size of the fibrocartilage region, looser collagen organization and a lower glycosaminoglycan content in the tissue[228]. It was also reported that re-establishing cyclic compression *in vitro* enhanced the expression of aggrecan, biglycan and versican in bovine flexor tendons[230]. Collectively, these findings suggest that compressive loading modulates fibrocartilage formation and may be responsible for matrix remodeling in tendon tissue.

7.1.2 Objectives

To address the challenge of achieving biological fixation of soft tissue grafts, the goal of this study is to develop functional methods to regenerate an anatomic fibrocartilage transition on ACL reconstruction grafts. To this end, a novel mechanoactive graft collar will be evaluated. This collar is composed of an aligned poly(lactic-*co*-glycolic) acid (PLGA) nanofiber mesh which is biodegradable and undergoes anisotropic contraction when placed in a physiological environment[24;36;232]. This collar is designed to be secured to the proximal and distal ends of the graft during surgery and remain in the bone tunnels during the healing process (*Fig. 7.1).* Furthermore, to mimic the heterogeneity of the native ligament-to-bone interface, a multi-phasic collar with both PLGA and composite PLGA-hydroxyapatite nanofiber components has been developed to provide region-specific enhancement of fibrocartilage and mineralized tissue formation. The efficacy of the mechnoactive collar was previously demonstrated *in vitro* as it was report to upregulate the expression of fibrocartilage markers, such as transforming growth

factor-beta 3 (TGF-β3), aggrecan and type II collagen when applied to bovine patellar tendons *in vitro*[36]. The objective of the current study is to evaluate the use of a mechanoactive collar system *in vivo* using a rat ACL reconstruction model. It is hypothesized that the composite nanofiber collar will promote fibrocartilage formation, enhance osteointegration and improve graft fixation strength following ACL reconstruction. It is anticipated that the impact of this work will extend beyond orthopaedic repair techniques as similar approaches could be developed to apply mechanical stimulation *in situ* to improve a variety of surgical procedures and also enhance the clinical potential of tissue engineering strategies.

7.2 Materials and Methods

7.2.1 Collar Fabrication

Aligned nanofiber collars composed of polylactide-*co*-glycolide (PLGA, 85:15, M_w = 123.6 kDa; Lakeshore Biomaterials) were produced via electrospinning[24;246]. Briefly, a polymer solution consisting of 35% PLGA (w/v) in 55% N,N-dimethylformamide (Sigma-Aldrich, St. Louis, MO) and 10% ethanol (Pharmco-AAPER, Brookfield, CT) was loaded into a syringe fitted with an 18.5-gauge blunt tip needle (Becton Dickinson, Franklin Lakes, NJ). Composite PLGA-hydroxyapatite (PLGA-HA) nanofiber collars were fabricated similarly by adding a suspension of HA nanoparticles immersed in DMF to the PLGA solution, resulting in a 15% HA (w/w) polymer-ceramic suspension. Aligned fibers were obtained using an aluminum mandrel rotating at a velocity of 20m/s with a constant polymer flow rate of 1 mL/hr maintained via a syringe pump (Harvard Apparatus, Holliston, MA)[233]. An electrical potential was applied between the needle and the drum using a high-voltage DC power supply (Spellman, Hauppauge, NY). The bi-phasic (BP) collar was fabricated by electrospinning parallel regions of PLGA and PLGA-HA nanofibers. After depositing a layer of aligned PLGA nanofibers on the mandrel, a custom masking system was applied upon which a layer of PLGA-HA nanofibers was deposited. The resulting multi-phase collar consisted of a PLGA region, a PLGA/PLGA-HA overlapping region (1mm in length) and a PLGA-HA region (*Fig. 7.1*).

7.2.2 ACL Reconstruction Procedure

The ACL reconstruction procedure was performed on male Lewis rats (weight, 275–300 g) using a flexor digitorum longus tendon graft[247] following approval by the Institutional Animal Care and Use Committee. The rats were kept in soft-bedding cages with free access to food and water. Animals were anesthetized with a mixture of 80 mg/kg ketamine hydrochloride and 5 mg/kg xylazine administered intraperitoneally through a 25-gauge needle. A longitudinal incision was first made on the medial aspect of the right distal leg and ankle. The flexor digitorum longus tendon was identified and cut just distal to the ankle in order to harvest the full length of the flexor digitorum longus tendon (average length, 30 mm). A second incision was made over the knee and a medial parapatellar arthrotomy was performed to open the joint and excise the ACL. Bone tunnels 1.6mm in diameter were made in the proximal tibia and the distal femur by entering the joint at the attachment sites of the ACL. In the experimental groups (PLGA, PLGA-HA, and bi-phasic), a nanofiber collar was wrapped once around a 5 mm section of each end of the tendon graft, corresponding to the regions inserted into the bone tunnels (*Fig 7.1*). The collar was secured to the graft using 7-0 Prolene suture (Ethicon, Somerville, NJ) and a 4–0 Ethibond suture (Ethicon, Somerville, NJ) was passed through each end of the graft. Control groups received a graft without a nanofiber collar. The graft was passed through the bone tunnels to replace the ACL and the proximal and distal ends were secured to the femur and tibia, respectively. Wounds were closed in standard fashion. No negative effects of the autologous graft harvest were observed other than expected swelling and all animals resumed normal gait by 2 to 3 days after surgery. The animals remained healthy and infection-free throughout the duration of the study. All animals resumed normal cage activity by the first postoperative day. Careful inspection of the articular surfaces after euthanasia revealed no arthritis or advanced joint degeneration.

7.2.3 Matrix Deposition & Fibrocartilage Formation

Two animals per group were euthanized at 4 and 8 weeks after surgery via carbon dioxide inhalation and prepared for histologic analysis. At each time point, one specimen was decalcified and embedded in paraffin for histology and immunohistochemistry. The remaining specimen for each time point was embedded in methacrylate.

Harvested tissues for decalcified histology were fixed for 4 days in 10% neutral buffered formalin and then decalcified for 48 hours in a solution of formalin, formic acid and ion exchange beads (Dowex HCS-5, Dow Chemical, Midland, MI). Excess bone and soft tissue surrounding the femoral and tibial tunnels was removed and the tissues were dehydrated in serial alcohol concentrations (70%–100%), cleared thrice in xylenes and then embedded in paraffin (Fisher Scientific) at 60ºC. Seven-micrometer-thick sections were cut perpendicular to the axes of the bone tunnels and stained with a Modified Goldner's Masson trichrome stain and picrosirius red to visualize collagen distribution, and alcian blue to visualize sulfated glycosaminoglycans (GAG). Images were obtained using a light microscope (Zeiss Axiovert 25, Zeiss, Germany) and a polarized light microscope (Olympus BX60, Olympus, Center Valley, PA).

Immunohistochemical analysis was performed to evaluate collagen distribution and the presence of fibrocartilage-related proteins[2]. Specifically, monoclonal antibodies against type I collagen (1:20 dilution, Abcam, Cambridge, MA), type II collagen (1:100 dilution, Santa Cruz Biotechnology, Santa Cruz, CA), type I pro-collagen (1:50 dilution, Developmental Studies Hybridoma Bank, Iowa City, IA), aggrecan (1:100 dilution, Santa Cruz Biotechnology) and TGF-β3 (1:100, Abcam) were applied to serial sections after retrieval with 1% hyaluronidase for 30 minutes (aggrecan and type II collagen) or hot citrate buffer (pH = 6.0) for 20 minutes (type I procollagen and TGF-β3) at 37˚C. All sample sections were incubated with primary antibody overnight at 4˚C. Following a rinse with PBS, FITC-conjugated secondary antibody (1:200 dilution, Abcam) was added for one hour at 25˚C. Propidium iodide (Invitrogen) was used as a nuclear counterstain. Images were obtained using a confocal microscope (Leica TCS-SP5, Leica, Bannockburn, IL).

7.2.4 Mineralization

Mineral distribution with the tibial and femoral bone tunnels was determined using micro-computed tomography (micro-CT, n=2/group). Briefly, following fixation for 96 hours in 10% neutral buffered formalin, histological samples were scanned with a micro-computed tomography system (VivaCT 40, Scanco Medical, Switzerland). The length of the tibia and femur surrounding the bone tunnel was scanned with a 17μm voxel size. Three-dimensional reconstructions were then performed by tracing the

edges of the bone and using a mineral density of 268 mg HA/cm^3. Tunnel diameter was measured by taking measurements in tripliciate down the length of each tunnel in the resulting three-dimensional figures.

Bone volume surrounding the tunnel was quantified by performing volumetric reconstruction of a uniform cylinder of bone including the tibial bone tunnel. A 2.0cm circular contour surrounding the bone tunnel was placed on 315 slices as acquired via micro-CT and reconstructed at a density of 268 mg HA/cm^3, the bone volume and bone volume fraction were quantified using the vivaCT software.

Samples for calcified histology were dehydrated in serial alcohol concentrations (70%–100%). Rat tibiae were embedded in poly(methylmethacrylate) using a modification of the methods of Erben *et al.*[248]. Seven-micrometer-thick sections were cut perpendicular to the bone tunnels and von Kossa staining was used to visualize mineralized tissue[249]. Images were obtained using a light microscope (Zeiss Axiovert 25, Zeiss, Germany).

7.2.5 Biomechanical Properties

Biomechanical testing (n=10) was performed to evaluate the strength of the reconstruction after 8 weeks[38;247]. Limbs used for biomechanical testing were disarticulated at the hip and all muscles were removed leaving the joint capsule and the ligaments intact to protect the ACL graft until testing. Specimens were stored in a freezer at −80°C until testing. Prior to testing, each limb was defrosted overnight at 4°C and thawed at room temperature. The joint capsule, tendons, ligaments (except the ACL) and the suture material at the graft ends were excised prior to testing. The bony ends were potted in bonding cement at the proximal femur and the distal tibia to allow secure fixation in the testing machine. The specimen was positioned on a custom device for rat knees. Knee flexion was maintained at 45° with the tensile load passing parallel to the ACL graft and the bone tunnels. A preload of 15 g was applied to the graft for five cycles, following which a tensile load to failure test was performed at a displacement rate of 0.17 mm/second. The load-deformation curve was recorded on a personal computer. Results are reported in terms of the ultimate load-to-failure (N) and stiffness (N/mm) which were calculated from the linear portion of the load-deformation curve. The site of failure was recorded as pull-out from the bone tunnel versus mid-substance rupture.

7.2.6 Statistical Analysis

Results are presented in the form of mean ± standard deviation, with *n* equal to the number of samples per group. Two-way analysis of variance (ANOVA) was performed to evaluate the effect of time and composition on collar contraction and also to assess the effect of time and collar composition on tunnel diameter. One-way ANOVA was used to evaluate the effect of the bi-phasic collar on bone volume and biomechanical properties. The Tukey-Kramer post-hoc test was used for pair-wise comparisons. Significance was attained at $p<0.05$. Statistical analyses were performed with JMP IN (4.0.4, SAS Institute).

7.3 Results

7.3.1 Matrix Deposition & Fibrocartilage Formation

A vascularized bone tunnel was evident surrounding the collagenous tendon graft in the control, PLGA and PGLA-HA groups as shown in the series of trichrome stains (*Fig. 7.2*), in which the collagenous matrix appears green, erythrocytes in red and cell nuclei in black. After 4 weeks, similar collagen distribution was displayed within and surrounding the grafts in all groups with vascularized tissue evident within the mid-substance of grafts wrapped with the PLGA-HA. After 8 weeks, the presence of vascularized tissue was more prominent in the PLGA-HA group and a statistically significant decrease in tunnel diameter (*Fig. 7.2*) was also observed in this group. Histological sections of the PLGA and PLGA-HA regions of specimens wrapped with the bi-phasic collar also displayed vasculature present within the graft at both 4 and 8 weeks.

Visualization of the collagenous matrix via picrosirius red staining revealed similar collagen distribution within grafts of all groups at both week 4 and week 8 (*Fig. 7.3*). Evaluation of collagen orientation, as shown with polarized light microscopy, indicated minimal differences in collagen orientation in the control and PLGA groups at both week 4 and week 8. Interestingly, collagen fibers appearing green under polarized light, indicative of smaller diameter fibers, were distinctly present within the graft in both the PLGA-HA and HA region of the bi-phasic collar after 8 weeks. Fibers appearing green were also evident surrounding the grafts in all groups, corresponding to the outline of the bone tunnel.

Collagen distribution was further evaluated using immunohistochemistry. At 4 weeks, type I collagen was uniformly distributed in all groups and similar findings were observed after 8 weeks. Additionally, intracellular type I procollagen was stained to determine regions of new collagen synthesis and neo-tissue formation[250] (*Fig. 7.4*). Type I procollagen was revealed to be present surrounding all grafts and was most abundant around grafts wrapped with a collar at 4 weeks. After 8 weeks, type I procollagen was similarly uniform in all groups. Type II collagen was found to be present only within the grafts of experimental groups (PGLA, PLGA-HA and bi-phasic collars) at 4 weeks and was found in all groups after 8 weeks, though most abundantly in the groups wrapped with nanofiber collars (*Fig. 7.4*).

The deposition of proteoglycans and the formation of fibrocartilage were evaluated with Alcian Blue staining as well as immunohistochemical staining for type II collagen and aggrecan. In addition, the presence of TGF-β3 was also evaluated as it has been shown to be an important factor related to proteoglycan production in tendons[230]. At 4 weeks, Alcian Blue staining revealed glycosaminoglycans (GAG) present surrounding grafts in all groups but only within the midsubstance of grafts wrapped with a PLGA-HA collar. No substantial GAG content was observed within the grafts of any group after 8 weeks (*Fig. 7.5*). Aggrecan was found only within the adjacent cartilaginous tissue in the control group at week 4 but was present in the midsubstance of all grafts wrapped with a collar. Minimal regions of aggrecan deposition were found within the graft of the control group at 8 weeks and it was more abundantly present within the PLGA, PLGA-HA and bi-phasic groups at this time point (*Fig. 7.5*). TGF-β3 deposition was found to correlate with aggrecan deposition as it was not present in the control group graft at 4 weeks and only minimally present in the control after 8 weeks. More abundant TGB-β3 deposition was observed in the PLGA, PLGA-HA and bi-phasic groups after 8 weeks (*Fig. 7.6*).

7.3.2 Mineralization

In terms of mineral distribution, micro-CT analysis revealed that mineralized tissue was present within grafts wrapped with collars containing HA at 4 weeks (PLGA-HA and bi-phasic groups, *Fig. 7.7*). The most abundant mineral was detected within the tunnels of the PLGA-HA and bi-phasic groups as a cylindrical ring of mineral evident in the tunnel of both groups. The presence of mineralized tissue within the graft was confirmed with von Kossa staining, which stained positive for mineral within grafts wrapped

with HA and bi-phasic collars. Nodules of mineralized tissue formation were found to be larger after 8 weeks in these groups.

Mineralized tissue formation was further evaluated by quantifying the amount of bone present surrounding and within the tibial bone tunnels of each specimen. This analysis revealed that a greater amount of mineral was present after 8 weeks with the bi-phasic collar in comparison with the control group (*Fig. 7.8*). The total bone volume (9.36±1.31 mm^3 vs. 7.58±1.67 mm^3) and bone volume fraction (0.27±0.03 vs. 0.22±0.05) of the analyzed region were significantly greater with the bi-phasic collar as compared to the control group.

7.3.3 Biomechanical Properties

Uniaxial tensile testing of reconstructed knees revealed no significant difference in stiffness or failure load between the bi-phasic group and the control group. The failure load of grafts in the control group was measured as 11.10±5.97N as compared to 10.17±3.94N with the bi-phasic collar. Similarly, the stiffness in the control group was 8.27±4.79 N/mm as compared to 7.92±3.30 with the bi-phasic collar. Samples in both groups failed at both the mid-substance of the graft as well as at the tibial and femoral bone tunnels.

7.4 Discussion

Our long-term goal is to facilitate biological fixation by engineering a functional and anatomical fibrocartilage interface directly on soft tissue and synthetic grafts used in orthopaedic repair techniques[251]. To this end, this study focused on the *in vivo* evaluation of a mechanoactive and osteointegrative collar system, guided by the working hypothesis that compression applied to tendon grafts via the inherent contraction of the polymeric nanofiber meshes would result in matrix remodeling and fibrocartilage formation while the addition of a ceramic component would enhance bone formation and tendon-to-bone integration. Specifically, the primary objective of this study was to evaluate this graft collar system *in vivo* to test the hypothesis that a composite nanofiber collar will promote fibrocartilage formation, enhance osteointegration and increase graft fixation strength.

We previously reported that the PLGA nanofiber collar induced the upregulation of fibrocartilage-related markers *in vitro* after 24 hours when applied to bovine patellar tendon samples, as compared to samples with pre-contracted PLGA collars[36]. This study extended the collar system to an *in vivo* rat model and indicates that tendon graft compression via collar contraction resulted in the acceleration of type II collagen, aggrecan and TGF-β3 formation after 4 weeks *in vivo* and also increased the production of these proteins after 8 weeks. As the native enthesis of tendons is largely comprised of types I and II collagen and proteoglycans[22;35;227] and native fibrocartilage formation from tendon and ligament tissue has been shown to correlate with the expression and production of these proteins[252], these results indicate that compressive loading can initiate matrix remodeling. It should be noted however, that no *in situ* monitoring of tendon compression was performed and that physical loads at the graft-bone interface may also have played a role due to the fact that knee motion was not constrained. However, these findings demonstrate the potential of the nanofiber collar system for use *in vivo* to induce fibrocartilage-like tissue formation on tendon grafts following ACL reconstruction.

The incorporation of hydroxyapatite nanoparticles within the PLGA-HA and bi-phasic graft collars resulted in the formation of calcified tissue within the bone tunnels of these groups. In addition, an increase in total bone volume surrounding the graft was measured with in bi-phasic collar group as compared to the control group. These findings are likely due to the presence of a physiological mineral within the collar as several groups have reported similar results when evaluating calcium phosphate-based cements to augment tendon-to-bone integration. For example, Wen *et al.* applied a calcium phosphate-based brushite within the tendon-to-bone interface of the bone tunnels in a rabbit ACL reconstruction model[253]. It was reported that the application of the cement resulted in increased peri-tendon bone volume and also promoted bone growth into the healing interface. Additionally, Ishikawa *et al.* studied the effect of a collagen gel mixed with a hydroxyapatite powder on tendon-to-bone integration in a rabbit model[62]. The gel, applied between the grafted Achilles tendon and bone in a femoral bone tunnel, resulted in greater bone volume and Sharpey-like fibers integrating the tendon with bone. Our results are in agreement with these findings and demonstrate the potential of a ceramic component within the graft collar to enhance bone formation and tendon-to-bone integration.

The functional outcomes of the nanofiber collar were evaluated with uniaxial tensile testing of the bi-phasic collar as compared to the control group[38;247]. No significant difference in stiffness or failure load was measured between the two groups. This finding may be due to the relatively short 8-week study duration as compared to the traditional 6 to 12 month healing process following ACL reconstruction. It is anticipated that future studies may need to be extended beyond the 8-week time point to allow for sufficient healing and interface formation to impact biomechanical outcomes.

We reported on the evaluation of three collar systems (PLGA, PLGA-HA and bi-phasic) for enhancing ligament-to-bone integration. The PLGA collar demonstrated the potential of collar-mediated compression to initiate the formation of fibrocartilage-like tissue while the PLGA-HA collar included a mineral component and resulted in mineralized tissue formation throughout the length of the bone tunnels. The bi-phasic collar, extending upon these designs, resulted in region-specific mineralized tissue formation and demonstrates the potential of a multi-phase collar to recapitulate the inherent complexity of the ligament-to-bone interface. It is anticipated that this system would result in long-term enhancement of bone formation within the tunnel and also induce fibrocartilage formation, thereby regenerating the anatomical transition between ligament and bone.

While the rat ACL reconstruction model is well established in the literature, interpretations of these results must take into account the limitation of this model. Specifically, due to the fact that the rat growth plate does not close during the lifetime of the animal[254], further evaluation is necessary in a larger, skeletally mature animal model. Therefore, future studies will focus on extending the use of our system to more clinically relevant animal models, such as a caprine model.

7.5 Conclusions

In summary, a mechanoactive nanofiber collar was evaluated to assess the efficacy of applying mechanical loading to tendon grafts *in situ*. Collar-induced compression of the flexor digitorum tendon graft accelerated and increased the formation of key components of fibrocartilage, including type II collagen, aggrecan and TGF-β3. In addition, the inclusion of a physiological mineral component within the collar resulted in bone formation within the graft midsubstance. These promising results demonstrate the clinical potential of a multi-phasic mechanoactive polymer-ceramic collar, as it is envisioned that the collar

can be used to apply both biochemical and mechanical stimuli to induce the formation of a fibrocartilaginous interface on tendon grafts. Based on these results, the bi-phasic nanofiber collar system will be used to induce interface tissue formation on the multi-phased synthetic ACL graft. In addition, this approach has the potential for immediate clinical translation in order to augment current ACL reconstruction methods by enhancing graft osteointegration and stimulating the formation of native ligament-to-bone interfacial tissue. In the next chapter, a multi-phased scaffold comprised of all three optimized phases will be fabricated and evaluated *in vitro*.

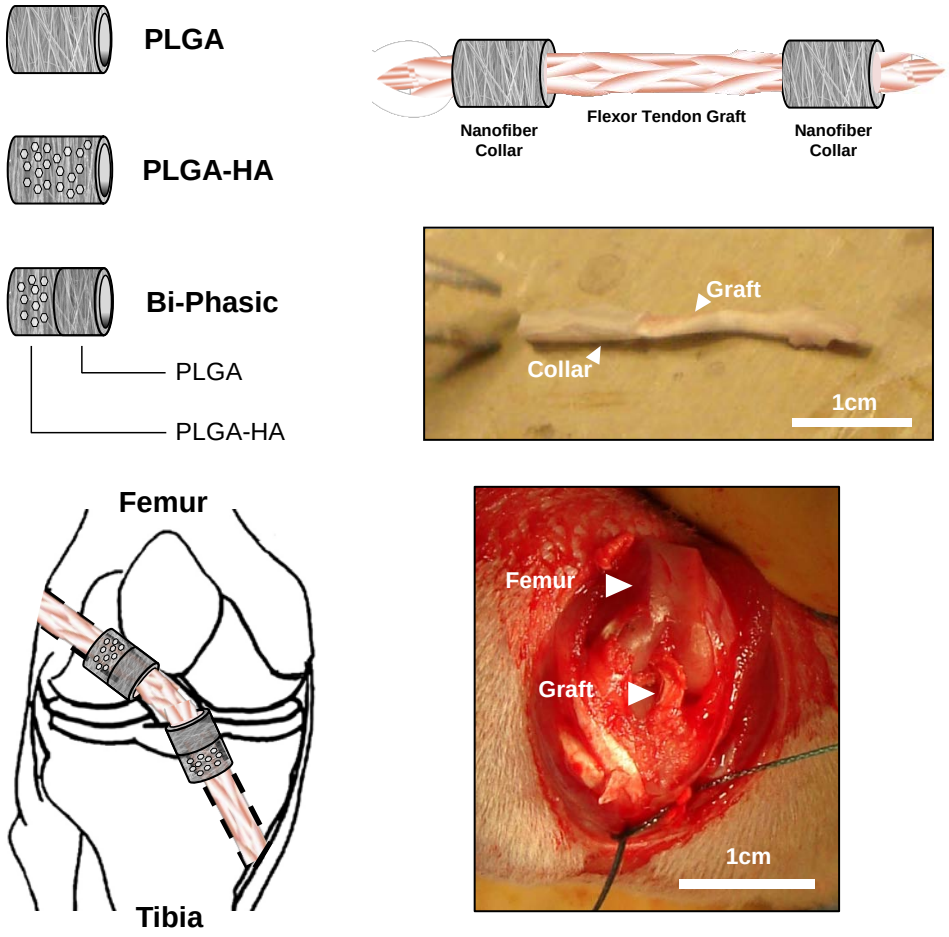

Figure 7.1. Mechanoactive nanofiber collar application. The ACL reconstruction procedure was performed on Lewis rats. Rats in the experimental groups received either a PLGA, PLGA-HA, or a bi-phasic collar on each end of the flexor tendon graft, corresponding to the regions inserted within the bone tunnels.

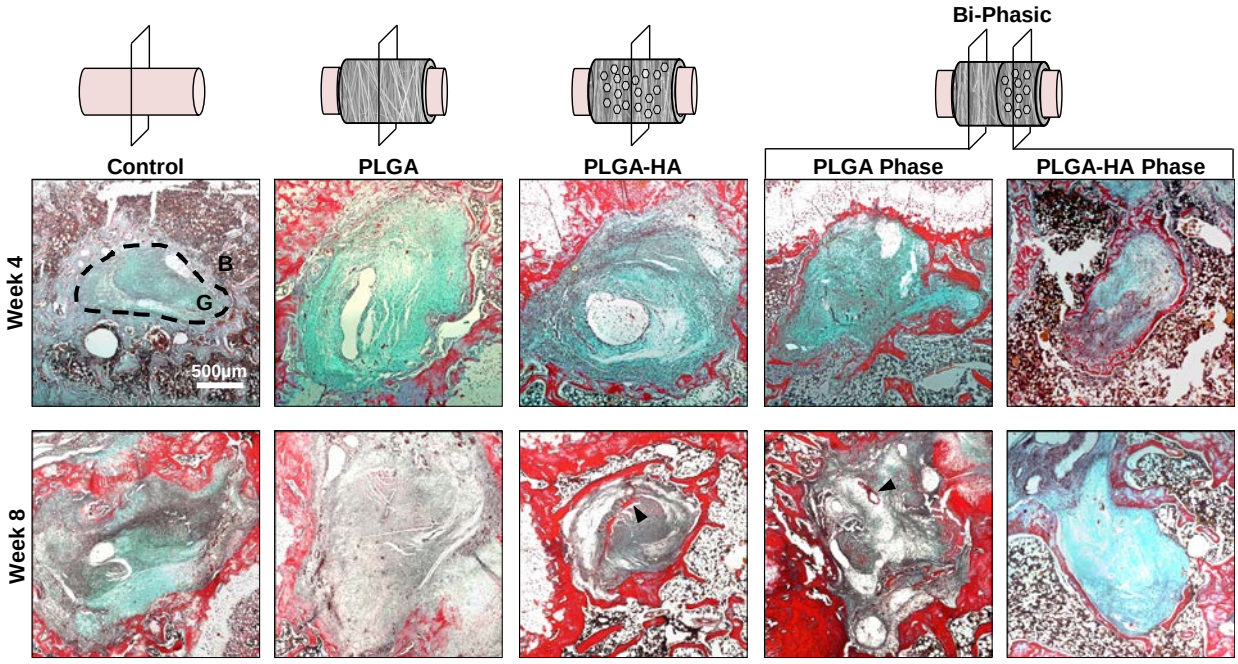

Figure 7.2. Effect of nanofiber collar on matrix deposition. A modified Goldner's Masson Trichrome Stain of histological sections. Collagen is stained in green, erythrocytes in red and cell nuclei in black (5x, scale bar = 500μm) to delineate the bone (B) from the graft (G). Similar collagen distribution is evident in all groups over time, with vascularized tissue formation most evident within the graft of the PLGA-HA and BP groups (arrow).

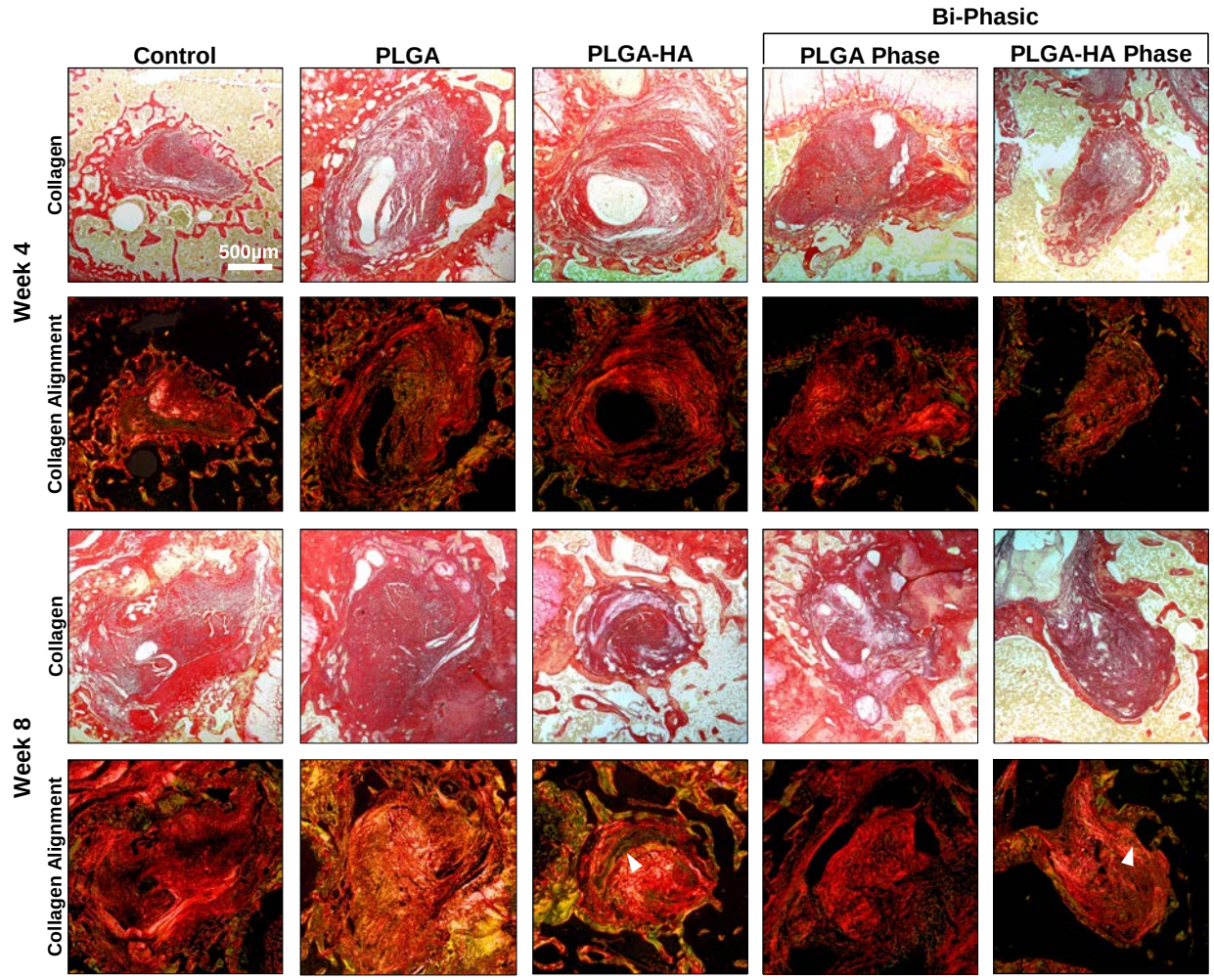

Figure 7.3. Effect of nanofiber collar on collagen distribution and orientation. Picrosirius red staining of histological specimens with corresponding polarized light micrographs showing that collagen distribution is uniform in all groups (5x, scale bar = 500μm). Polarized light microscopy revealed the presence of smaller diameter fibers (green, arrow) within the grafts of the PLGA-HA group and the HA regions of the BP group.

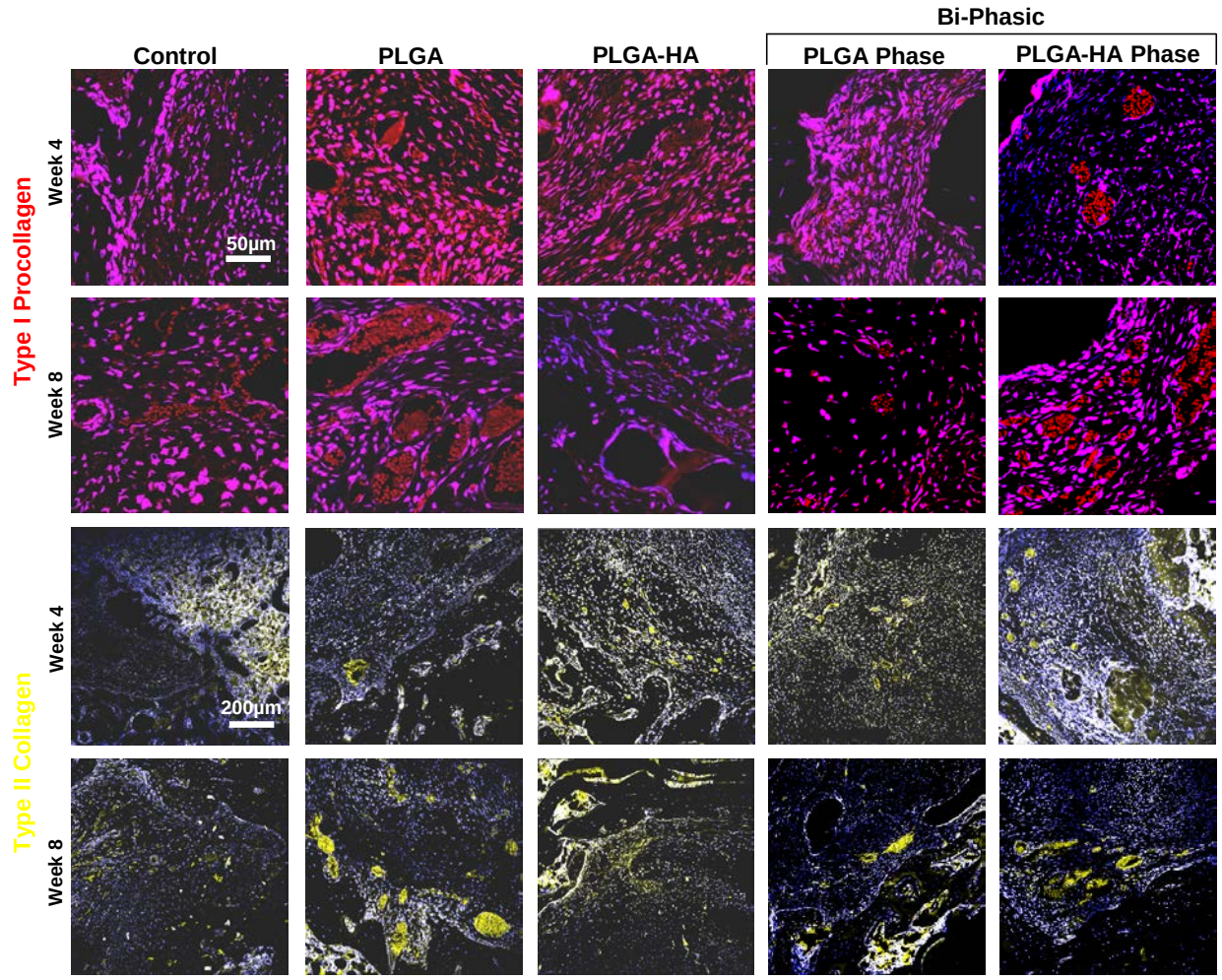

Figure 7.4. Effect of nanofiber collar on neo-tissue formation. Type I procollagen (red; cell nuclei: blue; 63x, scale bar = 50μm) was found to be most abundant surrounding the experimental groups at week four. Type II collagen (yellow; blue: cell nuclei; 20x, bar = 200μm) was present only within the graft of experimental groups at week four and was present within all grafts at week eight.

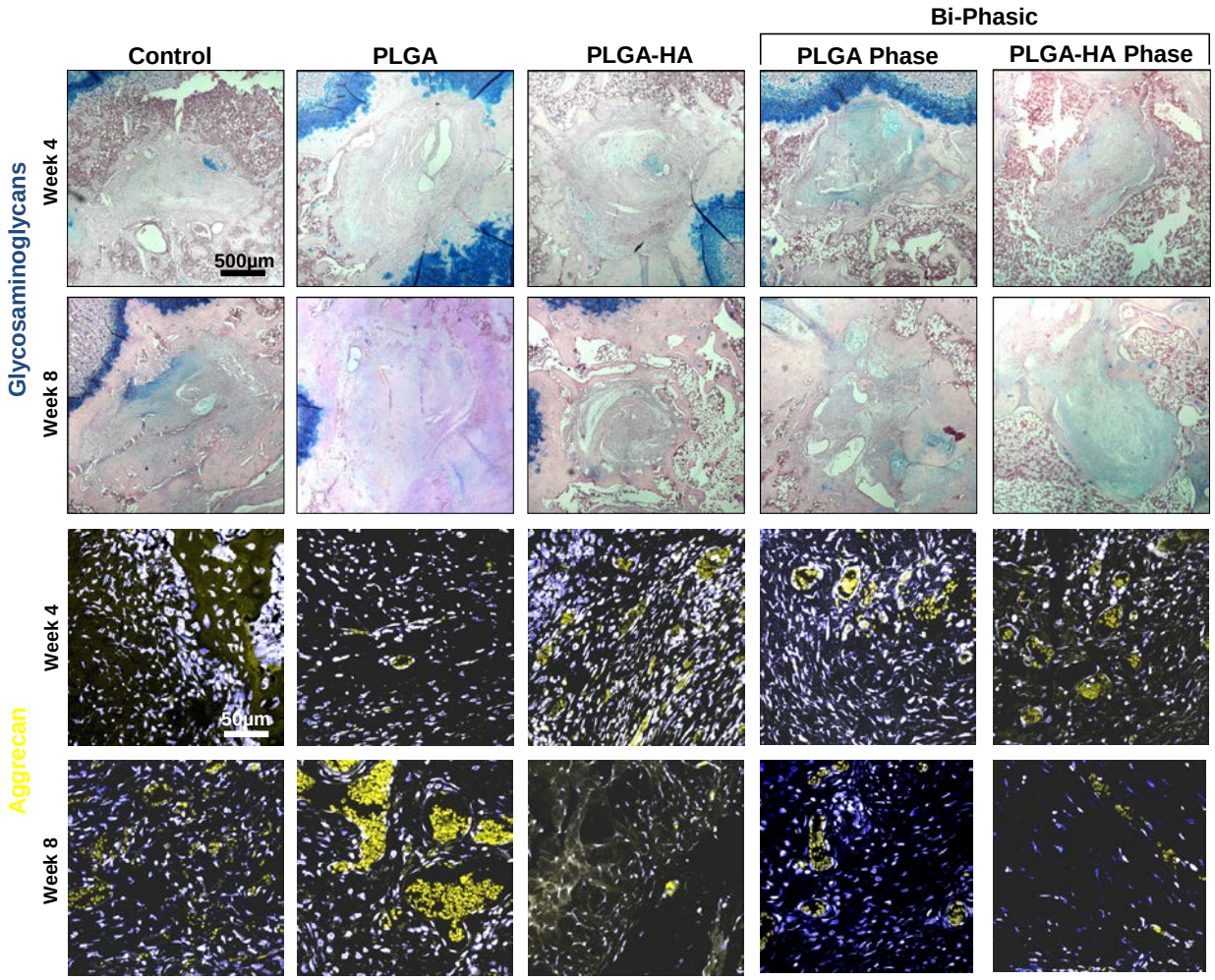

Figure 7.5. Effect of nanofiber collar on cartilaginous tissue formation. Alcian Blue staining indicated the presence of GAG (blue) only within grafts wrapped with a PLGA-HA collar after four weeks (5x, scale bar = 500μm). No positive staining was indicated within the graft of any groups after eight weeks. Aggrecan (yellow; cell nuclei: blue; 63x, scale bar = 50μm) was present within the graft of all experimental groups at week four but absent in the control group. After eight weeks, aggrecan was present within all grafts but was more abundantly evident in the experimental groups.

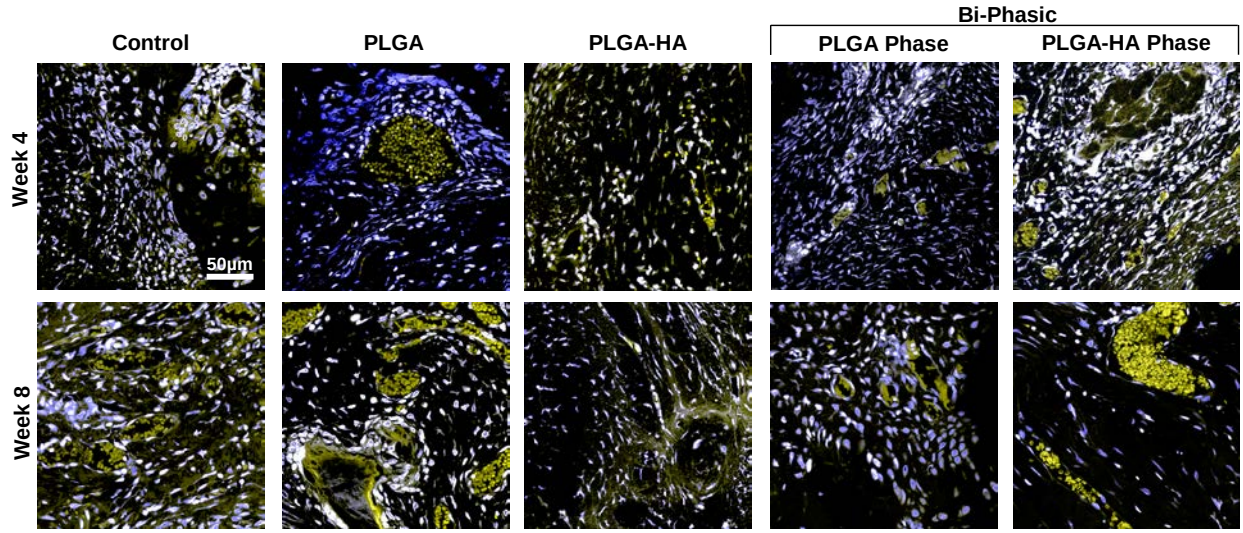

Figure 7.6. Effect of nanofiber collar on fibrocartilage formation. Staining for TGF-β3 (yellow; cell nuclei: blue; 63x, scale bar = 50µm) indicated that it was present near regions of aggrecan. Similarly, it was only present in experimental groups at week four and absent in the control group. It was most abundantly evident in the experimental groups at week eight.

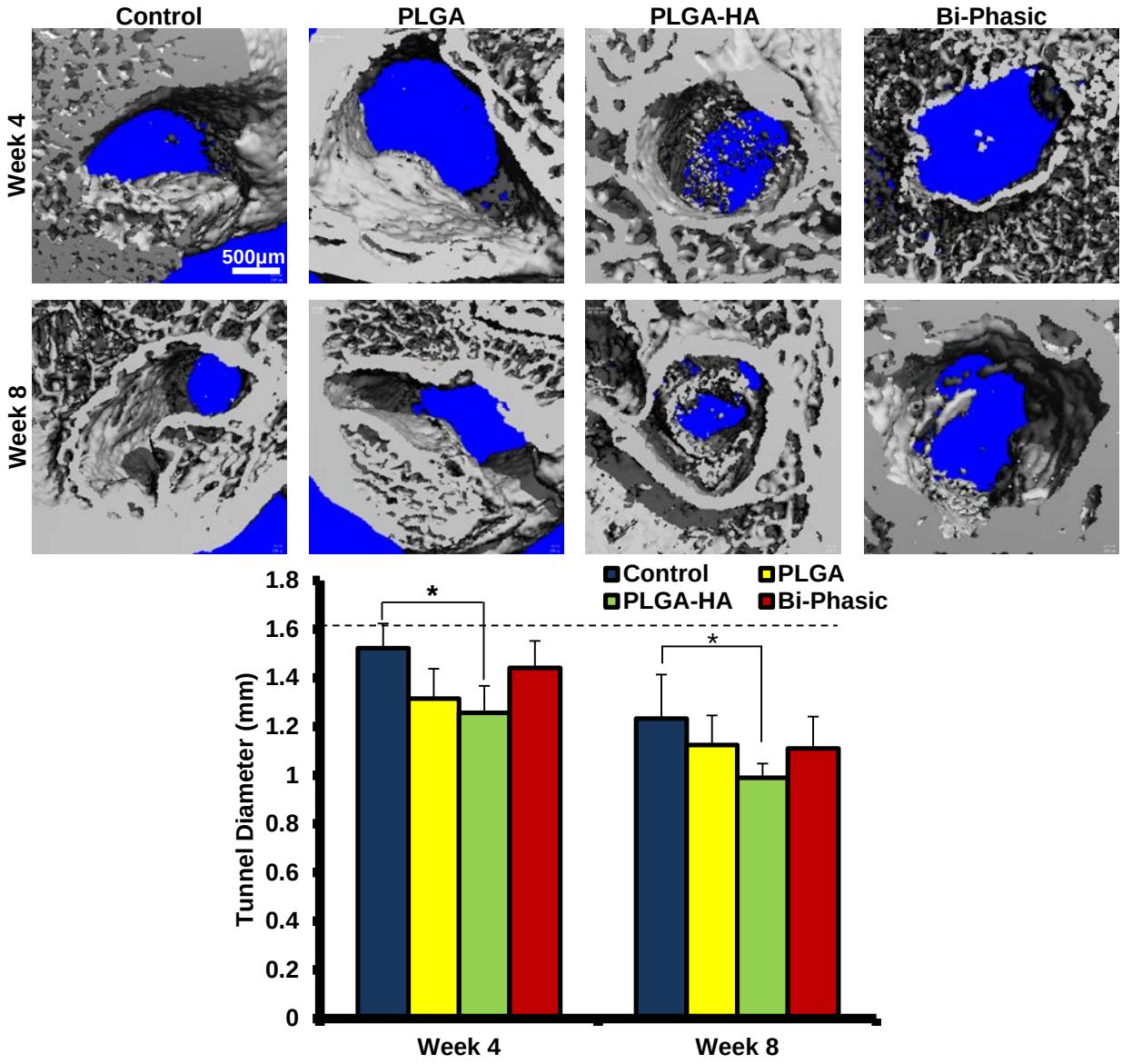

Figure 7.7. Effect of nanofiber collar on mineralized tissue formation and tunnel diameter. Three-dimensional reconstructions (bar = 500µm) of tibiae via µCT revealed the presence of mineralized tissue within the tunnels of grafts wrapped with the PLGA-HA and BP scaffold after four weeks. More abundant mineralized tissue was found within the grafts of these groups after eight weeks. Both the PLGA-HA and Bi-Phasic collar groups measured a significant decrease in tunnel diameter between weeks four and eight (#$p<0.05$). A significant decrease in tunnel diameter was observed with the PLGA-HA collar after four weeks of implantation(*$p<0.05$).

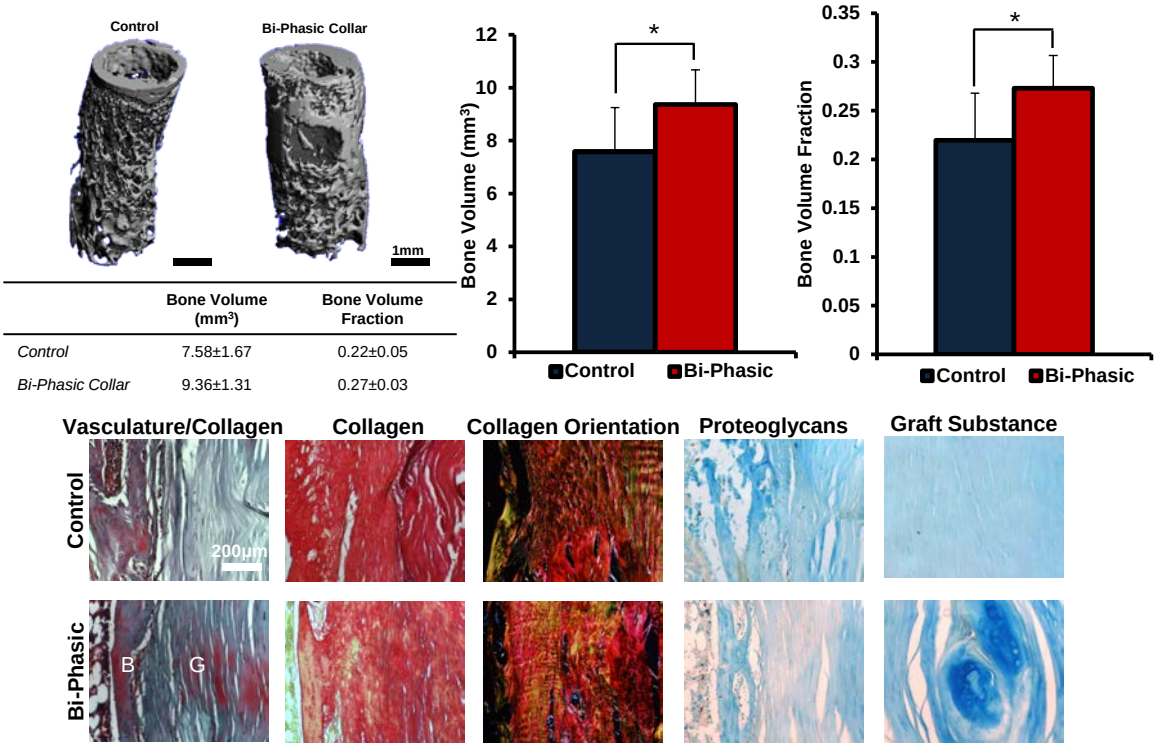

Figure 7.8. Effect of nanofiber collar on tunnel mineralization. Bone volume surrounding the bone tunnel was analyzed using μCT. Total bone volume (BV) and bone volume fraction (BVF) of uniform cylindrical sections of bone surrounding the bone tunnel was assessed using the vivaCT software. A significant increase in BV and BVF were measured in the bi-phasic collar group as compared to the control group. Similar tissue morphology was evident with the bi-phasic collar as compared to the control group. Regions of cartilage-like tissue were found within the tendon substance with the bi-phasic collar but not in the control group.

CHAPTER 8: *IN VITRO* EVALUATION OF THE MULTI-PHASED SYNTHETIC ACL GRAFT

8.1 Introduction

The previous chapters focused on optimizing the individual phases of the synthetic ACL graft to enable bone, interface and ligament regeneration. The focus of this chapter is the incorporation of all three phases in order to produce a single construct to induce the formation of an integrated bone-ligament-bone complex *in vitro*. In this chapter, the three phases will be incorporated, the cell seeding density will be optimized and the optimal construct will be cultured under in a physiologically-relevant bioreactor system to evaluate the formation of a pre-integrated ligament tissue *in vitro*.

8.1.1 Background and Motivation

Optimization of cell seeding density of tissue engineered scaffolds is necessary to maximize the utility of donor cells and provide a basis for uniform tissue regeneration[255]. In particular, higher cell-seeding densities have been reported to be desirable due to increased matrix production[256], likely due to the increased cell-cell contact and enhanced cell-matrix interactions[257-259]. Previous studies investigating cell-seeded synthetic ligament grafts have been performed using a range of cell seeding densities. For example, Cooper *et al.* and Fan *et al.* seeded ligament scaffolds at a density of 3 million cells per scaffold[18;108] and 4 million cells[109] per scaffold prior to implantation in a rabbit model and goat model, respectively. Therefore, prior to *in vivo* implantation, the cell seeding density for the synthetic ligament graft must be optimized.

8.1.2 Objectives

The objectives of this study are three-fold: the first objective is to optimize the architecture of the ligament phase of the scaffold as that phase is responsible for its bulk mechanical properties, the second is to determine the optimal seeding density for the synthetic ACL graft and the last is to the culture the system to evaluate the formation of a pre-integrated bone-ligament-bone complex *in vitro*. Grafts seeded at the optimal seeding density, as determined by matrix deposition and cell phenotype, will then be cultured in a bioreactor to simulate the physiological environment and evaluate the formation of an integrated bone-ligament-bone complex *in vitro*. It is hypothesized that a multi-bundle architecture, similar to the characterization of the structure of the native ligament will be necessary for optimal mechanical

characteristics. In addition, it is hypothesized that increasing initial cell seeding density will result in accelerated differentiation of MSCs towards specific phenotypes and increased matrix deposition.

8.2 Materials and Methods

8.2.1 Synthetic ACL Phase Fabrication

Each phase of the nanofiber-based synthetic ACL was fabricated via electrospinning. For the ligament phase, a mixture of 18% (w/v) poly(ε-caprolactone) (PCL, Sigma-Aldrich, Mw=70,000-90,000) and PLGA (85:15, M_w=123.6 kDa; Lakeshore Biomaterials) was dissolved in a mixture of 60/40 dichloromethane (DCM, Sigma-Aldrich, St. Louis, MO) and DMF. The polymer solution was loaded into a 5 mL syringe with a 18.5-gauge stainless steel blunt tip needle, and electrospun at 8-10kV using a custom electrospinning device. The polymer solution was deposited (1 mL/hour) using a syringe pump (Harvard Apparatus, Holliston, MA) onto a custom rotating mandrel (20 m/s) to produce aligned fibers.

For the interface phase, bi-phasic nanofiber collars were fabricated. Briefly, a polymer solution consisting of 35% PLGA (w/v, 85:15, Lakeshore Biomaterials) in 55% N,N-dimethylformamide (Sigma-Aldrich) and 10% ethanol (Pharmco-AAPER, Brookfield, CT) was loaded into a syringe fitted with an 18.5-gauge blunt tip needle (Becton Dickinson, Franklin Lakes, NJ). Composite PLGA-hydroxyapatite (PLGA-HA) nanofibers were fabricated similarly by adding a suspension of HA nanoparticles immersed in DMF to the PLGA solution, resulting in a 15% HA (w/w) polymer-ceramic suspension. Aligned fibers were obtained using an aluminum mandrel rotating at a velocity of 20m/s with a constant polymer flow rate of 1 mL/hr maintained via a syringe pump (Harvard Apparatus, Holliston, MA)[233]. An electrical potential was applied between the needle and the drum using a high-voltage DC power supply (Spellman, Hauppauge, NY). The bi-phasic collar system was fabricated by electrospinning parallel regions of PLGA and PLGA-HA nanofibers. After depositing a layer of aligned PLGA nanofibers on the mandrel, a custom masking system was applied upon which a layer of PLGA-HA nanofibers was deposited. The resulting multi-phase collar consisted of a PLGA region, a PLGA/PLGA-HA overlapping region (1mm in length) and a PLGA-HA region.

For the bone phase, composite polymer-ceramic nanofibers were fabricated. Briefly, a 5:1 mixture of PLGA and PCL was dissolved in a 60:40 mixture of dichloromethane and dimethyl formamide (DMF)

and mixed for one hour. Simultaneously, a suspension of HA nanoparticles (Nanocerox, Ann Arbor, MI) and DMF was sonicated for one hour. The nanoparticle suspension and polymer solution were then mixed rigorously to produce an 18% (wt%) polymer solution containing 35% (wt ceramic/wt polymer) HA. To produce the nanofibers, the polymer solution was loaded into a 5 mL syringe with a 18.5-gauge stainless steel blunt tip needle, and electrospun at 8-10kV using a custom electrospinning device. The polymer solution was deposited (1 mL/hour) using a syringe pump (Harvard Apparatus, Holliston, MA) onto a rotating mandrel (20m/s) to produce the aligned fibers.

8.2.2 Cells and Cell Culture

Mesenchymal stem cells were obtained from the long bones of Lewis rats. Rats were euthanized by carbon dioxide inhalation, and the femurs and tibiae were harvested under sterile conditions. The MSCs were harvested by lavaging the intramedullary canals of the long bones into 50mL conical tubes using DMEM containing 10% fetal bovine serum (FBS), 1% penicillin-streptomycin, 1% non-essential amino acids, 0.1% amphotericin B and 0.1% gentamicin. Harvested cells were plated directly into 150cm2 culture dishes for 48 hours in an incubator at 37°C, humidified with 5% CO2. After 2 days, the contents of the flask were removed and washed with phosphate buffered saline (PBS), leaving behind MSCs that adhered to the bottom of the flask. Once confluent, the MSCs were detached with 0.25% trypsin (Cellgro) and serially sub-cultured. Cells from passages three and four were used for all studies.

Grafts were seeded dynamically using an orbital shaker. Briefly, after sterilization, grafts were placed in conical tubes (BD Biosciences, Franklin Lakes, NJ) containing cell suspension with a density of 1 million MSC/ml. Tubes containing grafts were placed on an orbital shaker, rotating at a rate of 100 RPM, while placed in a cell culture incubator. It was determined through previous optimization studies that cell seeding density could be controlled by varying the amount of time that scaffolds were agitated in the cell suspension. Seeding for 2 hours resulted in $2.5x10^5$ cells per scaffold, 3 hours resulted in $5x10^5$ cells per scaffold and 4 hours resulted in $1x10^6$ cells per scaffold.

8.2.3 Cell Proliferation

Total DNA content was measured using the PicoGreen dsDNA assay (Invitrogen). At each time point, the samples (n=5/group) were homogenized in 0.1% Triton-X (Sigma-Aldrich) and subjected to 20 seconds of ultrasonication at 5W. Fluorescence was measured using a microplate reader (Tecan, Research Triangle Park, NC) at an excitation wavelength of 485 nm and an emission wavelength of 535 nm. A standard curve was derived and used to correlate DNA concentration to fluorescence intensity, and cell number was determined based on a conversion factor of 8pg DNA/cell[104].

8.2.4 Cell Biosynthesis

Total collagen content per sample (n=5/group) was calculated using the hydroxyproline assay[142]. Briefly, the samples were first desiccated for 24 hours and then digested for 16 hours at 60^{o}C with papain (600 µg protein/ml) in 0.1M sodium acetate (Sigma), 10 mM cysteine HCl (Sigma), and 50 mM ethylenediaminetetraacetate (Sigma). A 40 µl aliquot of the digest was hydrolyzed with 10 µl 10 M sodium hydroxide and autoclaved for 25 minutes. The hydrolyzate was then oxidized by a buffered chloramine-T reagent for 25 minutes before the addition of Ehrlich's reagent. Sample absorbance was measured at 550nm (Tecan), and the collagen content was obtained by interpolation along a standard curve of bovine type I collagen (Sigma).

Mineralization potential was determined by measuring ALP activity (n=5) using an colorimetric assay based on the hydrolysis of p-nitrophenyl phosphate (pNP-PO4) to p-nitrophenol (pNP)[202]. Briefly, the samples were lysed in 0.1% Triton-X solution, then added to pNP-PO4 solution (Sigma) and allowed to react for 30 min at 37°C. Sample absorbance was measured at 415nm using a microplate reader (Tecan).

Sample glycosaminogylcan content (GAG, n=5) was determined with a modified 1, 9-dimethylmethylene blue (DMMB) binding assay[234-236], with chondrotin-6-sulfate (Sigma) as the standard. To account for the anionic nature of the carboxyl groups on the alginate hydrogel, the pH of the DMMB dye solution was adjusted to 1.5 with concentrated formic acid (Sigma) so that only the sulfated GAG-DMMB complexes were detectable. Additionally, the absorbance difference between 540nm and 595nm was used to improve the sensitivity in signal detection.

8.2.5 Cell Differentiation

The phenotype of MSCs was assessed quantitative real-time reverse transcriptase polymerase chain reaction (n=5/group). Total RNA was isolated using the Trizol extraction method (Invitrogen). Isolated RNA was then reverse-transcribed into complementary DNA using the SuperScript First-Strand Synthesis System (Invitrogen), and the cDNA product was amplified using recombinant Taq DNA polymerase (Invitrogen). Phase-specific gene expression analysis was performed using the primers listed in *Table 8.1*. GAPDH served as the house-keeping gene. All primer sequences are listed in Table 2. All genes were amplified for 50 cycles in a thermocycler (Bio-Rad iCycler, Hercules, CA) with a fluorescent probe (SYBR Green, Invitrogen). Quantitative analysis of gene expression was performed using the delta-delta CT method.

8.2.6 Tensile Mechanical Properties

For tensile testing, the scaffolds were secured with custom clamps and mounted on an Instron (Model 8841, Norwood, MA), equipped with a 250 lb load cell. The samples had an average gauge length of 3.5 cm and were tested to failure along the scaffold long axis at a strain rate of 5 mm/min. Scaffold yield strength, ultimate tensile stress and ductility were determined, and elastic modulus was calculated from the linear region of the stress-strain curve.

8.2.7 Effect of Architecture on Graft Mechanical Properties and Integrity

The effect of ligament phase architecture was first evaluated to select the optimal configuration for the ligament phase in terms of mechanical properties. Ligament phase nanofibers were rolled into cylindrical bundles to mimic the organization of the native ACL. To standardize the amount of fibers in each bundle, ligament phase nanofibers were fabricated by electrospinning for 45 minutes to create a 20μm-thick nanofiber mesh. The resulting meshes were rolled into bundles 0.8mm in diameter.

Five architecture configurations were tested. Single, double and triple parallel bundle designs were evaluated, which consisted of one, two or three ligament phase bundles in parallel (*Fig. 8.1*). Additionally, two braided structures were assessed, the first consisted of three fibrous bundles were then

braided together while the second was made up of three triple bundles braided together (*Fig 8.1*). Once fabricated, the ends of the ligament phase constructs were melted to maintain integrity.

Once the ligament phase architecture was optimized, a multi-phased scaffold incorporating the ligament, bone and interface phases was constructed. To incorporate the ligament and bone phases, multi-phased bundles were first constructed. To standardize the number of fibers in each phase, composite polymer-ceramic bone phase nanofibers were first electrospun onto a mandrel for 45 minutes. Subsequently, a region of fibers 0.5mm in width was excised from the mandrel and ligament phase nanofibers were electrospun over the remaining bone phase fibers for 45 minutes. The resulting mesh consisted of a region with a layer of bone phase fibers over a layer of ligament phase fibers and a central region of ligament phase-only fibers. The meshes were then rolled into cylindrical bundles and interface phase collars were secured to these ligament/bone phase bundles using a 7-0 Prolene suture (Ethicon, Somerville, NJ). The resulting multi-phased scaffold consisted of a 1cm bone phase at each end, 0.5cm interface phases and a central 0.5cm ligament phase. Tensile testing was performed on multi-phased ACL scaffold to ensure construct integrity between phases.

8.2.8 Effect of Cell Density

Following validation of the multi-phased ACL scaffold, cell seeding density on the scaffold was optimized. Multi-phased ACL scaffolds were fabricated and seeded with rat MSCs. Three densities were evaluated: $2.5x10^5$ cells per scaffold, $5x10^5$ cells per scaffold and $1x10^6$ cells per scaffold. The effect of culture duration on cell proliferation, biosynthesis, and differentiation was determined over the course of 7 days. For end point analyses, the scaffolds were carefully separated into bone, ligament and interface phases to perform phase-specific analyses.

8.2.9 Bioreactor Culture

After optimizing cell density, the multi-phased ACL construct was cultured *in vitro* at the optimal cell density using a bioreactor to apply mechanical stimulation and simulate the in vivo environment. The bioreactor system and mechanical loading parameters were identical to those used in a previously published study[176]. The effect of bioreactor culture duration on cell proliferation, biosynthesis, and

differentiation as well as scaffold tensile mechanical properties was assessed over 21 days. Similar to the cell density optimization study, for end point analyses, the scaffolds were carefully separated into bone, ligament and interface phases to perform phase-specific analyses.

8.3 Results

8.3.1 Effect of Architecture on Mechanical Properties

A parallel-bundle and a braid design were evaluated to determine the optimal architecture for the ligament phase of the graft. Three different parallel bundle designs, ranging from one to three parallel bundles, were tested to simulate the architecture of the native ACL. No difference in tensile mechanical properties was measured by changing the parameters of the parallel-bundle design (*Fig. 8.1*). In contrast, braiding resulted in a significant increase in the length of the toe region of the ligament phase as well as a significant decrease in elastic modulus. No significant difference was measured between the single-bundle braid system and the triple-bundle braid.

The tensile properties of the synthetic graft were also evaluated after incorporating all three phases to ensure that no delamination occurred once the phases were combined. No significant difference in tensile properties was measured between a single ligament-phase-only graft and the multi-phased graft incorporating the bone and interface phases (*Fig. 8.2*).

8.3.2 Effect of Cell Density on Cell Proliferation and Biosynthesis

A seven day study was conducted to evaluate the effect of cell density on MSC response. In terms of cell attachment and proliferation, a significantly greater number of cells was measured on all phases of grafts seeded with 1M cells as compared to the 250K and 500K cell seeded group at day 1 (*Fig 8.3*). On the bone phase, a significantly greater number of cells was measured in the 1M cell seeded group as compared to the 500K cell seeded group, which also had significantly more cells than the 250K cell seeded group. After seven days, no significant difference in cell number was measured between the 250K and 500K cell seeded groups though the 1M cell seeded group had significantly greater cells than both. On the interface and ligament phases, the 250K and 500K cell seeded groups had similar numbers

of cells at day 3 with significantly greater cells attached in the 1M cell seeded group. At day 7, the 1M cell seeded group had a significantly greater number of cells than the 250K cell seeded group only.

A significant increase in ALP activity per cell was measured on the bone phase of grafts seeded with 1M cells at day 7, as compared to grafts seeded with 250K cells (*Fig. 8.4*). In addition, this increase was significant as compared to the ALP activity for the same group at day 3. No significant difference in ALP activity was measured for the other groups on the bone phase nor was any difference measured between groups or over time on the interface or ligament phases.

Total collagen content on each phase was also quantified and normalized per cell with no significant difference measured between groups or over time on any of the phases (*Fig. 8.5*). A mean increase, however, was observed over time for the 1M cell seeded group on all phases.

A significant increase in sulfated GAG content per cell was measured on the interface phase of grafts seeded with 1M cells at day 7, as compared to grafts seeded with 250K cells (*Fig. 8.6*). No significant difference in total GAG content was measured for the other groups on the interface phase nor was any difference measured between groups or over time on the bone or ligament phases.

8.3.3 Effect of Cell Density on Cell Differentiation

The effect of cell density on MSC differentiation was assessed at day 1 (*Fig. 8.7*). On the bone phase, no difference in osteocalcin or osteopontin expression was measured as a function of seeding density. On the interface phase, type II collagen and aggrecan were upregulated at day 1 with a 1M cells/scaffold seeding density, as compared to the 250K cell seeded group. No difference in type X collagen expression was observed between groups. For the ligament phase, several ligament-specific markers were measured including types I and III collagen, fibronectin, tenascin-C, scleraxis and tenomodulin. However, cell density had no significant effect on the expression of any of these markers.

8.3.4 Effect of Bioreactor Culture on Cell Proliferation and Biosynthesis

Based on the results of the cell-density study, synthetic grafts seeded with 1M cells were cultured for 21 days in a bioreactor which applied controlled tensile stimulation to mimic the *in vivo* environment. Evaluating cell attachment and proliferation, a significantly greater number of cells was measured on the

bone phase at day 7 as compared to day 1. No difference in cell number was measured over time on the interface or ligament phases.

A significant increase in ALP activity was only measured on the bone phase with a significant increase at day 7 as compared to day 1. The ALP activity remained elevated at day 21 on the bone phase. No difference in ALP activity was measured over time on the interface or ligament phases. Collagen content per cell was significantly greater on the ligament phase after 21 days of culture as compared to day 1 and day 7. No difference was measured over time on the bone phase or interface phase. Lastly, GAG content was measured over time and normalized per cell. A significant increase in GAG content was measured at day 7 as compared to day 1 and remained elevated at day 21. No significant difference was measured over time on the bone or ligament phases.

8.3.5 Effect of Bioreactor Culture on Cell Differentiation

Cell differentiation was assessed by measuring the expression of relevant genes for each phase at day 21 as compare to day 1. On the bone phase, a significant increase in osteocalcin and osteopontin expression was measured at day 21. On the interface phase, type II collagen and aggrecan were significantly upregulated at day 21. However, no difference in type X collagen was observed as compared to day 1. Similarly, the expression of several fibroblastic markers was measured for the ligament phase. It was observed that types I and III collagen, fibronectin, tenascin-C, and tenomodulin were all upregulated at day 21 as compared to day 1. No difference in scleraxis expression was measured over time.

8.3.6 Effect of Bioreactor Culture on Tensile Properties

Tensile mechanical properties of the cell-seeded synthetic grafts were measured at day 1, 7 and 21. No significant difference in mechanical properties was observed over time though a mean decrease in elastic modulus and ultimate tensile strength was measured beginning at day 7 (*Fig. 8.10*). Conversely, a mean increase was observed for yield strength and ductility over time.

8.4 Discussion

The goal of this study is to optimize the architecture and seeding density of synthetic ACL scaffold and subsequently evaluate the optimized scaffold for the formation of an integrated bone-ligament-bone complex *in vitro*. To address the first objective, five different configurations for the ligament phase of the scaffold were evaluated. It was determined that a multi-bundle braided structure was optimal for this phase based on the physiologically relevant mechanical properties that it exhibited, specifically an elongated toe-region similar to the native ligament. Following optimization of the architecture, the cell seeding density for the scaffold was optimized. Three densities were evaluated: $2.5x10^5$, $5x10^5$ and $1x10^6$ cells per scaffold. It was demonstrated that the highest seeding density, $1x10^6$ cells per scaffold, resulted in increased ALP activity and GAG production on the bone and ligament phases, respectively, at day 7 as well as an upregulation of type II collagen and aggrecan on the interface phase at day 1. No such response was observed at the other seeding densities indicating that the $1x10^6$ cells per scaffold density was optimal for further investigation. Lastly, the scaffold incorporating the optimal architecture and cell density was culture *in vitro* using a bioreactor system to apply physiologically relevant mechanical loading. A phase-specific response was measured over 21 days with increase ALP activity and osteogenic marker expression on the bone phase, increase GAG production on the interface phase and increased collagen synthesis and fibroblastic marker expression on the ligament phase.

Controlling the bundle architecture of the ligament phase was shown to enable control of scaffold bulk mechanical properties. All scaffold configuration displayed elastic mechanical properties within the range of the native ACL in terms of the elastic modulus, which is reportedly between 49-163 MPa[186], yield strength (13.7-36.4MPa in humans[186]), and ductility (19-36% [186]). However, in addition to elastic mechanical properties, the viscoelastic properties of soft tissue grafts are critical for long-term functionality. In particular, the low stiffness region known was the ‘toe region’ of the stress-strain cure reported to be approximately 5% for the native human ACL. This mechanical behavior is due to the straightening of collagen fibrils that occurs and enables the tissue to lengthen without damaging the fiber structure[185;260;261]. In this study, it was demonstrated that using a braided structure resulted in a toe region upwards of 5% enabling the same viscoelastic behavior as the native ligament. Previous efforts in

ligament tissue engineering have similarly focused on a braided design due to mechanical considerations[18;19;100;103;104].

For *in vitro* culture, the highest cell seeding density evaluated in this study was found to be optimal as increased ALP activity and GAG content was only measured on the bone and interface phases, respectively, after 7 days of culture with $1x10^6$ cells per scaffold. Previous studies investigating the effect of seeding density on ligament tissue engineered constructs have similarly found that greater cell density enhances biosynthetic activity. For example, Awad *et al.* reported that collagen gel constructs seeded at 4 million cells per ml resulted in greater cell alignment and contractile properties[262]. Studies investigating cell seeding density for bone and cartilage tissue engineering construct have also reported that a minimum number of cells is required for an optimal response, beyond which additional cells have little effect on biosynthesis and tissue formation[255;262;263]. Increased cell density is thought to lead to an enhanced response due to greater cell-cell and cell-material interactions that occur with higher cell number[255].

Using the optimized parameters, the scaffold was cultured *in vitro* using a bioreactor to apply mechanical stimulation similar to that experienced when the scaffold is used for ACL reconstruction. The scaffold supported the formation of distinct tissue types on each phase. On the interface phase, increased GAG production was measured after 7 days of culture. These proteins are indicative of a cartilage-like phenotype as proteoglycans and type II collagen make up cartilaginous tissues as well as the fibrocartialginous insertion sites between soft and hard tissues[75]. The expression of types II and X collagen as well as aggrecan, however, was not upregulated in this study suggesting that additional chemical or mechanical factors may be necessary to induce long-term interface formation. Type X collagen is of particular importance because it is has been identified at the ACL-bone interface and is thought to play a role in the attachment of ligament to bone[220]. A bone-specific response was measured on the bone phase, including an increase in ALP activity at day 7 and the upregulation of osteocalcin and osteopontin after 21 days which are early and late markers of bone formation, respectively[264;265]. Lastly, similar to previous studies performed on an aligned PLGA nanofiber system using human MSCs[176], collagen production was increased and the expression of several fibroblastic markers was upregulated indicating that the rat MSC differentiated towards a fibroblastic phenotype.

Collectively, these findings suggest that the physical and chemical parameters of each phase coupled with the tensile mechanical loading resulted in the formation of a heterogeneous tissue similar to the native bone-ACL-bone complex.

8.5 Conclusions

The results of this study demonstrate that a braided architecture seeded at a density of 1 million cells per graft is the optimal seeding density for the synthetic nanofiber graft. In addition, these findings show that a phase-specific response is elicited at this density when cultured under physiologically relevant mechanical conditions and that a bone-ligament-bone complex containing distinct yet continuous regions of bone, interface and ligament tissue can be formed *in vitro* on the synthetic nanofiber graft. Based on these findings, the multi-phased scaffold will be evaluated *in vivo* in the following chapter.

Table 8.1. List of rat PCR primers.

Gene	*Sense*	*Anti-Sense*
GAPDH	5'-TGTATCCGTTGTGGATCTGACATGC-3'	5'-CCCTGTTGCTGTAGCCATATTCATTGT-3'
Osteocalcin	5'-AGGGCAGTAAGGTGGTGAAT-3'	5'-CTAAACGGTGGTGCCATAGA-3'
Osteopontin	5'-TGTGTCCTCTGAAGAAACGG-3'	5'-AGAATCCTCGCTCTCTGCAT-3'
Type II Collagen	5'-GGACATAGGGCCTGTCTGTT-3'	5'-CCGGACTGTGAGGTTAGGAT-3'
Aggrecan	5'-CAGATCTGCATGGAATCACC-3'	5'-AAGTGCCTGCATCTATGTCG-3'
Type X Collagen	5'-CTCCTGGTGTGAATGGACAG-3'	5'-TCACCTCTTCTTCCCACTCC-3'
Type I Collagen	5'-CTGCTGGTCCTAAGGGAGAG-3'	5'-GACAGCACCATCGTTACCAC-3'
Type III Collagen	5'-GATGCTGGTGCTGAGAAGAA-3'	5'-GGCTGGAAAGAAGTCTGAGG-3'
Fibronectin	5'-AGAAATTGACAAGCCATCCC-3'	5'-CACAGGAGAAGTTGAAGGCA-3'
Tenascin C	5'-CAGAAGCTGAACCGGAAGTTG-3'	5'-GGCTGTTGTTGCTATGGCACT-3'
Scleraxis	5'-AACACGGCCTTCACTGCGCTG-3'	5'-CAGTAGCACGTTGCCCAGGTG-3'
Tenomodulin	5'-TCGAGTCATCTGTCGTGTCA-3'	5'-GCAAATGCAGAAATTCATGG-3'

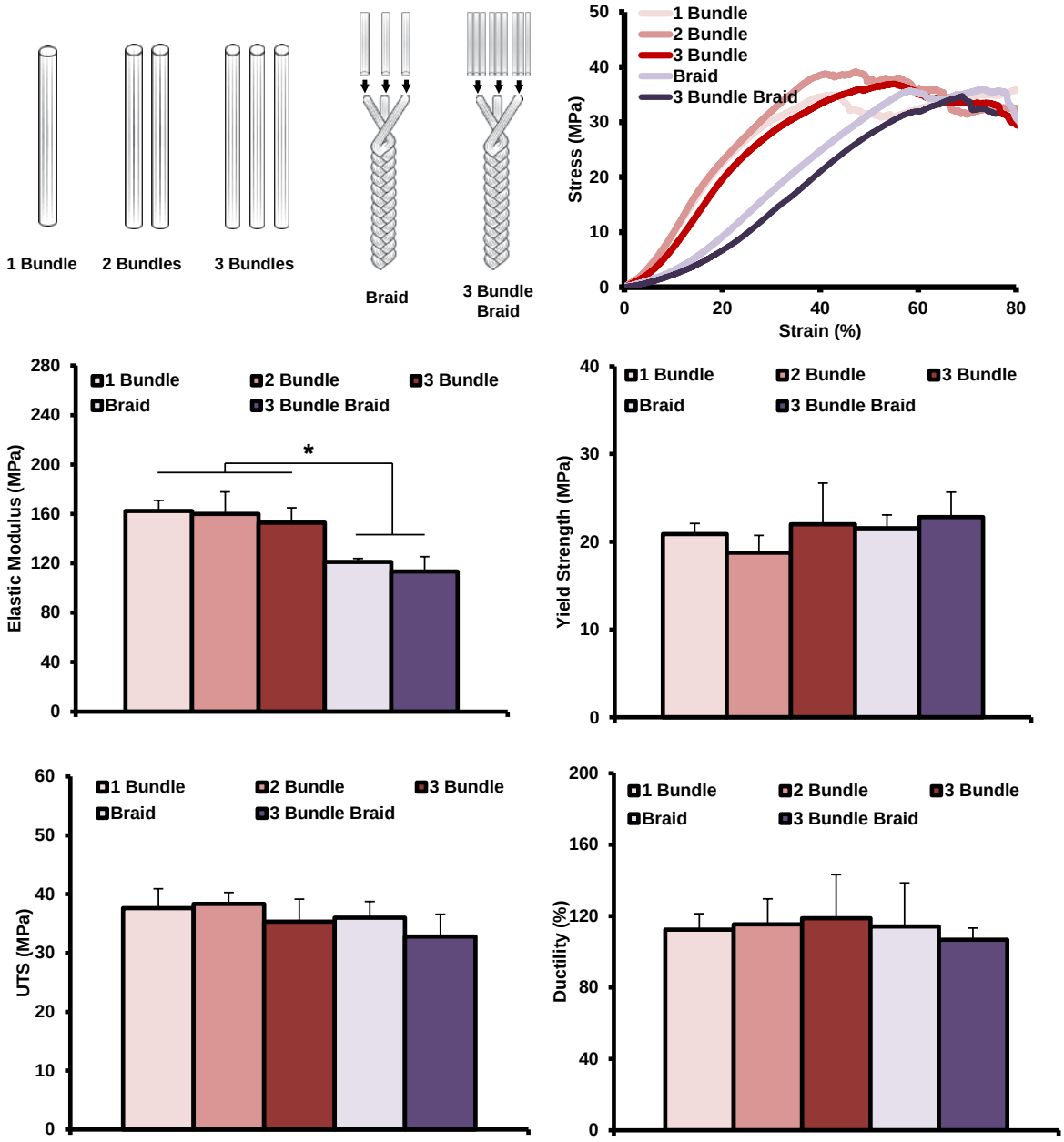

Figure 8.1. Effect of ligament phase architecture. No difference in tensile properties was measured with multiple parallel bundles. Braiding of the bundles resulted in a significantly elongated toe region and decreased construct elastic modulus. Similarly, no difference in mechanical properties was observed between the single-bundle braid and the triple-bundle braid.

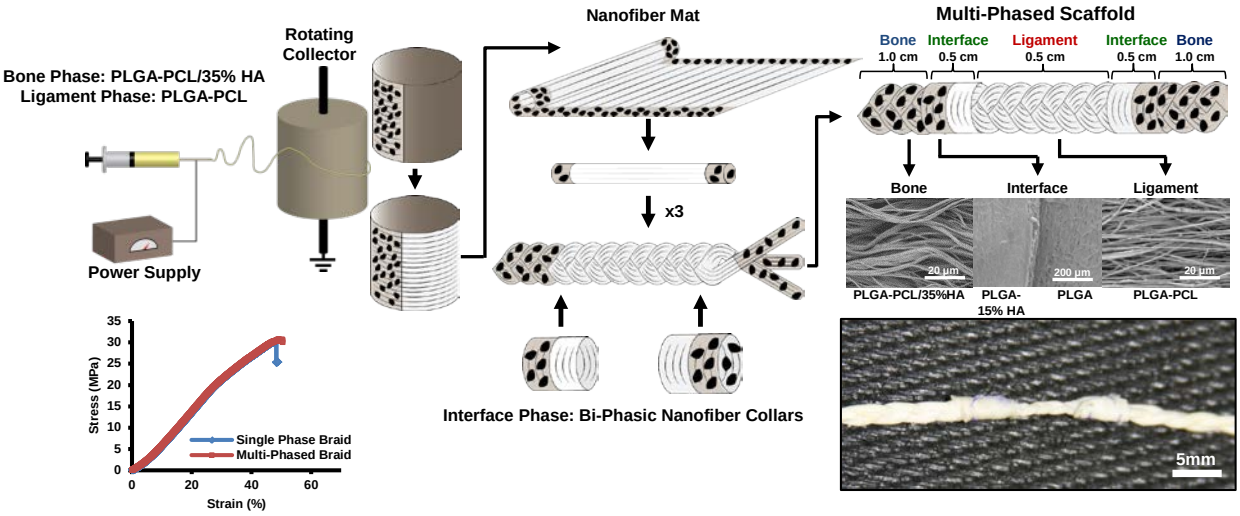

Figure 8.2. Multi-phased ACL scaffold fabrication. The multi-phased ACL scaffold was fabricated via electrospinning the bone and ligament phases together and then attaching the bi-phasic collars as the interface phase. Incorporating the ligament and bone phases had no effect on scaffold mechanical properties.

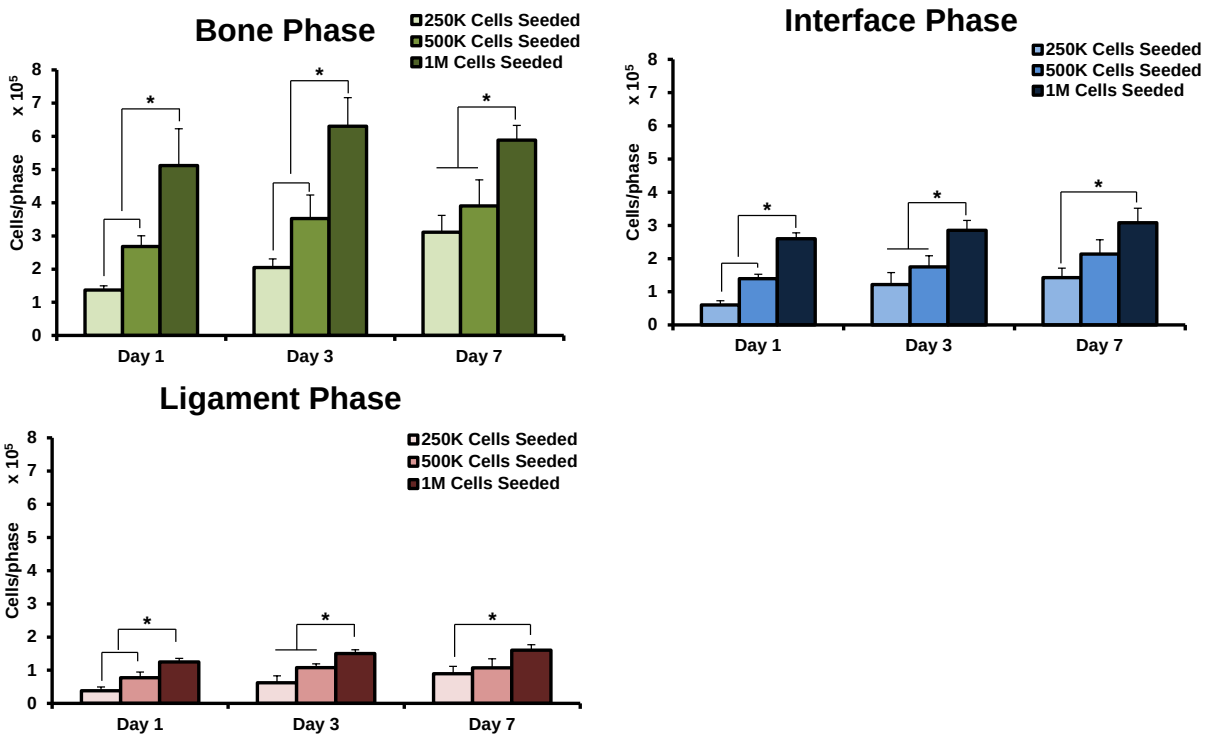

Figure 8.3. Cell attachment and proliferation. A significantly greater number of cells was measured on all phases of grafts seeded with 1M cells as compared to the 500K and 250K cell group at day 1. A significantly greater number of cells was measured in the 1M cell seeded group on all phases at all time points.

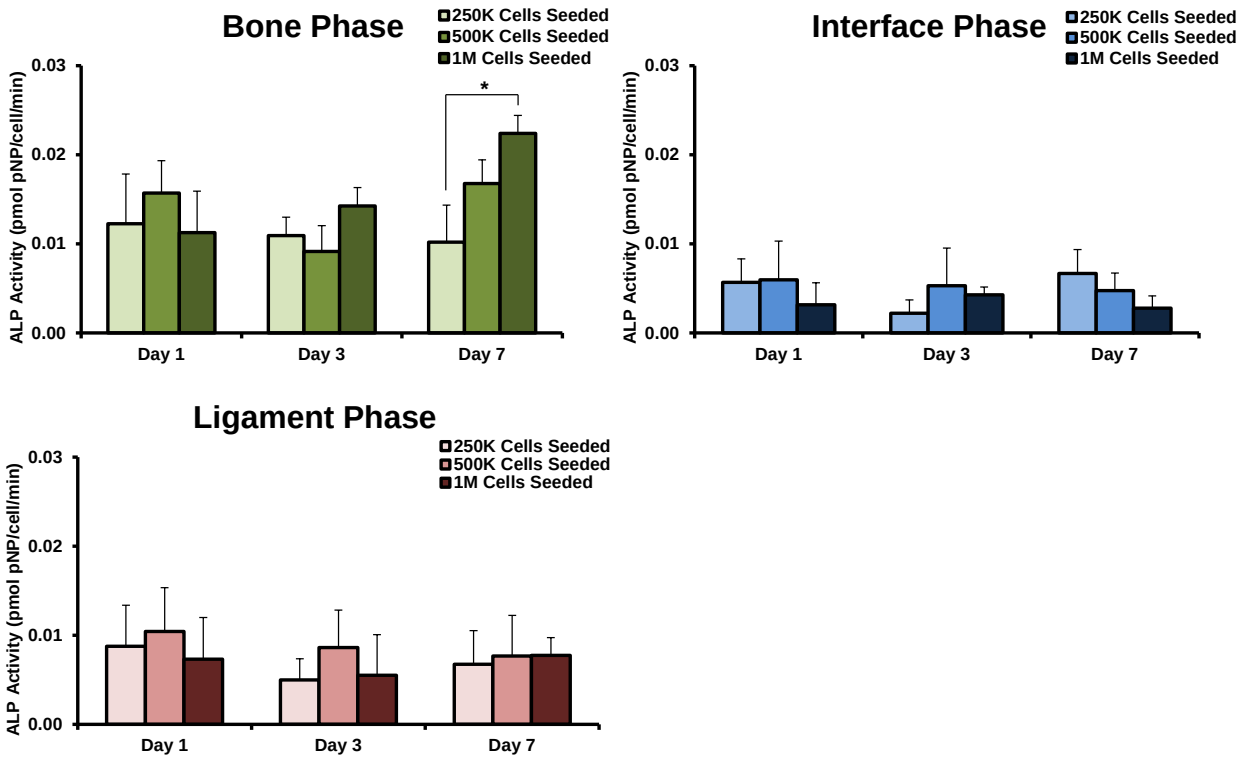

Figure 8.4. Effect of cell density on ALP activity. Increased ALP activity was measured on the bone phase of grafts seeded with 1M cells at day 7, as compared to grafts seeded with 250K cells. No effect of cell density on ALP activity was observed on the interface or ligament phase at any time point.

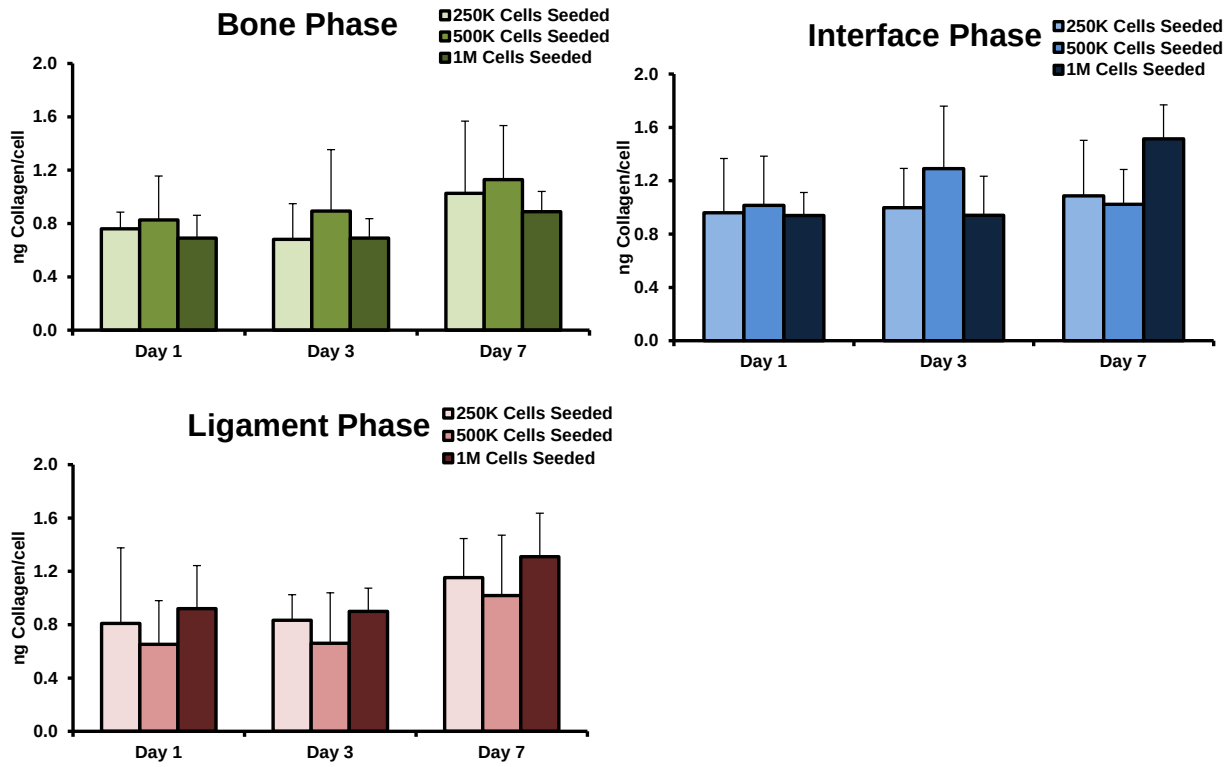

Figure 8.5. Effect of cell density on collagen synthesis. Cell density had no significant effect on collagen synthesis per cell though a mean increase was observed over time in all groups.

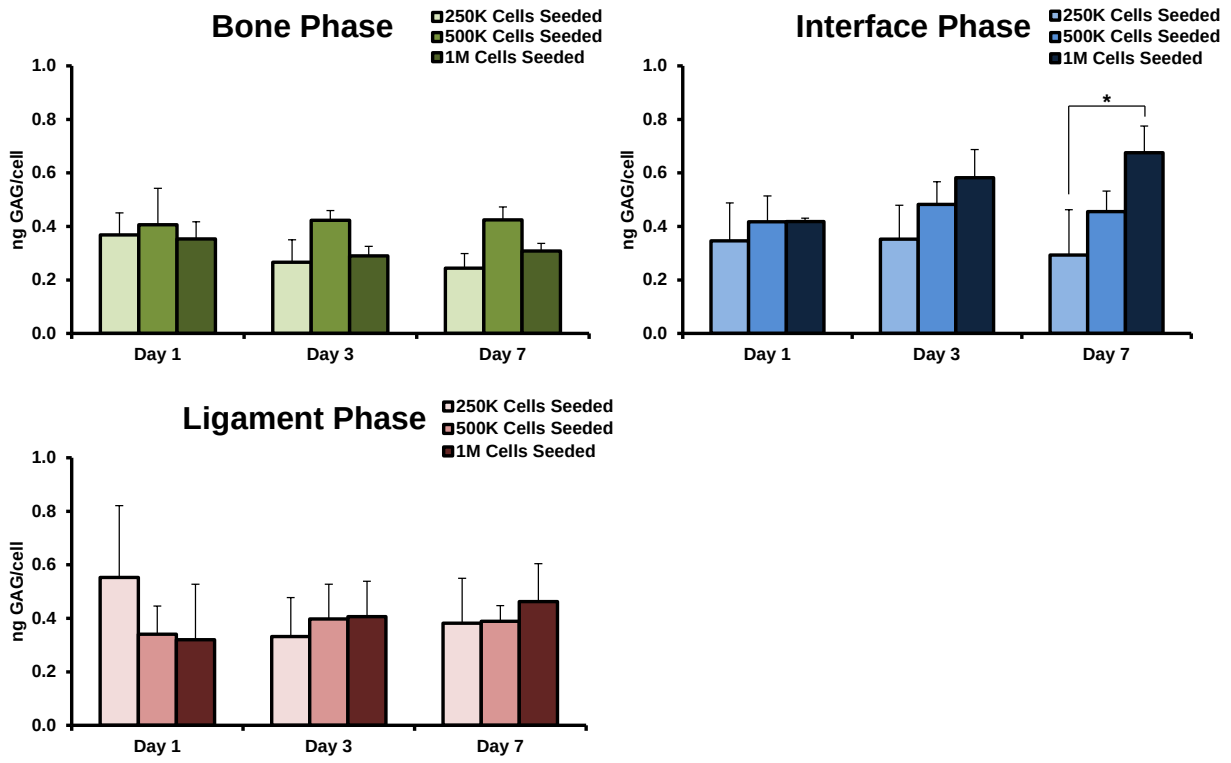

Figure 8.6. Effect of cell density on GAG production. Increased sulfated GAG was measured on the interface phase of grafts seeded with 1M cells, as compared to grafts seeded with 250K cells. No effect of cell density on GAG production was observed on the interface or ligament phase at any time point.

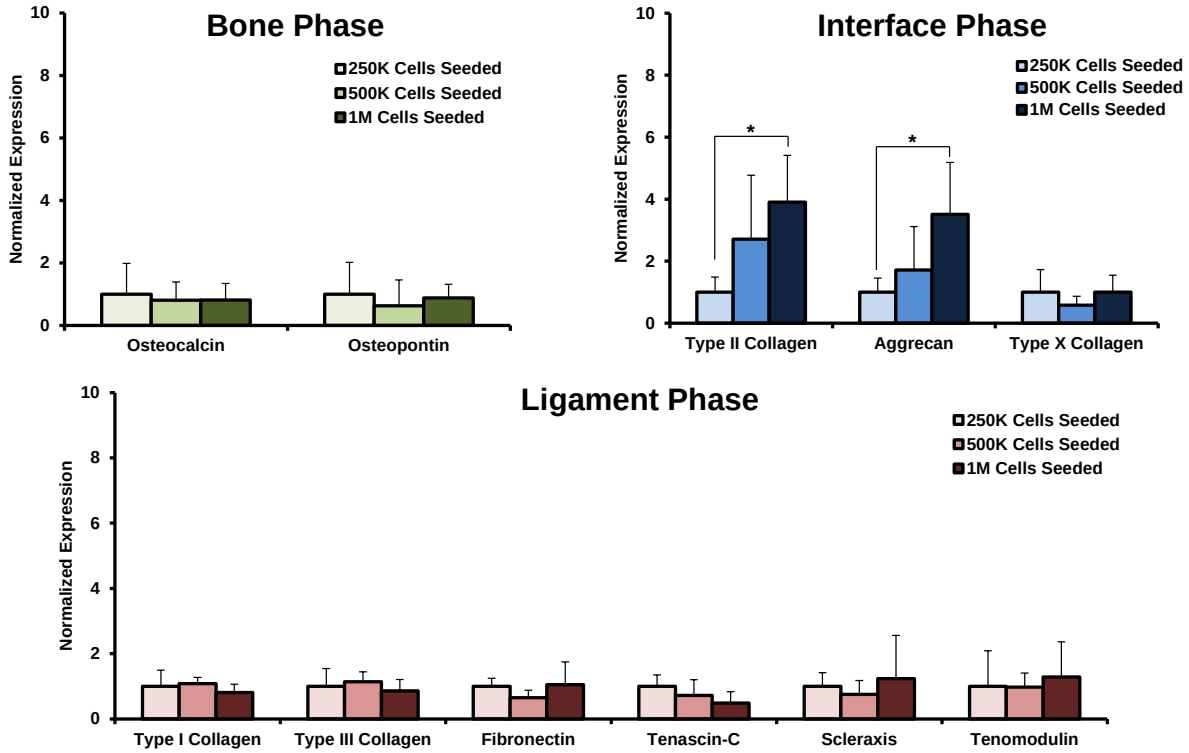

Figure 8.7. Effect of cell density on cell differentiation at day 1. Type II collagen and aggrecan expression was significantly upregulated on the interface phase only in the 1M cell seeded group at day 1. Cell density had no effect on the expression of osteogenic or fibroblastic markers on the bone and ligament phases, respectively.

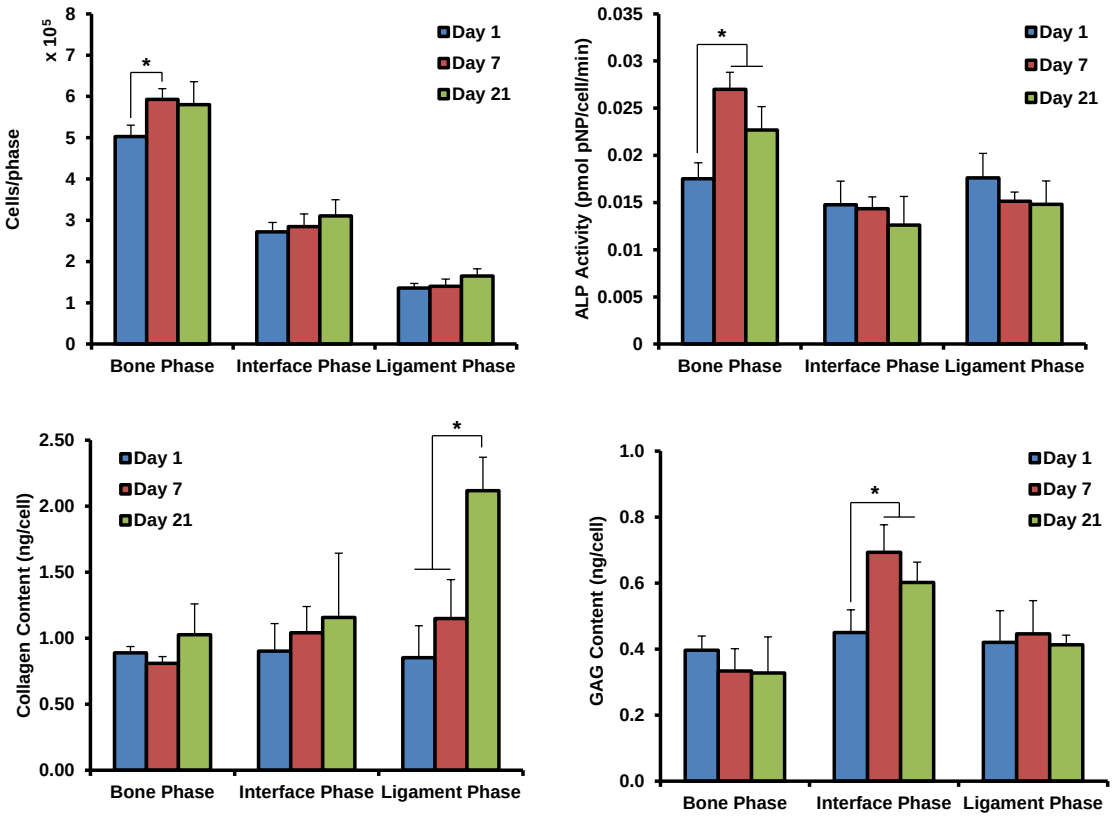

Figure 8.8. Cell proliferation and biosynthesis over time with bioreactor culture. A significant increase in cell number was only measured on the bone phase at day 7 compared to day 1. A phase-specific response was measured in terms of biosynthesis with increase ALP activity per cell on the bone phase beginning at day 7, increased collagen per cell on the ligament phase at day 21 and increased GAG per cell on the interface phase at day 7.

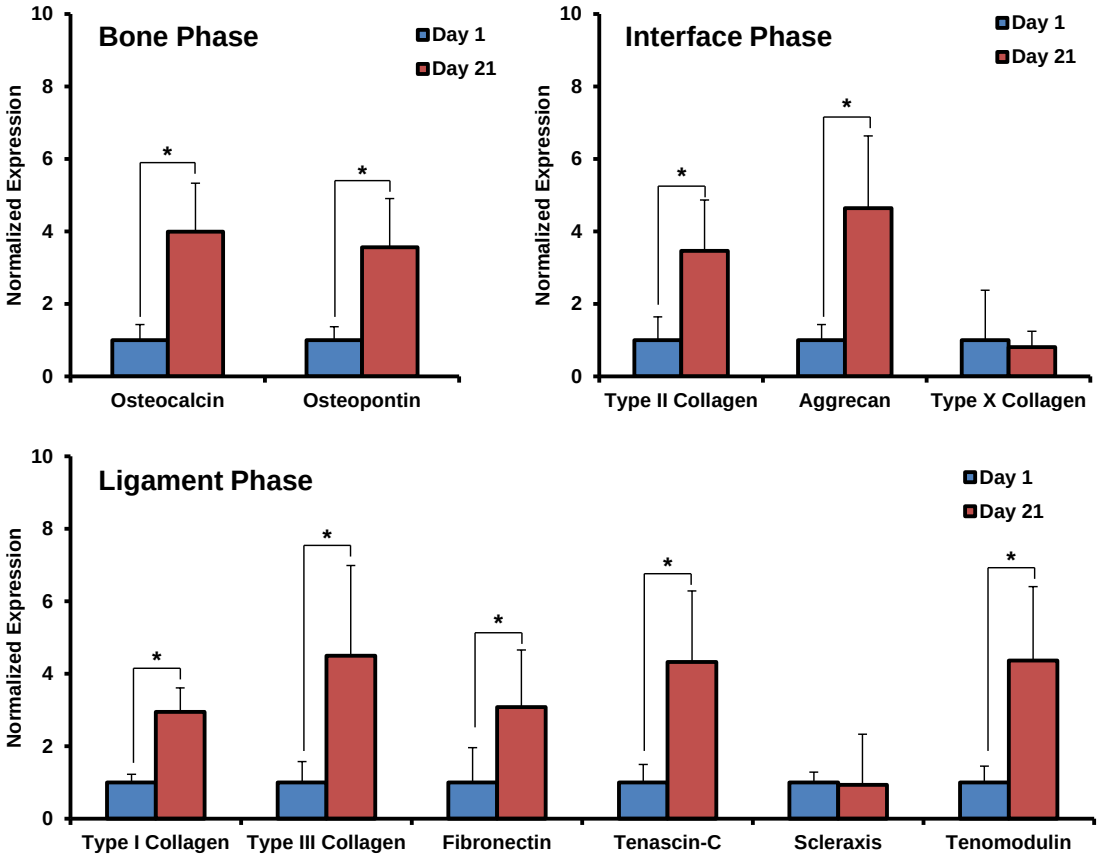

Figure 8.9. Cell differentiation on each phase with bioreactor culture. A phase-specific differentiation response was observed on the graft. On the bone phase, osteocalcin and osteopontin were upregulated at day 21 as compared to day 1. On the interface phase, type II collagen and aggrecan were upregulated at day 21. On the ligament phase, types I and III collagen, fibronectin, tenascin-C, and tenomodulin were all upregulated after 21 days of culture.

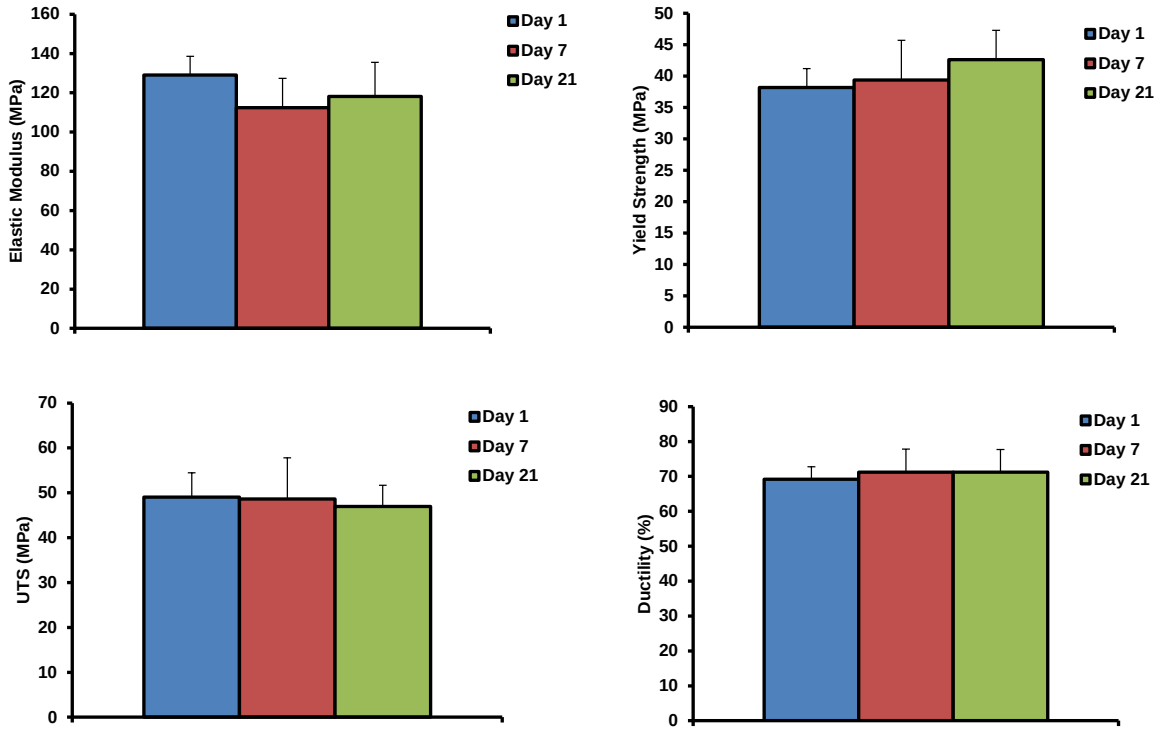

Figure 8.10. Effect of bioreactor culture on tensile mechanical properties. No significant difference in tensile mechanical properties was measured over the 21 day culture period.

CHAPTER 9: IN VIVO EVALUATION OF THE MULTI-PHASED SYNTHETIC ACL GRAFT

9.1 Introduction

The previous chapters of this thesis focused on the design and optimization of the multi-phased synthetic scaffold for the formation of an integrated bone-ligament-bone complex *in vitro*. While the results from *Chapter 8* demonstrate the ability of the scaffold to induce the formation of distinct regions of bone, ligament and interface tissue *in vitro*, an animal model will be used in *Chapter 9* to assess the formation of an integrated bone-ligament-bone complex *in vivo*. In this study, the three different scaffold modalities will be evaluated. The first modality consists of a multi-phased scaffold pre-cultured with cells *in vitro* prior to implantation into the patient. The second modality is an acellular multi-phased scaffold which is implanted to direct the response of host cells. Lastly, a single-phase scaffold consisting of the ligament phase only will be implanted to assess how the multi-phased design affects subsequent tissue formation.

9.1.1 Background and Motivation

The development of scaffold systems for tissue engineering necessitates the use of relevant *in vivo* models to account for the presence of vasculature, the full complement of in vivo cytokines, hormones, growth factors, cell types, and physiologic loading which are essential for graft-to-host interaction. *In vitro* models alone are not adequate to evaluate the full spectrum of the biologic response due to the complexity of the processes being studied. Moreover, there is insufficient data available for the design of non-living models. This *in vivo* evaluation will provide invaluable feedback for future scaffold optimization and guidelines for implant evaluation in larger animal models.

9.1.2 Objectives

The goal of this study is to test the multi-phased scaffold in vivo by assessing bone, fibrocartilage and ligament formation and integration. It is hypothesized that the multi-phased design of the synthetic ACL scaffold will enable for the regeneration of distinct-yet-continuous bone, interface and ligament tissue. Specifically, the bone phase will support mineralized bone tissue formation and scaffold osteointegration, the nanofiber collar interface phase will support fibrocartilaginous tissue and the ligament phase will maintain joint stability and promote collagenous ligament tissue formation. In addition,

it is hypothesized that the seeding of cells on the multi-phased scaffold prior to implantation result in more abundant tissue formation. To this end, ACL reconstruction will be performed using a control soft tissue graft, a single phase (ligament phase only) scaffold to demonstrate the effect of the multi-phased design, as well as an acellular and cell-seeded multi-phased scaffold.

Several animal models have been developed for ACL reconstruction including the rodent[266], rabbit[18], canine[12], porcine[267] and goat[268] models. While large animal models provide a more accurate representation of human anatomical size and biomechanical loads, they are significantly more costly to obtain and maintain. These animals are also quadrupeds with differences in anatomy and joint biomechanics as compared to bipedal humans. The rodent model is a well-developed model of ACL reconstruction that has been extensively studied to assess tendon-to-bone healing[11;56;57;266;269]. A syngeneic rodent model, in particular, is optimal for this study as it allows for the use of primary rodent stem cells without the need to harvest cells from each animal, a procedure that would increase study complexity and time. The rat is also the smallest animal and lowest species in which the response can be evaluated *in vivo*, but is much larger compared to mice, making the technically-challenging ACL reconstruction procedure feasible.

9.2 Materials and Methods

9.2.1 Synthetic ACL Scaffold Fabrication

Each phase of the nanofiber-based synthetic ACL was fabricated via electrospinning. For the ligament phase, a mixture of 18% (w/v) poly(ε-caprolactone) (PCL, Sigma-Aldrich, Mw=70,000-90,000) and PLGA (85:15, M_w=123.6 kDa; Lakeshore Biomaterials) was dissolved in a mixture of 60/40 dichloromethane (DCM, Sigma-Aldrich, St. Louis, MO) and DMF. The polymer solution was loaded into a 5 mL syringe with a 18.5-gauge stainless steel blunt tip needle, and electrospun at 8-10kV using a custom electrospinning device. The polymer solution was deposited (1 mL/hour) using a syringe pump (Harvard Apparatus, Holliston, MA) onto a custom rotating mandrel (20 m/s) to produce aligned fibers.

For the interface phase, bi-phasic nanofiber collars were fabricated. Briefly, a polymer solution consisting of 35% PLGA (w/v, 85:15, Lakeshore Biomaterials) in 55% N,N-dimethylformamide (Sigma-Aldrich) and 10% ethanol (Pharmco-AAPER, Brookfield, CT) was loaded into a syringe fitted with an 18.5-

gauge blunt tip needle (Becton Dickinson, Franklin Lakes, NJ). Composite PLGA-hydroxyapatite (PLGA-HA) nanofibers were fabricated similarly by adding a suspension of HA nanoparticles immersed in DMF to the PLGA solution, resulting in a 15% HA (w/w) polymer-ceramic suspension. Aligned fibers were obtained using an aluminum mandrel rotating at a velocity of 20m/s with a constant polymer flow rate of 1 mL/hr maintained via a syringe pump (Harvard Apparatus, Holliston, MA)[233]. An electrical potential was applied between the needle and the drum using a high-voltage DC power supply (Spellman, Hauppauge, NY). The bi-phasic collar system was fabricated by electrospinning parallel regions of PLGA and PLGA-HA nanofibers. After depositing a layer of aligned PLGA nanofibers on the mandrel, a custom masking system was applied upon which a layer of PLGA-HA nanofibers was deposited. The resulting multi-phase collar consisted of a PLGA region, a PLGA/PLGA-HA overlapping region (1mm in length) and a PLGA-HA region.

For the bone phase, composite polymer-ceramic nanofibers were fabricated. Briefly, a 5:1 mixture of PLGA and PCL was dissolved in a 60:40 mixture of dichloromethane and dimethyl formamide (DMF) and mixed for one hour. Simultaneously, a suspension of HA nanoparticles (Nanocerox, Ann Arbor, MI) and DMF was sonicated for one hour. The nanoparticle suspension and polymer solution were then mixed rigorously to produce an 18% (wt%) polymer solution containing 35% (wt ceramic/wt polymer) HA. To produce the nanofibers, the polymer solution was loaded into a 5 mL syringe with a 18.5-gauge stainless steel blunt tip needle, and electrospun at 8-10kV using a custom electrospinning device. The polymer solution was deposited (1 mL/hour) using a syringe pump (Harvard Apparatus, Holliston, MA) onto a rotating mandrel (20m/s) to produce the aligned fibers.

A multi-phased scaffold incorporating the ligament, bone and interface phases was constructed. To incorporate the ligament and bone phases, multi-phased bundles were first constructed. To standardize the number of fibers in each phase, composite polymer-ceramic bone phase nanofibers were first electrospun onto a mandrel for 45 minutes. Subsequently, a region of fibers 0.5mm in width was excised from the mandrel and ligament phase nanofibers were electrospun over the remaining bone phase fibers for 45 minutes. The resulting mesh consisted of a region with a layer of bone phase fibers over a layer of ligament phase fibers and a central region of ligament phase-only fibers. The meshes were then rolled into cylindrical bundles and interface phase collars were secured to these ligament/bone

phase bundles using a 7-0 Prolene suture (Ethicon, Somerville, NJ). The resulting multi-phased scaffold consisted of a 1cm bone phase at each end, 0.5cm interface phases and a central 0.5cm ligament phase. Single phase (ligament phase only) scaffolds were similarly fabricated using the layering technique though both layers consisted of ligament phase fibers and no interface phase collar was attached.

9.2.2 Cells and Cell Culture

Mesenchymal stem cells were obtained from the long bones of Lewis rats. Rats were euthanized by carbon dioxide inhalation, and the femurs and tibiae were harvested under sterile conditions. The MSCs were harvested by lavaging the intramedullary canals of the long bones into 50mL conical tubes using DMEM containing 10% fetal bovine serum (FBS), 1% penicillin-streptomycin, 1% non-essential amino acids, 0.1% amphotericin B and 0.1% gentamicin. Harvested cells were plated directly into 150cm^2 culture dishes for 48 hours in an incubator at 37°C, humidified with 5% CO2. After 2 days, the contents of the flask were removed and washed with phosphate buffered saline (PBS), leaving behind MSCs that adhered to the bottom of the flask. Once confluent, the MSCs were detached with 0.25% trypsin (Cellgro) and serially sub-cultured. Cells from passages three were used for implantation.

9.2.3 Cell Seeding

For rats receiving cell-seeded synthetic scaffolds, the scaffolds were seeded dynamically using an orbital shaker. Briefly, after sterilization, scaffolds were placed in conical tubes (BD Biosciences) containing cell suspension with a density of 1 million MSC/mL. Tubes containing scaffolds were placed on an orbital shaker, rotating at a rate of 100 RPM, for four hours in a cell culture incubator. It was determined through previous optimization studies that this technique resulted in the adhesion of approximately 1 million cells per scaffold. The scaffolds were pre-cultured with cells for one day prior to implantation.

9.2.4 Surgical Procedure

The ACL reconstruction procedure was performed on male Lewis rats (weight, 275–325 g) following approval by the Institutional Animal Care and Use Committee. The rats were kept in soft-

bedding cages with free access to food and water. Animals were anesthetized with a mixture of 80 mg/kg ketamine hydrochloride and 5 mg/kg xylazine administered intraperitoneally through a 25-gauge needle.

For the control group, the flexor digitorum longus (FDL) tendon was harvested and used as a graft[247]. Briefly, a longitudinal incision was made on the medial aspect of the right distal leg and ankle. The FDL tendon was identified and cut just distal to the ankle in order to harvest the full length of the flexor digitorum longus tendon (average length, 30 mm). The experimental groups received either a single-phase synthetic scaffold, acellular multi-phased synthetic scaffold, or a cell-seeded multi-phased synthetic scaffold.

To perform the ACL reconstruction, an incision was made over the knee and a medial parapatellar arthrotomy was performed to open the joint and excise the ACL. Bone tunnels 1.4mm in diameter were made in the proximal tibia and the distal femur by entering the joint at the attachment sites of the ACL. The graft or scaffold was passed through the bone tunnels to replace the ACL and the proximal and distal ends were secured to the femur and tibia, respectively. Wounds were closed in standard fashion. No negative effects of the autologous graft harvest were observed other than expected swelling and all animals resumed normal gait by 2 to 3 days after surgery. The animals remained healthy and infection-free throughout the duration of the study. All animals resumed normal cage activity by the first postoperative day. Careful inspection of the articular surfaces after euthanasia revealed no arthritis or advanced joint degeneration.

9.2.5 Mineralization

Mineral distribution with the tibial and femoral bone tunnels was determined using micro-computed tomography (micro-CT, n=3/group). Briefly, following fixation for 96 hours in 10% neutral buffered formalin, histological samples were scanned with a micro-computed tomography system (VivaCT 40, Scanco Medical, Switzerland). The length of the tibia and femur surrounding the bone tunnel was scanned with a 17μm voxel size. Three-dimensional reconstructions were then performed by tracing the edges of the bone and using a mineral density of 268 mg HA/cm^3. Tunnel diameter was measured by taking measurements in triplicate down the length of each tunnel in the resulting three-dimensional figures.

Bone volume surrounding the tunnel was quantified by performing volumetric reconstruction of a uniform cylinder of bone including the tibial bone tunnel. A 2.0cm circular contour surrounding the bone tunnel was placed on 315 slices as acquired via micro-CT and reconstructed at a density of 268 mg HA/cm^3, the bone volume and bone volume fraction were quantified using the vivaCT software.

Samples for calcified histology were dehydrated in serial alcohol concentrations (70%–100%). Rat tibiae were embedded in poly(methylmethacrylate) using a modification of the methods of Erben *et al.*[248]. Seven-micrometer-thick sections were cut perpendicular to the bone tunnels and von Kossa staining was used to visualize mineralized tissue[249]. Images were obtained using a light microscope (Zeiss Axiovert 25, Zeiss, Germany).

9.2.6 Matrix Deposition

Three animals per group were euthanized at 4 and 10 weeks after surgery via carbon dioxide inhalation and prepared for histologic analysis. At each time point, two specimens were decalcified and embedded in paraffin for histology and immunohistochemistry. The remaining specimen for each time point was embedded in methacrylate.

Harvested tissues for decalcified histology were fixed for two days in 10% neutral buffered formalin and then decalcified for 48 hours in a solution of formalin, formic acid and ion exchange beads (Dowex HCS-5, Dow Chemical, Midland, MI). Excess bone and soft tissue surrounding the femoral and tibial tunnels was removed and the tissues were dehydrated in serial alcohol concentrations (70%–100%), cleared thrice in xylenes and then embedded in paraffin (Fisher Scientific) at 60ºC. Seven-micrometer-thick sections were cut perpendicular to the axes of the bone tunnels and stained with a Modified Goldner's Masson trichrome stain and picrosirius red to visualize collagen distribution, and safranin-O to visualize glycosaminoglycans (GAG). Images were obtained using a light microscope (Zeiss Axiovert 25, Zeiss, Germany) and a polarized light microscope (Olympus BX60, Olympus, Center Valley, PA).

9.2.7 Biomechanical Testing

Biomechanical testing (n=10) was performed to evaluate the strength of the reconstruction after 10 weeks[38;247]. Limbs used for biomechanical testing were disarticulated at the hip and all muscles were removed leaving the joint capsule and the ligaments intact to protect the ACL graft/scaffold until testing. Specimens were stored in a freezer at −80°C until testing. Prior to testing, each limb was defrosted overnight at 4°C and thawed at room temperature. The joint capsule, tendons, ligaments (except the ACL) and the suture material at the graft/scaffold ends were excised prior to testing. The bony ends were potted in bonding cement at the proximal femur and the distal tibia to allow secure fixation in the testing machine. The specimen was positioned in a tensile testing system (Instron 8800) with custom clamps to maintain knee flexion at 45° with the tensile load passing parallel to the ACL graft/scaffold and the bone tunnels. A preload of 15 g was applied to the graft/scaffold for five cycles, following which a tensile load to failure test was performed at a displacement rate of 0.17 mm/second. The load-deformation curve was recorded on a personal computer. Results are reported in terms of the ultimate load-to-failure (N) and stiffness (N/mm) which were calculated from the linear portion of the load-deformation curve. The site of failure was recorded as pull-out from the bone tunnel versus mid-substance rupture.

9.3 Results

The surgery was well tolerated by rats regardless of the graft or scaffold utilized for the procedure. All animals regained mobility within 24 hours of surgery and had resumed normal gait within 7 days of the procedure. Inspection of the joints after euthanasia showed that control grafts and synthetic scaffolds remained intact. The articular cartilage surfaces appeared normal with no evidence of advanced joint degeneration.

9.3.1 Reconstruction with Flexor Tendon Graft

Reconstruction with the flexor digitorum longus graft served as a positive control for the scaffold groups in terms of joint stability and surrounding tissue integrity, as well as negative control in terms of

graft osteointegration and interface formation. Analysis of mineral formation via micro-CT at 4 weeks revealed a cylindrical bone tunnel (*Fig. 9.2*), as expected. Similarly, histological analysis demonstrated that the graft was intact as a dense collagenous structure and surrounded by bone within the bone tunnels, as shown via trichrome and picrosirius red staining. A disorganized fibrovascular interface was evident between the graft and the bone with no cartilage damage was noted to the surfaces of the tibia or femur, as evidenced via safranin-O staining. After 4 weeks, a mineralization front was noted extending from the periphery of the bone tunnel and surrounding the graft indicating the formation of new bone tissue (*Fig 9.3*).

9.3.2 Reconstruction with Single Phase Synthetic Scaffold

Reconstruction was performed with a single phase scaffold as a negative control for interface formation and osteointegration, as compared to the multi-phased scaffold. Analysis of mineralization via micro-CT demonstrated a bone tunnel similar in structure to that of the FDL graft control surrounding the scaffold (*Fig. 9.2*). Histologically, neo-collagenous tissue was evident surrounding the single-phase scaffold within the joint and the bone tunnels (*Fig 9.4*). Similar activity as the FDL graft control group surrounding the bone tunnel in terms of bone formation (*Fig 9.4*) was noted and no evidence of cartilage damage or degeneration was visible histologically.

9.3.3 Reconstruction with Acellular Multi-Phased Scaffold

The acellular multi-phased scaffold was similarly well-tolerated as the single-phased grafts. Nodules indicative of new bone formation were present within the bone tunnels when visualized via micro-CT corresponding to the location of the bone phase of the scaffold (*Fig. 9.2*). Histologically, abundant collagenous tissue was evident surrounding each phase of the scaffold. Collagenous tissue was also evident around the individual bundles of the synthetic scaffold (*Fig 9.5*). Tissue staining positive for proteoglycans, via safranin-O, was visible adjacent to the interface phase. Qualitatively more accelerated bone formation, as compared to the FDL graft and single phase controls, was noted from the periphery of the bone tunnel towards the scaffold indicating more rapid bone formation (*Fig 9.5*). No evidence of cartilage degeneration was found in any of the specimens.

9.3.4 Reconstruction with Cell-seeded Multi-Phased Graft

The cell-seeded scaffold performed similarly at 4 weeks as the acellular multi-phased scaffold. As shown via micro-CT, mineralized tissue was present within the bone tunnels thereby indicating new bone formation on the bone phase of the scaffold (*Fig. 9.2*). Histologically, similarly, abundant collagenous tissue was evident surrounding the bone phase of the scaffold within the bone tunnels and spanning the individual bundles of the ligament phase of the cell-seeded scaffold (*Fig 9.6*). Small regions of tissue staining positive for proteoglycans, via safranin-O, were visible adjacent to the interface phase. Again, similar to the corresponding acellular scaffold, qualitatively more accelerated bone formation was visible as compared to the FDL graft and single phase controls (*Fig 9.6*). All joint surfaces appeared intact and no cartilage damage was noted.

9.4 Discussion

The long-term research goal of this thesis is to facilitate integrative anterior cruciate ligament regeneration, by engineering a multi-phased synthetic scaffold that mimics the native structure and composition characteristic of bone, ligament and bone-ligament interfaces. Specifically, this study assesses the efficacy of a biomimetic multi-phased scaffold to promote ACL regeneration and integration. The ACL reconstruction procedure was performed in a rat model with groups evaluating an acellular and cell-seeded multi-phased scaffold as well as a single-phased scaffold and tendon graft to serve as controls. While all synthetic scaffold systems supported joint stability and ligament-like tissue formation, it was found that the multi-phased design accelerated bone formation and enabled the formation of interface-like tissue.

The implantation of tissue engineered scaffolds into animal models is a pre-requisite for further clinical development and eventual regulatory approval. While the *in vivo* response can be evaluated using a simple subcutaneous model, the synovial environment of the knee is a unique environment due to its low vascularity[18]. As a result, an intra-articular model provides a more accurate representation of scaffold performance. In this study, a histological analysis was performed to observe any inflammatory response the biomechanical response of the scaffold to maintain normal knee function was tested. The

synthetic ACL scaffold tested in this study was well-tolerated by all animals and reduced the duration of the reconstruction procedure. A histological evaluation showed minimal inflammatory response and no scaffolds ruptured nor was any cartilage damage observed, indicating that joint stability was maintained.

Hydroxyapatite presence within the bone phase of the multi-phased scaffold resulted in accelerated mineralization surrounding the scaffold as well as the formation of mineralized tissue within the scaffold. Several groups have reported similar results when evaluating the use of composite polymer-ceramic scaffolds for bone tissue regeneration[224;270;271]. For example, Hasegawa *et al.* reported that porous poly(D,L)-lactide/hydroxyapatite composite scaffold induced bone formation by rat MSCs in subcutaneous rodent model which did not occur when the same scaffold was implanted without HA particles[271]. In addition, calcium phosphate-based cements have also been shown to be effective in augmenting tendon-to-bone integration[62;253]. Our results are in agreement with these findings and demonstrate the potential of a ceramic component within the scaffold to enhance bone formation osteointegration.

The multi-phased scaffold supported the formation of heterogeneous tissue, localized to the phases of the scaffold. Bone formation was limited to within the bone tunnels, with no ectopic bone formation on interface or ligament phases. Collagenous tissue was observed within the joint cavity indicating neo-ligament tissue formation on the ligament phase and regions of cartilaginous interface-like tissue were observed surrounding the interface-phase of the scaffold. These findings validate the multi-phased design as compared to the single-phase synthetic graft, in which no interface-like tissue formation was observed nor was significant bone formation displayed within the bone tunnels.

In summary, the findings of this study demonstrate that a synthetic nanofiber-based scaffold can effectively regenerate the ACL. As compared to the single-phase scaffold, the multi-phased design accelerated the formation of bone tissue, likely due to the presence of hydroxyapatite within the bone phase, and displayed evidence of preliminary interface-like tissue formation. Cell-seeding was shown to have minimal effects on tissue formation at 4 weeks. While the rat ACL reconstruction model has been well developed in the literature, interpretations of these findings must take into account the limitations of this model. Specifically, due to the fact that the rat growth plate does not close during the lifetime of the animal[254], further evaluation is necessary in a larger, skeletally mature animal model. To

better evaluate the scaffold for long-term ligament regeneration, future studies should focus on longer time points and also the use of larger animal models that more closely parallel the biomechanical loads experienced by the human knee.

9.5 Conclusions

The results of this study collectively demonstrate that the multi-phased ACL scaffold is an effective replacement for conventional soft tissue grafts and is capable of supporting joint stability and driving the formation of a bone, ligament and interface tissues. Further evaluation at longer time points and in larger animal models is necessary to evaluate long-term tissue formation, scaffold degradation and the ability to support loads approximating those of the human knee.

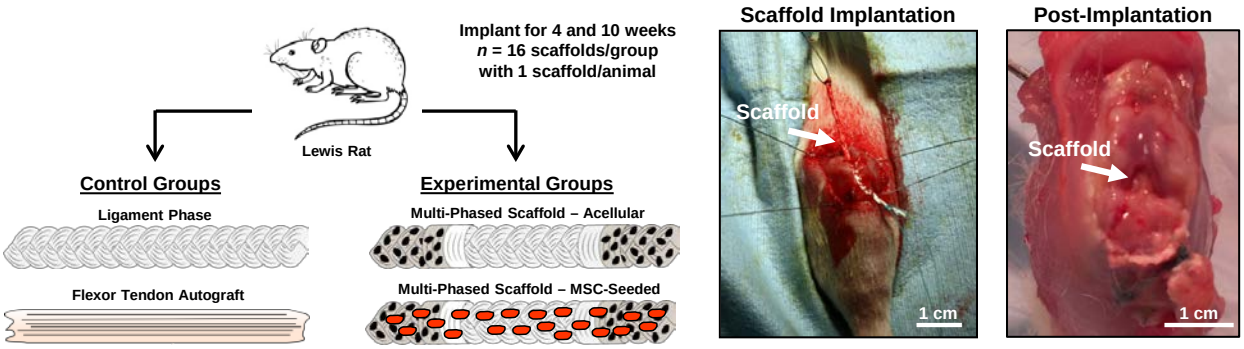

Figure 9.1. Schematic of scaffold design and ACL reconstruction. A multi-phased ACL scaffold was developed for ACL regeneration and ACL reconstruction was performed on Lewis rats. Rats received either a flexor tendon graft, a single phase scaffold, an acellular multi-phased scaffold or a MSC-seeded multi-phased scaffold. Animals were sacrificed after 4 or 10 weeks for histological analysis and biomechanical testing.

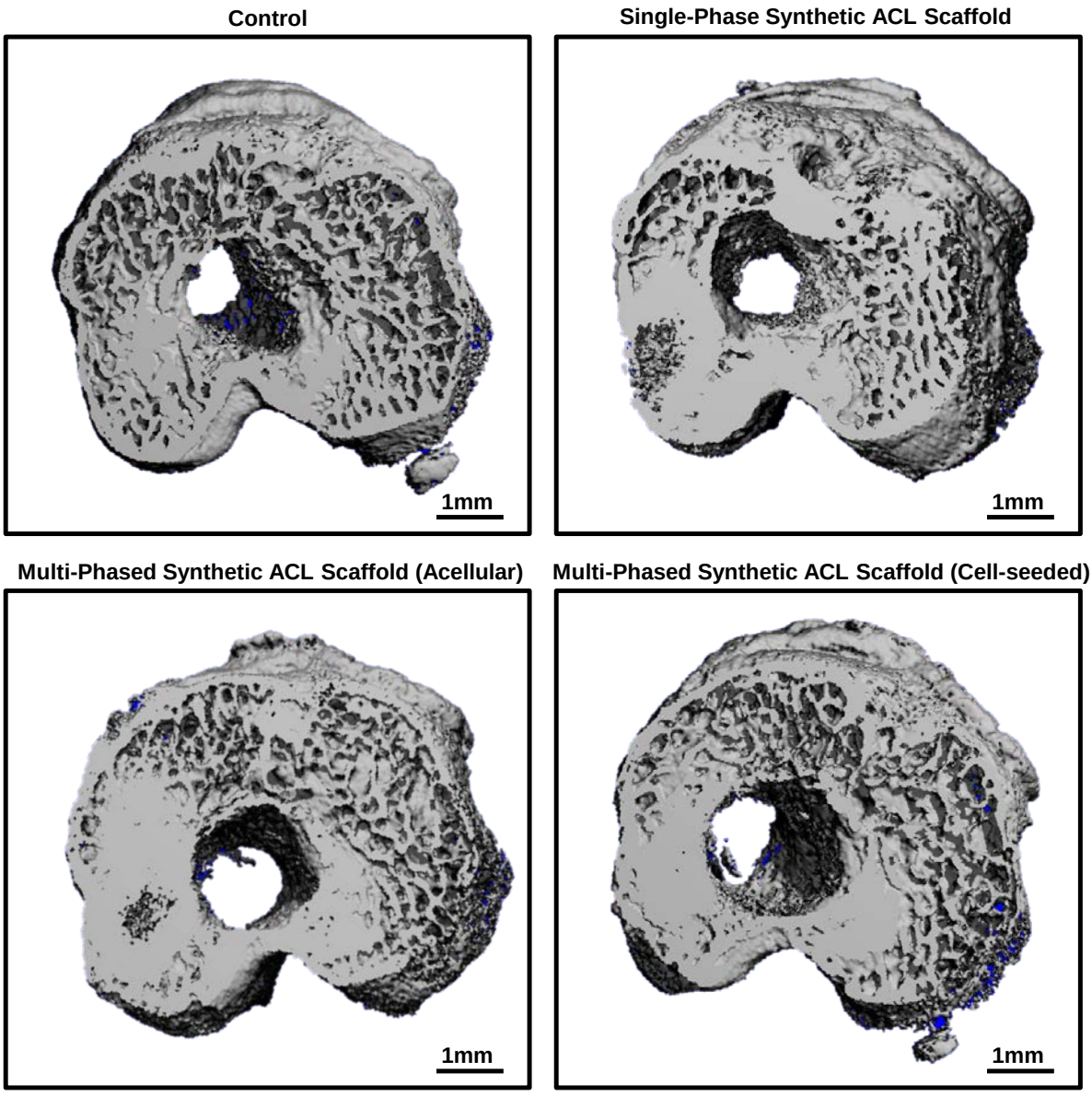

Figure 9.2. Mineralization within the tibial bone tunnels. Mineralization within the bone tunnels was evaluated via micro-CT. Bone formation was evident within the bone tunnels only for animals that received the multi-phased synthetic ACL.

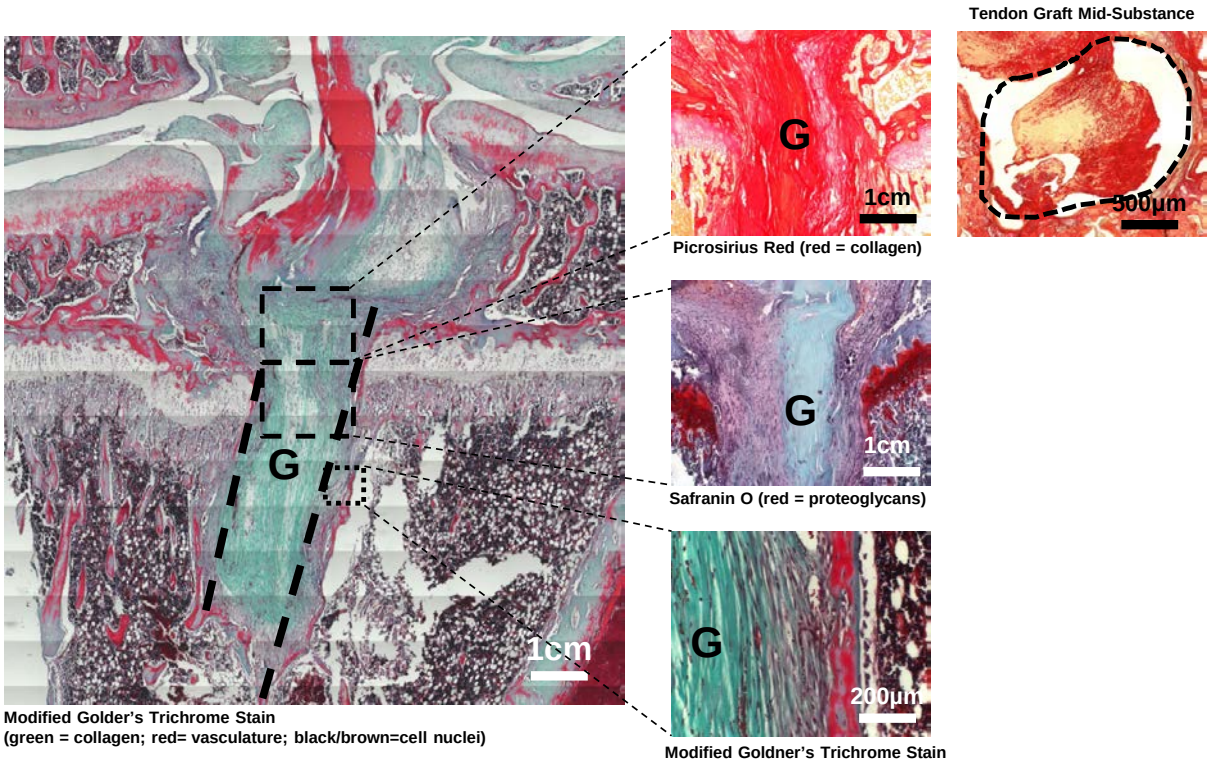

Figure 9.3. Control reconstruction with flexor tendon graft. Histological analysis demonstrated that the graft (G) was intact as a dense collagenous structure and surrounded by bone within the bone tunnels. A disorganized fibrovascular interface was evident between the graft and the bone. After 4 weeks, a mineralization front was noted extending from the periphery of the bone tunnel and surrounding the graft indicating the formation of new bone tissue. No fibrocartilaginous tissue was found forming within the graft.

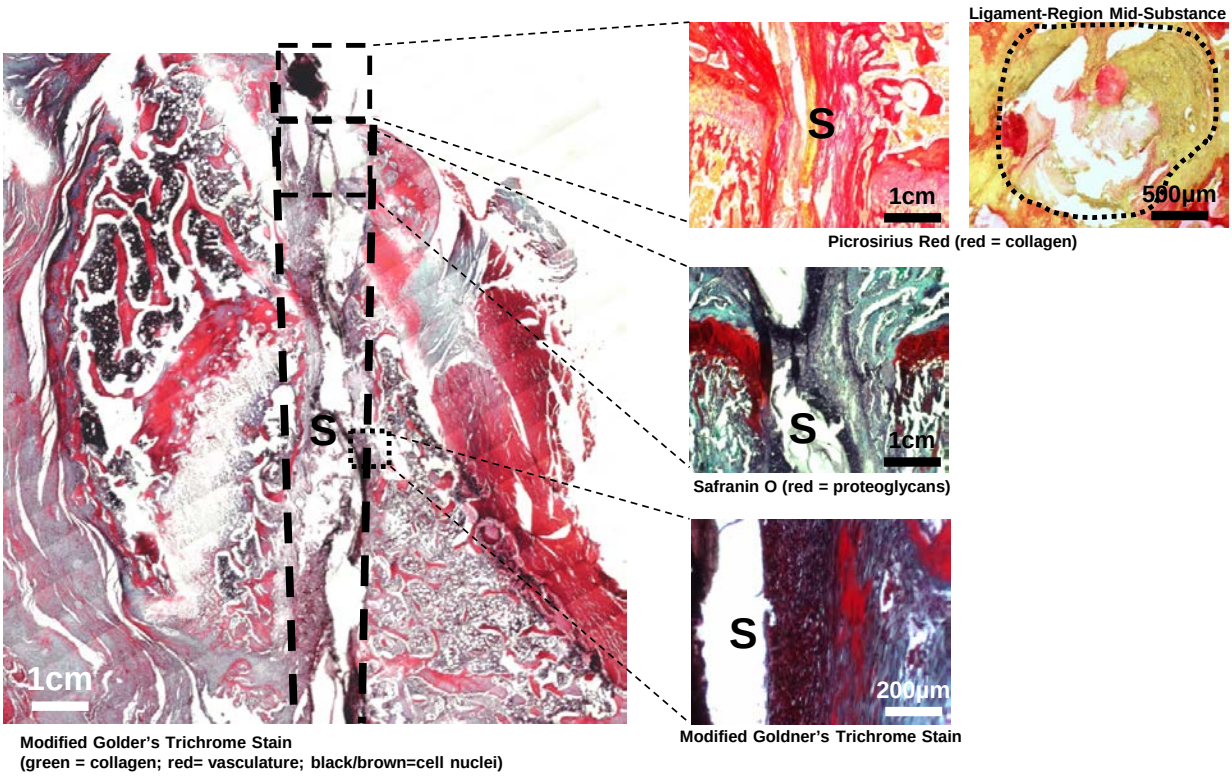

Figure 9.4. Reconstruction with single-phase graft. Neo-collagenous tissue was evident surrounding synthetic (S) graft and spanning the bone tunnels, surrounding the individual bundles of the scaffold. Similar activity as the FDL graft control group surrounding the bone tunnel in terms of bone formation was noted and no fibrocartilage formation was visible histologically surrounding the insertion regions.

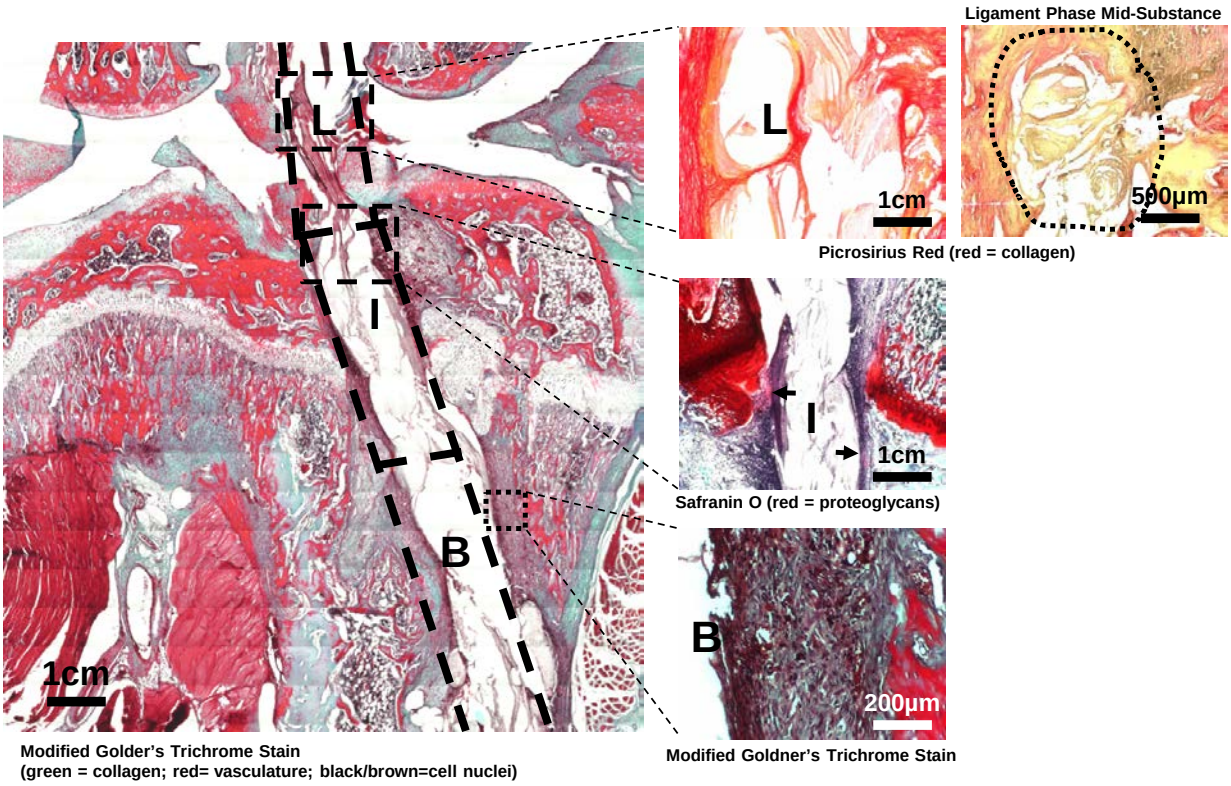

Figure 9.5. Reconstruction with acellular multi-phased graft. Collagenous tissue was evident surrounding the ligament phase (L) of the graft and within the individual bundles of the synthetic scaffold. Qualitatively more accelerated bone formation was noted from the periphery of the bone tunnel towards the bone phase (B) of the graft indicating more rapid bone formation. Small regions of tissue staining positive for proteoglycans, via safranin-O, was visible adjacent to the interface phase (I).

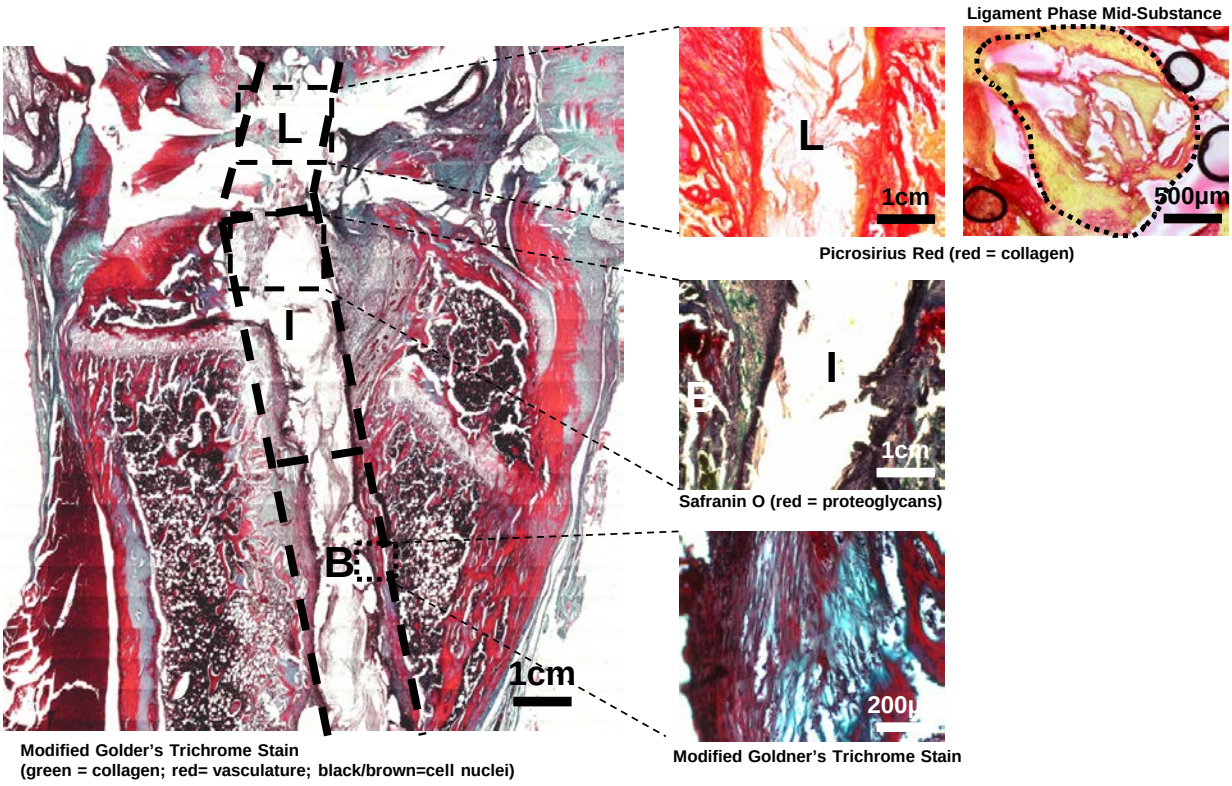

Figure 9.6. Reconstruction with MSC-seeded multi-phased graft. Similar to the aceullular multi-phased scaffold, collagenous tissue was evident surrounding the ligament (L) phase of the scaffold. Small regions of tissue staining positive for proteoglycans, via safranin-O were visible adjacent to the interface phase (I). Qualitatively more accelerated bone formation was visible around the bone phase (B) as compared to the FDL graft and single phase controls.

CHAPTER 10: SUMMARY AND FUTURE DIRECTIONS

10.1 Summary

The objective of this thesis was to design a multi-phased integrative scaffold for anterior cruciate ligament regeneration. As this integrative scaffold was intended to replace traditional soft tissue grafts used for ACL reconstruction, there are several key design criteria for the ideal system. First, it must be able to withstand the functional demands of the native tissue by demonstrating physiologically equivalent viscoelastic and elastic mechanical properties as immediate joint stability is required following reconstruction. Second, the scaffold must be comprised of compositionally varying phases in order to recapitulate the inherent heterogeneity of the native ligament to bone transition. Lastly, the scaffold must be biodegradable such that it is gradually replaced by the regenerated tissue following implantation. It was hypothesized that a biomimetic, multi-phased scaffold comprised of optimized bone, interface and ligament regions coupled with controlled chemical and/or mechanical stimulation *in vitro* will guide phase-specific mesenchymal stem cell differentiation and result in a biologically integrated bone-ligament-bone complex *in vivo*. To evaluate these hypotheses, studies were designed to address five specific aims.

The first three aims focused on individually optimizing each phase of the multi-phased scaffold to enable MSC-mediated integrative ACL reconstruction. **Aim 1** focused on the formation of a ligament-like tissue on polymeric nanofibers by inducing the differentiation of MSC into the ligament fibroblast-like phenotype. To this end, the effect of mechanical stimulation and nanofiber architecture were assessed to determine the optimal parameters to induce fibroblastic differentiation (*Chapter 2*). It was demonstrated that both physiologically-relevant mechanical stimulation and an aligned nanofiber substrate were required for the upregulation of fibroblastic markers and the production of a ligament-like extracellular matrix. Next, the addition of fibrogenic growth factors[28] was evaluated to determine if concurrent chemical and mechanical stimulation was necessary(*Chapter 3*). Lastly, the effect of nanofiber composition was assessed to select the optimal material based on mechanical properties, degradation and cell response for the ligament phase (*Chapter 4*).

Following development of the ligament phase, **Aim 2** addressed the optimization of the bone phase by guiding MSC-mediated bone formation. To accomplish this, hydroxyapatite (HA) particles, the primary mineral identified in bone[32], were incorporated into nanofibers to induce MSC differentiation

towards an osteoblastic phenotype[33]. The osteogenic differentiation of MSCs was evaluated as a function of nanofiber mineral content to determine the optimal nanofiber mineral content (Chapter 5).

Aim 3 focused on optimizing the interface phase. As fibrocartilage formation has been shown to be induced by compressive loading[35], this aim incorporated the application of compression to induce MSC-mediated formation of a matrix rich in types I and II collagen and proteoglycans. To this end, a mechanoactive, nanofiber-based collar composed of PLGA was used to apply compression to MSCs as it contracts when placed in a physiological environment. Compressive loading via a nanofiber collar system has previously been shown to induce upregulation of fibrocartilage-related markers when applied to soft tissue *in vitro*[36]. Similarly, compression has also been shown to enhance MSC chondrogenesis[30;37]. The effect of compression via nanofiber scaffold contraction on MSCs was first assessed *in vitro* (*Chapter 6*) and the system was further validated by assessing its ability to induce fibrocartilage formation on biological grafts *in vivo* (*Chapter 7*).

Incorporating the outcomes of the first three aims, **Aim 4** encompassed the design, characterization and *in vitro* evaluation of a stratified scaffold that incorporates all three optimized phases to form an integrated bone-ligament-bone complex. This multi-phased scaffold was designed to guide MSC differentiation in order to form distinct-yet-continuous regions of bone, interface and ligament tissues *in vitro*. Graft architecture and seeding density were optimized and the optimal multi-phased graft was evaluated *in vitro* (*Chapter 8*) to assess the formation of bone, interface and ligament tissue. Subsequently, in **Aim 5**, the system was evaluated *in vivo* using a well-established rodent model of ACL reconstruction[38] to assess its efficacy for integrative ACL reconstruction (*Chapter 9*) in terms of biomechanical properties and matrix formation, focusing on regenerating a biologically integrated bone-ligament-bone complex. The major findings of each chapter are briefly highlighted below.

10.1.1 Nanofiber Phase Design and Optimization for MSC-Mediated Ligament Formation

The first aim focused on optimization of the ligament phase of the multi-phased ACL scaffold. As this system uses MSCs to produce three different tissue types, it was necessary to identify the parameters required to differentiate MSCs into fibroblasts, the primary cell type of ligaments. In *Chapter 2*, the effects of nanofiber alignment and mechanical stimulation on fibroblastic differentiation of MSCs

were assessed. A custom built bioreactor was used to apply physiological levels of dynamic tensile stimulation to MSCs seeded on aligned and unaligned nanofibers. It was demonstrated that fibroblastic differentiation of MSCs only, in terms of type III collagen production and the expression of several key fibroblast-related markers, occurs with a combination of aligned nanofibers and mechanical strain. These findings established the architecture for the scaffold and demonstrated that mechanical stimulation alone could differentiate these cells.

In *Chapter 3*, the effect of combined mechanical and chemical stimulation was investigated to determine if chemical stimulation could synergistically enhance fibroblastic differentiation of MSCs. Cells were stimulated with bFGF prior to the application of mechanical stimulation as this growth factor has been shown to promoted fibrogenesis of MSCs. It was shown that sequential chemical and mechanical stimulation enhanced MSC proliferation and collagen synthesis and established bFGF stimulation as a viable method to enhanced cell response if necessary.

Optimization of nanofiber composition was the focus *Chapter 4*. Nanofibers were fabricated from a blend of two degradable polymers, PLGA and PCL as these both have mechanical properties within range of the native ACL with differing degradation characteristics. It was demonstrated that nanofibers with controlled mechanical and degradation properties could be generated by blending the two polymers at various ratios. The response of human ACL fibroblasts on each composition was studied to select the optimal parameters based on cell response. Fibroblast proliferation, matrix production and fibroblast gene expression were shown to be greatest on scaffolds with higher PCL content, including pure PCL nanofibers and 1:5 PLGA:PCL blend nanofibers. Based on these findings, the 1:5 PLGA:PCL nanofibers were selected as the composition of the ligament phase. Collectively, these findings provide the rationale for the parameters of the ligament phase of the integrative ACL graft.

10.1.2 Nanofiber Phase Design and Optimization for MSC-Mediated Bone Formation

The focus of **Aim 2** was to optimize the bone phase of the graft to induce osteogenic differentiation of MSCs. In *Chapter 5*, Composite polymer-ceramic nanofibers were fabricated by incorporating hydroxyapatite, as HA is the primary mineral found in bone and has been shown to enhance both osteoblast response and osteogenesis of stem cells[33;196;197]. The response of MSCs, in terms of

mineralized matrix formation and osteogenic marker expression, was studied as a function of nanofiber HA content. The production of ALP was increased on nanofibers containing 25% and 35% HA and the expression of several osteogenic markers was greatest on the 35% HA nanofibers. These findings established that the optimal ceramic content of the bone phase as 35% HA.

10.1.3 Mechanoactive Nanofiber Collar Design and Optimization for MSC-mediated Interface Formation

The focus of **Aim 3** shifted to the design and optimization of a nanofiber collar system to induce fibrocartilage formation by MSCs on the multi-phased ACL scaffold. A system to apply compression was investigated as this mode of stimulation has been shown to be responsible for fibrocartilage formation *in vivo* and has been shown to enhance cartilage-like tissue production by MSCs. To this end, a nanofiber collar system was designed and evaluated *in vitro* (*Chapter 6*) to induce cartilage formation by MSCs, as this system had been previously shown to enhance proteoglycan production and fibrocartilage-related marker production on tendon grafts *in vitro*. It was demonstrated that compressive stimuli enhanced the expression of fibrocartilage-related markers by MSCs thereby indicating that the collar system could be used to promote interface formation by these cells when seeded on the multi-phased ACL scaffold. This system was further validated *in vivo* using a rodent ACL reconstruction model (*Chapter 7*). It was shown that the multi-phased nanofiber collar, composed of parallel regions of polymer and polymer-ceramic nanofibers, enhanced graft osteointegration and increase the production of fibrocartilage-related proteins. These findings established the ability of the collar system to promote fibrocartilage formation.

10.1.4 Fabrication and In Vitro Evaluation of the Multi-Phased ACL Scaffold

Based on the phases optimized in the first seven chapters, in **Aim 4**, a multi-phased nanofiber-based graft for integrative ACL reconstruction was fabricated and optimized in terms of architecture and cell seeding density (*Chapter 8*). The architecture of the ligament phase was optimized by designing a braided three-bundle system that mimicked the organization of the native ACL while also mimicking the elastic and viscoelastic properties of the native ligament tissue. The system was cultured *in vitro* with rodent MSCs at three different densities, $2.5x10^5$, $5x10^5$ and $1x10^6$ cells per scaffold, to evaluate the effect of cell seeding density and determine the optimal cell density for further evaluation (*Chapter 8*). A

seeding density of 1 million cells/scaffold resulted in increased ALP activity and GAG production on the bone and ligament phase, respectively, at day 7 as compared to the other groups thereby indicating that this seeding density was optimal. The optimized multi-phased graft was then cultured *in vitro* using a bioreactor to simulate the in vivo mechanical environment (*Chapter 8*). Over 21 days, a phase-specific response by cells was measured with distinct regions of bone, interface and ligament tissue formed *in vitro*.

10.1.5 In Vivo Evaluation of the Multi-Phased ACL Scaffold

To address **Aim 5**, the final chapter of this thesis focused on establishing the efficacy of the multi-phased ACL scaffold *in vivo* using a rodent model of ACL reconstruction. A cell-seeded multi-phased scaffold was compared with an acellular multi-phased scaffold, acellular single-phase scaffold, consisting of the ligament phase only, and a flexor tendon graft. All scaffold configurations were well tolerated *in vivo* and no cartilage damage in any animals, indicating that the joint stability was maintained. As compared to the single phase scaffold, accelerated bone formation was noted surrounding the multi-phased scaffold. These findings demonstrate the efficacy of the multi-phased ACL scaffold for ligament reconstruction.

10.2 Future Directions

The findings of this thesis demonstrate the feasibility of using a multi-phased scaffold to regenerate the ACL, ACL-to-bone interface and subchondral bone. However, to realize the clinical translation of the scaffold system, several areas of further study are needed as described below.

10.2.1 Large Animal Model

Although the rat model has been well-established for ACL reconstruction, it is still necessary to evaluate scaffold designs in large animal models for clinical translation. Compared to the rat, larger animal models such as the rabbit[18], canine[12], porcine[267] or goat[268] models would provide a more physically demanding environment with dimensions and biomechanical loads more closely approximating those of the human knee.

10.2.2 Growth Factor Delivery for Interface Formation

Due to the complexity of the current multi-phased graft design, future work may require simplifying the structure of the graft for high-throughput fabrication. One potential approach is the incorporation of chemical factors into the interface phase of the graft, as opposed to using the nanofiber collar system. In particular, TGF-β3 has been shown to induce chondrogenic differentiation of MSCs[272] and can enhance cartilage formation on tissue engineered scaffolds[273;274]. In addition, growth factor release from nanofibers has been well investigated[131;275;276] .

10.2.3 Alternative Stem Cell Source

While MSCs can be readily obtained and have been well characterized in the literature, other sources of stem cells such as tendon-derived stem cells and synovium-derived stem cells may be better suited for musculoskeletal tissue regeneration. In addition, the recent development of induced pluripotent stem cells (iPSC) may enable cell-based approaches which do not require an additional surgical procedure.

REFERENCES

[1] Moisala AS, Jarvela T, Paakkala A, Paakkala T, Kannus P, Jarvinen M. Comparison of the bioabsorbable and metal screw fixation after ACL reconstruction with a hamstring autograft in MRI and clinical outcome: a prospective randomized study. Knee Surgery, Sports Traumatology, Arthroscopy 2008 Dec 1;16(12):1080-6.

[2] Wang IE, Mitroo S, Chen FH, Lu HH, Doty SB. Age-dependent changes in matrix composition and organization at the ligament-to-bone insertion. J Orthop Res 2006 Jun 15;24(8):1745-55.

[3] Kondo E, Yasuda K, Yamanaka M, Minami A, Tohyama H. Effects of administration of exogenous growth factors on biomechanical properties of the elongation-type anterior cruciate ligament injury with partial laceration. Am J Sports Med 2005 Feb;33(2):188-96.

[4] Johnson RJ. The anterior cruciate: a dilemma in sports medicine. Int J Sports Med 1982 May;3(2):71-9.

[5] Gordon MD, Steiner ME. Orthopaedic Knowledge Update: Sports Medicine. In: Garrick JG, editor. Orthopaedic Knowledge Update: Sports Medicine.Rosemont, Ill: American Academy of Orthopaedic Surgeons; 2004. p. 169-81.

[6] Noyes FR, Mangine RE, Barber S. Early knee motion after open and arthroscopic anterior cruciate ligament reconstruction. Am J Sports Med 1987 Mar;15(2):149-60.

[7] Daniel DM, Stone ML, Dobson BE, Fithian DC, Rossman DJ, Kaufman KR. Fate of the ACL-injured patient. A prospective outcome study. Am J Sports Med 1994 Sep;22(5):632-44.

[8] Tom JA, Rodeo SA. Soft tissue allografts for knee reconstruction in sports medicine. Clin Orthop 2002 Sep;402:135-56.

[9] Barrett GR, Noojin FK, Hartzog CW, Nash CR. Reconstruction of the anterior cruciate ligament in females: A comparison of hamstring versus patellar tendon autograft. Arthroscopy 2002 Jan;18(1):46-54.

[10] Beynnon BD, Johnson RJ, Fleming BC, Kannus P, Kaplan M, Samani J, et al. Anterior cruciate ligament replacement: comparison of bone-patellar tendon-bone grafts with two-strand hamstring grafts. A prospective, randomized study. J Bone Joint Surg Am 2002 Sep;84-A(9):1503-13.

[11] Rodeo SA, Suzuki K, Deng XH, Wozney J, Warren RF. Use of recombinant human bone morphogenetic protein-2 to enhance tendon healing in a bone tunnel. Am J Sports Med 1999 Jul;27(4):476-88.

[12] Rodeo SA, Arnoczky SP, Torzilli PA, Hidaka C, Warren RF. Tendon-healing in a bone tunnel. A biomechanical and histological study in the dog. J Bone Joint Surg Am 1993 Dec;75(12):1795-803.

[13] Robertson DB, Daniel DM, Biden E. Soft tissue fixation to bone. Am J Sports Med 1986 Sep;14(5):398-403.

[14] Salmon LJ, Refshauge KM, Russell VJ, Roe JP, Linklater J, Pinczewski LA. Gender Differences in Outcome After Anterior Cruciate Ligament Reconstruction With Hamstring Tendon Autograft. The American Journal of Sports Medicine 2006 Apr 1;34(4):621-9.

[15] Getelman MH, Friedman MJ. Revision anterior cruciate ligament reconstruction surgery. Journal of the American Academy of Orthopaedic Surgeons 1999 May 1;7(3):189-98.

[16] Vunjak-Novakovic G, Altman G, Horan R, Kaplan DL. Tissue engineering of ligaments. Annu Rev Biomed Eng 2004;6:131-56.

[17] Altman GH, Horan RL, Weitzel P, Richmond JC. The use of long-term bioresorbable scaffolds for anterior cruciate ligament repair. J Am Acad Orthop Surg 2008 Apr;16(4):177-87.

[18] Cooper JA, Jr., Sahota JS, Gorum WJ, Carter J, Doty SB, Laurencin CT. Biomimetic tissue-engineered anterior cruciate ligament replacement. Proc Natl Acad Sci U S A 2007 Feb 27;104(9):3049-54.

[19] Barber JG, Handorf AM, Allee TJ, Li WJ. Braided Nanofibrous Scaffold for Tendon and Ligament Tissue Engineering. Tissue Eng Part A 2011 Sep 6.

[20] Ottani V, Raspanti M, Ruggeri A. Collagen structure and functional implications. Micron 2001 Apr;32(3):251-60.

[21] Altman GH, Horan RL, Lu HH, Moreau J, Martin I, Richmond JC, et al. Silk matrix for tissue engineered anterior cruciate ligaments. Biomaterials 2002 Oct;23(20):4131-41.

[22] Benjamin M, Evans EJ, Copp L. The histology of tendon attachments to bone in man. J Anat 1986 Dec;149:89-100.

[23] Moffat KL, Sun WH, Pena PE, Chahine NO, Doty SB, Ateshian GA, et al. Characterization of the structure-function relationship at the ligament-to-bone interface. Proc Natl Acad Sci U S A 2008 Jun 10;105(23):7947-52.

[24] Moffat KL, Kwei AS, Spalazzi JP, Doty SB, Levine WN, Lu HH. Novel nanofiber-based scaffold for rotator cuff repair and augmentation. Tissue Eng Part A 2009 Jan;15(1):115-26.

[25] Wang IE, Doty SB, Rubino VJ, Lu HH. Age-Dependent Characterization of the Anterior Cruciate Ligament to Bone Insertion. Transactions of the Orthopeadic Research Society , poster # 1525. 2005.
Ref Type: Abstract

[26] Pittenger MF, Mackay AM, Beck SC, Jaiswal RK, Douglas R, Mosca JD, et al. Multilineage potential of adult human mesenchymal stem cells. Science 1999 Apr 2;284(5411):143-7.

[27] Altman GH, Horan RL, Martin I, Farhadi J, Stark PR, Volloch V, et al. Cell differentiation by mechanical stress. FASEB J 2002 Feb;16(2):270-2.

[28] Moreau JE, Chen J, Bramono DS, Volloch V, Chernoff H, Vunjak-Novakovic G, et al. Growth factor induced fibroblast differentiation from human bone marrow stromal cells in vitro. J Orthop Res 2005 Jan;23(1):164-74.

[29] Toquet J, Rohanizadeh R, Guicheux J, Couillaud S, Passuti N, Daculsi G, et al. Osteogenic potential in vitro of human bone marrow cells cultured on macroporous biphasic calcium phosphate ceramic. J Biomed Mater Res 1999 Jan;44(1):98-108.

[30] Angele P, Schumann D, Angele M, Kinner B, Englert C, Hente R, et al. Cyclic, mechanical compression enhances chondrogenesis of mesenchymal progenitor cells in tissue engineering scaffolds. Biorheology 2004;41(3-4):335-46.

[31] Woo S., An K., Frank C.B. Anatomy, biology, and biomechanics of tendon and ligament. In: Buckwalter JA, Einhorn T.A., Simon S.R., editors. Orthopaedic Basic Science. 2 ed. Rosemont: American Academy of Orthopaedic Surgery; 2000. p. 581-616.

[32] Boskey AL, Posner AS. Bone structure, composition, and mineralization. Orthop Clin North Am 1984 Oct;15(4):597-612.

[33] Polini A, Pisignano D, Parodi M, Quarto R, Scaglione S. Osteoinduction of human mesenchymal stem cells by bioactive composite scaffolds without supplemental osteogenic growth factors. PLoS ONE 2011 Oct 12;6(10):e26211.

[34] Lin L, Chow KL, Leng Y. Study of hydroxyapatite osteoinductivity with an osteogenic differentiation of mesenchymal stem cells. J Biomed Mater Res Part A 2009;89A(2):326-35.

[35] Evanko SP, Vogel KG. Proteoglycan synthesis in fetal tendon is differentially regulated by cyclic compression in vitro. Arch Biochem Biophys 1993;307(1):153-64.

[36] Spalazzi JP, Vyner MC, Jacobs MT, Moffat KL, Lu HH. Mechanoactive scaffold induces tendon remodeling and expression of fibrocartilage markers. Clin Orthop Relat Res 2008 Aug;466(8):1938-48.

[37] Mauck RL, Yuan X, Tuan RS. Chondrogenic differentiation and functional maturation of bovine mesenchymal stem cells in long-term agarose culture. Osteoarthritis Cartilage 2006 Feb;14(2):179-89.

[38] Dagher E, Hays PL, Kawamura S, Godin J, Deng XH, Rodeo SA. Immobilization modulates macrophage accumulation in tendon-bone healing. Clin Orthop Relat Res 2009 Jan;467(1):281-7.

[39] Woo SL, Livesay GA, Engle C. Biomechanics of the human anterior cruciate ligament. ACL structure and role in knee motion. [Review] [21 refs]. Orthopaedic Review 1992 Jul;21(7):835-42.

[40] Goldblatt JP, Fitzsimmons SE, Balk E, Richmond JC. Reconstruction of the anterior cruciate ligament: meta-analysis of patellar tendon versus hamstring tendon autograft. Arthroscopy 2005 Jul;21(7):791-803.

[41] Sherman OH, Banffy MB. Anterior cruciate ligament reconstruction: which graft is best? Arthroscopy 2004 Nov;20(9):974-80.

[42] Wagner M, Kaab MJ, Schallock J, Haas NP, Weiler A. Hamstring tendon versus patellar tendon anterior cruciate ligament reconstruction using biodegradable interference fit fixation: a prospective matched-group analysis. Am J Sports Med 2005 Sep;33(9):1327-36.

[43] Wilson TW, Zafuta MP, Zobitz M. A biomechanical analysis of matched bone-patellar tendon-bone and double-looped semitendinosus and gracilis tendon grafts. Am J Sports Med 1999 Mar;27(2):202-7.

[44] Otto D, Pinczewski LA, Clingeleffer A, Odell R. Five-year results of single-incision arthroscopic anterior cruciate ligament reconstruction with patellar tendon autograft. Am J Sports Med 1998 Mar;26(2):181-8.

[45] Adam F, Pape D, Schiel K, Steimer O, Kohn D, Rupp S. Biomechanical properties of patellar and hamstring graft tibial fixation techniques in anterior cruciate ligament reconstruction: experimental study with roentgen stereometric analysis. Am J Sports Med 2004 Jan;32(1):71-8.

[46] Tashiro T, Kurosawa H, Kawakami A, Hikita A, Fukui N. Influence of Medial Hamstring Tendon Harvest on Knee Flexor Strength after Anterior Cruciate Ligament Reconstruction. The American Journal of Sports Medicine 2003 Jul 1;31(4):522-9.

[47] Kurosaka M, Yoshiya S, Andrish JT. A biomechanical comparison of different surgical techniques of graft fixation in anterior cruciate ligament reconstruction. Am J Sports Med 1987 May;15(3):225-9.

[48] Eriksson K, Anderberg P, Hamberg P, Olerud P, Wredmark T. There are differences in early morbidity after ACL reconstruction when comparing patellar tendon and semitendinosus tendon graft. Scandinavian Journal of Medicine & Science in Sports 2001;11(3):170-7.

[49] West RV, Harner CD. Graft Selection in Anterior Cruciate Ligament Reconstruction. Journal of the American Academy of Orthopaedic Surgeons 2005 May;13(3):197-207.

[50] Jackson DW, Grood ES, Goldstein JD, Rosen MA, Kurzweil PR, Cummings JF, et al. A comparison of patellar tendon autograft and allograft used for anterior cruciate ligament reconstruction in the goat model. Am J Sports Med 1993 Mar;21(2):176-85.

[51] Fleming B, Beynnon B, Howe J, McLeod W, Pope M. Effect of tension and placement of a prosthetic anterior cruciate ligament on the anteroposterior laxity of the knee. J Orthop Res 1992 Mar;10(2):177-86.

[52] Beynnon BD, Johnson RJ, Fleming BC, Peura GD, Renstrom PA, Nichols CE, et al. The effect of functional knee bracing on the anterior cruciate ligament in the weightbearing and nonweightbearing knee. Am J Sports Med 1997 May;25(3):353-9.

[53] Loh JC, Fukuda Y, Tsuda E, Steadman RJ, Fu FH, Woo SL. Knee stability and graft function following anterior cruciate ligament reconstruction: Comparison between 11 o'clock and 10 o'clock femoral tunnel placement. Arthroscopy 2003 Mar;19(3):297-304.

[54] Markolf KL, Hame S, Hunter DM, Oakes DA, Zoric B, Gause P, et al. Effects of femoral tunnel placement on knee laxity and forces in an anterior cruciate ligament graft. J Orthop Res 2002 Sep;20(5):1016-24.

[55] Brand J, Jr., Weiler A, Caborn DN, Brown CH, Jr., Johnson DL. Graft fixation in cruciate ligament reconstruction. Am J Sports Med 2000 Sep;28(5):761-74.

[56] Dagher E, Hays P, Deland K, Ying L, Deng X, Rodeo S. Effect of human mesenchymal stem cells on tendon-to-bone healing in a rat model of ACL reconstruction. Transactions of the Orthopaedic Research Society . 2006.
Ref Type: Abstract

[57] Gulotta LV, Kovacevic D, Ying L, Ehteshami JR, Montgomery S, Rodeo SA. Augmentation of tendon-to-bone healing with a magnesium-based bone adhesive. Am J Sports Med 2008 Jul;36(7):1290-7.

[58] Tien YC, Chih TT, Lin JH, Ju CP, Lin SD. Augmentation of tendon-bone healing by the use of calcium-phosphate cement. J Bone Joint Surg Br 2004 Sep;86(7):1072-6.

[59] Huangfu X, Zhao J. Tendon-bone healing enhancement using injectable tricalcium phosphate in a dog anterior cruciate ligament reconstruction model. Arthroscopy 2007 May;23(5):455-62.

[60] Mutsuzaki H, Sakane M, Nakajima H, Ito A, Hattori S, Miyanaga Y, et al. Calcium-phosphate-hybridized tendon directly promotes regeneration of tendon-bone insertion. J Biomed Mater Res A 2004 Aug 1;70(2):319-27.

[61] Mutsuzaki H, Sakane M, Hattori S, Kobayashi H, Ochiai N. Firm anchoring between a calcium phosphate-hybridized tendon and bone for anterior cruciate ligament reconstruction in a goat model. Biomed Mater 2009 Aug;4(4):045013.

[62] Ishikawa H, Koshino T, Takeuchi R, Saito T. Effects of collagen gel mixed with hydroxyapatite powder on interface between newly formed bone and grafted achilles tendon in rabbit femoral bone tunnel. Biomaterials 2001 Jun;22(12):1689-94.

[63] Shen H, Qiao G, Cao H, Jiang Y. An histological study of the influence of osteoinductive calcium phosphate ceramics on tendon healing pattern in a bone tunnel with suspensory fixation. Int Orthop 2010 Aug;34(6):917-24.

[64] Mutsuzaki H, Sakane M. Calcium phosphate-hybridized tendon graft to enhance tendon-bone healing two years after ACL reconstruction in goats. Sports Med Arthrosc Rehabil Ther Technol 2011;3(1):31.

[65] Amiel D, Frank C, Harwood F, Fronek J, Akeson W. Tendons and ligaments: A morphological and biochemical comparison. Journal of Orthopaedic Research 1983;1(3):257-65.

[66] Amiel D, Kleiner JB, Roux RD, Harwood FL, Akeson WH. The phenomenon of "ligamentization": anterior cruciate ligament reconstruction with autogenous patellar tendon. J Orthop Res 1986;4(2):162-72.

[67] Butler DL. Kappa Delta Award paper. Anterior cruciate ligament: its normal response and replacement. J Orthop Res 1989;7(6):910-21.

[68] Iwahashi T, Shino K, Nakata K, Nakamura N, Yamada Y, Yoshikawa H, et al. Assessment of the ΓÇ£functional lengthΓÇ¥ of the three bundles of the anterior cruciate ligament. Knee Surgery, Sports Traumatology, Arthroscopy 2008 Feb 1;16(2):167-74.

[69] Butler DL, Kay MD, Stouffer DC. Comparison of material properties in fascicle-bone units from human patellar tendon and knee ligaments. Journal of Biomechanics 1986;19(6):425-32.

[70] Matyas JR, Anton MG, Shrive NG, Frank CB. Stress governs tissue phenotype at the femoral insertion of the rabbit MCL. J Biomech 1995 Feb;28(2):147-57.

[71] Spalazzi JP, Gallina J, Fung-Kee-Fung SD, Konofagou EE, Lu HH. Elastographic imaging of strain distribution in the anterior cruciate ligament and at the ligament-bone insertions. J Orthop Res 2006 Oct;24(10):2001-10.

[72] Woo SL, Gomez MA, Seguchi Y, Endo CM, Akeson WH. Measurement of mechanical properties of ligament substance from a bone-ligament-bone preparation. J Orthop Res 1983;1(1):22-9.

[73] Woo SL, Buckwalter JA. AAOS/NIH/ORS workshop. Injury and repair of the musculoskeletal soft tissues. Savannah, Georgia, June 18-20, 1987. J Orthop Res 1988;6(6):907-31.

[74] Benjamin M, Kumai T, Milz S, Boszczyk BM, Boszczyk AA, Ralphs JR. The skeletal attachment of tendons--tendon "entheses". Comp Biochem Physiol A Mol Integr Physiol 2002 Dec;133(4):931-45.

[75] Benjamin M, Ralphs JR. Fibrocartilage in tendons and ligaments--an adaptation to compressive load. J Anat 1998 Nov;193 (Pt 4):481-94.

[76] Bercovy M, Goutallier D, Voisin MC, Geiger D, Blanquaert D, Gaudichet A, et al. Carbon-PGLA prostheses for ligament reconstruction. Experimental basis and short-term results in man. Clin Orthop Relat Res 1985 Jun;(196):159-68.

[77] Bolton CW, Bruchman WC. The GORE-TEX expanded polytetrafluoroethylene prosthetic ligament. An in vitro and in vivo evaluation. Clin Orthop Relat Res 1985 Jun;(196):202-13.

[78] Ahlfeld SK, Larson RL, Collins HR. Anterior cruciate reconstruction in the chronically unstable knee using an expanded polytetrafluoroethylene (PTFE) prosthetic ligament. Am J Sports Med 1987 Jul;15(4):326-30.

[79] Richmond JC, Manseau CJ, Patz R, McConville O. Anterior cruciate reconstruction using a Dacron ligament prosthesis. A long-term study. Am J Sports Med 1992 Jan;20(1):24-8.

[80] Mody BS, Howard L, Harding ML, Parmar HV, Learmonth DJ. The ABC carbon and polyester prosthetic ligament for ACL-deficient knees. Early results in 31 cases. J Bone Joint Surg Br 1993 Sep;75(5):818-21.

[81] Roth JH, Kennedy JC, Lockstadt H, McCallum CL, Cunning LA. Polypropylene braid augmented and nonaugmented intraarticular anterior cruciate ligament reconstruction. Am J Sports Med 1985 Sep;13(5):321-36.

[82] Therin M, Christel P, Crespeau F, Durselen L, Claes L. Functional evaluation of polyarylamide fibers for use in a prosthesis for anterior cruciate ligament replacement in the sheep. Clinical Materials 1994;15(1):69-75.

[83] Guidoin MF, Marois Y, Bejui J, Poddevin N, King MW, Guidoin R. Analysis of retrieved polymer fiber based replacements for the ACL. Biomaterials 2000 Dec;21(23):2461-74.

[84] Bolton CW, Bruchman WC. The GORE-TEX expanded polytetrafluoroethylene prosthetic ligament. An in vitro and in vivo evaluation. Clin Orthop 1985 Jun;(196):202-13.

[85] Dunn MG, Tria AJ, Kato YP, Bechler JR, Ochner RS, Zawadsky JP, et al. Anterior cruciate ligament reconstruction using a composite collagenous prosthesis. A biomechanical and histologic study in rabbits. Am J Sports Med 1992 Sep;20(5):507-15.

[86] Chvapil M, Speer DP, Holubec H, Chvapil TA, King DH. Collagen fibers as a temporary scaffold for replacement of ACL in goats. J Biomed Mater Res 1993 Mar;27(3):313-25.

[87] Cai C, Chen C, Chen G, Wang F, Guo L, Yin L, et al. Type I collagen and polyvinyl alcohol blend fiber scaffold for anterior cruciate ligament reconstruction. Biomed Mater 2013 Jun;8(3):035001.

[88] Panas-Perez E, Gatt CJ, Dunn MG. Development of a silk and collagen fiber scaffold for anterior cruciate ligament reconstruction. J Mater Sci Mater Med 2013 Jan;24(1):257-65.

[89] Chen J, Horan RL, Bramono D, Moreau JE, Wang Y, Geuss LR, et al. Monitoring mesenchymal stromal cell developmental stage to apply on-time mechanical stimulation for ligament tissue engineering. Tissue Eng 2006 Nov;12(11):3085-95.

[90] Horan RL, Toponarski I, Boepple HE, Weitzel PP, Richmond JC, Altman GH. Design and characterization of a scaffold for anterior cruciate ligament engineering. J Knee Surg 2009 Jan;22(1):82-92.

[91] Moreau JE, Bramono DS, Horan RL, Kaplan DL, Altman GH. Sequential biochemical and mechanical stimulation in the development of tissue-engineered ligaments. Tissue Eng Part A 2008 Jul;14(7):1161-72.

[92] Richmond JC, Weitzel PP. Bioresorbable scaffolds for anterior cruciate ligament reconstruction: do we need an off-the-shelf ACL substitute? Sports Med Arthrosc 2010 Mar;18(1):40-2.

[93] Li X, Snedeker JG. Wired silk architectures provide a biomimetic ACL tissue engineering scaffold. J Mech Behav Biomed Mater 2013 Jun;22:30-40.

[94] Lin VS, Lee MC, O'Neal S, McKean J, Sung KL. Ligament tissue engineering using synthetic biodegradable fiber scaffolds. Tissue Eng 1999 Oct;5(5):443-52.

[95] Freeman JW, Woods MD, Cromer DA, Wright LD, Laurencin CT. Tissue engineering of the anterior cruciate ligament: the viscoelastic behavior and cell viability of a novel braid-twist scaffold. J Biomater Sci Polym Ed 2009;20(12):1709-28.

[96] Freeman JW, Woods MD, Laurencin CT. Tissue engineering of the anterior cruciate ligament using a braid-twist scaffold design. J Biomech 2007;40(9):2029-36.

[97] Freeman JW, Woods MD, Cromer DA, Ekwueme EC, Andric T, Atiemo EA, et al. Evaluation of a hydrogel-fiber composite for ACL tissue engineering. Journal of Biomechanics 2011 Feb 24;44(4):694-9.

[98] Walters VI, Kwansa AL, Freeman JW. Design and analysis of braid-twist collagen scaffolds. Connect Tissue Res 2012;53(3):255-66.

[99] Barber JG, Handorf AM, Allee TJ, Li WJ. Braided Nanofibrous Scaffold for Tendon and Ligament Tissue Engineering. Tissue Eng Part A 2011 Sep 6.

[100] Surrao DC, Waldman SD, Amsden BG. Biomimetic poly(lactide) based fibrous scaffolds for ligament tissue engineering. Acta Biomaterialia 2012 Nov;8(11):3997-4006.

[101] Vaquette C, Kahn C, Frochot C, Nouvel C, Six JL, De Isla N, et al. Aligned poly(L-lactic-co-e-caprolactone) electrospun microfibers and knitted structure: A novel composite scaffold for ligament tissue engineering. J Biomed Mater Res A 2010 Sep 15;94A(4):1270-82.

[102] Bach JS, Detrez F, Cherkaoui M, Cantournet S, Ku DN, Corte L. Hydrogel fibers for ACL prosthesis: Design and mechanical evaluation of PVA and PVA/UHMWPE fiber constructs. J Biomech 2013 May 31;46(8):1463-70.

[103] Cooper JA, Lu HH, Ko FK, Freeman JW, Laurencin CT. Fiber-based tissue-engineered scaffold for ligament replacement: design considerations and in vitro evaluation. Biomaterials 2005 May;26(13):1523-32.

[104] Lu HH, Cooper JA, Jr., Manuel S, Freeman JW, Attawia MA, Ko FK, et al. Anterior cruciate ligament regeneration using braided biodegradable scaffolds: in vitro optimization studies. Biomaterials 2005 Aug;26(23):4805-16.

[105] Kimura Y, Hokugo A, Takamoto T, Tabata Y, Kurosawa H. Regeneration of anterior cruciate ligament by biodegradable scaffold combined with local controlled release of basic fibroblast growth factor and collagen wrapping. Tissue Eng Part C Methods 2008 Mar;14(1):47-57.

[106] Sahoo S, Ouyang H, Goh JC, Tay TE, Toh SL. Characterization of a novel polymeric scaffold for potential application in tendon/ligament tissue engineering. Tissue Eng 2006 Jan;12(1):91-9.

[107] Liu H, Fan H, Wang Y, Toh SL, Goh JC. The interaction between a combined knitted silk scaffold and microporous silk sponge with human mesenchymal stem cells for ligament tissue engineering. Biomaterials 2008 Feb;29(6):662-74.

[108] Fan H, Liu H, Wong EJ, Toh SL, Goh JC. In vivo study of anterior cruciate ligament regeneration using mesenchymal stem cells and silk scaffold. Biomaterials 2008 Aug;29(23):3324-37.

[109] Fan H, Liu H, Toh SL, Goh JC. Anterior cruciate ligament regeneration using mesenchymal stem cells and silk scaffold in large animal model. Biomaterials 2009 Oct;30(28):4967-77.

[110] Fan H, Liu H, Wang Y, Toh SL, Goh JC. Development of a silk cable-reinforced gelatin/silk fibroin hybrid scaffold for ligament tissue engineering. Cell Transplant 2008;17(12):1389-401.

[111] Sahoo S, Toh SL, Goh JC. A bFGF-releasing silk/PLGA-based biohybrid scaffold for ligament/tendon tissue engineering using mesenchymal progenitor cells. Biomaterials 2010 Apr;31(11):2990-8.

[112] Chen K, Sahoo S, He P, Ng KS, Toh SL, Goh JC. A Hybrid Silk/RADA-Based Fibrous Scaffold with Triple Hierarchy for Ligament Regeneration. Tissue Eng Part A 2012 Apr 23.

[113] Teh TK, Toh SL, Goh JC. Aligned hybrid silk scaffold for enhanced differentiation of mesenchymal stem cells into ligament fibroblasts. Tissue Eng Part C Methods 2011 Jun;17(6):687-703.

[114] Ma J, Goble K, Smietana M, Kostrominova T, Larkin L, Arruda EM. Morphological and functional characteristics of three-dimensional engineered bone-ligament-bone constructs following implantation. J Biomech Eng 2009 Oct;131(10):101017.

[115] Ma J, Smietana MJ, Kostrominova TY, Wojtys EM, Larkin LM, Arruda EM. Three-dimensional engineered bone-ligament-bone constructs for anterior cruciate ligament replacement. Tissue Eng Part A 2012 Jan;18(1-2):103-16.

[116] Paxton JZ, Grover LM, Baar K. Engineering an in vitro model of a functional ligament from bone to bone. Tissue Eng Part A 2010 Jul 1.

[117] Paxton JZ, Donnelly K, Keatch RP, Baar K, Grover LM. Factors affecting the longevity and strength in an in vitro model of the bone-ligament interface. Ann Biomed Eng 2010 Jun;38(6):2155-66.

[118] Spalazzi JP, Doty SB, Moffat KL, Levine WN, Lu HH. Development of controlled matrix heterogeneity on a triphasic scaffold for orthopedic interface tissue engineering. Tissue Eng 2006;12(12):3497-508.

[119] Spalazzi JP, Dagher E, Doty SB, Guo XE, Rodeo SA, Lu HH. In vivo evaluation of a tri-phasic composite scaffold for anterior cruciate ligament-to-bone integration. Conf Proc IEEE Eng Med Biol Soc 2006;1:525-8.

[120] Shanti RM, Li WJ, Nesti LJ, Wang X, Tuan RS. Adult mesenchymal stem cells: biological properties, characteristics, and applications in maxillofacial surgery. Journal of oral and maxillofacial surgery : official journal of the American Association of Oral and Maxillofacial Surgeons 65[8], 1640-1647. 8-1-2007.
Ref Type: Abstract

[121] Engler AJ, Sen S, Sweeney HL, Discher DE. Matrix elasticity directs stem cell lineage specification. Cell 2006 Aug 25;126(4):677-89.

[122] Takahashi Y, Yamamoto M, Tabata Y. Osteogenic differentiation of mesenchymal stem cells in biodegradable sponges composed of gelatin and beta-tricalcium phosphate. Biomaterials 2005 Jun;26(17):3587-96.

[123] Grayson WL, Frohlich M, Yeager K, Bhumiratana S, Chan ME, Cannizzaro C, et al. Engineering anatomically shaped human bone grafts. Proc Natl Acad Sci U S A 2010 Feb 23;107(8):3299-304.

[124] Yoshimoto H, Shin YM, Terai H, Vacanti JP. A biodegradable nanofiber scaffold by electrospinning and its potential for bone tissue engineering. Biomaterials 2003 May;24(12):2077-82.

[125] Garreta E, Gasset D, Semino C, Borros S. Fabrication of a three-dimensional nanostructured biomaterial for tissue engineering of bone. Biomol Eng 2007 Feb;24(1):75-80.

[126] Baker BM, Mauck RL. The effect of nanofiber alignment on the maturation of engineered meniscus constructs. Biomaterials 2007 Apr;28(11):1967-77.

[127] Nerurkar NL, Elliott DM, Mauck RL. Mechanics of oriented electrospun nanofibrous scaffolds for annulus fibrosus tissue engineering. J Orthop Res 2007 Aug;25(8):1018-28.

[128] Li WJ, Danielson KG, Alexander PG, Tuan RS. Biological response of chondrocytes cultured in three-dimensional nanofibrous poly(epsilon-caprolactone) scaffolds. J Biomed Mater Res A 2003 Dec 15;67(4):1105-14.

[129] Kumbar SG, James R, Nukavarapu SP, Laurencin CT. Electrospun nanofiber scaffolds: engineering soft tissues. Biomed Mater 2008 Sep;3(3):034002.

[130] Li WJ, Mauck RL, Cooper JA, Yuan X, Tuan RS. Engineering controllable anisotropy in electrospun biodegradable nanofibrous scaffolds for musculoskeletal tissue engineering. J Biomech 2007;40(8):1686-93.

[131] Sahoo S, Ang LT, Cho-Hong GJ, Toh SL. Bioactive nanofibers for fibroblastic differentiation of mesenchymal precursor cells for ligament/tendon tissue engineering applications. Differentiation 2010 Feb;79(2):102-10.

[132] Pham QP, Sharma U, Mikos AG. Electrospun poly(epsilon-caprolactone) microfiber and multilayer nanofiber/microfiber scaffolds: characterization of scaffolds and measurement of cellular infiltration. Biomacromolecules 2006 Oct;7(10):2796-805.

[133] Murugan R, Ramakrishna S. Design strategies of tissue engineering scaffolds with controlled fiber orientation. Tissue Eng 2007 Aug;13(8):1845-66.

[134] Ma J, He X, Jabbari E. Osteogenic differentiation of marrow stromal cells on random and aligned electrospun poly(L-lactide) nanofibers. Ann Biomed Eng 2011 Jan;39(1):14-25.

[135] Skutek M, Griensven M, Zeichen J, Brauer N, Bosch U. Cyclic mechanical stretching modulates secretion pattern of growth factors in human tendon fibroblasts. European Journal of Applied Physiology 2001 Nov 7;86(1):48-52.

[136] Schofer M, Boudriot U, Wack C, Leifeld I, Gr+ñbed++nkel C, Dersch R, et al. Influence of nanofibers on the growth and osteogenic differentiation of stem cells: a comparison of biological collagen nanofibers and synthetic PLLA fibers. Journal of Materials Science: Materials in Medicine 2009 Mar 1;20(3):767-74.

[137] Jiang X, Cao HQ, Shi LY, Ng SY, Stanton LW, Chew SY. Nanofiber topography and sustained biochemical signaling enhance human mesenchymal stem cell neural commitment. Acta Biomater 2012 Mar;8(3):1290-302.

[138] Terraciano V, Hwang N, Moroni L, Park HB, Zhang Z, Mizrahi J, et al. Differential response of adult and embryonic mesenchymal progenitor cells to mechanical compression in hydrogels. Stem Cells 2007 Nov;25(11):2730-8.

[139] Reneker DH, Chun I. Nanometre diameter fibres of polymer, produced by electrospinning. Nanotechnology 1996;7 :216-23.

[140] De ZM, Bojsen-Moller F, Voigt M. Dynamic viscoelastic behavior of lower extremity tendons during simulated running. J Appl Physiol 2000 Oct;89(4):1352-9.

[141] Nirmalanandhan VS, Shearn JT, Juncosa-Melvin N, Rao M, Gooch C, Jain A, et al. Improving linear stiffness of the cell-seeded collagen sponge constructs by varying the components of the mechanical stimulus. Tissue Eng Part A 2008;14(11).

[142] Reddy GK, Enwemeka CS. A simplified method for the analysis of hydroxyproline in biological tissues. Clin Biochem 1996 Jun;29(3):225-9.

[143] Costa KD, Lee EJ, Holmes JW. Creating alignment and anisotropy in engineered heart tissue: role of boundary conditions in a model three-dimensional culture system. Tissue Eng 2003 Aug;9(4):567-77.

[144] Wang N, Tytell JD, Ingber DE. Mechanotransduction at a distance: mechanically coupling the extracellular matrix with the nucleus. Nat Rev Mol Cell Biol 2009 Jan;10(1):75-82.

[145] Ruoslahti E. Stretching is good for a cell. Science 1997 May 30;276(5317):1345-6.

[146] Friedl G, Schmidt H, Rehak I, Kostner G, Schauenstein K, Windhager R. Undifferentiated human mesenchymal stem cells (hMSCs) are highly sensitive to mechanical strain: transcriptionally controlled early osteo-chondrogenic response in vitro. Osteoarthritis and Cartilage 2007 Nov;15(11):1293-300.

[147] Bhargava MM, Beavis AJ, Edberg JC, Warren RF, Attia ET, Hannafin JA. Differential expression of integrin subunits in canine knee ligament fibroblasts. J Orthop Res 1999 Sep;17(5):748-54.

[148] Huang C, Fu X, Liu J, Qi Y, Li S, Wang H. The involvement of integrin beta1 signaling in the migration and myofibroblastic differentiation of skin fibroblasts on anisotropic collagen-containing nanofibers. Biomaterials 2012 Feb;33(6):1791-800.

[149] Henshaw DR, Attia E, Bhargava M, Hannafin JA. Canine ACL fibroblast integrin expression and cell alignment in response to cyclic tensile strain in three-dimensional collagen gels. J Orthop Res 2006 Mar;24(3):481-90.

[150] Wang JH, Grood ES. The strain magnitude and contact guidance determine orientation response of fibroblasts to cyclic substrate strains. Connect Tissue Res 2000;41(1):29-36.

[151] Baker BM, Shah RP, Huang AH, Mauck RL. Dynamic tensile loading improves the functional properties of mesenchymal stem cell-laden nanofiber-based fibrocartilage. Tissue Eng Part A 2011 May;17(9-10):1445-55.

[152] Lee CH, Shin HJ, Cho IH, Kang YM, Kim IA, Park KD, et al. Nanofiber alignment and direction of mechanical strain affect the ECM production of human ACL fibroblast. Biomaterials 2005 Apr;26(11):1261-70.

[153] Waggett AD, Ralphs JR, Kwan APL, Woodnutt D, Benjamin M. Characterization of collagens and proteoglycans at the insertion of the human achilles tendon. Matrix Biology 1998 Mar;16(8):457-70.

[154] Eriksen HA, Pajala A, Leppilahti J, Risteli J. Increased content of type III collagen at the rupture site of human Achilles tendon. Journal of Orthopaedic Research 2002;20(6):1352-7.

[155] Hsieh AH, Tsai CM, Ma QJ, Lin T, Banes AJ, Villarreal FJ, et al. Time-dependent increases in type-III collagen gene expression in medical collateral ligament fibroblasts under cyclic strains. J Orthop Res 2000 Mar;18(2):220-7.

[156] Murphy PG, Loitz BJ, Frank CB, Hart DA. Influence of exogenous growth factors on the synthesis and secretion of collagen types I and III by explants of normal and healing rabbit ligaments. Biochem Cell Biol 1994 Sep;72(9-10):403-9.

[157] Brent AE, Schweitzer R, Tabin CJ. A somitic compartment of tendon progenitors. Cell 2003 Apr 18;113(2):235-48.

[158] Schweitzer R, Chyung JH, Murtaugh LC, Brent AE, Rosen V, Olson EN, et al. Analysis of the tendon cell fate using Scleraxis, a specific marker for tendons and ligaments. Development 2001 Oct;128(19):3855-66.

[159] Kuo CK, Tuan RS. Mechanoactive tenogenic differentiation of human mesenchymal stem cells. Tissue Eng Part A 2008 Oct;14(10):1615-27.

[160] Shukunami C, Takimoto A, Oro M, Hiraki Y. Scleraxis positively regulates the expression of tenomodulin, a differentiation marker of tenocytes. Dev Biol 2006 Oct 1;298(1):234-47.

[161] Docheva D, Hunziker EB, Fassler R, Brandau O. Tenomodulin is necessary for tenocyte proliferation and tendon maturation. Mol Cell Biol 2005 Jan;25(2):699-705.

[162] Shukunami C, Takimoto A, Oro M, Hiraki Y. Scleraxis positively regulates the expression of tenomodulin, a differentiation marker of tenocytes. Dev Biol 2006 Oct 1;298(1):234-47.

[163] Garcia AJ. Get a grip: integrins in cell-biomaterial interactions. Biomaterials 2005 Dec;26(36):7525-9.

[164] Hannafin JA, Attia EA, Henshaw R, Warren RF, Bhargava MM. Effect of cyclic strain and plating matrix on cell proliferation and integrin expression by ligament fibroblasts. J Orthop Res 2006 Feb;24(2):149-58.

[165] Lin TW, Cardenas L, Soslowsky LJ. Biomechanics of tendon injury and repair. J Biomech 2004 Jun;37(6):865-77.

[166] Petrie TA, Capadona JR, Reyes CD, Garcia AJ. Integrin specificity and enhanced cellular activities associated with surfaces presenting a recombinant fibronectin fragment compared to RGD supports. Biomaterials 2006 Nov;27(31):5459-70.

[167] Giancotti FG. Integrin signaling: specificity and control of cell survival and cell cycle progression. Curr Opin Cell Biol 1997 Oct;9(5):691-700.

[168] Song G, Ju Y, Soyama H, Ohashi T, Sato M. Regulation of cyclic longitudinal mechanical stretch on proliferation of human bone marrow mesenchymal stem cells. Mol Cell Biomech 2007 Dec;4(4):201-10.

[169] Timmenga EJF, Andreassen TT, Houthoff HJ, Klopper PJ. The effect of mechanical stress on healing skin wounds: an experimental study in rabbits using tissue expansion. British Journal of Plastic Surgery 1991;44(7):514-9.

[170] Schiro JA, Chan BM, Roswit WT, Kassner PD, Pentland AP, Hemler ME, et al. Integrin alpha 2 beta 1 (VLA-2) mediates reorganization and contraction of collagen matrices by human cells. Cell 1991 Oct 18;67(2):403-10.

[171] Zemel A, Rehfeldt F, Brown AEX, Discher DE, Safran SA. Optimal matrix rigidity for stress-fibre polarization in stem cells. Nat Phys 2010 Jun;6(6):468-73.

[172] Effect of scaffold material, construct length and mechanical stimulation on the in vitro stiffness of the engineered tendon construct 2008.

[173] Juncosa-Melvin N, Shearn JT, Boivin GP, Gooch C, Galloway MT, West JR, et al. Effects of mechanical stimulation on the biomechanics and histology of stem cell-collagen sponge constructs for rabbit patellar tendon repair. Tissue Eng 2006 Aug;12(8):2291-300.

[174] Butler DL, Juncosa-Melvin N, Boivin GP, Galloway MT, Shearn JT, Gooch C, et al. Functional tissue engineering for tendon repair: A multidisciplinary strategy using mesenchymal stem cells, bioscaffolds, and mechanical stimulation. J Orthop Res 2007 Aug 3.

[175] Butler DL, Shearn JT, Juncosa N, Dressler MR, Hunter SA. Functional tissue engineering parameters toward designing repair and replacement strategies. Clin Orthop Relat Res 2004 Oct;(427 Suppl):S190-S199.

[176] Subramony SD, Dargis BR, Castillo M, Azeloglu EU, Tracey MS, Su A, et al. The guidance of stem cell differentiation by substrate alignment and mechanical stimulation. Biomaterials 2013 Mar;34(8):1942-53.

[177] Hankemeier S, Keus M, Zeichen J, Jagodzinski M, Barkhausen T, Bosch U, et al. Modulation of proliferation and differentiation of human bone marrow stromal cells by fibroblast growth factor 2: potential implications for tissue engineering of tendons and ligaments. Tissue Eng 2005 Jan;11(1-2):41-9.

[178] The Effects of Local bFGF Release and Uniaxial Strain on Cellular Adaptation and Gene Expression in a 3D Environment: Implications for Ligament Tissue Engineering 2007.

[179] Shin HY, Schwartz EA, Bizios R, Gerritsen ME. Receptor-mediated basic fibroblast growth factor signaling regulates cyclic pressure-induced human endothelial cell proliferation. Endothelium 2004 Sep;11(5-6):285-91.

[180] Vincent T, Hermansson M, Bolton M, Wait R, Saklatvala J. Basic FGF mediates an immediate response of articular cartilage to mechanical injury. Proc Natl Acad Sci U S A 2002 Jun 11;99(12):8259-64.

[181] Vincent TL, Hermansson MA, Hansen UN, Amis AA, Saklatvala J. Basic fibroblast growth factor mediates transduction of mechanical signals when articular cartilage is loaded. Arthritis Rheum 2004 Feb;50(2):526-33.

[182] Jenner JM, Van EF, Saris DB, Willems WJ, Dhert WJ, Creemers LB. Effect of transforming growth factor-beta and growth differentiation factor-5 on proliferation and matrix production by human bone marrow stromal cells cultured on braided poly lactic-co-glycolic acid scaffolds for ligament tissue engineering. Tissue Eng 2007 Jul;13(7):1573-82.

[183] James R, Kumbar SG, Laurencin CT, Balian G, Chhabra AB. Tendon tissue engineering: adipose-derived stem cell and GDF-5 mediated regeneration using electrospun matrix systems. Biomed Mater 2011 Apr;6(2):025011.

[184] Matthews JA, Wnek GE, Simpson DG, Bowlin GL. Electrospinning of Collagen Nanofibers. Biomacromolecules 2002;3 :232-8.

[185] Vieira AC, Guedes RM, Marques AT. Development of ligament tissue biodegradable devices: A review. Journal of Biomechanics 2009 Nov 13;42(15):2421-30.

[186] Chandrashekar N, Mansouri H, Slauterbeck J, Hashemi J. Sex-based differences in the tensile properties of the human anterior cruciate ligament. Journal of Biomechanics 2006;39(16):2943-50.

[187] Burkersroda Fv, Schedl L, G+¦pferich A. Why degradable polymers undergo surface erosion or bulk erosion. Biomaterials 2002 Nov;23(21):4221-31.

[188] Kweon H, Yoo MK, Park IK, Kim TH, Lee HC, Lee HS, et al. A novel degradable polycaprolactone networks for tissue engineering. Biomaterials 2003 Feb;24(5):801-8.

[189] Baker SC, Rohman G+, Southgate J, Cameron NR. The relationship between the mechanical properties and cell behaviour on PLGA and PCL scaffolds for bladder tissue engineering. Biomaterials 2009 Mar;30(7):1321-8.

[190] Boskey AL. Current concepts of the physiology and biochemistry of calcification. Clin Orthop 1981 Jun;(157):225-57.

[191] LeGeros RZ. Calcium phosphate-based osteoinductive materials. Chem Rev 2008 Nov;108(11):4742-53.

[192] LeGeros RZ. Properties of osteoconductive biomaterials: calcium phosphates. Clin Orthop Relat Res 2002 Feb;(395):81-98.

[193] Liu X, Smith LA, Hu J, Ma PX. Biomimetic nanofibrous gelatin/apatite composite scaffolds for bone tissue engineering. Biomaterials 2009 Apr;30(12):2252-8.

[194] Kim HW, Kim HE. Nanofiber generation of hydroxyapatite and fluor-hydroxyapatite bioceramics. J Biomed Mater Res B Appl Biomater 2006 May;77(2):323-8.

[195] Song JH, Kim HE, Kim HW. Electrospun fibrous web of collagen-apatite precipitated nanocomposite for bone regeneration. J Mater Sci Mater Med 2008 Aug;19(8):2925-32.

[196] Yeo M, Lee H, Kim G. Three-Dimensional Hierarchical Composite Scaffolds Consisting of Polycaprolactone, +¦-Tricalcium Phosphate, and Collagen Nanofibers: Fabrication, Physical Properties, and In Vitro Cell Activity for Bone Tissue Regeneration. Biomacromolecules 2010 Dec 28;12(2):502-10.

[197] Ko EK, Jeong SI, Rim NG, Lee YM, Shin H, Lee BK. In vitro osteogenic differentiation of human mesenchymal stem cells and in vivo bone formation in composite nanofiber meshes. Tissue Eng Part A 2008 Dec;14(12):2105-19.

[198] Meinel L, Karageorgiou V, Fajardo R, Snyder B, Shinde-Patil V, Zichner L, et al. Bone tissue engineering using human mesenchymal stem cells: effects of scaffold material and medium flow. Ann Biomed Eng 2004 Jan;32(1):112-22.

[199] McCullen SD, Zhu Y, Bernacki SH, Narayan RJ, Pourdeyhimi B, Gorga RE, et al. Electrospun composite poly(L-lactic acid)/tricalcium phosphate scaffolds induce proliferation and osteogenic differentiation of human adipose-derived stem cells. Biomed Mater 2009 Jun;4(3):035002.

[200] M++ller P, Bulnheim U, Diener A, L++then F, Teller M, Klinkenberg ED, et al. Calcium phosphate surfaces promote osteogenic differentiation of mesenchymal stem cells. Journal of cellular and molecular medicine 2008 Jan 1;12(1):281-91.

[201] He J, Genetos DC, Leach JK. Osteogenesis and trophic factor secretion are influenced by the composition of hydroxyapatite/poly(lactide-co-glycolide) composite scaffolds. Tissue Eng Part A 2010 Jan;16(1):127-37.

[202] Lu HH, Kofron MD, El Amin SF, Attawia MA, Laurencin CT. In vitro bone formation using muscle-derived cells: a new paradigm for bone tissue engineering using polymer-bone morphogenetic protein matrices. Biochemical & Biophysical Research Communications 2003 Jun 13;305(4):882-9.

[203] Wang IE, Shan J, Choi R, Oh S, Kepler CK, Chen FH, et al. Role of osteoblast-fibroblast interactions in the formation of the ligament-to-bone interface. J Orthop Res 2007 Aug 3;25(12):1609-20.

[204] Lu HH, Tang A, Oh SC, Spalazzi JP, Dionisio K. Compositional effects on the formation of a calcium phosphate layer and the response of osteoblast-like cells on polymer-bioactive glass composites. Biomaterials 2005 Nov;26(32):6323-34.

[205] Walters MA, Leung YC, Blumenthal NC, LeGeros RZ, Konsker KA. A Raman and infrared spectroscopic investigation of biological hydroxyapatite. J Inorg Biochem 1990 Jul;39(3):193-200.

[206] Rehman I, Bonfield W. Characterization of hydroxyapatite and carbonated apatite by photo acoustic FTIR spectroscopy. J Mater Sci Mater Med 1997 Jan;8(1):1-4.

[207] Golub EE, Boesze-Battaglia K. The role of alkaline phosphatase in mineralization. Current Opinion in Orthopaedics 2007;18(5).

[208] Kunzler TP, Drobek T, Schuler M, Spencer ND. Systematic study of osteoblast and fibroblast response to roughness by means of surface-morphology gradients. Biomaterials 2007 May;28(13):2175-82.

[209] Lincks J, Boyan BD, Blanchard CR, Lohmann CH, Liu Y, Cochran DL, et al. Response of MG63 osteoblast-like cells to titanium and titanium alloy is dependent on surface roughness and composition. Biomaterials 1998 Dec;19(23):2219-32.

[210] Mwale F, Wang HT, Nelea V, Luo L, Antoniou J, Wertheimer MR. The effect of glow discharge plasma surface modification of polymers on the osteogenic differentiation of committed human mesenchymal stem cells. Biomaterials 2006 Apr;27(10):2258-64.

[211] Dulgar-Tulloch AJ, Bizios R, Siegel RW. Differentiation of human mesenchymal stem cells on nano- and micro-grain size titania. Materials Science and Engineering: C 2011 Mar 12;31(2):357-62.

[212] Wall I, Donos N, Carlqvist K, Jones F, Brett P. Modified titanium surfaces promote accelerated osteogenic differentiation of mesenchymal stromal cells in vitro. Bone 2009 Jul;45(1):17-26.

[213] Balloni S, Calvi EM, Damiani F, Bistoni G, Calvitti M, Locci P, et al. Effects of titanium surface roughness on mesenchymal stem cell commitment and differentiation signaling. Int J Oral Maxillofac Implants 2009 Jul;24(4):627-35.

[214] Mwale F, Tchetina E, Wu CW, Poole AR. The assembly and remodeling of the extracellular matrix in the growth plate in relationship to mineral deposition and cellular hypertrophy: an in situ study of collagens II and IX and proteoglycan. J Bone Miner Res 2002 Feb;17(2):275-83.

[215] Wu LN, Ishikawa Y, Sauer GR, Genge BR, Mwale F, Mishima H, et al. Morphological and biochemical characterization of mineralizing primary cultures of avian growth plate chondrocytes: evidence for cellular processing of Ca2+ and Pi prior to matrix mineralization. J Cell Biochem 1995 Feb;57(2):218-37.

[216] Hongju Peng and Zi Yin and Huanhuan Liu and Xiao Chen and Bei Feng and Huihua Yuan and Bo Su and Hongwei Ouyang and Yanzhong Zhang. Electrospun biomimetic scaffold of hydroxyapatite/chitosan supports enhanced osteogenic differentiation of mMSCs. Nanotechnology 2012;23(48):485102.

[217] Lu LX, Zhang XF, Wang YY, Ortiz L, Mao X, Jiang ZL, et al. Effects of Hydroxyapatite-Containing Composite Nanofibers on Osteogenesis of Mesenchymal Stem Cells In vitro and Bone Regeneration In vivo. ACS Appl Mater Interfaces 2012 Dec 25;5(2):319-30.

[218] Phipps MC, Clem WC, Catledge SA, Xu Y, Hennessy KM, Thomas V, et al. Mesenchymal Stem Cell Responses to Bone-Mimetic Electrospun Matrices Composed of Polycaprolactone, Collagen I and Nanoparticulate Hydroxyapatite. PLoS ONE 2011 Feb 8;6(2):e16813.

[219] Messner K. Postnatal development of the cruciate ligament insertions in the rat knee. morphological evaluation and immunohistochemical study of collagens types I and II. Acta Anatomica 1997;160(4):261-8.

[220] Niyibizi C, Sagarrigo VC, Gibson G, Kavalkovich K. Identification and immunolocalization of type X collagen at the ligament-bone interface. Biochem Biophys Res Commun 1996 May 15;222(2):584-9.

[221] Petersen W, Tillmann B. Structure and vascularization of the cruciate ligaments of the human knee joint. Anat Embryol (Berl) 1999 Sep;200(3):325-34.

[222] Sagarriga VC, Kavalkovich K, Wu J, Niyibizi C. Biochemical analysis of collagens at the ligament-bone interface reveals presence of cartilage-specific collagens. Arch Biochem Biophys 1996 Apr 1;328(1):135-42.

[223] Wei X, Messner K. The postnatal development of the insertions of the medial collateral ligament in the rat knee. Anat Embryol (Berl) 1996 Jan;193(1):53-9.

[224] Spalazzi JP, Dagher E, Doty SB, Guo XE, Rodeo SA, Lu HH. In vivo evaluation of a multiphased scaffold designed for orthopaedic interface tissue engineering and soft tissue-to-bone integration. J Biomed Mater Res A 2008 Jul;86(1):1-12.

[225] Gao J, Messner K, Ralphs JR, Benjamin M. An immunohistochemical study of enthesis development in the medial collateral ligament of the rat knee joint. Anat Embryol (Berl) 1996 Oct;194(4):399-406.

[226] Nawata K, Minamizaki T, Yamashita Y, Teshima R. Development of the attachment zones in the rat anterior cruciate ligament: changes in the distributions of proliferating cells and fibrillar collagens during postnatal growth. J Orthop Res 2002 Nov;20(6):1339-44.

[227] Koob TJ, Clark PE, Hernandez DJ, Thurmond FA, Vogel KG. Compression loading in vitro regulates proteoglycan synthesis by tendon fibrocartilage. Arch Biochem Biophys 1992 Oct;298(1):303-12.

[228] Malaviya P, Butler DL, Boivin GP, Smith FN, Barry FP, Murphy JM, et al. An in vivo model for load-modulated remodeling in the rabbit flexor tendon. J Orthop Res 2000 Jan;18(1):116-25.

[229] Perez-Castro AV, Vogel KG. In situ expression of collagen and proteoglycan genes during development of fibrocartilage in bovine deep flexor tendon. J Orthop Res 1999 Jan;17(1):139-48.

[230] Robbins JR, Evanko SP, Vogel KG. Mechanical loading and TGF-beta regulate proteoglycan synthesis in tendon. Arch Biochem Biophys 1997 Jun 15;342(2):203-11.

[231] Vogel KG. The effect of compressive loading on proteoglycan turnover in cultured fetal tendon. Connect Tissue Res 1996;34(3):227-37.

[232] Zong X, Ran S, Kim KS, Fang D, Hsiao BS, Chu B. Structure and Morphology Changes during in Vitro Degradation of Electrospun Poly(glycolide-co-lactide) Nanofiber Membrane. Biomacromolecules 2003 Mar;4(2):416-23.

[233] Yang F, Murugan R, Wang S, Ramakrishna S. Electrospinning of nano/micro scale poly(L-lactic acid) aligned fibers and their potential in neural tissue engineering. Biomaterials 2005 May;26(15):2603-10.

[234] Enobakhare BO, Bader DL, Lee DA. Quantification of sulfated glycosaminoglycans in chondrocyte/alginate cultures, by use of 1,9-dimethylmethylene blue. Anal Biochem 1996 Dec 1;243(1):189-91.

[235] Farndale RW, Sayers CA, Barrett AJ. A direct spectrophotometric microassay for sulfated glycosaminoglycans in cartilage cultures. Connect Tissue Res 1982;9(4):247-8.

[236] Seibel MJ, Macaulay W, Jelsma R, Saed-Nejad F, Ratcliffe A. Antigenic properties of keratan sulfate: influence of antigen structure, monoclonal antibodies, and antibody valency. Arch Biochem Biophys 1992 Aug 1;296(2):410-8.

[237] Silver FH, Kato YP, Ohno M, Wasserman AJ. Analysis of mammalian connective tissue: relationship between hierarchical structures and mechanical properties. [Review] [214 refs]. J Long Term Eff Med Implants 1992;2(2-3):165-98.

[238] Mauck RL, Byers BA, Yuan X, Tuan RS. Regulation of cartilaginous ECM gene transcription by chondrocytes and MSCs in 3D culture in response to dynamic loading. Biomech Model Mechanobiol 2007 Jan;6(1-2):113-25.

[239] Kisiday JD, Frisbie DD, McIlwraith CW, Grodzinsky AJ. Dynamic compression stimulates proteoglycan synthesis by mesenchymal stem cells in the absence of chondrogenic cytokines. Tissue Eng Part A 2009 Oct;15(10):2817-24.

[240] Huang AH, Farrell MJ, Kim M, Mauck RL. Long-term dynamic loading improves the mechanical properties of chondrogenic mesenchymal stem cell-laden hydrogel. Eur Cell Mater 2010;19:72-85.

[241] Wozney JM, Rosen V, Celeste AJ, Mitsock LM, Whitters MJ, Kriz RW, et al. Novel regulators of bone formation: molecular clones and activities. Science 1988 Dec 16;242(4885):1528-34.

[242] Seyedin SM, Rosen DM, Segarini PR. Modulation of chondroblast phenotype by transforming growth factor-beta. Pathology & Immunopathology Research 1988;7(1-2):38-42.

[243] Mackay AM, Beck SC, Murphy JM, Barry FP, Chichester CO, Pittenger MF. Chondrogenic differentiation of cultured human mesenchymal stem cells from marrow. Tissue Eng 1998;4(4):415-28.

[244] Thomopoulos S, Das R, Birman V, Smith L, Ku K, Elson EL, et al. Fibrocartilage tissue engineering: the role of the stress environment on cell morphology and matrix expression. Tissue Eng Part A 2011 Apr;17(7-8):1039-53.

[245] He P, Ng KS, Toh SL, Goh JC. In vitro ligament-bone interface regeneration using a trilineage coculture system on a hybrid silk scaffold. Biomacromolecules 2012 Sep 10;13(9):2692-703.

[246] Doshi J, Reneker DH. Electrospinnig process and applications of electrospun fibers. Journal of Electrostatics 35 , 151-160. 1995.
Ref Type: Journal (Full)

[247] Hays PL, Kawamura S, Deng XH, Dagher E, Mithoefer K, Ying L, et al. The role of macrophages in early healing of a tendon graft in a bone tunnel. J Bone Joint Surg Am 2008 Mar;90(3):565-79.

[248] Erben RG. Embedding of bone samples in methylmethacrylate: an improved method suitable for bone histomorphometry, histochemistry, and immunohistochemistry. J Histochem Cytochem 1997 Feb;45(2):307-13.

[249] von Kossa J. Ueber die im Organismus kunstlich erzeugen Verkalkungen. Beitr Path Anat 1901;29:163-202.

[250] Doty SB. Space flight and bone formation. Materwiss Werksttech 2004 Dec;35(12):951-61.

[251] Karaoglu S, Celik C, Korkusuz P. The effects of bone marrow or periosteum on tendon-to-bone tunnel healing in a rabbit model. Knee Surg Sports Traumatol Arthrosc 2009 Feb;17(2):170-8.

[252] Ralphs JR, Benjamin M, Waggett AD, Russell DC, Messner K, Gao J. Regional differences in cell shape and gap junction expression in rat Achilles tendon: relation to fibrocartilage differentiation. J Anat 1998 Aug;193 (Pt 2):215-22.

[253] Wen CY, Qin L, Lee KM, Chan KM. The use of brushite calcium phosphate cement for enhancement of bone-tendon integration in an anterior cruciate ligament reconstruction rabbit model. J Biomed Mater Res B Appl Biomater 2009 May;89B(2):466-74.

[254] Moen CT, Pelker RR. Biomechanical and histological correlations in growth plate failure. J Pediatr Orthop 1984 Mar;4(2):180-4.

[255] Vunjak-Novakovic G, Obradovic B, Martin I, Bursac PM, Langer R, Freed LE. Dynamic cell seeding of polymer scaffolds for cartilage tissue engineering. Biotechnol Prog 1998 Mar;14(2):193-202.

[256] Almarza AJ, Athanasiou KA. Effects of initial cell seeding density for the tissue engineering of the temporomandibular joint disc. Ann Biomed Eng 2005 Jul;33(7):943-50.

[257] Gurdon JB. A community effect in animal development. Nature 1988 Dec 22;336(6201):772-4.

[258] Kruyt M, De BJ, Rouwkema J, Van BC, Oner C, Verbout A, et al. Analysis of the dynamics of bone formation, effect of cell seeding density, and potential of allogeneic cells in cell-based bone tissue engineering in goats. Tissue Eng Part A 2008 Jun;14(6):1081-8.

[259] Wang L, Tran I, Seshareddy K, Weiss ML, Detamore MS. A comparison of human bone marrow-derived mesenchymal stem cells and human umbilical cord-derived mesenchymal stromal cells for cartilage tissue engineering. Tissue Eng Part A 2009 Aug;15(8):2259-66.

[260] Woo SL, Hollis JM, Adams DJ, Lyon RM, Takai S. Tensile properties of the human femur-anterior cruciate ligament-tibia complex. The effects of specimen age and orientation. Am J Sports Med 1991 May;19(3):217-25.

[261] Chen EH, Black J. Materials design analysis of the prosthetic anterior cruciate ligament. J Biomed Mater Res 1980 Sep;14(5):567-86.

[262] Awad HA, Butler DL, Harris MT, Ibrahim RE, Wu Y, Young RG, et al. In vitro characterization of mesenchymal stem cell-seeded collagen scaffolds for tendon repair: Effects of initial seeding density on contraction kinetics. J Biomed Mater Res 2000 Aug;51(2):233-40.

[263] Grayson WL, Bhumiratana S, Cannizzaro C, Chao PH, Lennon DP, Caplan AI, et al. Effects of initial seeding density and fluid perfusion rate on formation of tissue-engineered bone. Tissue Eng Part A 2008 Nov;14(11):1809-20.

[264] Lian JB, Gundberg CM. Osteocalcin. Biochemical considerations and clinical applications. Clin Orthop 1988 Jan;(226):267-91.

[265] Aubin JE, Liu F, Malaval L, Gupta AK. Osteoblast and chondroblast differentiation. Bone 1995 Aug;17(2 Suppl):77S-83S.

[266] Kawamura S, Ying L, Kim HJ, Dynybil C, Rodeo SA. Macrophages accumulate in the early phase of tendon-bone healing. J Orthop Res 2005 Nov;23(6):1425-32.

[267] Murray MM, Spindler KP, Abreu E, Muller JA, Nedder A, Kelly M, et al. Collagen-platelet rich plasma hydrogel enhances primary repair of the porcine anterior cruciate ligament. J Orthop Res 2007 Jan;25(1):81-91.

[268] Schwartz HE, Matava MJ, Proch FS, Butler CA, Ratcliffe A, Levy M, et al. The effect of gamma irradiation on anterior cruciate ligament allograft biomechanical and biochemical properties in the caprine model at time zero and at 6 months after surgery. Am J Sports Med 2006 Nov;34(11):1747-55.

[269] Anderson K, Seneviratne AM, Izawa K, Atkinson BL, Potter HG, Rodeo SA. Augmentation of tendon healing in an intraarticular bone tunnel with use of a bone growth factor. Am J Sports Med 2001 Nov;29(6):689-98.

[270] Livingston T, Ducheyne P, Garino J. In vivo evaluation of a bioactive scaffold for bone tissue engineering. J Biomed Mater Res 2002 Oct;62(1):1-13.

[271] Hasegawa S, Tamura J, Neo M, Goto K, Shikinami Y, Saito M, et al. In vivo evaluation of a porous hydroxyapatite/poly-DL-lactide composite for use as a bone substitute. J Biomed Mater Res A 2005 Dec 1;75(3):567-79.

[272] Mackay AM, Beck SC, Murphy JM, Barry FP, Chichester CO, Pittenger MF. Chondrogenic Differentiation of Cultured Human Mesenchymal Stem Cells from Marrow. Tissue Eng 1998;4(4):415-28.

[273] Park JS, Woo DG, Yang HN, Na K, Park KH. Transforming growth factor beta-3 bound with sulfate polysaccharide in synthetic extracellular matrix enhanced the biological activities for neocartilage formation in vivo. J Biomed Mater Res A 2009 Nov;91(2):408-15.

[274] Bian L, Zhai DY, Tous E, Rai R, Mauck RL, Burdick JA. Enhanced MSC chondrogenesis following delivery of TGF-beta3 from alginate microspheres within hyaluronic acid hydrogels in vitro and in vivo. Biomaterials 2011 Sep;32(27):6425-34.

[275] Sahoo S, Ang LT, Goh JC, Toh SL. Growth factor delivery through electrospun nanofibers in scaffolds for tissue engineering applications. J Biomed Mater Res A 2010 Jun 15;93(4):1539-50.

[276] Valmikinathan CM, Defroda S, Yu X. Polycaprolactone and bovine serum albumin based nanofibers for controlled release of nerve growth factor. Biomacromolecules 2009 May 11;10(5):1084-9.